FYSAST
Examensarbete 30 hp
March 2011

Numerical Modelling of Langmuir Probe Measurements for the Swarm Spacecraft

Marco Chiaretta

UPPSALA
UNIVERSITET

Teknisk- naturvetenskaplig fakultet
Institutionen för fysik och astronomi

Besöksadress:
Ångströmlaboratoriet
Lägerhyddsvägen 1

Postadress:
Box 516
751 21 Uppsala

Telefon:
018 – 471 5952

Telefax:
018 – 471 5999

Hemsida:
http://www.teknat.uu.se/student

Abstract

Numerical Modelling of Langmuir Probe Measurements for the Swarm Spacecraft

Marco Chiaretta

This work studies the current collected by the spherical Langmuir probes to be mounted on the ESA Swarm satellites in order to quantify deviations from idealized cases caused by non-ideal probe geometry. The finite-element particle-in-cell code SPIS is used to model the current collection of a realistic probe, including the support structures, for two ionospheric plasma conditions with and without drift velocity. SPIS simulations are verified by comparing simulations of an ideal sphere at rest to previous numerical results by Laframboise parametrized to sufficient accuracy. It is found that for probe potentials much above the equivalent electron temperature, the deviations from ideal geometry decrease the current by up to 25 % compared to the ideal sphere case and thus must be corrected if data from this part of the probe curve has to be used for plasma density derivations. In comparison to the non-drifting case, including a plasma ram flow increases the current for probe potentials around and below the equivalent ion energy, as the contribution of the ions to the shielding is reduced by their high flow energy.

Handledare: Anders Eriksson, Swedish Institute of Space Physics, Uppsala
Ämnesgranskare: Mats André
Examinator: Bengt Lindgren
FYSAST

DIPLOMA THESIS

NUMERICAL MODELLING OF LANGMUIR PROBE MEASUREMENTS FOR THE SWARM SPACECRAFT

MARCO CHIARETTA

Swedish Institute of Space Physics
and
Department of Astronomy and Space Physics, Uppsala University, Sweden

MARCH 15, 2011

With their round dance the electrons spin
chrysalises of that which abides,
the inmost cocoons
which do not open of their own accord
but are of that which abides.

There it is not a matter of hatching out.
There it is a matter of tending and protecting
the metamorphoses of the inmost
deeper-down swaying,
the innermost playing of women in dance.

The Electrons by Harry Martinson

ABSTRACT

This work studies the current collected by the spherical Langmuir probes to be mounted on the ESA Swarm satellites in order to quantify deviations from idealized cases caused by non-ideal probe geometry. The finite-element particle-in-cell code SPIS is used to model the current collection of a realistic probe, including the support structures, for two ionospheric plasma conditions with and without drift velocity. SPIS simulations are verified by comparing simulations of an ideal sphere at rest to previous numerical results by Laframboise parametrized to sufficient accuracy. It is found that for probe potentials much above the equivalent electron temperature, the deviations from ideal geometry decrease the current by up to 25 % compared to the ideal sphere case and thus must be corrected if data from this part of the probe curve has to be used for plasma density derivations. In comparison to the non-drifting case, including a plasma ram flow increases the current for probe potentials around and below the equivalent ion energy, as the contribution of the ions to the shielding is reduced by their high flow energy.

SUMMARY

Space environment modelling in the near surroundings of the Swarm spacecraft

As part of the Earth Science Observation program of the European Space Agency, three satellites known as Swarm will be launched together with the objective to investigate the Earth's interior and the climate. Data are acquired by electric and magnetic sensors probing the atmosphere at satellites orbits.

The space environment at such altitudes carries the informations the Swarm mission aims to collect. This environment is characterized by charged particles (electrons and ions) that together constitute what is called a plasma. To disclose informations about this plasma, on board of each spacecraft are mounted dedicated instruments. The Electric Filed Instrument (EFI) is in focus in this thesis that is dedicated to support the accuracy of EFI measurements. Such accuracy is perfected by a pair of sensors called Langmuir probes (LP) mounted onboard of each spacecraft. These are a pair of spherical probes of 7.61 mm in diameter, mounted in the front portion of the spacecraft and are designed and built by the Swedish Institute for Space Physics, IRF-U (Institutet fr Rymdfysik), section of Uppsala, Sweden. Langmuir probes determine local properties of the plasma such as temperature and density by measuring the collected current due to electrons and ions. This current is related to the voltages imposed on the probe and current and voltages can be plotted together in a characteristic curve.

In the Swarm scenario, the LP support and the spacecraft body may effect the measurements, hence the shape of the characteristic curve, by introducing local variations on the density of electrons and ions. As the mission objectives push for accurate determination of plasma local properties, the quality and quantity of the disturbance have to be evaluated and this is done by looking at the shape of the characteristic curve. Beyond the theoretical model, an added amount of considerations, based on computer simulations, is performed to reproduce the essence of the plasma without all the details as to clarify main relations between the shape of the curve and the plasma parameters implemented in the simulation

process.

In this thesis are simulated Langmuir probe measurements in the ionosphere in conditions as close to reality as the simulation tools allow. Figure 1 shows the modelled environment within which the virtual measurement is performed. Determining the drivers of the plasma response will improve real data interpretation. To address the simulations of consistency and to determine deviations from ideal cases, simulations are compared to other results present in literature that have been previously obtained by other means and also to fully consistent theories. The results of this thesis show a good matching between simulations and literature.

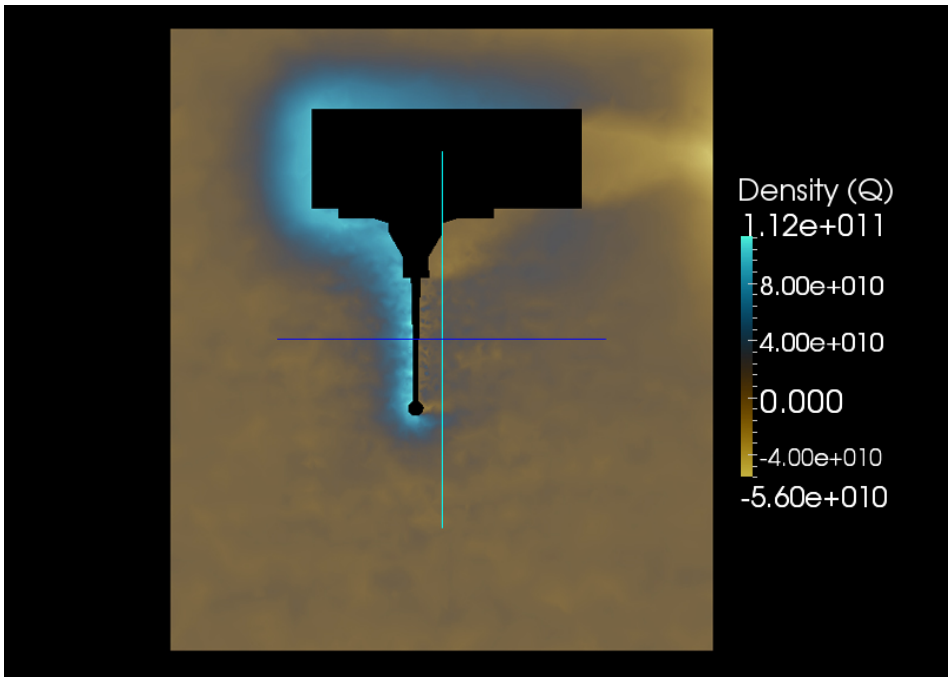

Figure 1: *Charge density around the LP and a portion of the spacecraft.*

ACKNOWLEDGEMENTS

I thank my supervisor, Dr Anders Eriksson, for giving me the opportunity to work at this interdisciplinary project made of an incredible combination of physics, engineering and numerics. I thank him for all the scientific talks and idea we exchanged that guided me while approaching various problems. I am grateful for having been allowed to work with a consistent degree of freedom while having, at the same time, a careful eye on my work. Through him, I acknowledge the ESA's Space Environment Section and people at Onera for the encouraging and constructive commments about the results of this work.

I thank Prof. Mats André and all the present and past members I met at the IRF-Uppsala for welcoming me into the group and for the hospitality they have dedicated during meetings, seminars, coffe breaks and trips. I am also grateful to Prof. Hermann Opgenoorth for his constructive attitude.

Special thanks to my coworkers Alexander Sjögren, Thomas Nilsson, Madeleine Holmberg and Christian Hanberg for the good time we shared together that kept me running when the simulations were unstable and uncooperative.

Gratitude goes to the direct influence of Mum and Dad for their never ending love, patience and support that I feel very close even if they live more than 2000 km away. Gratitute goes also to the indirect influence of my grandparents whose distinct 'heretical' spirit has finally come to inspire my life again.

CONTENTS

List of Abbreviations

EFI-Electric Field Instrument
EUV-Extreme Ultraviolet Radiation
FEM-Finite Element Method
IRF-Institutet för Rymdfysik (Swedish Institute of Space Physics)
JPL-Jet Propulsion Laboratory
LF-Laframboise
LP-Langmuir probe
NOAA-National Oceanic and Atmospheric Administration
OML-Orbital Motion Limited
PIC-Particles in Cell
S/C-Spacecraft
SL-Sheath Limited
SPIS-Space Plasma Interaction System
UV-Ultraviolet Radiation

1

INTRODUCTION

1.1 General background

As part of the ESA's Earth science observation, the Swarm mission has the objective to provide the best ever survey of the geomagnetic field, its evolution and new insights into our knowledge of the Earth's interior and into the climate. The Swarm mission will operate three identical satellites in constellation to assess properties of the Earth's geodynamo by providing high precision measurements of the geomagnetic field [1]. These informations are local and punctual in time and consist in strength and direction of the magnetic feld as it is resolved by a three point measurement collected by the satellites operating together. Data are acquired by electric and magnetic sensors probing the magnetosphere at ionospheric altitudes. The Electric Filed Instrument (EFI) is of interest for this thesis whose results are dedicated to support the accuracy of its measurements.

The EFI will determine the plasma conductivity from the near-polar orbit for each satellite: two satellites at 450 km (approximately in the same orbit and with a few seconds of delay from each other); one at 530 km (crossing by 90° the lower pair and introducing a second dimension into the measurements). In Section 2.5 it is discussed how the accuracy of the EFI is perfected by the pair of Langmuir probes (LP) mounted onboard of each spacecraft. These probes are designed and built by the Swedish Institute for Space Physics, IRF-U (Institutet för Rymdfysik), section of Uppsala, Sweden.

[1] The geomagnetic field is produced by a self sustaining dynamo (geodynamo) operating in the fluid deep inside the Earth.

(a) Artistic representation of the Swarm spacecrafts. Credits: Astrium.

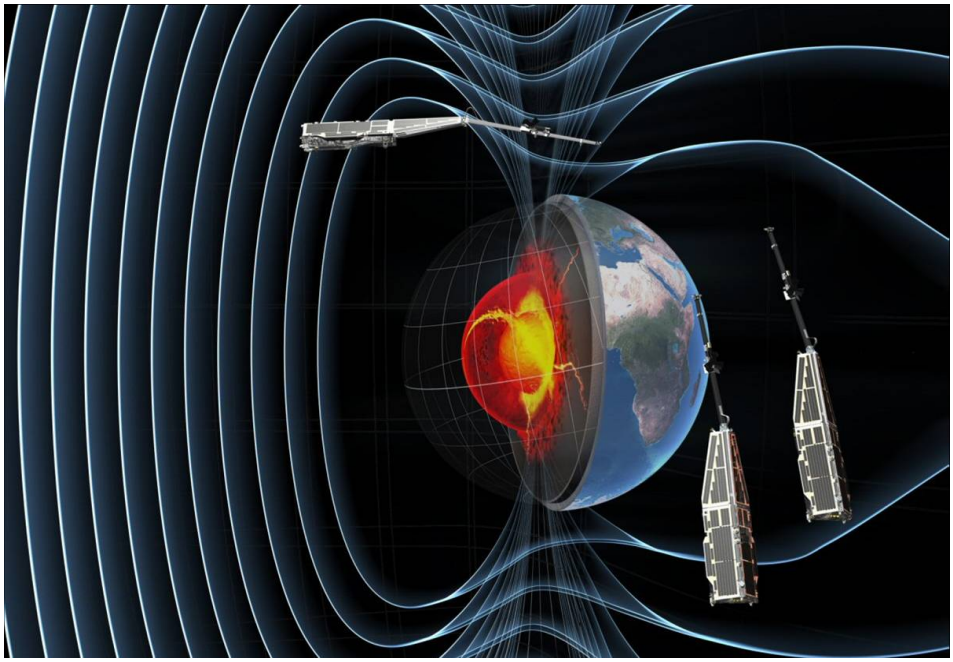

(b) Swarm mission scheme. Credits ESA.

Figure 1.1: *Two views of the Swarm constellation in formation.*

Langmuir probes determine local properties of the plasma such as temperature and density from the collected current. Theories for LP data interpretation are exact in only a few simplified cases which do not include the satellite motion and complex potential distributions associated to composite materials and/or sophisticated geometries. In the Swarm scenario, the LP support and the spacecraft body alter the symmetry of the potential distribution hence may effect the measurements by introducing local electromagnetic disturbances. As the Swarm mission objectives push for accurate determination of plasma local properties, the quality and quantity of the disturbance have to be evaluated. Beyond the theoretical model, an added amount of considerations, based on computer simulations, is performed to reproduce the essence of the plasma without all the details as to clarify main relations between the plasma parameters implemented in the simulation process and its outcome represented by the simulations results.

In this thesis are simulated LP measurements in the ionosphere in conditions as close to reality as the simulation tools allow. The goal is to determine the drivers of the plasma response to imposed probe potentials in order to refine algorithms for in situ data interpretation. The simulation problem is the sheath modelling and it is not linear. Among the numerical approaches, it is used the Particle-In-Cell (PIC) method which is one of the most reliable and established techniques used for short simulations time. With this technique, it is performed a three dimensional analysis of a dense, collisionless and unmagnetized plasma which is implemented in a finite element approximation also resolving the instrument's geometry to the highest possible realism. The software used is SPIS (Space Plama Interaction System) and it is developed to model electromagnetic effects on space systems by several Europeans contributors, particularly ONERA and Artenum with strong support from ESA. In order to validate the SPIS code and to determine deviations from ideal cases, simulations are compared to numerical results from Laframboise [1] and to the Orbit Motion Limited (OML) theory. The reliability of results is ensured via extensive comparison between the Spis and the Laframboise methods and via confrontations of various PIC simulations. The introduced simplifications concern the environmental parameters and the geometrical model of the sensor, both are discussed with respect of theory and literature.

1.2 Thesis structure

Elements of plasma theory used within the simulation are surveyed in Chapter 2. Numerical procedures for resolving nonlinear kinetic processes around the probe and the parametrization of Laframboise's results (preliminary to data confrontation with SPIS simulations) are described in Chapter 3. Ionspheric parameters are presented in Chapter 4. The simplified plasma model (resolved by macroparticles) and the LP models (resolved by a triangular mesh) are discussed as correlated arguments in Chapter 5. Simulations are logically ordered, collected species currents are mapped in time and averaged stable current values are listed in Chapter 6. Average values of collected currents are compared to each other on I-V maps as results are discussed; pictures of the sheath structure in different models support the discussion and conclude the thesis with Chapter 7.

2

PROBE THEORY & SHEATH PHYSICS

This chapter describes the essential physics for the interpretation of the Langmuir probe data including the influence of the artificially polarized region which surrounds the probe, the sheath.

2.1 Quasineutrality and thermal speed

A plasma is a quasi-neutral ($n_e \sim n_i$) ensamble of charged particles (electrons and ions) interacting with their neighbours via the electric potential. Electrodynamics complements gas kinetics and impose a description of the plasma in terms of collective behaviour. At thermal equilibrium ($T_e \sim T_i$), the ratio of the mean electron speed $v_{th_e} = (2k_B T_e/\pi m_e)^{1/2}$ to the mean ion speed $v_{th_i} = (2k_B T_i/\pi m_i)^{1/2}$ is simplified to the square root of the mass ratio between electrons and ions ($m_p/m_e = 1836$) [1]

$$\frac{v_e}{v_i} = \left(\frac{m_i}{m_e}\right)^{1/2} \approx 42.9, \tag{2.1}$$

where is assumed that the ions are protons. The higher electron mobility maintains electrons inhert enough along their trajectories towards the ions making it possible for them to escape the trapped orbits domain. This is verified for most of the electrons. However, at a given time, due to the long range electrostatic attraction, there are enough electrons near the ions to estabilish neutrality; as the electron

[1] where $m_e = 9.11 \cdot 10^{-31}$ kg, $m_p = 1.67 \cdot 10^{-27}$ kg

density is dynamically distorted by the presence of the ions, the charge balance is called quasi neutral.

2.2 Debye length

While reducing the size of the observed volume element down to the scale lengths at which charge neutrality does not hold any longer and the local charge density $\rho = e(n_i - n_e)$ is no longer zero, it comes to be resolved the presence of an electric potential which satisfies the Poisson's equation for an electron-proton plasma. The density of ions and electrons can still be modeled via the Boltzmann's law,

$$n_e(r) = n_0 \, exp\left(\frac{e\phi(r)}{k_B T_e}\right). \tag{2.2}$$

By expanding 2.2 in a Taylor series and combining with the Poisson equation

$$\Delta\phi = -\frac{\rho}{\epsilon}, \tag{2.3}$$

it results a differential spherical symmetic problem for the potential field centered on an ion and with radious r,

$$\nabla^2\phi = \frac{e^2 n_0}{\epsilon_0 k_B T_e}\phi = \left(\frac{1}{\lambda_D}\right)^2 \phi. \tag{2.4}$$

The right hand side describes a potential divided by the square of a characteristic lenght, the Debye (screening) length,

$$\lambda_D \equiv \left(\frac{e^2 n_0 \phi}{\epsilon_0 k_B T_e}\right)^{-1/2} \equiv \frac{v_{th_e}}{\omega_p} \tag{2.5}$$

which is the radius of the artificial polarized volume around the ion, the Debye sphere. The Debye length is numerically related to the electron thermal velocity v_{th_e} and to the plasma frequency ω_p.

2.3 Debye sheath

Section 2.2 has introduced the Debye sheath around a point ion. For a macroscopic body, the sheath is altered by the absorption of ions and electrons around

the body, complicating the sheath structure. Figure 2.1 shows the sheath around a Swarm satellite as simulated by SPIS. The sheath is comparable to the Debye length but varies to a certain extent depending on the applied bias voltage on the electrode. Sheaths control LP current collection by effecting the dynamic of incoming charges via electromagnetic interaction.

For simplicity, it is possible to approach the sheath problem by separating the effects of a plasma at rest and of a flowing plasma, there result a *stationary sheath* problem and a *streached sheath* problem due to the presence of the wake. Issues related to current collection from LP in the two cases are discussed together with the results in Chapter 7.

2.4 Langmuir class of electric probes

Electric probes have been adopted since the beginning of the 20^{th} century when Irving Langmuir carried his pioneering work in electric probes measurements for laboratory plasma diagnostics [2], [3]. Langmuir probes have been used in sounding rockets and in interplanetary spacecrafts to perform in situ measurements of the terrestral (and extraterrestral) ionosphere and as an indicator of spacecraft charging [4], [5], [6], [7], [8], [9]. The Langmuir probe technique is based on applying a voltage to a metallic conductor and on observing the collected total current I_{tot} which is a summation of various contrubutions,

$$I_{tot} = I_e + I_i + I_{se} + I_{si} + I_{ph}. \tag{2.6}$$

Figure 2.2 sketches the drivers for the currents contribution to the satellite and its subsystems. Surface currents are controlled by ultraviolet radiation and energetic particles and are functions of design parameters as the area of the sunlit surfaces and materials properties. I_e and I_i are the currents due to ionized particles impacting the probe surface. I_{se} and I_{si} are currents due to secondary emission when electrons and ions hit the spacecraft. I_{se} arises particularly in the auroral zones and is otherwise small with respect of currents due to incoming electrons. I_{ph} is the photoelectron current arising in response to ultraviolet radiation.

LP data are expressed in terms of $I_{collected} - V_{applied}$ curves, Figure 2.5. A satisfactory interpretation of all currents contributions, which includes sheath modelling, allows the accurate determination of the plasma density and temperature parameters: n_e, n_i, T_e, T_i. When mounted on a satellite, the LP is exposed to the

only disturbance of the ram velocity, outside of the spacecraft sheath. Figure 2.3 sketches the instrument components; measurements are achieved by biasing the stub at the same potential of the sensor in order to avoid perturbations of the sheath caused by complex geometries. Probes radii follow in size the length of the Debye parameter hence the properties of the plasma the instruments couple with.

2.5 Swarm langmuir probes

The Swarm Langmuir probes are a pair of spherical probes of 7.61 mm in diameter, mounted perpendicular at the edge of the ram side of the spacecraft, forming a part of the Electric Field Instrument (EFI) which also contains the Thermal Ion Imager (TII), Figure 2.4. The LP objective is to determine the spacecraft potential for the reduction of EFI data end to measure the plasma density and the electron temperature for conductivity estimations, Table 2.1 [10], [11], [12], [13].

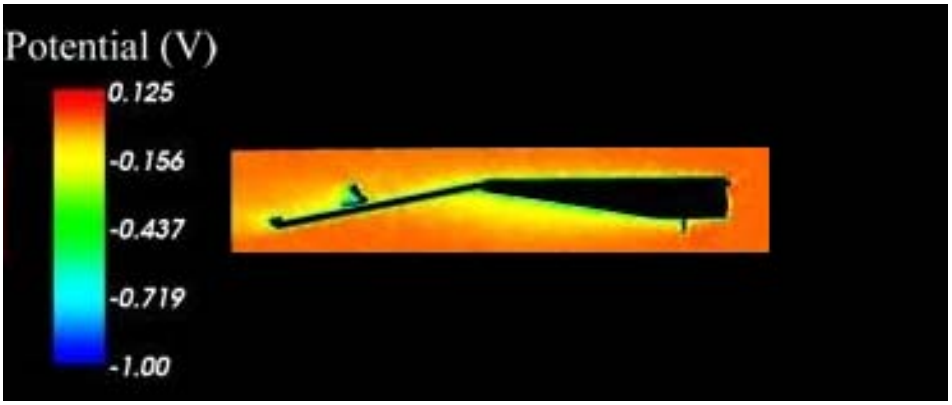

Figure 2.1: *Sheath structure around a Swarm satellite. Credits: ESA.*

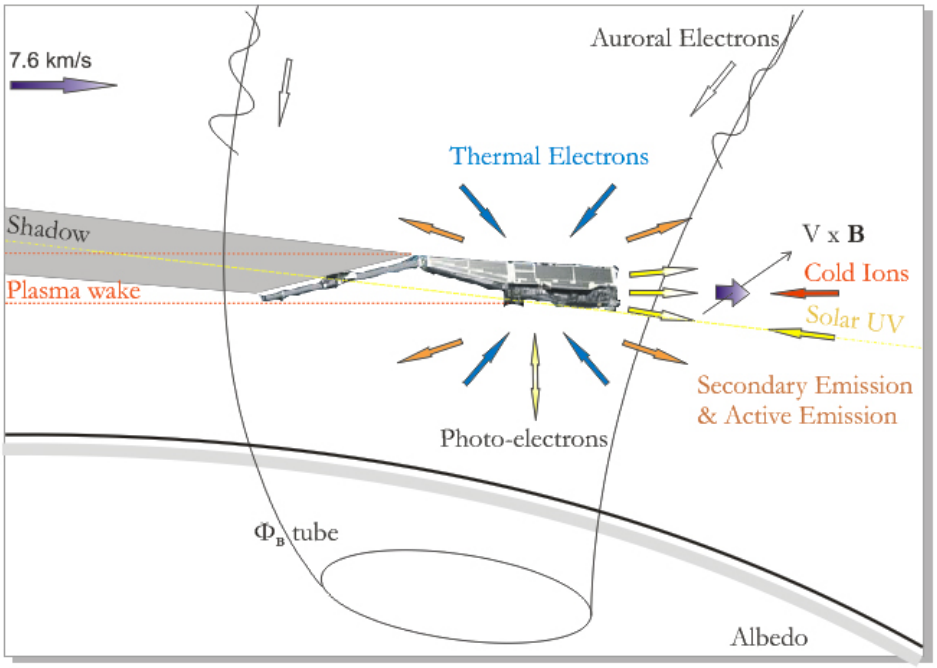

Figure 2.2: *Ambient orbit characteristics for a Swarm satellite.*

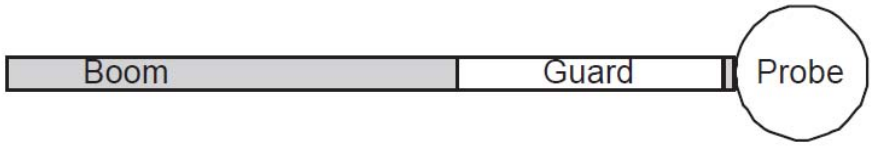

Figure 2.3: *Langmuir probe components scheme. The stub is also known as guard. Figure adapted from [6].*

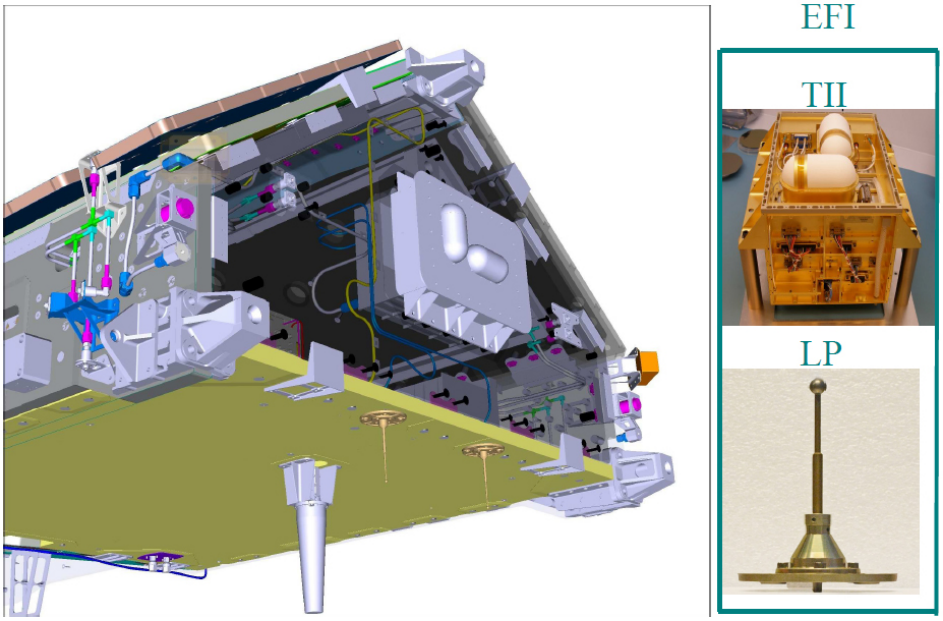

Figure 2.4: *Panoramic view of the Electric Field Instrument, EFI. Langmuir probes are mounted perpedicularly to the ram side. Credits: Astrium.*

Table 2.1: *EFI Measurements Objectives by subsystems.*

Objective	Instrument
Ion Temperature, T_i	(TII)
Electron Temperature, T_e	(LP)
Ion Density, n_i	$(TII) + (LP)$
Electron Density, n_e	(LP)
Spececraft Potential, $V_{s/c}$	(LP)
Ion Incident Angle, ϕ	(TII)

2.6 LP theory of operation

2.6.1 Current to the probe

It follows a description of the theory of operation for Langmuir probes for the interpretation of the collected current as the voltage is sweeped. The average magnitude of the velocity single direction component for a Maxwellian distribution of particle velocities [2] is given by

$$v_x = \left(\frac{2k_B T}{\pi m}\right), \tag{2.7}$$

where k_B is the Boltzmann constant and T and m are respectively the particle speces' temperature and mass. Recalling the thermal velocity, the random thermal current collected by a surface A at the same potential of the surrounding charged specie q_j in a Maxwellian plasma is

$$I_{th_j} = \frac{1}{2} n_j q_j A v_x = n_j q_j A \left(\frac{k_B T_j}{2\pi m_j}\right)^{1/2}, \tag{2.8}$$

where m_j is the mass, n_j is the density. The factor 1/2 enters Equation 2.8 because only half of the particles in the plasma have velocities directed towards the surface of the probe to be collected [14].

2.6.2 Current to the probe at various voltages: I-V curve

The I-V curve is characterized by three regions: ion saturation, electron retardation and electron saturation, Figure 2.5. As a convention, the current from the probe to the plasma is considered positive. The saturation regions are situated beyond Φ_p of for much less than Φ_f and are named after the dominant collected species. Beyond Φ_p no electric field propagates from the probe surface to the outer-sheath where the plasma is quasineutral. The currents in this regions are strongly influenced by the geometry of the probe, the sheath size and the velocity of the probe relative to the surrounding plasma. The ion dynamics is not a mirror of the electron dynamics because the potential structure acts as a "hill" for the electrons and as a "valley" for the ions, this behaviour is enhanced in the

[2] The Maxwellian distribution function is described in Chapter 3

exponential part (Φ_f<V<Φ_p) of the electron retardation region (V<Φ_p) where the electrons need more kinetic energy to overcome the maxima while the ions get accelerated towards the surface. V_p is not an equilibrium extreme for current collection since the electron thermal current prevails due to higher electron mobility. The equilibrium is reached at the floating potential where ion and electron thermal currents balance each other. The collected species current in the retardation region is given by

$$I_e(V) = I_{th_e} exp\left(\frac{e(V-\Phi_p)}{k_B T_e}\right), \tag{2.9}$$

where e is the fundamental electron charge and I_{th_e} is the electron thermal current.

2.7 Sheath modelling

Models that predict the motion of the charges in the sheath are accurate for symmetrical potential fields sustained by corresponding simple probe geometries (spherical and cylindrical). Furthermore, the theoretical expression for the current to the probe is given as exact within domains being asymptotic with respect of certain ratios of three parameters: λ_D, the probe radius r and the mean free path λ. This is clarified in Figure 2.6.

2.8 The Orbital-Motion-Limit theory

2.8.1 Generalities

Langmuir and Mott-Smith [3] have analyzed the current collection by cylindrical and spherical probes and named the limit of maximal current collection the Orbital-Motion-Limit. When the OML is valid, the ratio of the probe radius to Debye length is so small that the shielding becomes unimportant; at this limit, the number of electrons absorbed by the probe is determined by energy and angular momentum only. The Orbital-Motion-Limit theory has originally developed by assuming that the plasma is collisionless, isotropic, there is no external magnetic field and the surface properties of the probe are homogeneous.

Under OML conditions, the probe current is proportional to the plasma density and, at constant temperature, any density fluctuation can be measured by the

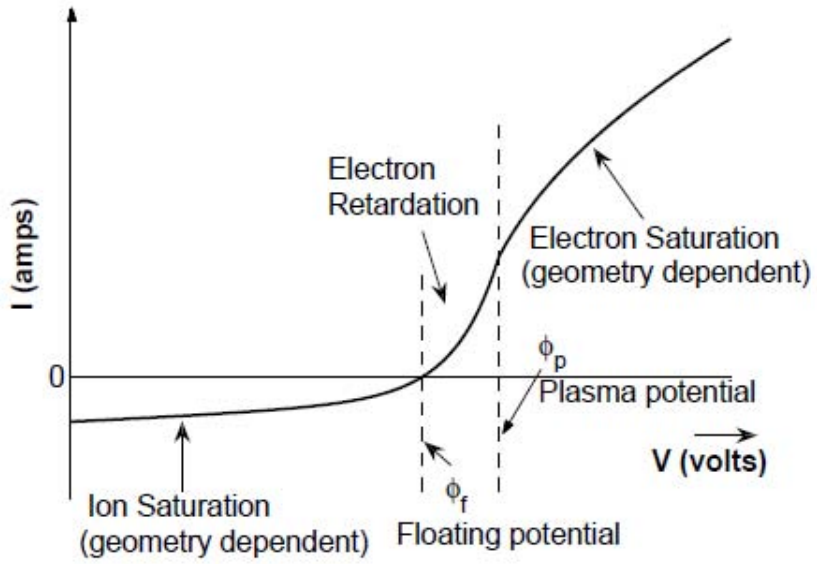

Figure 2.5: *I-V curve characteristics. The ion current has been amplified to ease the viewing. Figure adapted from [6].*

relative variation of the probe current. None of the undisturbed plasma particles placed at infinity and capable of reaching the probe on the basis of its energy and angular momentum is excluded from doing so; as to say that there is no intervening barriers of active potential to block its motion.

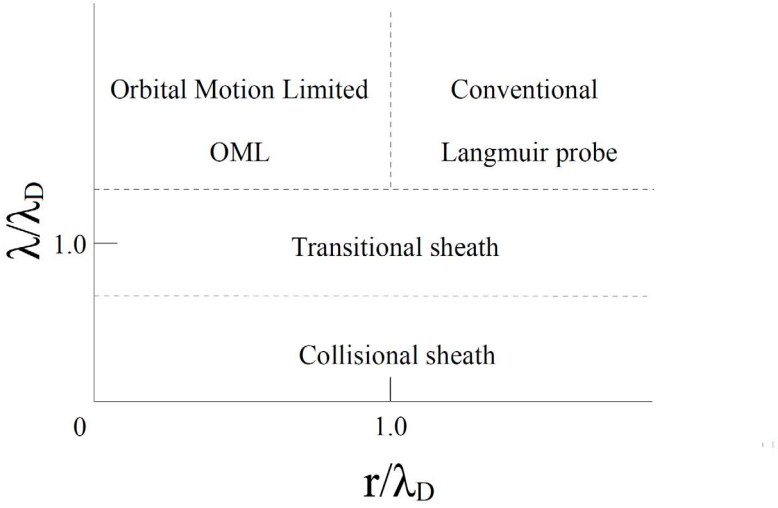

Figure 2.6: *Asymptotic probe-operation regimes, figure adapted from [5].*

2.8.2 Effective potential

The role of the sheath in particle collection is clarified by introducing the effective potential. It is possible to combine the conservation of energy E,

$$E = \frac{1}{2} m_e (v_r^2 + v_\theta^2) \tag{2.10}$$

and the conservation of angular momentum J,

$$J = m_e r v_\theta \tag{2.11}$$

and obtain the radial velocity v_r,

$$v_r^2 = \frac{2}{m_e}\left(E - q\phi - \frac{J^2}{2m_e r^2}\right) \tag{2.12}$$

which balances the energy E and the effective potential U,

$$U = q\phi + \frac{J^2}{2m_e r^2}. \tag{2.13}$$

r is the distance from the probe center, v_θ is the azimuthal velocity, ϕ is the local potential. The 2-dimensional motion can be treated as a 1-dimensional case by considering the normal part of the effective potential. A particle reaches the surface of the probe only if the right hand side of Equation 2.12 is positive along the path from infinity to the surface. There exist two cases: for thin sheath, the second term of Equation 2.12 becomes dominant near the probe and prevents certain attracted particles from reaching the probe; in such cases $v(r)$ has an intermediate minimum value. When the sheath is thick (OML limit), the first term of the equation becomes dominant across the whole region and the electric potential is large enough to overcome the bump in the effective potential [6].

2.8.3 OML current modelling

The general form for the collected current to a charged sphere follows the proportion [1],

$$I_{sphere} \sim 1 + \frac{V}{T}. \tag{2.14}$$

For $V < 0$ the species contribution is,

$$I_e = I_{e0} \exp\left(\frac{eV}{KT_e}\right) \tag{2.15}$$

$$I_i = I_{i0} \exp\left(1 - \frac{eV}{KT_i}\right), \tag{2.16}$$

while for $V > 0$ is

$$I_e = I_{e0}\left(1 + \frac{eV}{KT_e}\right) \tag{2.17}$$

$$I_i = -I_{i0}\left(-\frac{eV}{KT_i}\right). \tag{2.18}$$

Here the random currents are given by

$$I_{e0} = 4\pi r^2 ne \left(\frac{KT_e}{2\pi m_e}\right)^{1/2} \tag{2.19}$$

$$I_{i0} = 4\pi r^2 ne \left(\frac{KT_i}{2\pi m_i}\right)^{1/2}. \tag{2.20}$$

2.8.4 $(I-V)_{OML}$ as a background to evaluate sheath effects

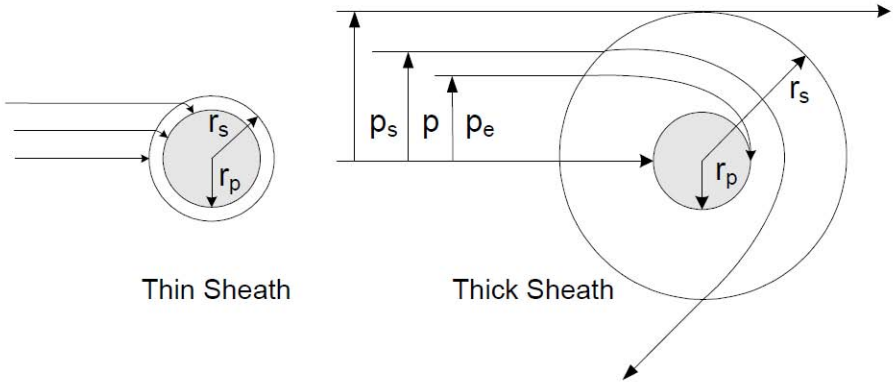

Figure 2.7: *Thin vs thick sheath domain; figure adapted from [6].*

OML theory accounts for a linear increase of the collecting area with probe potential and does not apply for high dense plasmas characterized by small Debye lengths for instance typical of the ionospheric plasma. The Debye length at Swarm altitudes ranges from about 1.7 mm to 10 mm and it is comparable to probe and stub radii. The Swarm probe sheaths, in terms of extension, are qualitatively in the between the two scenarios described in Figure 2.7. The reason for confronting the OML curves to simulated I-V curves is to quantify the effects on particle screening due to the bump in effective potential hence to sheath effects (Equation 2.13).

This problem is two dimensional in spherical geometry as it also depends on particles trajectories. The sketch on the left represents the thin sheath domain where about all the electrons crossing the sheath are collected. The current is determined by the thermal driven random transitions of particles coming from the quasineutral plasma. These currents are not anymore dependent from the sensor's geometry as all the probes behave like planar. For the Swarm LP the sheath is large enough to become a domain for curved orbital motions of particles more or less attracted towards the probe [3].

[3]Trapped particles are not considered in this thesis because this is the approximation done by

2.8.5 $(I-V)_{OML}$ for the Swarm scenario

Figure 2.8 is derived by Equations 2.15-2.18 for an electron-O^+ plasma and for the two densities and temparatures scenarios, translated into the two Debye lengths by Equation 2.5 that are considered and described further in Chapter 5: $\lambda_D \approx 1.7\,\text{mm}$, $\lambda_D \approx 10\,\text{mm}$.

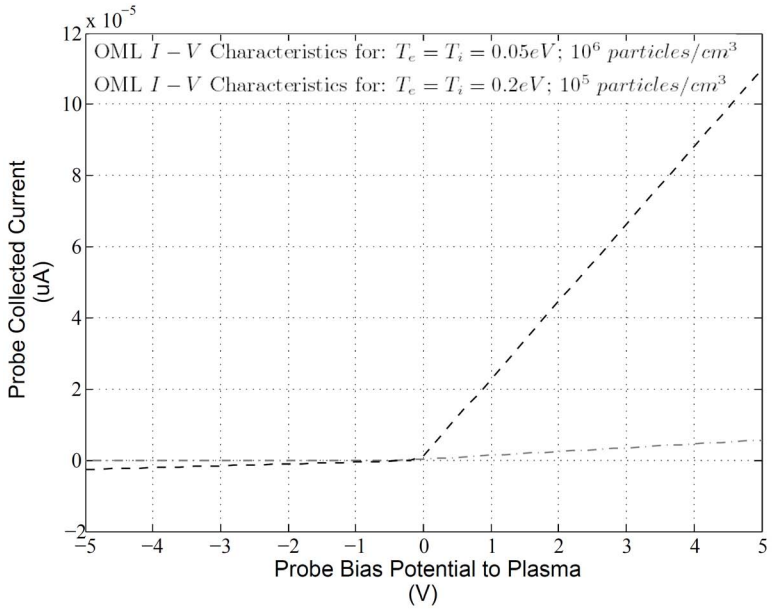

Figure 2.8: *OML I-V characteristics for $\lambda \approx 1.7\,mm$ and $\lambda \approx 10\,mm$.*

Laframboise in it's work in 1966

3

NUMERICAL METHODS

This chapter presents Laframboise's and the PIC solution schemes to LP modelling. The two approaches are introduced in the context of the kinetic theory. In the first part of the chapter, the collisionless kinetic equation, in its Vlasov form, is introduced to simplify the survey of the methods as it represents a common tool to approach the solution in the two cases whose conceptual difference consists in the treatment of the phase space. The PIC approach involves a phase space of discretized particle density while Laframboise's method treats the phase space as a continuum. In the second part of the chapter, Laframboise's results are parametrized and the procedure is described step by step in order to prepare the confrontation to PIC results. The relative digression of LF curves to PIC curves on the I-V plane is quantified in Chapter 7.

3.1 The general problem

Each particle in the plasma has an instantaneous state defined in terms of position and velocity which lies in a six-dimensional phase space described by six independent coordinates $x_1, x_2, x_3, v_1, v_2, v_3$ [1]. Tracking the trajectories of an ensamble of charged particles, moving within electric **E** and magnetic **B** fields and generating their individual contribution to such fields, is a multi-varible problem whose soluton requires the knowledge of the force exchange among the particles

[1] $\mathbf{r} = (x_1, x_2, x_3)$ is the position vector. $\mathbf{v} = (v_1, v_2, v_3)$ and $\mathbf{v} = \frac{d\mathbf{x}}{dt}$

and the fields. The Maxwell equations 3.1-3.4 give $\mathbf{E}(\mathbf{r},t)$ and $\mathbf{B}(\mathbf{r},t)$ from the knowledge of $\mathbf{r}$ and $\mathbf{v}$ and viceversa does the Lorentz force equation 3.5.

$$\nabla \times \mathbf{E} = -\frac{\partial \mathbf{B}}{\partial t} \tag{3.1}$$

$$\nabla \times \mathbf{B} = \mu_0 \mathbf{j} + \mu_0 \epsilon_0 \frac{\partial \mathbf{E}}{\partial t} \tag{3.2}$$

$$\nabla \cdot \mathbf{E} = \frac{1}{\epsilon_0} \sum q_\alpha n_\alpha \tag{3.3}$$

$$\nabla \cdot \mathbf{B} = 0 \tag{3.4}$$

$$\frac{d}{dt}(m\mathbf{v}) = q_\alpha(\mathbf{E} + \mathbf{v} \times \mathbf{B}). \tag{3.5}$$

Where the species α of electrons and ions have charge and mass q_α and m_α, n_α is the number density, $\mathbf{j}$ is the electric current density in the plasma, μ_0 is the permeability in vacuum and ϵ_0 is the dielectric constant in vacuum. Accounting for all the particles and the fields makes the treatment of full particle dynamics complex and its solution is analytical in only a few cases. The class of solvable problems concerns symmetrical potential distributions as the radial distribution surrounding a sphere. For non symmetrical geometries and for non symmetrical velocity fields (flowing plasma), it is necessary to take a PIC approach to map the potential distribution. For these situations, it is possible to integrate the Poisson equation 2.3 to construct the potential map and proceed further with iterations to edge closer to the exact solution.

3.2 Kinetic theory

3.2.1 Background

The kinetic theory is a description of statistical nature in terms of distribution functions $f_\alpha = f_\alpha(\mathbf{r}_\alpha, \mathbf{v}_\alpha, t)$. Distribution functions are probability densities in phase space whose evolution in time and space are described through the kinetic equation and the fields are governed by Maxwell's equations.

3.2.2 The Maxwellian distribution function

A convenient form for f_α is founded on the Maxwellian distribution function which maximizes the entropy of a set of gas particles and satisfies the three laws of thermodynamics [2]. A Maxwellian plasma is in thermal equilibrium because it does not have anymore free energy, hence there is no more energy exchange between the particles. This particle density distribution can be written as a function of the thermal velocity $v = (1k_BT/m)^{1/2}$, where m is the mass of the particle and k_B is the Boltzmann constant,

$$f_M(v) = \left(\frac{m_p}{2\pi k_B T}\right)^{3/2} \exp\left(-\frac{m(v-v_0)^2}{2k_B T}\right). \tag{3.6}$$

The number density can be written in terms of distribution function,

$$N_\alpha = \int f_M(r,v) d^3v. \tag{3.7}$$

3.2.3 The kinetic equations

The kinetic equations governs the number density of charged species hence the particle distribution. The general form is

$$\frac{\partial f_M}{\partial t} + \mathbf{v}\cdot\nabla_x f_M + \frac{q}{m}(\mathbf{E}+\mathbf{v}\times\mathbf{B})\cdot\nabla_v f_M = -\frac{q}{m}(\delta\mathbf{E}+\mathbf{v}\times\delta\mathbf{B})\cdot\nabla_v \delta F_M \tag{3.8}$$

where δF considers the fluctuations of the averaged phase space density F [15].

Uncorrelated fields and collisionless plasma

The Boltzman equation

$$\frac{\partial f_M}{\partial t} + \mathbf{v}\cdot\nabla_x f_M + \frac{q}{m}(\mathbf{E}+\mathbf{v}\times\mathbf{B})\cdot\nabla_v f_M = \left(\frac{\partial f_M}{\partial t}\right)_c \tag{3.9}$$

simplifies Equation 3.8 as it neglects the correlations between the fields and only considers the correlation among particles via collisions. Because collisions are

[2] A plasma differs from a gas but deviations from the Maxwellian ideal state of equilibrium are often small enough that this approximation results to be locally valid.

often negligible compared to the electrostatic forces, the Boltzmann equation can be furtherly simplified into the Vlasov equation [15],

$$\frac{\partial f_M}{\partial t} + \mathbf{v} \cdot \nabla_x f_M + \frac{q}{m}(\mathbf{E} + \mathbf{v} \times \mathbf{B}) \cdot \nabla_v f_M = 0. \tag{3.10}$$

3.3 Vlasov-Poisson system

The Vlasov equation can be combined with the Poisson equation (written in terms of number density 3.7 and charge density $\rho = eN$) to derive the electric field via the electric potential $\mathbf{E} = -\nabla\Phi$ and the charge number density from the distribution function according to the scheme in Figure 3.1. The Vlason-Poisson system for the distribution function f_M is

$$\frac{\partial f_M}{\partial t} + \mathbf{v} \cdot \nabla_x f_M + \frac{q}{m}(\mathbf{E} + \mathbf{v} \times \mathbf{B}) \cdot \nabla_v f_M = 0 \tag{3.11}$$

$$\epsilon_0 \nabla^2 \Phi = \sum q \int f_M d^3 v. \tag{3.12}$$

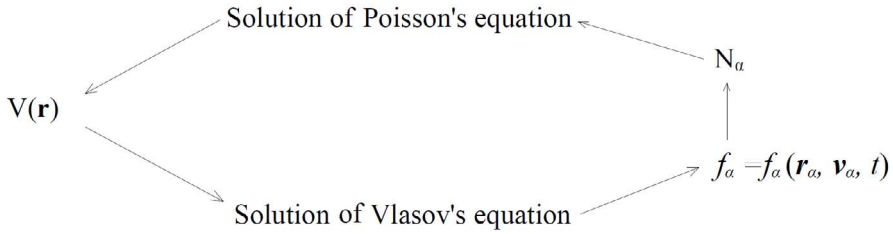

Figure 3.1: *Vlasov solvers scheme*

This scalar system 3.11-3.12 of non-linear partial differential equations is the non relativistic, electrostatic (no inductive electric field) and collisionless limit of the general kinetic problem represented by the Maxwell-Loretz system; it is the simplest kinetic model of a plasma. The solution of the system gives, for the considered volume, the structure of the charge density $\rho = n_i q_i + n_e q_e = \sum q_\alpha n_\alpha$ hence the potential map and current density $j = n_i q_i v_i + n_e q_e v_i = \sum q_\alpha n_\alpha v_\alpha$ at a certain

time t at which the system is in equilibrium.

3.4 Laframboise's numerical study (1966)

3.4.1 Introduction

The system 3.11 and 3.12 can be re-written by assuming an unmagnetized plasma. The force becomes proportional only to the electric filed and the Lorentz equation is simplified to the Newton's second law $\frac{d}{dt}(m\mathbf{v}) = \mathbf{F} = q\mathbf{E}$. This non-linear system of integral equations has been implemented numerically by LF [3] at the University of Toronto in 1966 to solve the problem of current collection on Langmuir probes. Numerical solutions are available in his report [1] in form of collected species current i_{LF} to spherical and cylindrical probes and are presented in the form

$$f\left(\frac{eV}{KT_e}, \frac{r_p}{\lambda_D}\right) = i_{LF} \tag{3.13}$$

as functions of non-dimensional parameters explicited as normalized potential $\pm e\Phi_P/kT_e$ and R_p/λ_D. The iterative procedure for the numerical solution of the equations starts by assuming an initial trial function for the net charge density. Poisson's equation is then integrated to reconstruct the electric potential map and its two first derivatives given as a function of radius. Using this information the electron and the ion current are calculated. The resulting charge density function is mixed with the previous net charge density to gain a closer approximation of the solution.

3.4.2 Parametrization of Laframboise's results

Data are parametrized to sufficient accuracy by following a method in two steps that reconstructs and extends to a continous domain the currents of Table 3.1; only columns containing at least six values are used to better conditioning the fit (grey coloumns). The Matlab codes written to parametrize LF results are listed in Appendix 2.

[3] on an IBM 7094 digital computer.

Step 1

Firstly, the collected species current of Table 3.1 are interpolated by 3rd order polynomial functions of potential as

$$f\left(\frac{eV}{KT_e},\frac{r_p}{\lambda_D}\right) = \\ = a_0\left(\frac{r_p}{\lambda_D}\right)+a_1\left(\frac{r_p}{\lambda_D}\right)\left(\frac{eV}{kT_e}\right)+a_2\left(\frac{r_p}{\lambda_D}\right)\left(\frac{eV}{kT_e}\right)^2+a_3\left(\frac{r_p}{\lambda_D}\right)\left(\frac{eV}{kT_e}\right)^3. \quad (3.14)$$

Current values and their fits are shown in Figure 3.2. The interpolation is conditioned by weighting 10 times the ratio $r_p/\lambda_D = 0$ in order ensure consistency with the OML limit where Laframboise's numerical results are exact and are fitted by a straight line [4]. The opposite case is $r_p/\lambda_D = 100$ is the worst fit which average standard deviation is 0.19.

Step 2

Secondly, the polynomial coefficients from step 1 are fitted to 4th order polynomial functions of R_p/λ_D as

$$\ln a_0\left(\frac{r_p}{\lambda_D}\right) = b_{00}+b_{01}\left(\frac{r_p}{\lambda_D}\right)+b_{02}\left(\frac{r_p}{\lambda_D}\right)^2+b_{03}\left(\frac{r_p}{\lambda_D}\right)^3+b_{04}\left(\frac{r_p}{\lambda_D}\right)^4 \quad (3.15)$$

where the standard deviation is 0.017 in the worst case. Fits are shown in Figure 3.3 and coefficients are listed in Table 3.3.

3.4.3 $(I-V)_{parametrized}$ for the Swarm scenario

We now have a tool for generating collected currents that reconstructs and extends the Laframboise's results of Table 3.1 to Table 3.2 and further to any value of R_p/λ_D. This method enables the access to the specific sub-set of current values to confront to SPIS simulated currents in the spherical case. Figure 3.4 presents

[4] Over-weighting the null ratio also ensures consistency in the low density limit for which OML theory is well representative.

I-V curves generated to model Swarm's LP collected current from an electron-O^+ plasma with the two densities and temperatures scenarios described further, in Chapter 5. In the figure's legend these parameters are given as the two corresponding Debye lengths: $\lambda_D \approx 1.7\,\text{mm}$, $\lambda_D \approx 10\,\text{mm}$.

Table 3.1: *Spherical Probe: Computed Values of Attracted-Maxwellian-Species Current (Laframboise's currents i_{LF}) for $T_i/T_e = 1$; from Laframboise's Report 100.*

$\pm\frac{e\Phi_p}{kT_e}$	R_p/λ_D 0	0.2	0.3	0.5	1	2	3	5	7.5	10	15	20	50	100
0	1.0	1.000	1.000	1.000	1.000	1.000	1.000	1.000	1.000	1.000	1.000	1.000	1.000	1.000
0.1	1.1				1.0999			1.099		1.098		1.097	1.095	1.094
0.3	1.3				1.299		1.293	1.288		1.280		1.269	1.255	1.246
0.6	1.6				1.595	1.584	1.572	1.552		1.518		1.481	1.433	1.402
1.0	2.0				1.987	1.955	1.922	1.869		1.783		1.694	1.592	1.534
1.5	2.5			2.493	2.469	2.399	2.329	2.219		2.050		1.887	1.719	1.632
2.0	3.0			2.987	2.945	2.824	2.709	2.529		2.266		2.030	1.803	1.694
3.0	4.0			3.970	3.878	3.632	3.406	3.068		2.609		2.235	1.910	1.762
5.0	6.0			5.917	5.687	5.126	4.640	3.957		3.119		2.516	2.037	1.833
7.5	8.5			8.324	7.871	6.847	6.007	4.887	4.094	3.620		2.779	2.148	1.891
10.0	11.0			10.704	9.990	8.460	7.258	5.710	4.658	4.050		3.002	2.241	1.938
15.0	16.0			15.403	14.085	11.482	9.542	7.167	5.645	4.796		3.383	2.397	2.022
20.0	21.0			20.031	18.041	14.314	11.636	8.473	6.518	5.453	4.318	3.716	2.532	2.097
25.0	26.0	25.763	25.462	24.607	21.895	17.018	13.603	9.676	7.318	6.053	4.719	4.018	2.658	2.166

Table 3.2: *Polynomial interpolation of Laframboise's attracted-Maxwellian-species current.*

$\pm\frac{e\Phi_p}{kT_e}$	R_p/λ_D										
	0	0.5	1	2	3	5	7.5	10	20	50	100
0	1.0	1.0000	1.0000	1.0000	1.0000	1.0000	1.0000	1.0000	1.0000	1.0000	1.0000
0.1	1.1	1.1001	1.1003	1.1005	1.1003	1.0997	1.0896	1.0973	1.0925	1.0848	1.0798
0.3	1.3	1.3001	1.2998	1.2979	1.2947	1.2890	1.2573	1.2762	1.2575	1.2317	1.2156
0.6	1.6	1.5994	1.5964	1.5855	1.5725	1.5507	1.4846	1.5110	1.4636	1.4057	1.3720
1.0	2.0	1.9974	1.9871	1.9549	1.9206	1.8650	1.7515	1.7741	1.6794	1.5750	1.5182
1.5	2.5	2.4931	2.4686	2.3977	2.3266	2.2146	2.0415	2.0443	1.8837	1.7210	1.6373
2.0	3.0	2.9870	2.9435	2.8228	2.7065	2.5273	2.2955	2.2682	2.0396	1.8212	1.7136
3.0	4.0	3.9697	3.8761	3.6314	3.4070	3.0739	2.7285	2.6257	2.2645	1.9459	1.7982
5.0	6.0	5.9172	5.6864	5.1280	4.6474	3.9721	3.4141	3.1453	2.5476	2.0675	1.8609
7.5	8.5	8.3236	7.8718	6.8495	6.0138	4.8964	4.0913	3.6292	2.7844	2.1487	1.8897
10.0	11.0	10.7043	9.9924	8.4617	7.2567	5.7032	4.6631	4.0341	2.9782	2.2147	1.9142
15.0	16.0	15.4028	14.0897	11.4763	9.5254	7.1377	5.6444	4.7517	3.3347	2.3540	1.9839
20.0	21.0	20.0326	18.0432	14.3095	11.6238	8.4527	6.5125	5.4291	3.6940	2.5166	2.0827
25.0	26.0	24.6057	21.8873	17.0240	13.6229	9.7121	7.3217	6.1038	4.0715	2.7025	2.2053

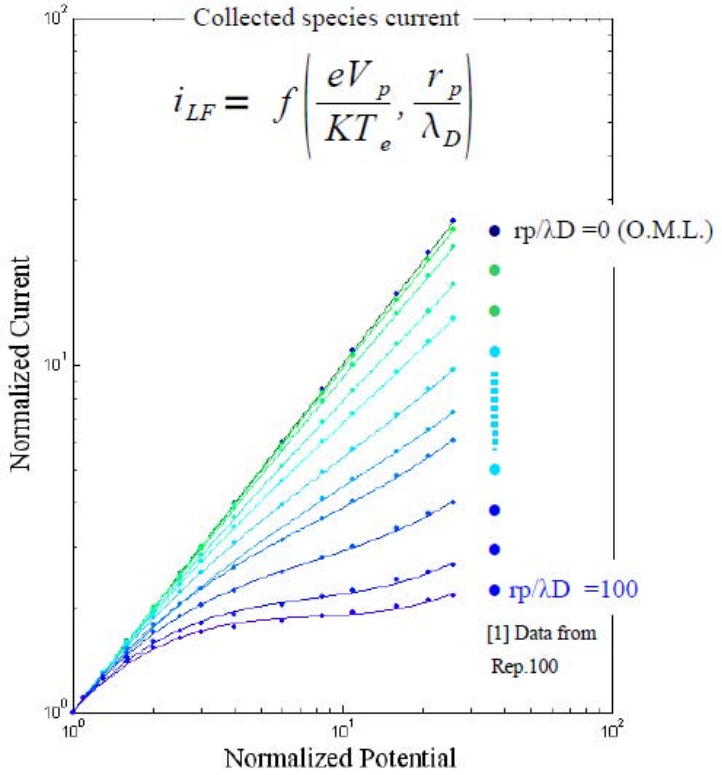

Figure 3.2: *Interpolation 1: Fit of Laframboise's numerical results from Table 3.1, std($r_p\lambda_D = 100$) = 0.19.*

Table 3.3: *Polynomial coefficients for attracted species current dependance on R_p/λ_D.*

	b_{0i}	b_{1i}	b_{2i}	b_{3i}	b_{4i}
a_0	2.9281446e-003	-3.5491135e-002	1.4509704e-001	-2.0890298e-001	9.7056427e-002
a_1	-1.4873920e-002	1.7707782e-001	-7.0123925e-001	9.2521630e-001	-3.8233420e-001
a_2	3.3132622e-003	-3.1747471e-002	7.9715839e-002	-5.0559405e-002	9.9636151e-001
a_3	-4.1035259e-008	2.6074208e-007	1.4802695e-007	-1.6380843e-006	1.3406175e-006

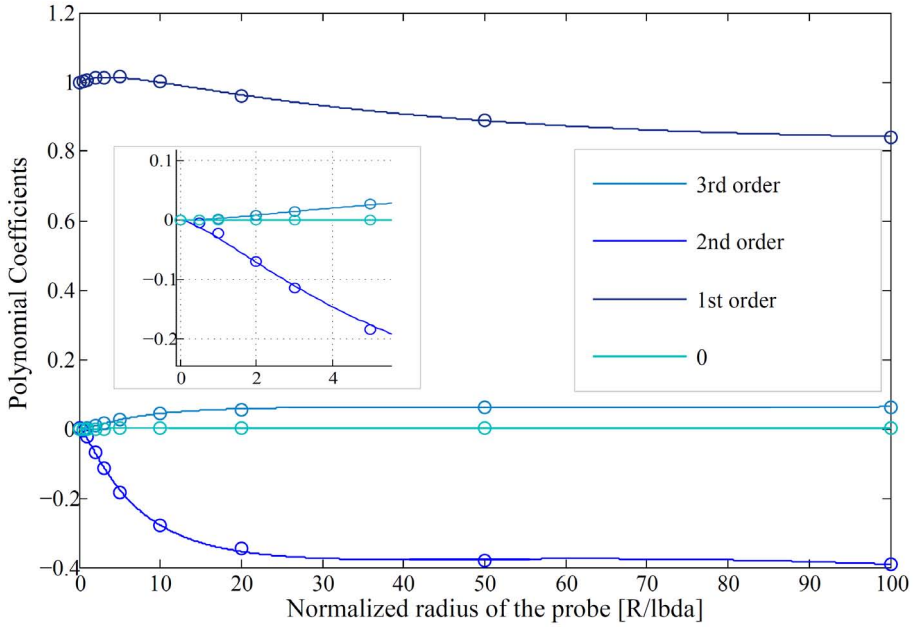

Figure 3.3: *Interpolation 2: Polynomial fits to R_p/λ_D for each polynomial coefficient from the eV_P/kT_e fit, std=0.017.*

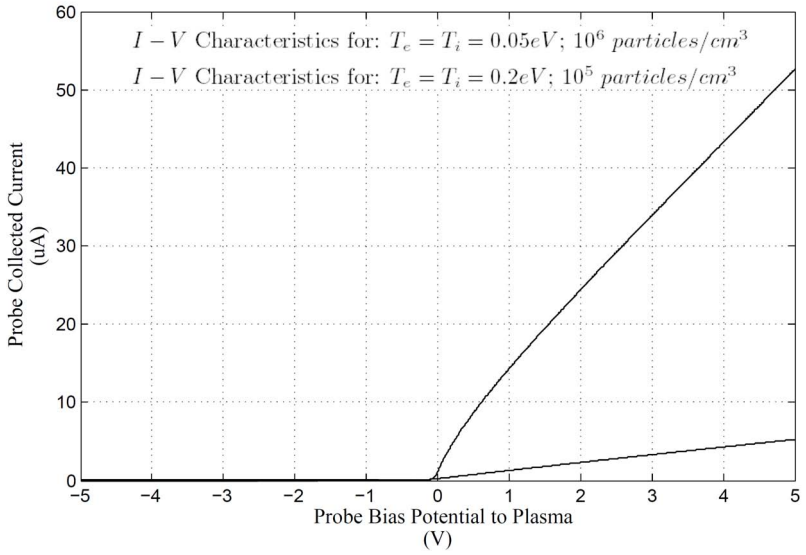

(a) Voltage bias range for the Swarm LP: V [-5, +5] .

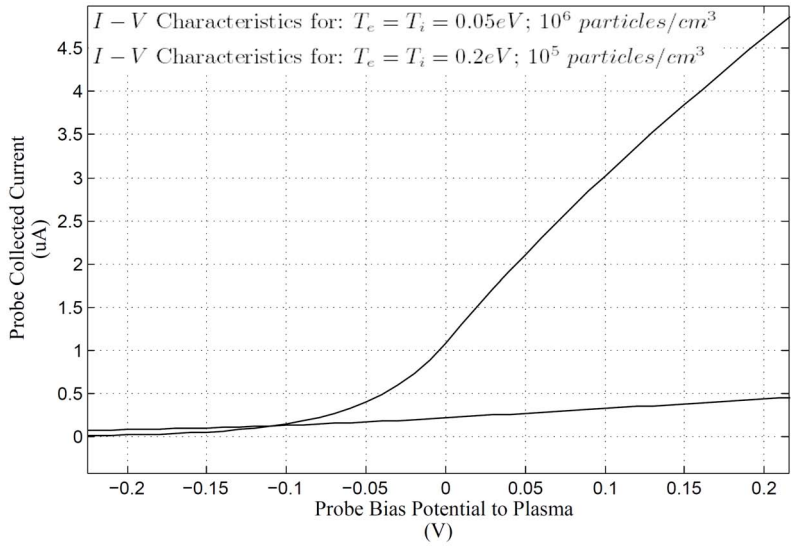

(b) Close-in on the electron retardation region: V[-0.2, +0.2].

Figure 3.4: *case 1:* $\lambda_D \approx 1.7\,mm \Leftrightarrow \rho_e{=}\rho_i{=}1\cdot 10^{12}\ m^{-3}$, $T_e = T_i = 0.05$*; case 2:* $\lambda_D \approx 10\,mm \Leftrightarrow \rho_e{=}\rho_i{=}1\cdot 10^{12}\ m^{-3}$, $T_e = T_i = 0.2\,eV$.

3.5 Particle-In-Cell (PIC) method

3.5.1 Overview

In PIC simulations, particles are distributed in a phase space where their motion is described in terms of position and velocity. The plasma dynamics is modeled from the coupling of matter and fields according to the scheme of Figure 3.5. For a given density n, the space charge is obtained from the Poisson equation and the electric field $\mathbf{E}$ with its boundary conditions, it is computed on a grid and interpolated for each particle position. The acceleration imposed by the forces acting on the particle (hence the trajectories) is then obtained from the Newton's second law. Finally a new space charge density is assigned to the volume element.

The number of particle considered in the actual computation is much less than in reality due to limitations in computational power [5]. The particles density is subsampled to macroparticles and their number is chosen by trading off computational power and kinetic resolution. The criteria for the choice of the number of macroparticles per cell in each model used in the thesis are presented in Chapter 5.

3.5.2 Outlook on a PIC simulation of collected species current

If the current is the objective of the simulation, the I-V curve introduced in Figure 2.5 is constructed by the interpolation of averaged stabilized current values obtained from different simulations, each one taken with a fixed bias. To better resolve the characteristic shape of the function, more runs are applied to the exponential part of the curve. The result is a set of simulations represented by a series of I-V-t maps an example of which is given in Figure 3.6. In the figure, it can be seen that the extracted values used to construct the I-V curve (traced in black in Figure 3.6) are averaged at equilibrium.

3.5.3 Spacecraft Plasma Interaction System, SPIS

The SPIS code runs modules for fields and matter and combines the PIC method to the leap-frog method and, when possible, solution is reached by exact integration

[5] Two different machines have been used: 1) RAM: 3.3 Gb, CPU: AMD Athlon (tn) 64bit Dual Core Processor, OS: Ubuntu 9. 2) RAM: 8Gb CPU: Dual Core AMD Opteron 875, 2.2 GHz, cache1MB, OS: Gentoo-r8.

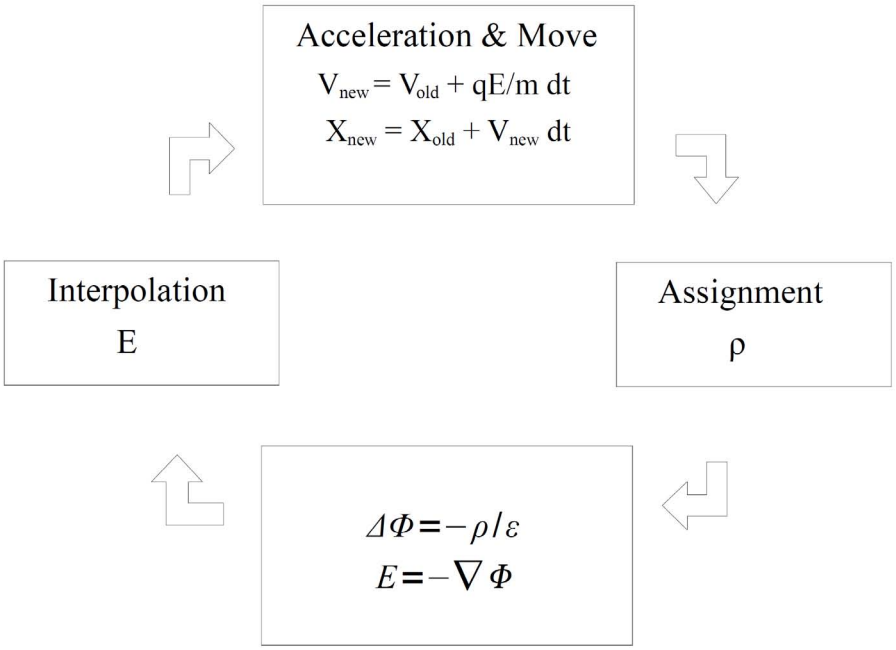

Figure 3.5: *A typical PIC cycle for unmagnetized plasma.*

in the elementary volume elements. Both full PIC and hybrid PIC with Boltzmann electrons (where the electrons density is modelled by the Boltzmann distribution) are implemented in the code [16]. [6].

3.5.4 Boundary properties

Boundary conditions can be time derivative dependent to describe the evolution of the collected current and potential distributions. At infinity, the electrostatic

[6] SPIS is a freely available and open source software designed to simulate the kinetic processes of ions and electrons by accounting their space charge and their interaction with spacecraft surfaces. Detailed documentation about the code and its modules and the program itself are availabe online http://www.spis.org/spis.

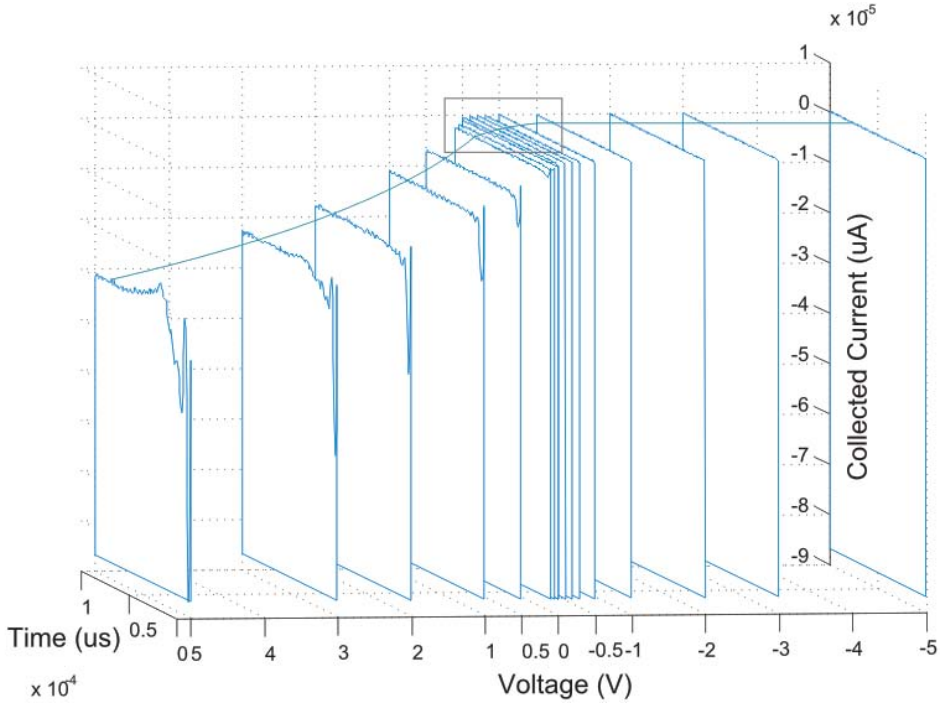

Figure 3.6: *Simulations set represented by I-V-t maps and I-V curve traced at averaged collected current values. The electron retardation and neightbour regions are more finely sampled.*

potential converges to 0,

$$\lim_{\|x\|\to\inf} \Phi(t,x) = 0. \tag{3.16}$$

Close to the probe the situation is more complex, external (and internal surfaces) and conductive elements connected to the surfaces, with possibly varying degree of conductivity, are a vehicle for currents propagation. Figure 3.7 illustrates the simplest material configuration in which a surface element is modeled as a bidimensional sandwich of composite material made of a conductive element on one side and a dielectric material on the other side. We model this surface element by assuming perfectly conductive elements at given potentials hence the

resistance at the interface between the dielectric and the surface is zero [7] [8].

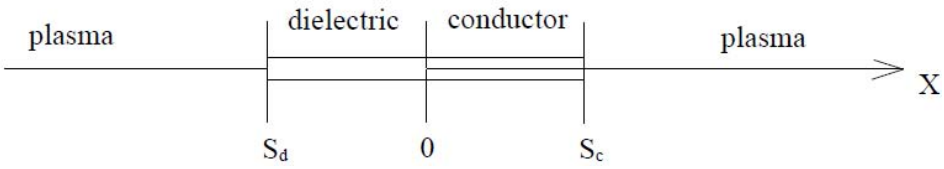

Figure 3.7: *Typical surface elements modellig.*

[7] SPIS assumes multilayered surfaces, the voltage is imposed on the element connected to the surface, this element is called electric node. Different material properties can be imposed to surface elements and the resistance can be tuned.

[8] Surface cathalisis allows charges recombination; neutralized species return the plasma leaving a negligible concentration of ionized species on the surface. This is what happents at the surface of the LP of Swarm which is made of titanium with a coating of titanium nitride. The assumption is consistent with the Laframboise's hypothesis of annihilation of ions and electrons at probe's surface.

4

THE IONOSPHERE AT SWARM ORBITS

The Swarm mission will use three satellites known as swarm A, B and C. During the five years of the mission the orbit of Swarm C will decay from 530 km to about 500 km and the lower pair Swarm A and B will decay from 450 km to 380 km. This chapter describes the structure of the ionosphere and its chemistry at these altitudes in order to set a background to model particles and density variations for the LP ambient orbits. These span and are contained within the F_2 layer.

4.1 The Ionosphere

4.1.1 Generalities

The ionosphere received its name by Sir Robert Watson-Watt in 1926, although Carl Friedrich Gauss had already speculated about its existence in 1839. The ionosphere is the permanently ionized upper part of the neutral atmosphere resulting from a balance of diverse phenomena that are in photochemical equilibrium to each other from an altitude of about 80 km. This balance is sustained by the ionization caused by solar UV radiation and by the neutralizing processes of recombination. The properties of the ionosphere result from the coupling of Sun and Earth of of which the ionosphere is a dynamic subsystem. The plasma in the ionosphere is subjected to the influence of external forces that transport mass hence charges (horizontal and vertical plasma transport) and energy. These forces are generated by the electric currents that arise from electron and ions distributions in the non neutral layers of the atmosphere. The ionosphere is a concern to

Figure 4.1: *Space Shuttle Endeavour taken by an astronaut on the ISS as it closes in to dock. Docking occurred at 11:06 p.m. (CST) on Feb. 9, 2010. The orbital outpost was at 46.9 south latitude and 80.5 west longitude, over the South Pacific Ocean off the coast of southern Chile with an altitude of 183 nautical miles when the image was recorded. The colour variation is due to the chemical structure of the atmosphere which is stratified. The orange layer is the troposphere, where all of the weather and clouds are generated and contained. This orange layer gives way to the whitish stratosphere and then into the mesosphere where most of the scattered light is blue due to nitrogen and oxygen molecules. Credits: NASA.*

space vehicle designers because it represents a chemically and electrically active medium which can potentially influence communications, guidance and tracking as it can carry electric currents and reflect, deflect and scatter radio waves.

4.1.2 Altitude dependent ionospheric patterns

The chemical composition of the ionosphere varies in space and time. The ionizing effect of the Sun, mostly due to UV radiation produces particles whose distribution is controlled by the structure of the Earth's magnetic field stretched by the pressure of the solar wind. The magnetic field develops from the Earth and crosses the ionosphere layers with a strength of a few tens of μT.

The number densities of electrons and ions are equal but undergo a strong daily variation, especially at sunrise and sunset and follows annual fluctuations. The vertical composition and the chemistry are described in Figures 4.2 and 4.3.

Figure 4.3 a divides the ionosphere into three main zones E, D and F that differ in primary ions constituents and absorbed UV wavelengths. The D-layer is the innermost layer which extends from about 60 km to about 90 km above the surface of the Earth, it is predominant in hydrated ions and does not exist at night due to the absence of solar ionization. The E-layer is the middle layer, mainly centered in the portion between 90 km and 120 km of altitude, it is abundant in NO^+ and O_2^+. Ionization is due to soft X-ray (1-10 nm) and far ultraviolet (UV) solar radiation ionization of molecular oxygen (O_2). The F layer or region, also known as the Appleton layer extends from about 200 km to more than 500 km above the surface of Earth. It is the denser part of the ionosphere and it constitutes a gateway for penetrating signals as it allows their escape into space, it is predominant in O^+. Beyond this layer there is the topside ionosphere. Standard ionospheric data are generated by the International Reference Ionosphere (IRI) model which is calculated over Logan, Utah (Lat. 41 44' 7'. Lon. -111 50' 3").

4.1.3 O^+ dominance and chemistry variability in the F layer

The F region is divided in two portions F_1 and F_2 respectively dominated by photochemical equilibrium and diffusive equilibrium. In both portions, the predominating ion in terms of number density is O^+ which presence is driven by the corresponding level of neutral oxygen ionized by UV radiation of high intensity (10-100 nm). Neutral oxygen density and chemical lifetime increases with altitude. In the F1-region, O^+ ions are produced at higher altitudes and cannot recombine dissociatively. The main chemical loss mechanism for O^+ is a relatively slow ions-neutrals reaction. The O^+ density is equal to the electron density for altitudes greater than about 160 km and n_{O+} (and n_e) reaches a maximum around 10^6cm^{-3} at about 250 km, Figure 4.2. Vertical transport of plasma is more impor-

tant than photochemistry from about 250 km where the F_2-region starts because life time of the ion specie exceed diffusive processes. Ions produced in this region diffuse down to the F1-region. The currents are also horizontal and their major effects are located in the polar regions where the magnetospheric electric fields extend their domain due to the dipolar structure of the magnetic field lines. Vertical and horizontal transport are complicated by a background of other species that are both locals and products of chemical reactions [18]. The geomagnetic system and the ionospheric chemistry are linked to the variability of the solar activity and the intensity of the solar wind.

4.2 In situ data from LEO missions

IRI modelling provides ionospheric parameters to model the effects of the solar activity and the geomagnetic activity on the ionosphere; unfortunately the day-to-day variability only mirrors the model provided average within 30 % and it diverges further for geomagnetically disturbed conditions [19]. Consequentely, in situ sampling becomes necessary for providing high resolution spatial and temporal observations of local plasma parameters. This is critical in the high density plasma F_2-region of the ionosphere which covers the Swarm, Hubble telescope, International Space Station and Shuttle altitudes and, in general, most of the Earth observing systems orbits. During the scheduled five years of the Swarm mission it is reasonable to assume that variations of plasma conditions resumed in Figure 4.3 will be covered at least by sudden events. The following chapter describes the method through which this variability is modelled in SPIS simulations. By following the arguments of Section 4.1.3 the representative ion considered is O^+.

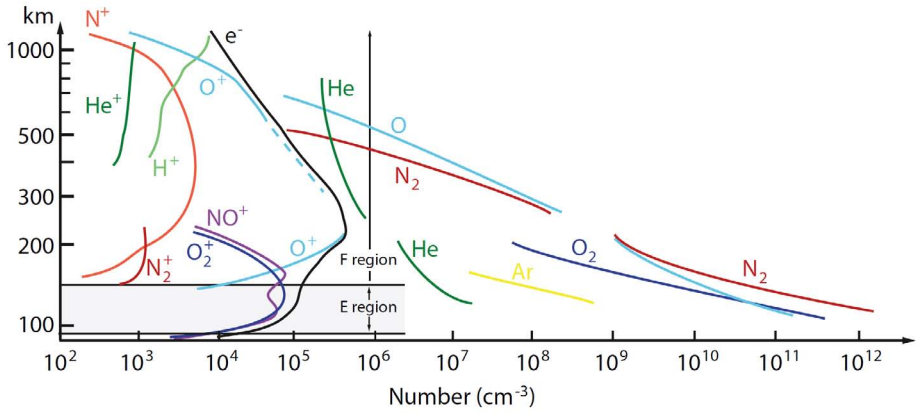

Figure 4.2: *Ionospheric species variation with altitude. Spacecrafts spanned altitudes are predicted to be: from* 530 *km to about* 500 *km for Swarm C and from* 450 *km to about* 380 *km for Swarm A and B. (Picture adapted from [17]).*

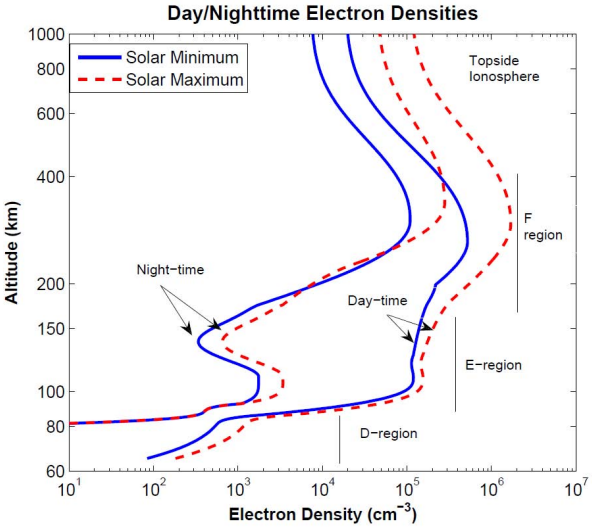

(a) Average mid-latitude daytime and night time electron denisty profiles featuring the D-, E-, F-layers of the ionosphere.

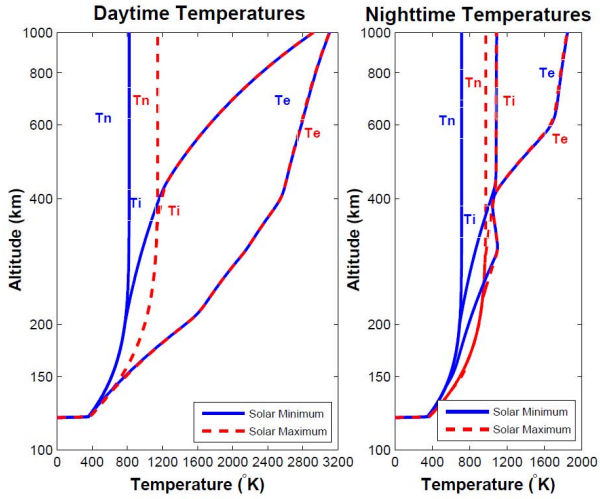

(b) Typical mid-latitude neutrals, ions and electrons temperature profiles.

Figure 4.3: *International-Reference-Ionosphere, IRI models [6].*

5

PLASMA MODEL & PROBE MODEL

This Chapter introduces the plasma parameters used to represent the the ionospheric environment described by IRI data in Chapter 4. Probe CAD models are further introduced and related to the plasma density which controls the mesh resolution.

5.1 Ambient model

5.1.1 Resume of parameters

From Figure 4.3 we see that electron density at Swarm altitudes (380-530 km) can be expected to mostly stay within the $3 \cdot 10^4 - 1 \cdot 10^6$ cm^{-3} range. Similarly, electron temperatures variations can be expected to stay in the 600-2000 K range. We obviously cannot run a SPIS simulation for every possible n_e and T_e, so we select two cases, given in Table 5.1. The best less sampled set of densities accounts one extreme value the satellite will probably encounter and another value which is either the other extreme either a conveniently chosen alternative.

5.1.2 Motivation for the used parameters

Extreme values with respect of different extreme conditions

In the Swarm scenario, the extreme is $1 \cdot 10^{12}$ particles m^{-3} per specie which is a peak condition for the ionospheric density at solar maxima, Figure 4.3. The

Table 5.1: *Plasma parameters.*

Plasma properties					
	Compounds	Density values m^{-3}		Temperature values eV	
Real particles	electrons	$1 \cdot 10^{11}$, $1 \cdot 10^{12}$	n_e	0.2, 0.05	T_e
	O^+ ions	$1 \cdot 10^{11}$, $1 \cdot 10^{12}$	n_{Q^+}	0.2, 0.05	T_i
Virtual particles	macroparticles	5 per cell			

associated temperature for both electrons and ions is 0.05 eV, the average night time temperature at solar minima, the lowest possible temperature characterizing the F2-layer. These choices produce the strongest possible deviation from the OML regime.

Average conditions just above the OML limit

The other parameters are chosen to represent a relatively dense scenario mirroring the ordinary conditions encountered by a satellite orbiting at Swarm altitudes. Within this range, adjustments have been done to reproduce a current closed to but still differentiable from the OML current. Such parameters have been identified through an initial set of simulations. $1 \cdot 10^{11}$ particles species per m^3 is the density while the associated temperature for both electrons and ions is 0.2 eV.

5.1.3 Synthetic density of species, macroparticles

The density of the ambient plasma is translated into an average number of 5 macroparticles per cell within the SPIS environment. The number of macroparticles [1] reduces the amount of objects to be physically traced in space. In order to avoid too long simulation time at high density, the solution scheme in Figure 3.5 is conveniently applied to a smaller problem and the integration of trajectories acts on such subsets. The macro particle number is chosen by trading off accuracy and computational time because the more macroparticles are used the longer the simulation lasts. Simulations should not include too many macroparticles because of computational power limitations and not too few because of the numerical noise. The drawback of low synthetic densities is in fact that the numerical noise which

[1] A macroparticle represents a distributed charge density.

only decreases as $1/\sqrt{N}$, where N is the number of macroparticles in any single cell **??**. Both the statistic character of the Maxwellian distribution function and sampling in time compensates for the low kinetic resolution adopted in the simulations. Averaging in time reconstructs the potential map due to the particles interactions as these move across the simulation volume during the overall simulation time. The confrontation to Laframboise's results verifies that the numerical noise is kept sufficiently low.

5.1.4 Ram velocity vs electron velocity

The different thermal kinetic energy of electrons and ions results in different thermal velocities. In a plasma at rest the two velocities scales according to Equation 2.1 as about 43. In a plasma made of oxygen ions the ratio is about 4 times bigger $v_{th_e}/v_{th_i} = (m_i/m_e)^{1/2} \sim 171$ as $v_e \approx 74800\,\text{m/s}$ and $v_i \approx 440\,\text{m/s}$ because the 8 neutron and 8 proton of the oxygen atom have to be accounted. The spacecraft orbital speed of v_d of about 7.800 m/s gives a ram flow in the spacecraft frame of the same magnitude, which is larger for ions but small for electrons, comparing to their thermal speed. The relevant electron to ion speed ratio thus is $74.8/7.8 \sim 10$ rather than 171.

When we consider the plasma drift, the SPIS parameter that accounts for the higher electron speed, the speed-up, has to be modified. The speed-up accounts for longest numerical time required by the ions to move with respect of the electrons; it is important not to exceed the ratios (or to be as close as possible to them) to resolve the plasma dynamics in the specific case under exam. 42 is maintained for the plasma at rest because is the default paramenter in SPIS and 13 is used for the flowing plasma.

5.2 Limitations vs physical realism

5.2.1 Overview

Potential digressions from physical data are here discussed. The unavoidable discretization (amount of macroparticles and tetrahedra size) is discussed with respect of the Debye length, the treatment of a collisionless and unmagnetized plasma is discussed with respect of literature.

5.2.2 Numerical (grid) heating

Some unphysical heating is caused by the discretization of the plasma model and by the necessary small number of macroparticles relative to the physical density. The numerical heating mechanism can alter the phase space and mime physical process leading to incorrect interpretation of computational results. This phenomena can be discussed through macroparticles number, grid resolution and Debye length according to the following mechanism.

As macroparticles drift from one cell to another there are fluctuations of their number per cell. Since the number of macroparticles is rather small, even fluctuations of 1 macroparticle contribute to large potential differences which can be non-realistic. These random fluctuations in the potential lead to localized electric fields which act on the macroparticles. In fact, when enough in number, macroparticles scatter off fluctuations of the potential which are typical in small Debye length plasmas (usually modelled by few macroparticles for hardware limitations). Problems with random potential fluctuations introduced by few macroparticles are augmented by the time scale of numerical phenomena involved that are not homogeneous. A kinetic instability arises by aliasing high frequency modes (not resolved by the grid) to low frequency. It is found that the growth rate of this instability is significantly reduced when $\lambda_D k_g \approx 1$ where $k_g = \pi/\Delta x$ is the smallest wave number supported by the grid [20]. This is the reason why the grid size in all the simulations is comparable to the Debye length in most of the volume except where geometrical details have to be resolved (in these regions of the simulation boxes the grid is smaller than λ_D). Effects of grid resolution on the quality of the simulations are discussed in Chapter 7 by exposing the results.

5.2.3 Collisionless plasma

Codes similar to SPIS as NASCAP/LEO and POLAR show that the collisionless approximation of LEO plasmas is reliable within 5 % of accuracy [21].

5.2.4 Magnetic field effects

In this work, the analysis of the probe-plasma response is not extended to the magnetized plasma domain. The presence of a magnetic field introduces complications and increases further the amount of variables to be handled. In fact, the magnetic field reduces the degree of symmetry of the problem because particles

are constrained to move along the field lines in gyromotion and this situation is further complicated by the collision rate [2]. An example of collisionless and magnetized plasma [23] whose density of species is comparable with Table 5.1 shows that, in presence of a weak B-field, the ion saturation current deviates of only a low number from the Laframboise's results obtained in the zero B-field hypothesis. Higher intensities of the magnetic field require a more complex modelling of collected currents. Deviations start to appear in medium B-field within the thin sheath domain and thick sheaths introduce further deviations [24]. According to such considerations, systematic errors, due to the assumption of a non-magnetized plasma, are expected to be more important in the less dense case. This is due to the broader sheath where the the magnetic field spread its influence to a larger set of charges crossing the polarized region along their orbits [5].

5.3 CAD models

5.3.1 Overview

The Langmuir probe of Figure 2.4 is simplified to replicas of different complexity that are modeled separately. The simulations mainly model the sphere and sphere plus stub (Figure 5.1) as runs are completed for these portions in the two ambient plasmas. In one case, for the lowest density, the full probe has been simulated.

5.3.2 Box features

The grid in which the plasma moves is represented by a fine texture of tertrahedra which maps the space and develops from the polygonal surface of the probe to the boudary of the simulation box. Models are made with Gmsh [3] and their Gmsh encodings are listed in Appendix 1.

[2] These class of situations is described as "magnetic bottle" by Laframboise in [22]. This is the situation of two "magnetic" mirrors facing each others; the dipole field of the Earth can be understood as a large magnetic bottle. A more complicate form of trapping is for example represented by Tokamaks.

[3] Gmsh is a 3D finite element grid generator with a build-in CAD (computer-aided design) engine and post-processor and with parametric input and advanced visualization capabilities. The specification of any input to Gmsh modules is done interactively using the graphical user interface or in ASCII text files using Gmsh's own scripting language.

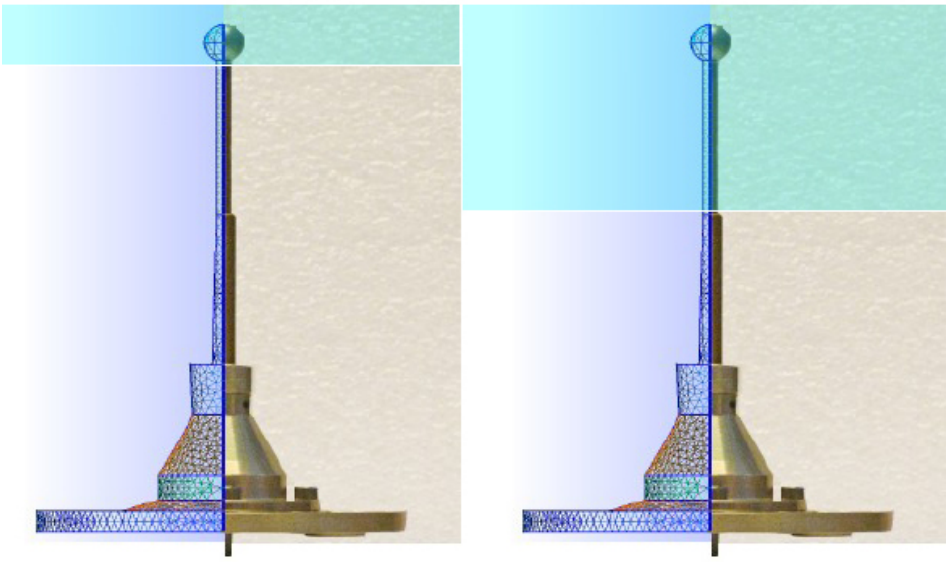

Figure 5.1: *The CAD model mirrors the real probe by a polygonal triangular surface. The blue-shaded areas at top show the components whose sweeps are simulated in the whole bias range: Sphere and Sphere-Stub.*

Because the mesh grid has to resolve the Debye length and because of Equation 2.5, the ambient parameters are related to the box dimensions via the density by λ_D as it is shown in Table 5.2. This relation clarifies the limit in box dimension which is imposed by the density the hardware can handle as the number of tetrahedra in the volume depends on the box dimensions and it grows by following a volume element scale factor k^3.

Table 5.2: *Plasma properties transfered on the grid.*

Link between physics and geometry		
Geometrical modelling: resolution	λ_D	*Chemical modelling:* $n_{(e^-,Q^+)}$

As the grid resolves the Debye length or gets close to it, the geometry of the instrument is well detailed for both sphere and stub. The high resolution

simplifies the confrontation of SPIS simulation to Laframboise's results because at CAD level the geometry is close enough to a perfect sphere. CAD models not only refers to the instrument but also to the box in which the plasma moves. The adaptive mesh generator increases the mesh density in the immediate regions around the probe to capture the dynamics of the macroparticles hence to resolve the sheath structure.

From a CAD point of view, the main goal is to make the simulation dependent to the less possible amount of geometrical parameters, for example, with sufficient computer power, box dimensions should not be discussed. In fact, in the situation of Maxwellian electrons, collisionless plasma and negligible sources and sinks in the sheath, the only length parameters that fully characterize the problem are the probe geometry, the Debye length and the sheath radius [25]. In order to achieve this goal, the box has to enclose the sheath and has to be big enough for the remainder of the potential imposed on the probe to pair or drop below the electron temperature at the boundaries [4]. For the simulations in this thesis, box length effects on the solutions are negligible in the less dense plasma case because boundaries are at enough Debye lengths of distance from the probe surface. Because of memory limitations, in the high dense plasma case, boxes are limited in size by the amount of tetrahedra they contain hence by the number of macroparticles the numerical engine has to track. In such situations box dimensions are an issue as it is discussed in Chapter 7 together with the results.

5.4 LP probe models

In Figure 5.2 we show the two main probe models used in the simulations: the sphere only model (Sphere) and the sphere +stub model (Sphere-Stub). The grid resolution appears sufficient for quite accurate geometric modelling. Figure 5.3 displays the simplified model for a probe mounted on a spacecraft represented by a box-like part of it.

[4] If this condition is not verified there is no quasineutral plasma left in the box.

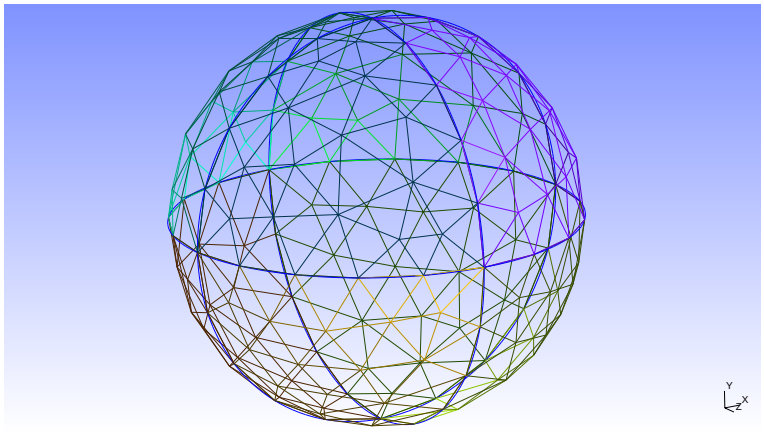

(a) Sphere.

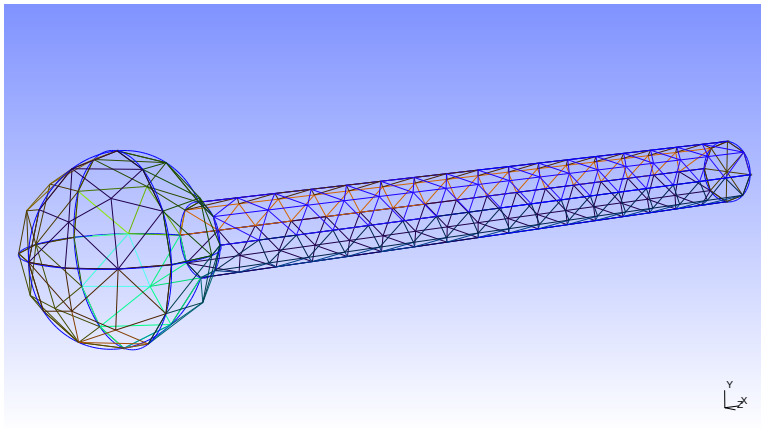

(b) Sphere-Stub.

Figure 5.2: *Spherical Probe and Probe-Stub model, realism is achieved via triangular patterning.*

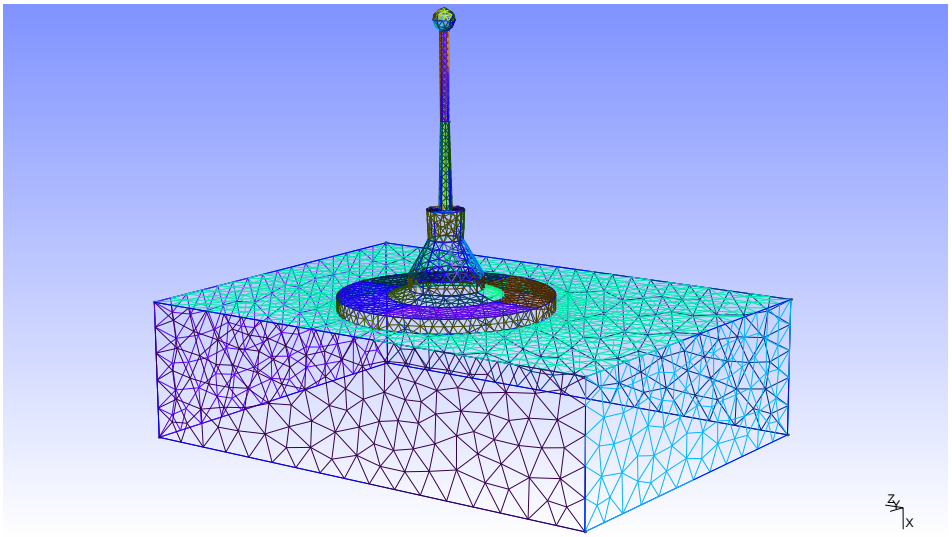

Figure 5.3: *Probe and simplified s/c geometry.*

5.5 Probe-in-the-box models

5.5.1 Overview

Different simulation boxes are applied to the LP models to simulate the two different densities according to Section 5.3.2. Boxes are chosen symmetrical because of simplicity and because of uniform distance from the probe to the boundaries. Boxes are spherical in the spherical probe case to conserve the radial symmetry. Boxes are kept spherical when the stub is added where possible. In the $\lambda_D \approx 1.7\,\text{mm}$ case only one hemisphere is maintained when the stub is added since a comprehensive spherical box would have required a longer radius hence too many tetrahedra. In this situation, the box is stretched into a cone in the stub portion and the area of the base of the cone is chosen as the largest the memory can handle for the mesh adopted. Figure 5.4 compares the spherical and the conical boxes. In the $\lambda_D \approx 10\,\text{mm}$ case, the spherical box form is conserved when the stub is added as shown in Figures 5.5, 5.6, 5.7. Figure 5.7 represents the largest spacecraft portion modelled in this thesis. The inner box is introduced to add an intermediate control on the mesh resolution.

5.5.2 Sphere and Sphere-Stub $\lambda_D \approx 1.7\,\text{mm}$

Geometrical parameters resumed in Table 5.3 and Table 5.4 are represented in Figure 5.4.

Table 5.3: *Geometrical and kinetic resolution of the probe model "Sphere" for* $\lambda_D \approx 1.7\,mm$.

Sphere				
Linked domains	*Parameter*		*Imposed Value*	
Geometry	Simulation box radius (outer box)	b_{r_o}	38	mm
	Simulation box radius (inner box)	b_{r_i}	8	mm
Plasma	Debye length	λ_D	1.7	mm
Geometry resolution	Tetrahedra side length (inner box)	$l_\bigtriangledown$	1	mm
	Typical tetrahedra side length (outer box)	$l_\bigtriangledown$	1.7	mm
	Numer of tetrahedrons	$N_\bigtriangledown$	$6 \cdot 10^5$	
Kinetic resolution	Number of macro particles	N_M	$3 \cdot 10^6$	

Table 5.4: *Geometrical and kinetic resolution of the probe model "Sphere-Stub" for* $\lambda_D \approx 1.7\,mm$.

Sphere-Stub				
Linked domains	*Parameter*		*Imposed Value*	
Geometry	Simulation box radius (hemisphere, outer box)	b_{r_o}	38	mm
	Simulation box length (cone, outer box)		51	mm
	Simulation box radius (circumference, outer box)		20	mm
	Simulation box radius (hemisphere, inner box)	b_{r_i}	8	mm
	Simulation box length (cylinder, inner box)		34	mm
Plasma	Debye length	λ_D	1.7	mm
Geometry resolution	Tetrahedra side length (inner box)	$l_\bigtriangledown$	1.7	mm
	Typical tetrahedra side length (outer box)	$l_\bigtriangledown$	2.0 ; 1.7	mm
	Numer of tetrahedrons	$N_\bigtriangledown$	$2.5 \cdot 10^5$	
Kinetic resolution	Number of macro particles	N_M	$1.25 \cdot 10^6$	

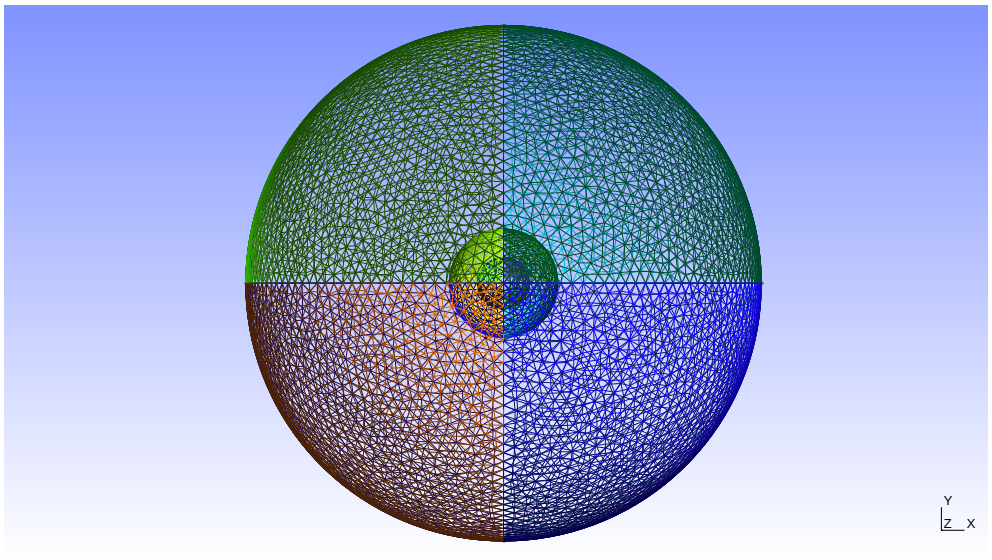

(a) Sphere and box.

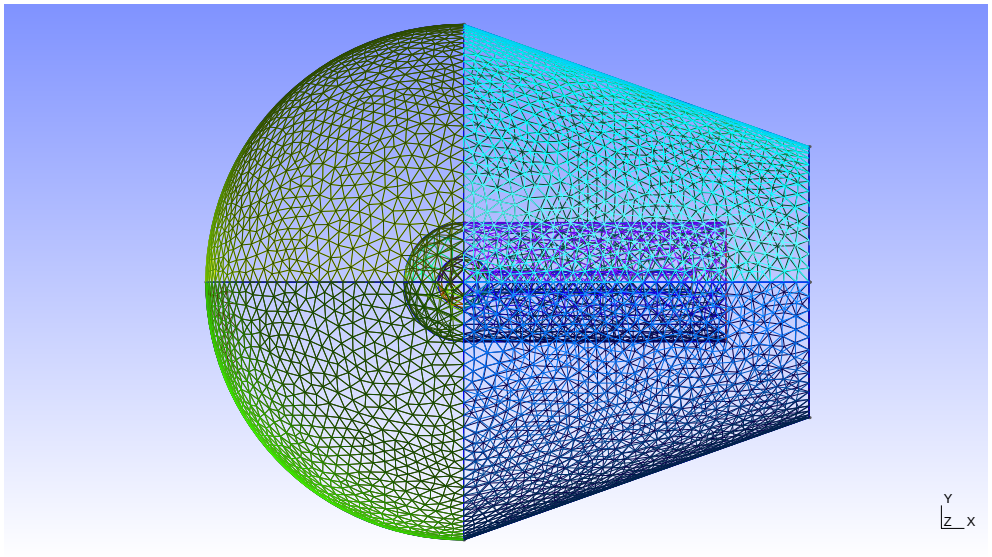

(b) Sphere-Stub and box.

Figure 5.4: n_e=n_e=$1 \cdot 10^{12}$ m^{-3}, $\lambda_D \approx 1.7\,mm$.

5.5.3 Sphere and Sphere-Stub $\lambda_D \approx 10\,\text{mm}$

Geometrical parameters resumed in Table 5.5 are represented in Figure 5.5; geometrical parameters resumed in Table 5.6 are represented in Figure 5.6; geometrical parameters resumed in Table 5.7 are represented in Figure 5.7.

Table 5.5: *Geometrical and kinetic resolution of the probe model "Sphere" for* $\lambda_D \approx 10\,mm$.

Sphere				
Linked domains	*Parameter*		*Imposed Value*	
Geometry	Simulation box radius (outer box)	b_{r_o}	95	mm
	Simulation box radius (inner box)	b_{r_i}	13.8	mm
Plasma	Debye length	λ_D	10	mm
Geometry resolution	Tetrahedra side length (inner box)	$l_\bigtriangledown$	1.7	mm
	Typical tetrahedra side length (outer box)	$l_\bigtriangledown$	6	mm
	Numer of tetrahedrons	$N_\bigtriangledown$	$2.1 \cdot 10^5$	
Kinetic resolution	Number of macro particles	N_M	$1.05 \cdot 10^6$	

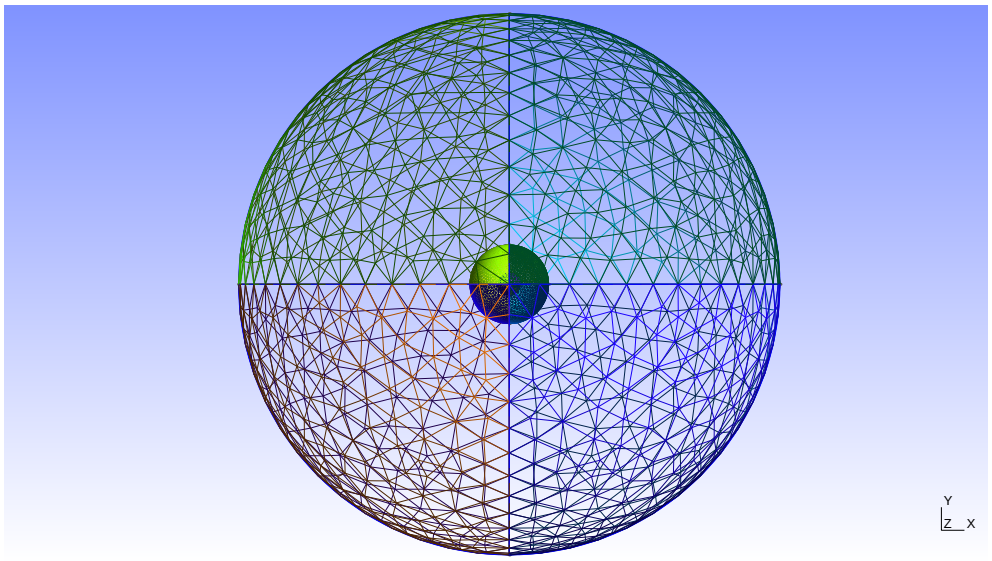

(a) Sphere and box.

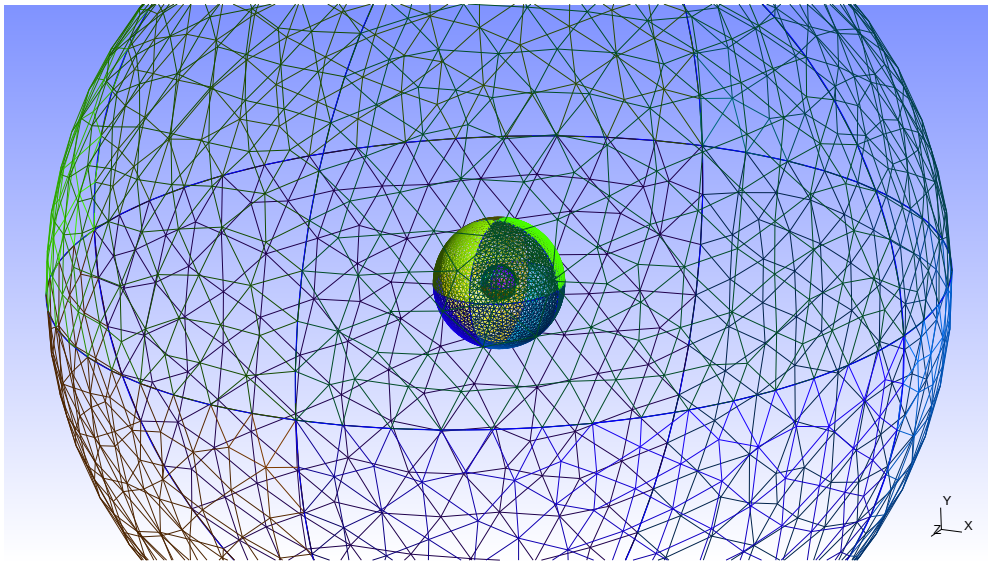

(b) Sphere and box, detail.

Figure 5.5: *Sphere,* n_e=n_e=$1 \cdot 10^{11}\ m^{-3}$, $\lambda_D \approx 10\,mm$.

Table 5.6: *Geometrical and kinetic resolution of the probe model "Sphere-Stub" for* $\lambda_D \approx 10\,mm$.

Sphere-Stub				
Linked domains	*Parameter*		*Imposed Value*	
Geometry	Simulation box radius	b_{r_o}	95	mm
	Simulation box radius (hemisphere, inner box)	b_{r_i}	8	mm
	Simulation box length (cylinder, inner box)		34	mm
Plasma	Debye length	λ_D	10	mm
Geometry resolution	Tetrahedra side length (inner box)	$l_\bigtriangledown$	1.7	mm
	Typical tetrahedra side length (outer box)	$l_\bigtriangledown$	6	mm
	Numer of tetrahedrons	$N_\bigtriangledown$	$2.5 \cdot 10^5$	
Kinetic resolution	Number of macro particles	N_M	$6 \cdot 10^5$	

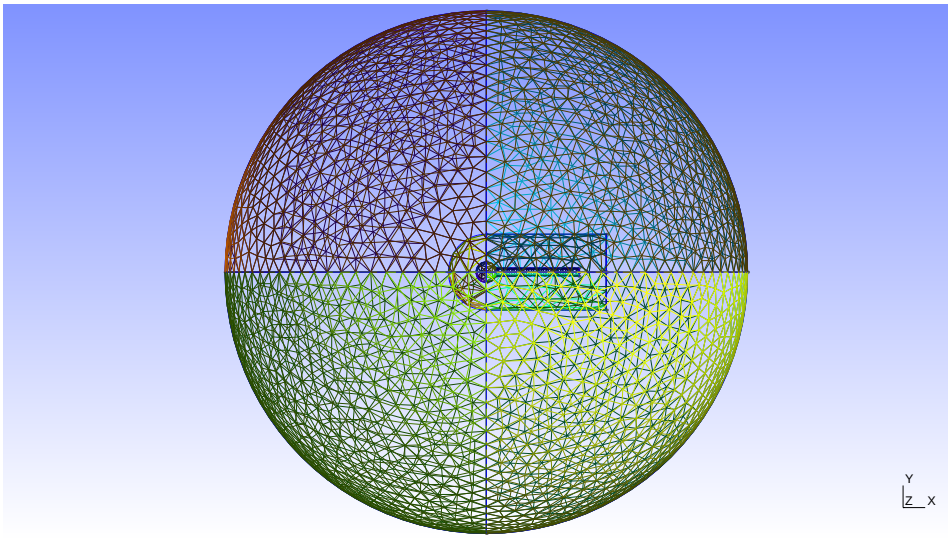

Figure 5.6: *Sphere-Stub,* n_e=n_e=$1 \cdot 10^{11}\ m^{-3}$, $\lambda_D \approx 10\,mm$.

A bigger box for the less dense plasma case is also used as the number of tetrahedra allows the extension of the boundaries. The limit at 190 mm is set by memory limitations.

Table 5.7: *Geometrical and kinetic resolution of the probe model "Sphere" for* $\lambda_D \approx 10\,mm$ *and large box.*

Sphere				
Linked domains	*Parameter*		*Imposed Value*	
Geometry	Simulation box radius (outer box)	b_{r_o}	190	mm
	Simulation box radius (inner box)	b_{r_i}	13.8	mm
Plasma	Debye length	λ_D	10	mm
Geometry resolution	Tetrahedra side length (inner box)	$l_{\bigtriangledown}$	1	mm
	Typical tetrahedra side length (outer box)	$l_{\bigtriangledown}$	5	mm
	Numer of tetrahedrons	$N_{\bigtriangledown}$	$2.1 \cdot 10^5$	
Kinetic resolution	Number of macro particles	N_M	$1.7 \cdot 10^6$	

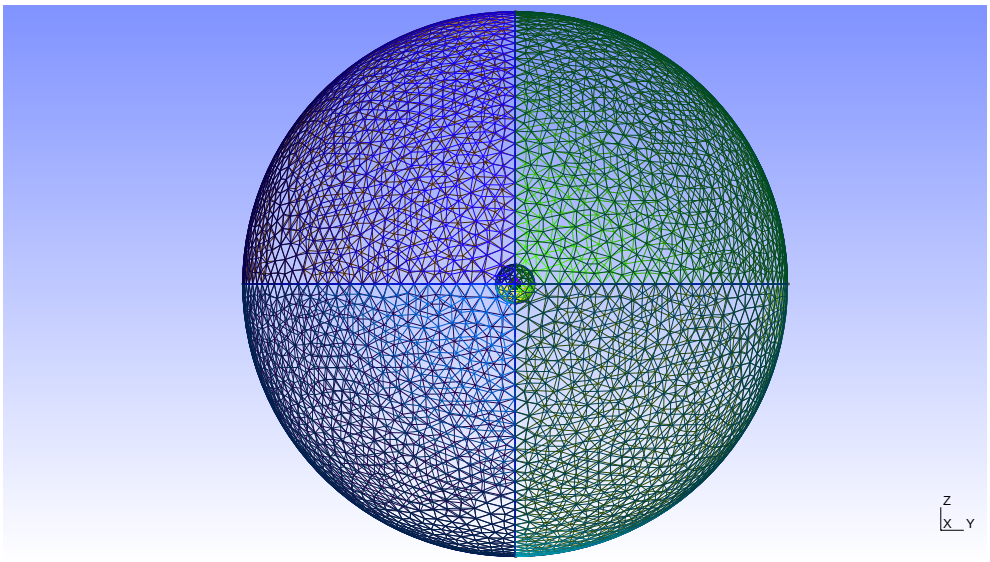

(a) Sphere and box.

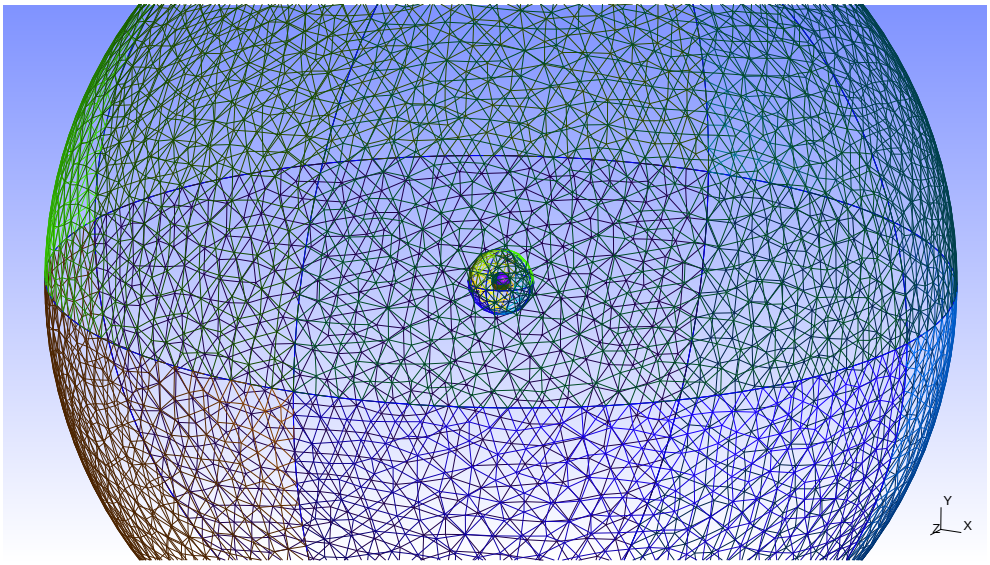

(b) Sphere and box, detail.

Figure 5.7: n_e=n_e=$1 \cdot 10^{11}\ m^{-3}$, $\lambda_D \approx 10\,mm$.

5.5.4 Probe $\lambda_D \approx 10\,\text{mm}$

Geometrical parameters resumed in Table 5.8 are represented in Figure 5.7.

Table 5.8: *Geometrical and kinetic resolution of the probe model for* $\lambda_D \approx 10\,mm$.

Probe				
Linked domains	*Parameter*		*Imposed Value*	
Geometry	Simulation box dimensions (x,y,z)	l_x, l_y, l_z	31x24x36	mm
Plasma	Debye length	λ_D	10	mm
Geometry resolution	Typical tetrahedra side length	$l_\bigtriangledown$	1.7-12	mm
	Numer of tetrahedrons	$N_\bigtriangledown$	$2.4 \cdot 10^5$	
Kinetic resolution	Number of macro particles	N_M	$1.2 \cdot 10^6$	

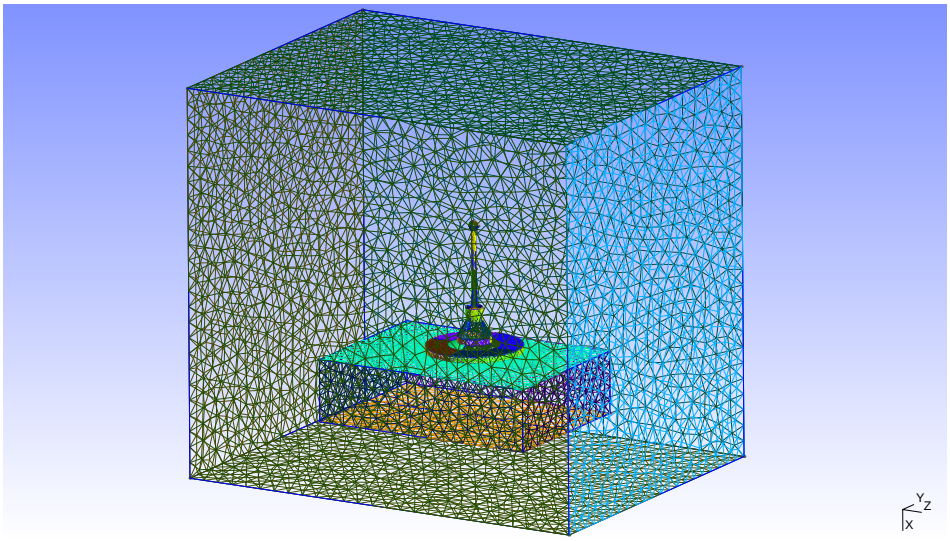

Figure 5.8: *Probe and simplified s/c geometry,* n_e=n_e=$1 \cdot 10^{12}\ m^{-3}$, $\lambda_D \approx 10\,mm$.

6

SIMULATIONS

This chapter presents all the simulation results for the $\lambda_D \approx 1.7$ mm case and for the $\lambda_D \approx 10$ mm case. To show the convergence of the simulations, the history of current collection for different bias voltages is exposed and grouped in form of I-V-t plots (introduced in Section 3.5.2). Such sets are listed in Table 5.1. SPIS runs are hierarchically organized in order to validate the simulations of the most complex probe model and the criteria for the adopted validation are hereby presented.

6.1 Modelling an increasingly complex situation

Figure 2.5 presents in scheme the method used to address the Sphere-Stub model in flowing plasma. Simulations are hierarchically ordered by starting from the spherical probe geometry because it is the only category for which numerical solutions exist. The second step consists in modelling an increasingly complex object (Sphere → Sphere-Stub [1]) but it is not straightforward as it requires an added amount of simulations with respect of the ones needed to just model the sphere for the two plasma environments presented in Chapter 5. Specific implementations in mesh density, speed up and box size are used to augment the accuracy of plasma modelling. Simulations whose grid does not resolve everywhere λ_D are compared to simulations that resolve λ_D with the mesh. Simulations whose box size may introduce boundary problems are compared to runs that adopt very large boxes.

[1] In one case, in the less dense scenario, the LP is modelled by Sphere-Stub and simplified s/c

Because memory consuming, it is found convenient to introduce the correct speed up on top of the process.

These relevant subsets of simulations are characterized by a completion time for single run that varies from 1 to 4 days. The current values obtained by these runs are confronted to the corresponding currents collected by the less refined models in order to ensure their consistency. As the validation is achieved, the current collection at remaining voltages is simulated in the less computationally expensive cases whose endurance is on average of about 8 hours. The auxiliary runs concern positive, moderate and high bias voltages (e.g: 2 V and 5 V) because collected current fluctuations at these potentials values are more significative as depend on the sheath shielding effects which is increasingly important as the bias grows.

Table 6.1: *Simulations,*
(letters R, V and B are only used to lable and differentiate the simulations in the following sections).

$T_e = 0.05V, n_{O^+} = n_{e^-} = 10^{12}m^{-3} \Rightarrow \lambda_D \approx 1.7\,mm$		
$\lambda_D \approx 1.7$ mm	Sphere PIC	
	Sphere MB	Maxwell Boltzmann electrons
	Sphere-Stub PIC	
	Sphere-Stub R PIC	λ_D resolved in the external box
	Sphere-Stub drift R PIC	
	Sphere-Stub drift V PIC	numerical speed up = 13
	Sphere PIC drift	numerical speed up = 13
	Stub PIC	
$T_e = 0.2V, n_{O^+} = n_{e^-} = 10^{-12}m^{-3} \Rightarrow \lambda_D \approx 10\,mm$		
$\lambda_D \approx 10$ mm	Sphere PIC	
	Sphere B PIC	larger simulation box
	Sphere-Stub PIC	
	Sphere-Stub drift PIC	
	Full probe-simplified s/c model drift PIC	

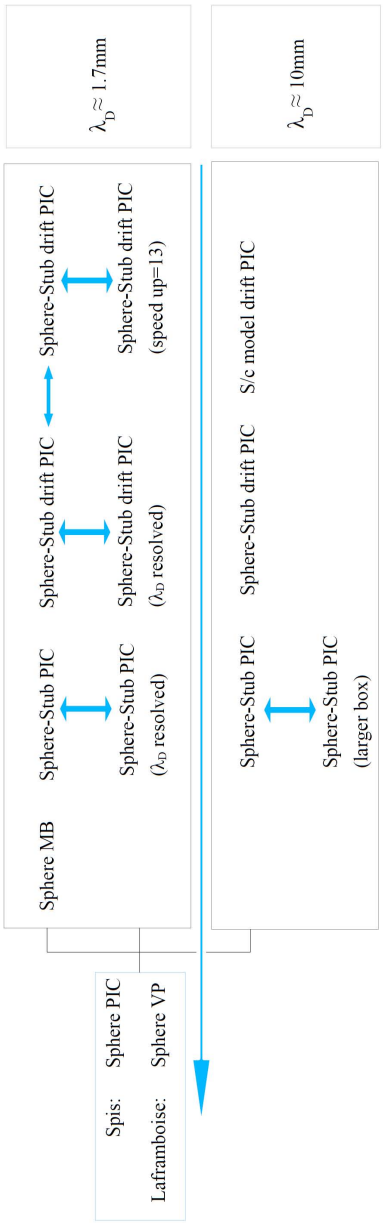

Figure 6.1: *Simulations hierarchy and logic ordering of the simulations exposed in Table 6.1. The direction of the arrow horizontal to the text points to the perfect sphere because it is the situation in which literature confronts the SPIS PIC simulations with numerical solutions of the VP (Vlasov-Poisson) system. The vertical arrows indicate the comparisons between simulations of identical scenarios modelled with different accuracy; the specific implementation introduced by the auxiliary sets are added in parenthesis. In the high density drifting plasma case two confrontations are implemented to verify that the respective digression is negligible. In the figure, labels R, V and B used in Table 6.1 have not been included.*

6.2 Check runs for high density plasma

$\lambda_D \approx 1.7\,\text{mm}$

This section presents the confrontations between simulations for the high dense case outlined in Figure 6.1. The discussion starts with an analysis of the potential remainder at the box boundaries because it easiers the discussion. A confrontation to Boltzmann electrons is performed as an added support for simulations of current collection at negative biases.

6.2.1 Potential remainder and electron temperature

The bias value for which the remainder of the potential stops at the order of the electron temperature at the box boundaries is about 2 V, Figure 6.2. The potential remainder drops within the electron temperature at the boundaries for values lower than about 2 V. At negative biases, the remainder at the boundaries stops at the order of the electron temperature at about −3 V, Figure 6.3.

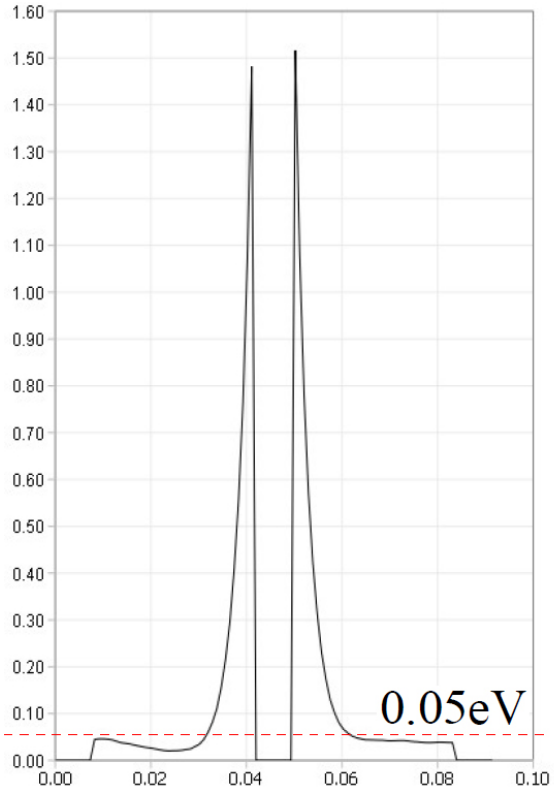

(a) Line cut plot of potential drop from probe surface to box boundaries and underneath T_e = 0.05 eV.

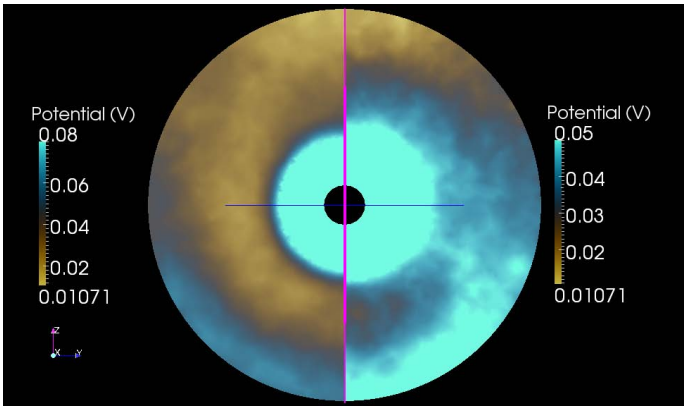

(b) Planar potential map (at two rescaled potential) correspondent to the line cut.

Figure 6.2: *Three plots of the same potential drop to box boundaries for* 2 *V biased spherical probe.*

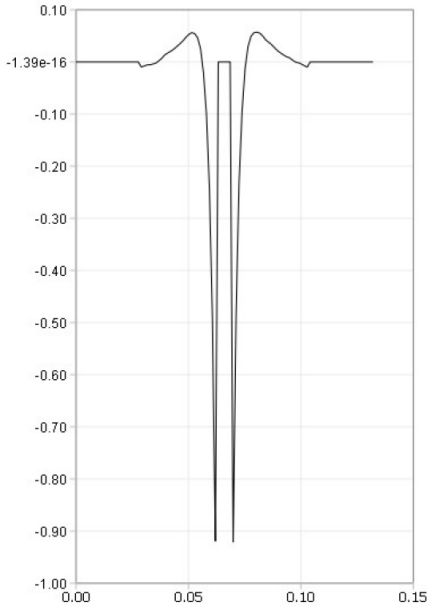

(a) Line cut type plot of potential drop from probe surface to box boundaries, -1 V bias.

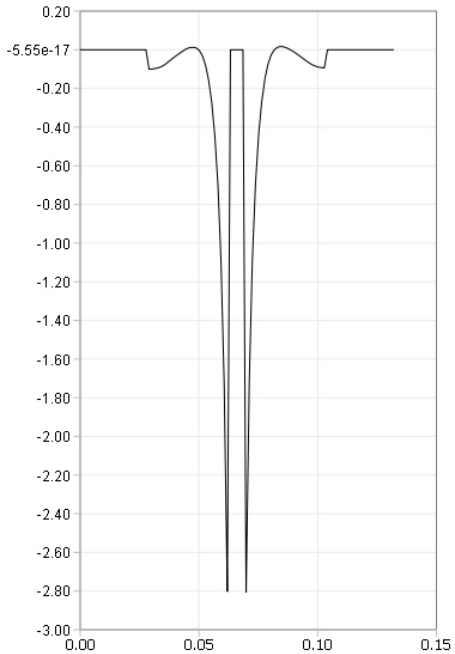

(b) Line cut type plot of potential drop from probe surface to box boundaries, -3 V bias. The potential at the boundaries is of the order of T_e.

Figure 6.3: *Potential drop to box boundaries for -1 V and -3 V bias potential.*

6.2.2 Maxwell-Boltzmann electrons

Boltzmann distributed electrons have been used as an alternative in some simulation runs for the negative voltages of the I-V curve in the high dense case. Results in Figure 6.4 show that curves well overlap to each other and deviations are negligible as they are not dependent on the applied voltage but scattered randomly due to numerical noise.

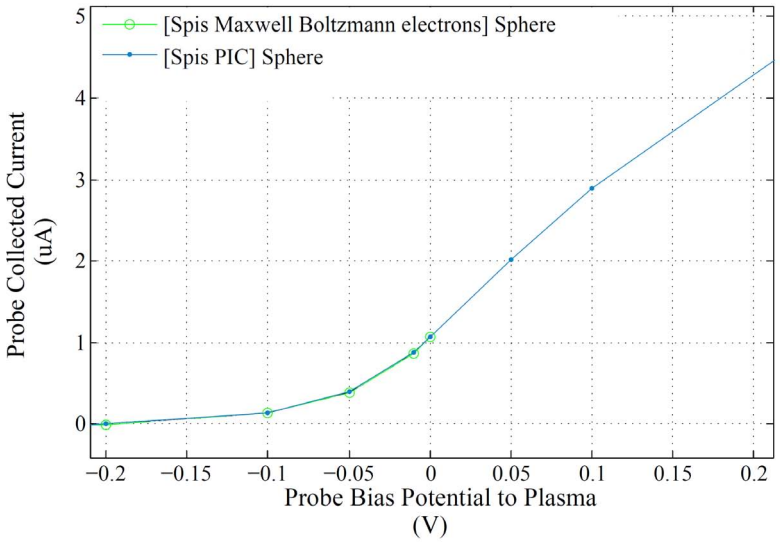

(a) Close-in over the electron retardation region to evaluate values correspondance.

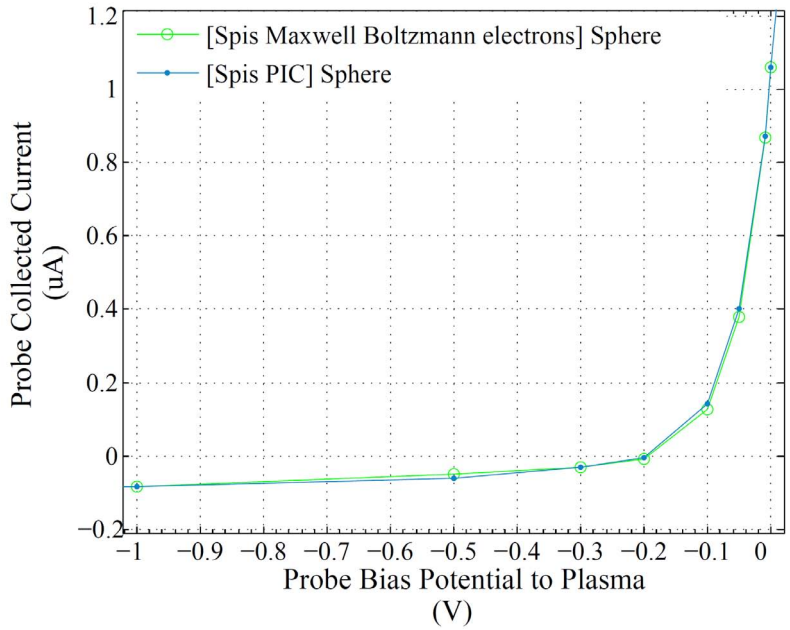

(b) Zoom out to evaluate overall coherence of simulations.

Figure 6.4: *Two details of Boltzmann simulations vs PIC simulations for probe model Sphere.*

6.2.3 Sphere-Stub, mesh ~ λ_D vs mesh exceeding λ_D of 15 % in outer box

Figure 7.1 confronts results obtained by two different models. In one case the mesh resolves λ_D, in the other the mesh exceeds λ_D of 15 % in the outher box. Part of the electron retardation region and the electron saturation region is compared between the plots. Curves coincide with each other with high confidence, less than 0.1 uA at 2 V and less than 0.5 uA at 5 V, the worst digression. We can thus adopt this grid in the simulations which saves computational time.

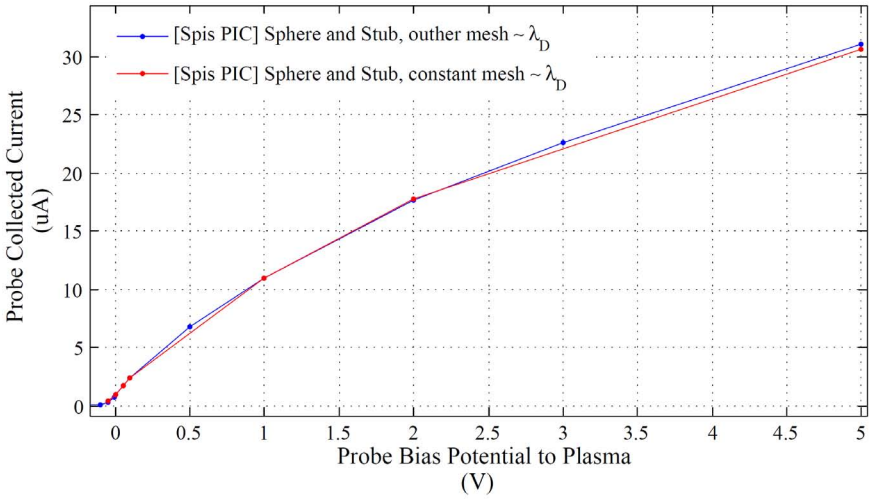

Figure 6.5: *I-V data comparison between mesh ~ λ_D vs mesh exceeding λ_D of 15 % in outher box*

6.2.4 Sphere-Stub in flowing plasma

We now put the model of the previous section which allows to save more computational (mesh exceeding λ_D of 15) in flowing plasma and rescale the speed up which is 13, then we compare this results to the model of the previous section that resolves λ_D everywhere but with speed up typical of the plasma at rest which is 42. Simulations with finer mesh and speed up 13 are not allowed by the used hardware settings. The scarcity of points taken by resolving λ_D in the drifted

plasma is motivated by the long computational time. Figure 6.6 shows that curves deviates from each other of less than 0.1 μA at 1 V and less than 0.5 μA at 2 V. 2 V is an extreme of interest for the considerations in Section 6.2. The comparison is also necessary because, at flowing plasma conditions, the potential drop at the boundary is significantly above the electron temperature as Figure 6.7 highlights. Figure 6.9 shows the similarity in the potential distribution across the whole space of the simulation box for the two cases as a comparative resume.

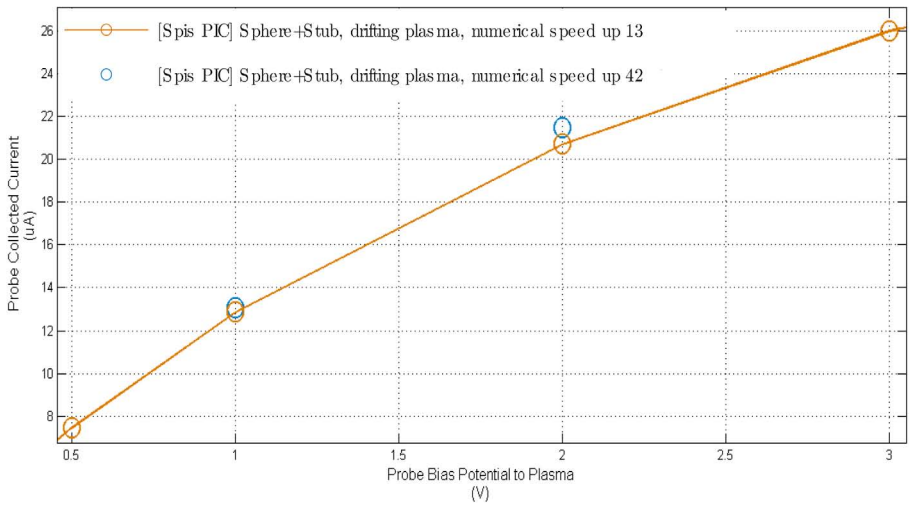

Figure 6.6: *I-V data comparison between mesh ~ λ_D and speed up=45 (orange) vs mesh exceeding λ_D of* 15 *% in outher box and speed up=13 (blue), flowing plasma.*

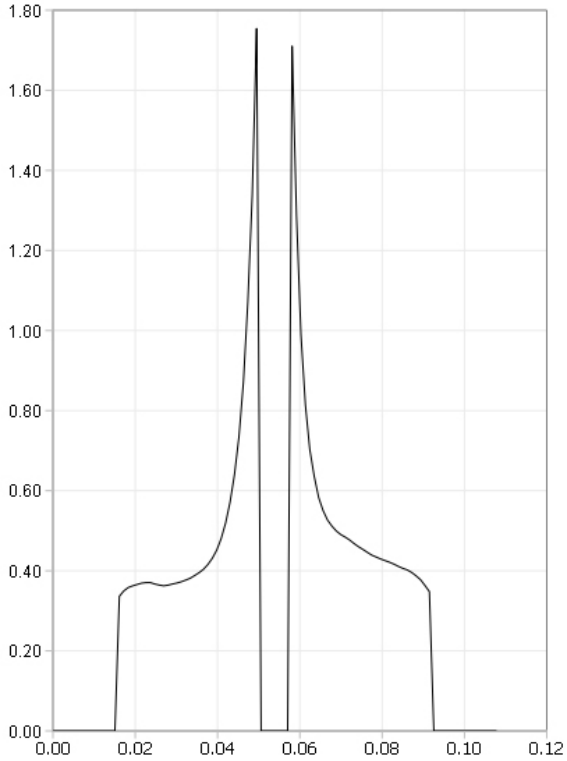

Figure 6.7: *Potential drop to box boundaries from sphere within the Sphere-Stub model biased at* $2\,V$*;* $\lambda_D \approx 1.7\,mm$*, flowing plasma, numerical speed up = 42.*

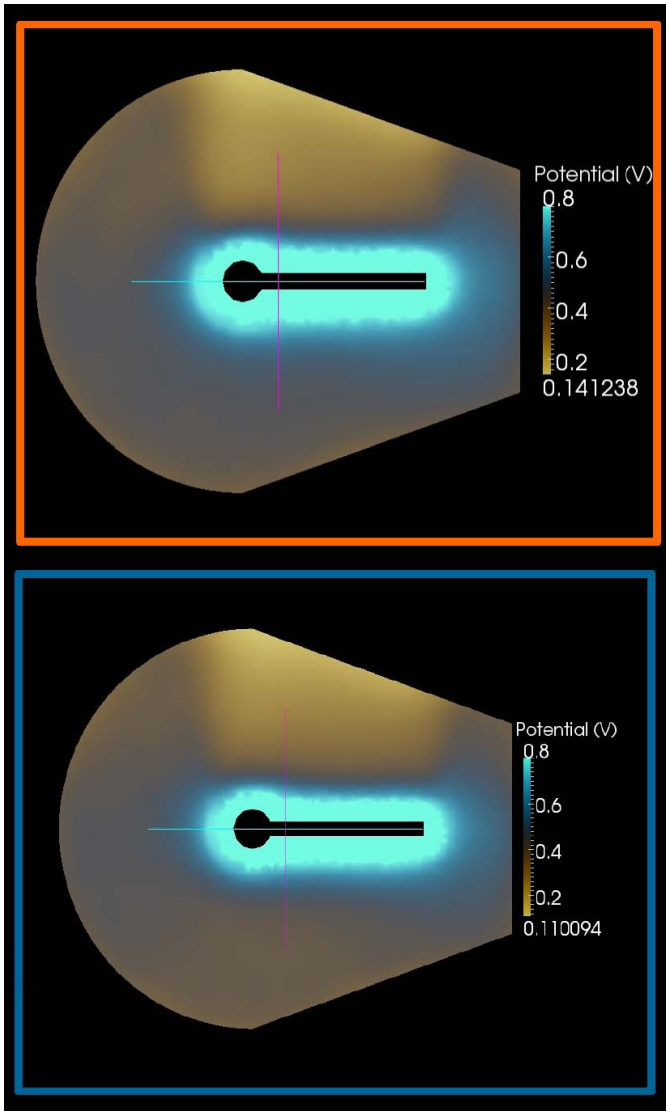

Figure 6.8: *Potential drop from 2 V biased surface to box boundaries, longitudinal section of the Probe-Stub models referred to Figure 6.6, colours are corresponding.*

6.3 Check runs for average density plasma

$\lambda_D \approx 10\,\mathrm{mm}$

In the low density scenario, larger boxes do not influence the simulation as the the collected current results to be about the same as it is shown in Figure 6.9. The potential drop at the boundary is smooth as Figure 6.10 points out and it does not exceed the electron temperature when the drift is added, Figure 6.11.

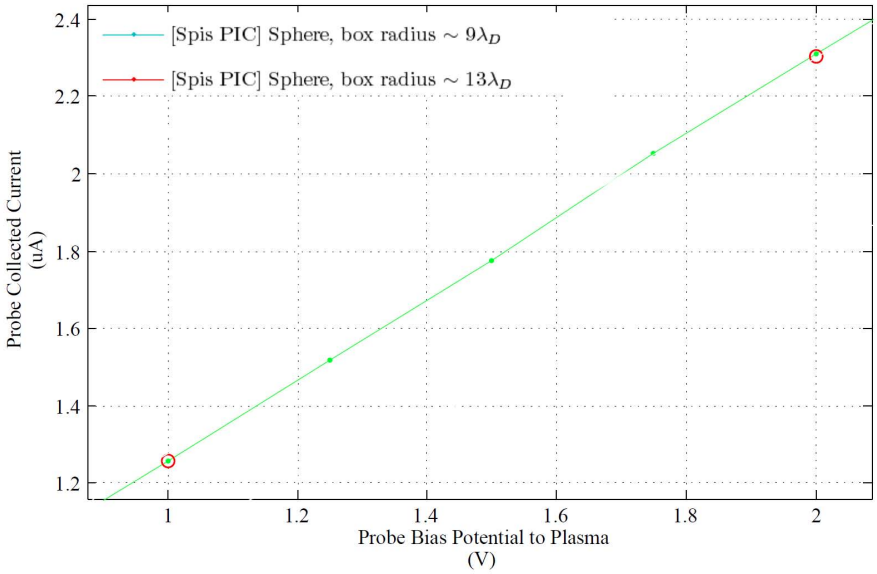

Figure 6.9: *I-V data comparison between different size boxes to verify the absence boudary effects on the solution.*

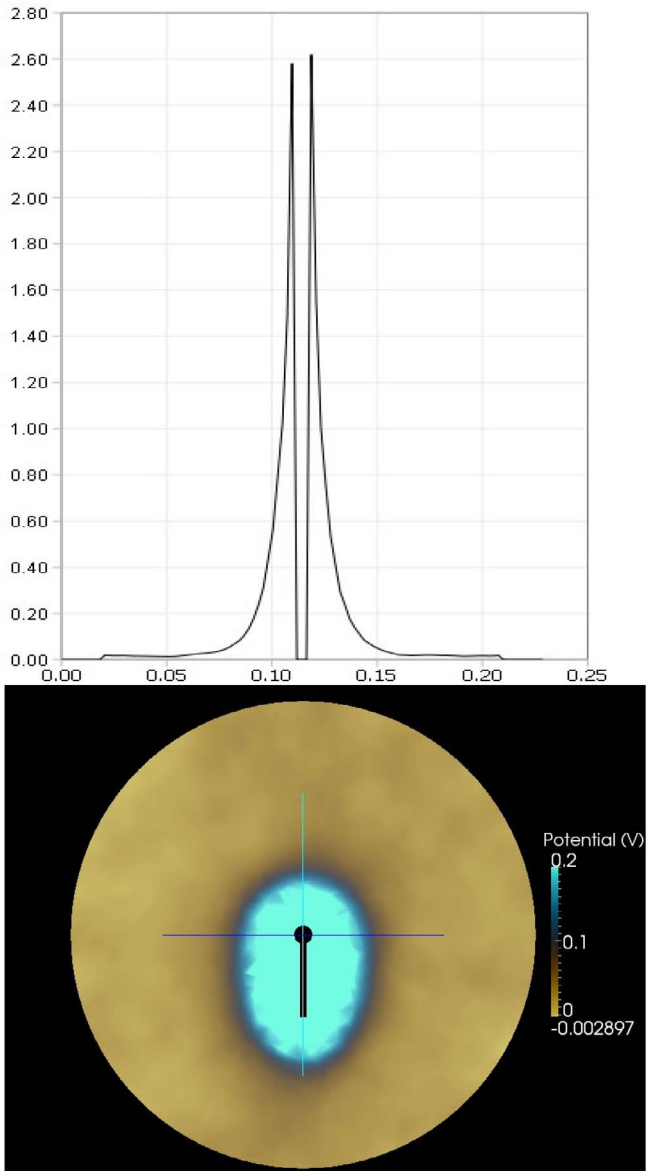

Figure 6.10: *Potential drop from a* $2\,V$ *biased probe to box boundaries;* $\lambda_D \approx 10\,mm$*, numerical speed up = 42.*

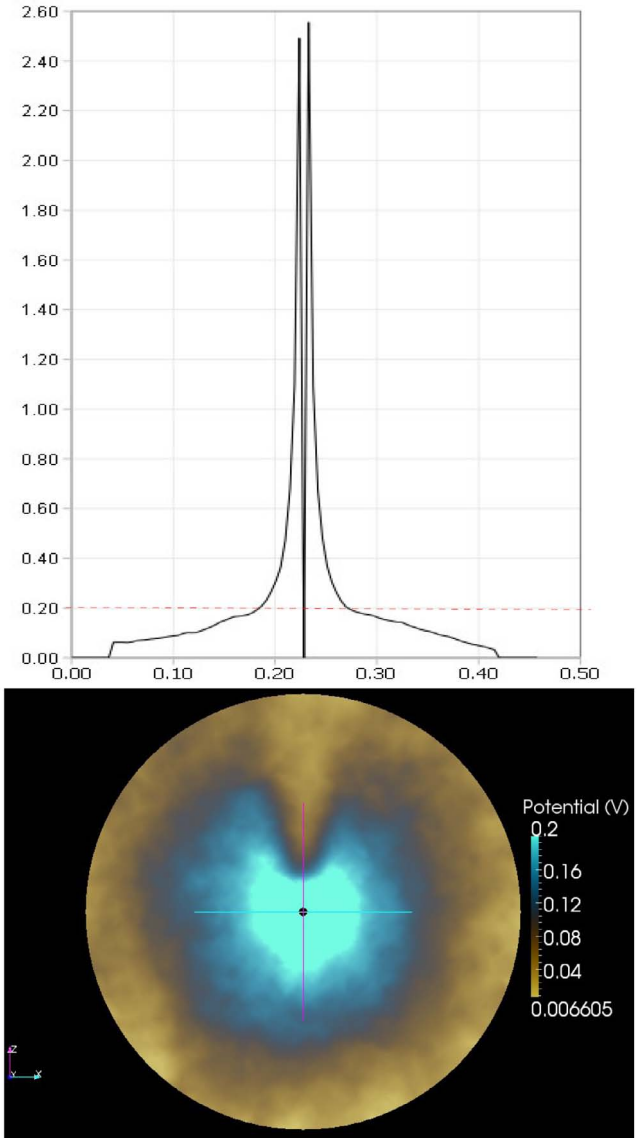

Figure 6.11: *Potential drop of a* $2\,V$ *biased probe;* $\lambda_D \approx 10\,mm$*, flowing plasma.*

6.4 I-V-t maps summary

In the following Sections the summary of all simulation is given. For the denser scenario, simulation runs are summarized by the values reported in Table 6.2 - Table 6.17 whose results are summarized from Figure 6.12 to Figure 6.19. For the less dense scenario, simulation runs are resumed via the values reported in Table 6.18 - Table 6.25 whose results are summarized from Figure 6.20 to Figure 6.24.

The I-V curves are detailed with different resolution depending if are check runs or complete runs. The extremes for the sweeps are ±5 V as the range will be used for the Swarm LP instrument. Currents are collected in 100μs and averages are calculated at stabilized current values usually occurring at 40μs but also after; values used for averages are listed in Appendix 3 for each case.

6.4.1 Collected current for high density plasma

Collected current for $\lambda_D \approx 1.7\,\text{mm}$ in simulations runs implementing the CAD model of Chapter 5.

Sphere PIC

Simulation runs implementing a CAD model of Figure 5.4 a whose geometrical properties are detailed in Table 5.3.

Table 6.2: *Imposed parameters, Sphere.*

Parameter		Imposed Value	
Electron temperature	T_e	0.05	eV
Ion temperature	T_i	0.05	eV
Electron density	n_e	$1 \cdot 10^{12}$	m^{-3}
Ion density	n_i	$1 \cdot 10^{12}$	m^{-3}
Debye length	λ_D	1.7	mm
Potential range	Φ	*Table*	V
Sphere radius	r_P	3.8	mm
Simulation box diameter	$b_\oslash$	38	mm
Numerical speed up		42	
Number of tetrahedrons		$6 \cdot 10^5$	
Number of macro-particles		$3 \cdot 10^6$	

Table 6.3: *Average collected current for various bias voltages, Sphere.*

Voltage (V)	5.0	3.0	2.0	1.5	1.0	0.5
Current (μA)	-47.89551	-32.96122	-24.16883	-19.39611	-14.27363	-14.27363
Voltage (V)	0.1	0.05	0.0	-0.01	-0.05	-0.1
Current (μA)	-8.50657	-2.89158	-2.01414	-0.87214	-0.40007	-0.1401
Voltage (V)	-0.2	-0.3	-0.5	-1.0	-3.0	
Current (μA)	0.00381	0.03201	0.06321	0.08471	0.19063	

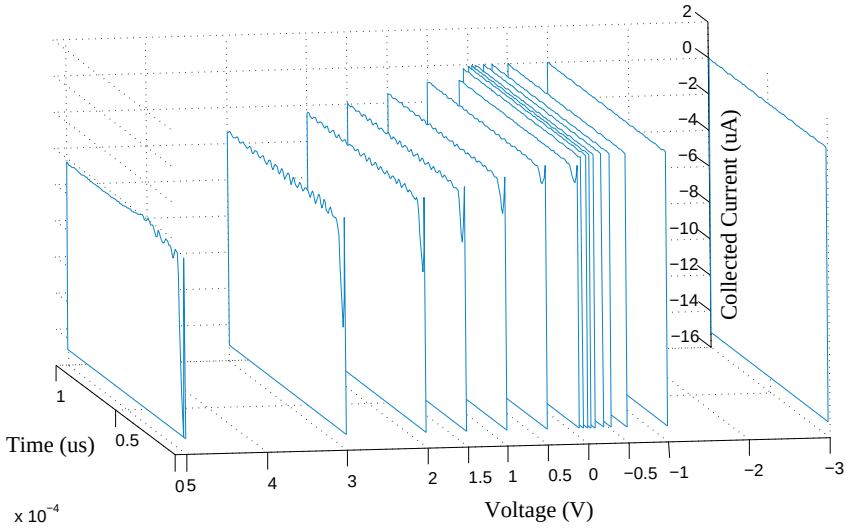

Figure 6.12: *Sampling of the current in time to reconstruct the sweep via the V values listed in Table 6.3.*

Sphere MB, Boltzmann electrons

Simulation runs implementing the CAD model of Figure 5.4 a whose geometrical properties are detailed in Table 5.3.

Table 6.4: *Imposed parameters, Sphere.*

Parameter		Imposed Value	
Electron temperature	T_e	0.05	eV
Ion temperature	T_i	0.05	eV
Electron density	n_e	$1 \cdot 10^{12}$	m^{-3}
Ion density	n_i	$1 \cdot 10^{12}$	m^{-3}
Debye length	λ_D	1.7	mm
Potential range	Φ	*Table*	V
Sphere radius	r_P	3.8	mm
Simulation box diameter	$b_\oslash$	38	mm
Numerical speed up		42	
Number of tetrahedrons		$6 \cdot 10^5$	
Number of macro-particles		$3 \cdot 10^6$	

Table 6.5: *Average collected current for various bias voltages range, Sphere.*

Voltage (V)	0.0	-0.01	-0.05	-0.1	-0.2	-0.3
Current (μA)	-1.06181	-0.86737	-0.38058	-0.12616	0.00818	0.03355
Voltage (V)	-0.5	-1.0	-1.5	-2.0	-5.0	
Current (μA)	0.05005	0.08406	0.08508	0.14331	0.28889	

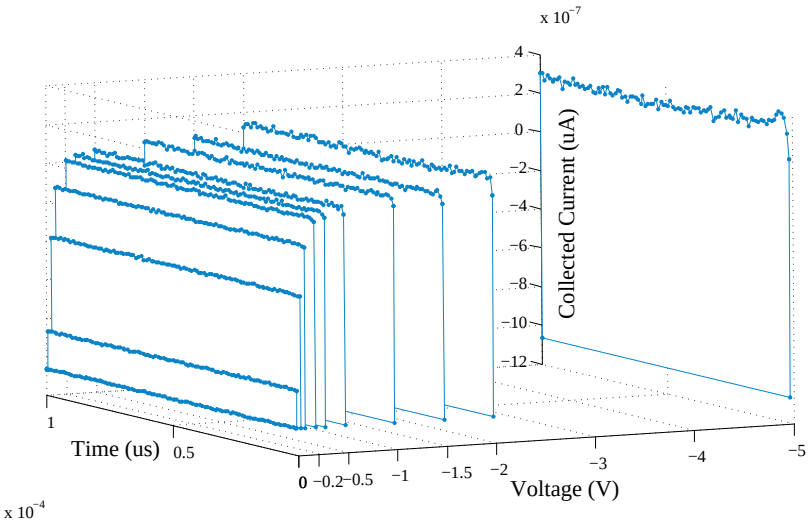

Figure 6.13: *Sampling of the current in time to reconstruct the sweep via the V values listed in Table 6.5.*

Sphere-Stub PIC

Simulation runs implementing the CAD model of Figure 5.4 b whose geometrical properties are detailed in Table 5.4.

Table 6.6: *Imposed parameters, Sphere.*

Parameter		Imposed Value	
Electron temperature	T_e	0.05	eV
Ion temperature	T_i	0.05	eV
Electron density	n_e	$1 \cdot 10^{12}$	m^{-3}
Ion density	n_i	$1 \cdot 10^{12}$	m^{-3}
Debye length	λ_D	1.7	mm
Potential range	Φ	*Table*	V
Sphere radius	r_P	3.8	mm
Stub radius	r_S	1.5	mm
Stub length	l_S	30	mm
Simulation box diameter (max extension)	$b_\varnothing$	38	mm
Numerical speed up		42	
Number of tetrahedrons		$2.5 \cdot 10^5$	
Number of macro-particles		$1.25 \cdot 10^6$	

Table 6.7: *Average collected current for various bias voltages range, Sphere and Stub.*

Voltage (V)	5.0	3.0	2.0	1.0	0.5	0.1
Current (μA)	-31.07232	-22.59314	-17.69486	-11.00537	-6.75019	-2.36675
Voltage (V)	0.05	0.0	-0.01	-0.05	-0.1	-0.2
Current (μA)	-1.68863	-0.91979	-0.77635	-0.34783	-0.12932	0.00202
Voltage (V)	-0.3	-1.0	-2.0	-3.0	-5.0	
Current (μA)	0.02479	0.06577	0.10313	0.13064	0.17946	

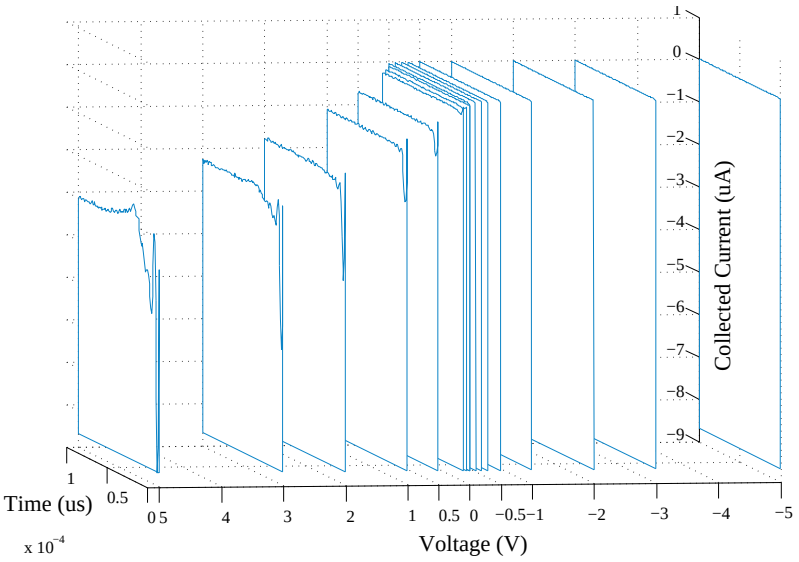

Figure 6.14: *Sampling of the current in time to reconstruct the sweep via the V values listed in Table 6.7.*

Sphere-Stub R PIC, λ_D resolved in the external box

Simulation runs implementing a CAD model similar to Figure 5.4 b.

Table 6.8: *Imposed parameters, Sphere.*

Parameter		Imposed Value	
Electron temperature	T_e	0.05	eV
Ion temperature	T_i	0.05	eV
Electron density	n_e	$1 \cdot 10^{12}$	m^{-3}
Ion density	n_i	$1 \cdot 10^{12}$	m^{-3}
Debye length	λ_D	1.7	mm
Potential range	Φ	*Table*	V
Sphere radius	r_P	3.8	mm
Stub radius	r_S	1.5	mm
Stub length	l_S	30	mm
Simulation box diameter (max extension)	$b_\varnothing$	38	mm
Numerical speed up		42	
Number of tetrahedrons		$4.5 \cdot 10^5$	
Number of macro-particles		$2.25 \cdot 10^6$	

Table 6.9: *Average collected current for various bias voltages range, Sphere and Stub.*

Voltage (V)	5.0	2.0	1.0	0.1	0.05	-0.05
Current (μA)	-30.67928	-17.74597	-11.01931	-2.39615	-1.68952	-0.38009

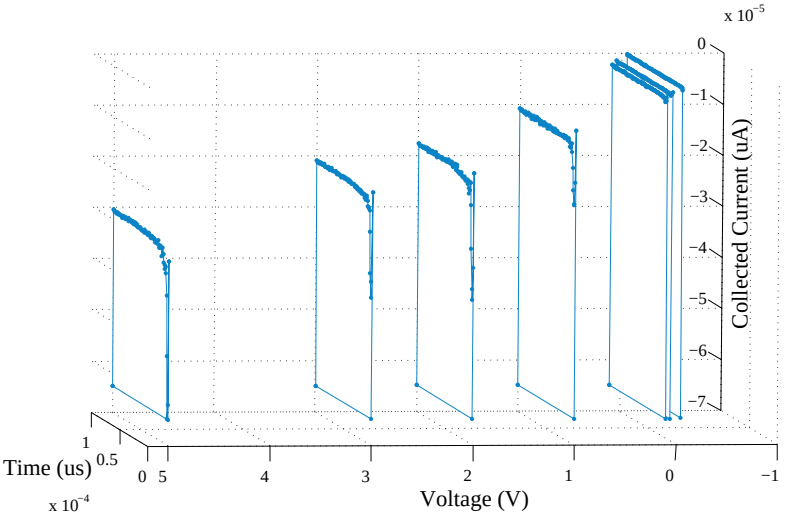

Figure 6.15: *Sampling of the current in time to reconstruct the sweep via the V values listed in Table 6.9.*

Sphere-Stub drift R PIC

Simulation runs implementing a CAD model similar to Figure 5.4 b.

Table 6.10: *Imposed parameters, Sphere.*

Parameter		Imposed Value	
Electron temperature	T_e	0.05	eV
Ion temperature	T_i	0.05	eV
Electron density	n_e	$1 \cdot 10^{12}$	m^{-3}
Ion density	n_i	$1 \cdot 10^{12}$	m^{-3}
Drift velocity	v_d	7800	m/s
Debye length	λ_D	1.7	mm
Potential range	Φ	*Table*	V
Sphere radious	r_P	3.8	mm
Stub radius	r_S	1.5	mm
Stub length	l_S	30	mm
Simulation box diameter (max extension)	$b_\varnothing$	38	mm
Numerical speed up		42	
Number of tetrahedrons		$4.5 \cdot 10^5$	
Number of macro-particles		$2.25 \cdot 10^6$	

Table 6.11: *Average collected current for various bias voltages range, Sphere and Stub.*

Voltage (V)	2.0	1.0	-0.5
Current (μA)	-21.48771	-13.09374	0.056591

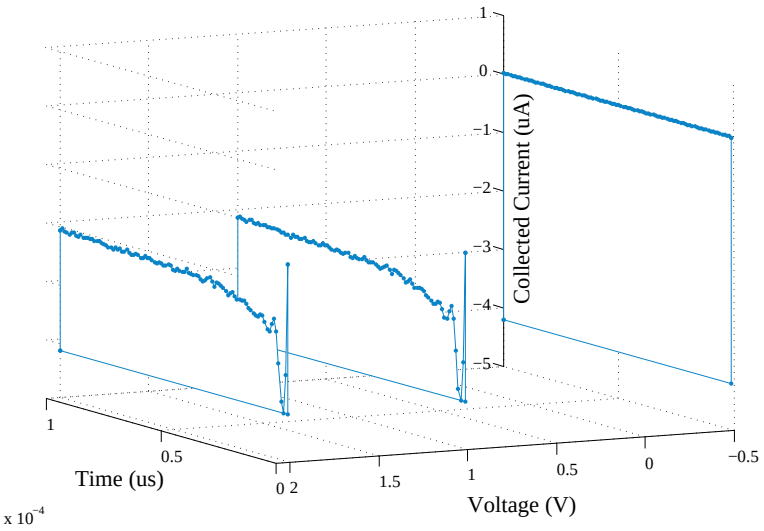

Figure 6.16: *Sampling of the current in time to reconstruct the sweep via the V values listed in Table 6.11.*

Sphere-Stub drift V PIC, numerical speed up = 13

Simulation runs implementing the CAD model of Figure 5.4 b whose geometrical properties are detailed in Table 5.4.

Table 6.12: *Imposed parameters, Sphere-Stub.*

Parameter		Imposed Value	
Electron temperature	T_e	0.05	eV
Ion temperature	T_i	0.05	eV
Electron density	n_e	$1 \cdot 10^{12}$	m^{-3}
Ion density	n_i	$1 \cdot 10^{12}$	m^{-3}
Drift velocity	v_d	7800	m/s
Debye length	λ_D	1.7	mm
Potential range	Φ	*Table*	V
Sphere radious	r_P	3.8	mm
Stub radius	r_S	1.5	mm
Stub length	l_S	30	mm
Simulation box diameter (max extension)	$b_\oslash$	38	mm
Numerical speed up		13	
Number of tetrahedrons		$2.5 \cdot 10^5$	
Number of macro-particles		$1.25 \cdot 10^6$	

Table 6.13: *Average collected current for variuos bias voltages range, Sphere and Stub.*

Voltage (V)	5.0	3.0	2.0	1.0	0.5	0.1	0.05	0.0
Current (μA)	-32.07453	-26.00494	-20.70815	-12.88028	-7.48714	-2.31279	-1.59498	-0.83596
Voltage (V)	-0.01	-0.05	-0.1	-0.2	-0.3	-0.5	-2.0	-5.0
Current (μA)	-0.69704	-0.29971	-0.08027	0.03642	0.05217	0.05681	0.06895	0.09408

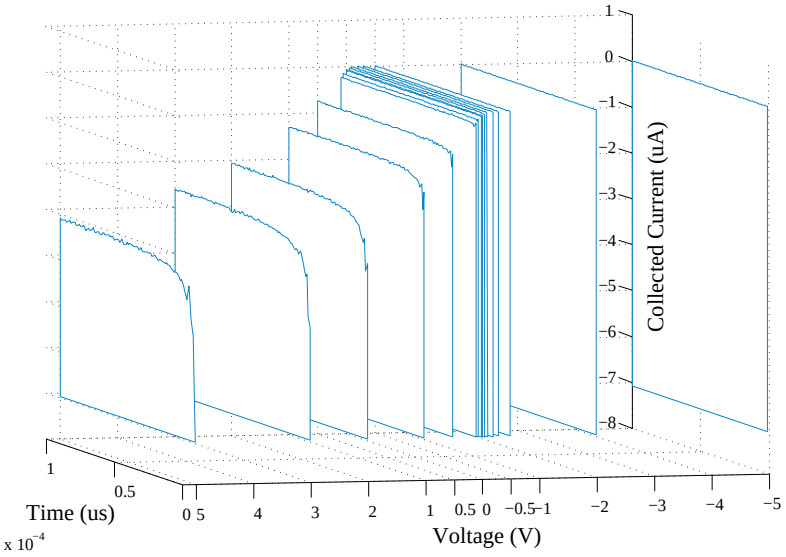

Figure 6.17: *Sampling of the current in time to reconstruct the sweep via the V values listed in Table 6.13.*

Sphere drift PIC, numerical speed up = 13

Simulation runs implementing a CAD model of Figure 5.4 a whose geometrical properties are detailed in Table 5.4.

Table 6.14: *Imposed parameters, Sphere.*

Parameter		Imposed Value	
Electron temperature	T_e	0.05	eV
Ion temperature	T_i	0.05	eV
Electron density	n_e	$1 \cdot 10^{12}$	m^{-3}
Ion density	n_i	$1 \cdot 10^{12}$	m^{-3}
Drift velocity	v_d	7800	m/s
Debye length	λ_D	1.7	mm
Potential range	Φ	*Table*	V
Sphere radius	r_P	3.8	mm
Simulation box diameter	$b_\varnothing$	38	mm
Numerical speed up		13	
Number of tetrahedrons		$2.5 \cdot 10^5$	
Number of macro-particles		$1.25 \cdot 10^6$	

Table 6.15: *Average collected current for various bias voltages range, Sphere and Stub.*

Voltage (V)	2.0	1.0	0.5	0.0	-0.01
Current (μA)	-34.12045	-18.74421	-10.2878	-0.95881	-0.78845
Voltage (V)	-0.05	-0.2	-5		
Current (μA)	- 0.33366	0.03618	0.11114		

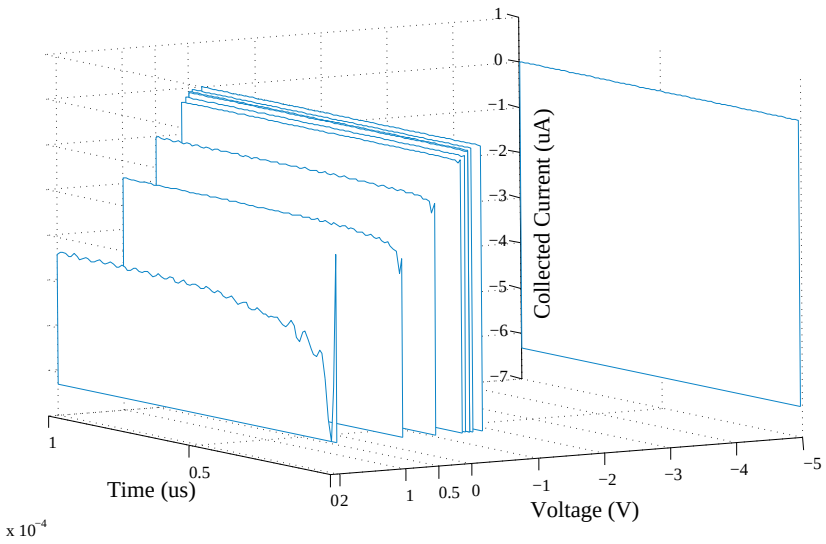

Figure 6.18: *Sampling of the current in time to reconstruct the sweep via the V values listed in Table 6.15.*

Stub PIC

Simulation runs implementing a CAD model of Figure 5.4 b whose geometrical properties are detailed in Table 5.4.

Table 6.16: *Imposed parameters, Sphere.*

Parameter		Imposed Value	
Electron temperature	T_e	0.05	eV
Ion temperature	T_i	0.05	eV
Electron density	n_e	$1 \cdot 10^{12}$	m^{-3}
Ion density	n_i	$1 \cdot 10^{12}$	m^{-3}
Debye length	λ_D	1.7	mm
Potential range	Φ	*Table*	V
Stub radius	r_S	1.5	mm
Stub length	l_S	30	mm
Simulation box diameter (max extension)	$b_\varnothing$	38	mm
Numerical speed up		42	
Number of tetrahedrons		$2.5 \cdot 10^5$	
Number of macro-particles		$1.25 \cdot 10^6$	

Table 6.17: *Average collected current for various bias voltages range, Sphere and Stub.*

Voltage (V)	5.0	3.0	2.0	1.0	0.5	0.1	0.05	0.0
Current (μA)	-33.855	-24.04242	-18.46331	-12.01453	-7.48714	-3.51832	-2.69521	-1.59446
Voltage (V)	-0.01	-0.05	-0.1	-0.2	-0.3	-0.5	-1.0	-2.0
Current (μA)	-1.33824	-0.61078	-0.23888	0.00877	0.03088	0.04753	0.07271	0.11244
Voltage (V)	-3.0	-5						
Current (μA)	0.14777	0.20597						

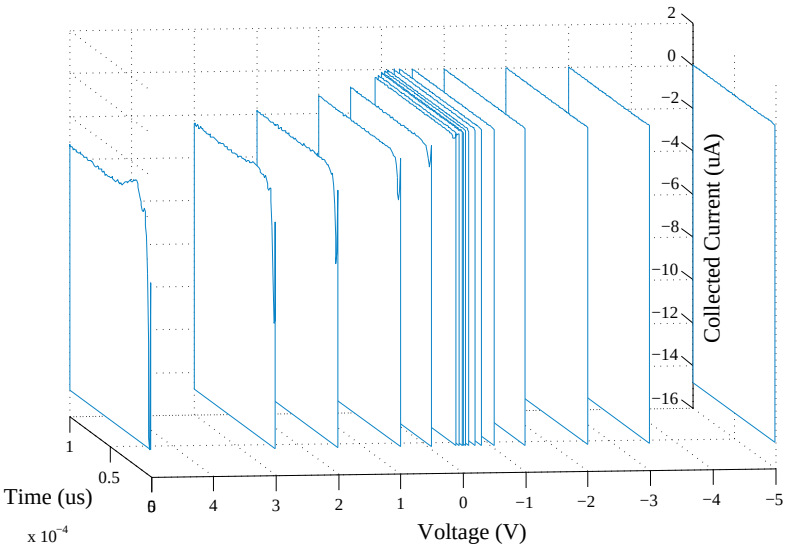

Figure 6.19: *Sampling of the current in time to reconstruct the sweep via the V values listed in Table 6.17.*

6.4.2 Collected current for average density plasma

Collected current for $\lambda_D = 10\,\text{mm}$ in simulation runs implementing the CAD model of Chapter 5.

Sphere PIC

Simulation runs implementing a CAD model of Figure 5.5 whose geometrical properties are detailed in Table 5.5.

Table 6.18: *Imposed parameters, Sphere.*

Parameter		Imposed Value	
Electron temperature	T_e	0.2	eV
Ion temperature	T_i	0.2	eV
Electron density	n_e	$1 \cdot 10^{12}$	m^{-3}
Ion density	n_i	$1 \cdot 10^{12}$	m^{-3}
Drift velocity	v_d	7800	m/s
Debye length	λ_D	10	mm
Potential range	Φ	*Table*	V
Sphere radious	r_P	3.8	mm
Simulation box diameter	$b_\oslash$	95	mm
Numerical speed up		42	
Number of tetrahedrons		$6 \cdot 10^5$	
Number of macro-particles		$3 \cdot 10^6$	

Table 6.19: *Average collected current for various bias voltages range, Sphere.*

Voltage (V)	5.0	3.0	2.0	1.75	1.5	1.25	1.0
Current (μA)	-5.34149	-3.31681	-2.31	-2.051	-1.7761	-1.517	-1.25643
Voltage (V)	0.75	0.5	0.25	0.0	-0.1	-0.25	-0.5
Current (μA)	1.00648	0.74268	0.47404	-0.20925	-0.12815	0.05768	-0.01424
Voltage (V)	-0.75	-1.0	-2.0	-3.0	-5.0		
Current (μA)	-0.00187	0.00640	0.01456	0.02071	0.03315		

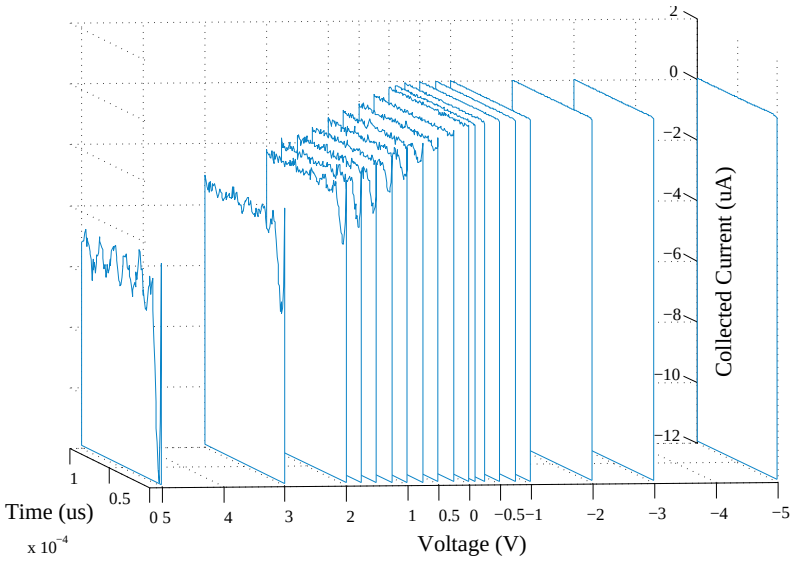

Figure 6.20: *Sampling of the current in time to reconstruct the sweep via the V values listed in Table 6.19.*

Sphere and stub PIC

Simulation runs implementing a CAD model of Figure 5.6 whose geometrical properties are detailed in Table 5.6

Table 6.20: *Imposed parameters, Sphere-Stub.*

Parameter		Imposed Value	
Electron temperature	T_e	0.2	eV
Ion temperature	T_i	0.2	eV
Electron density	n_e	$1 \cdot 10^{11}$	m^{-3}
Ion density	n_i	$1 \cdot 10^{11}$	m^{-3}
Debye length	λ_D	1.7	mm
Potential range	Φ	*Table*	V
Sphere radious	r_P	3.8	mm
Stub radius	r_S	1.5	mm
Stub length	l_S	30	mm
Simulation box diameter (max extension)	$b_\varnothing$	95	mm
Numerical speed up		42	
Number of tetrahedrons		$1.25 \cdot 10^5$	
Number of macro-particles		$6.25 \cdot 10^6$	

Table 6.21: *Average collected current for various bias voltages range, Sphere.*

Voltage (V)	5.0	3.0	2.0	1.75	1.5	1.25	1.0
Current (μA)	-3.86281	-2.55882	-1.80248	-1.62565	-1.43859	-1.25821	-1.05659
Voltage (V)	0.75	0.5	0.25	0.0	-0.1	-0.25	-0.5
Current (μA)	-0.85444	0.62414	0.41576	-0.19202	-0.11539	-0.05253	-0.01407
Voltage (V)	-0.75	-1.0	-2.0	-3.0	-5.0		
Current (μA)	-0.00002	0.00534	0.01186	0.01652	0.02521		

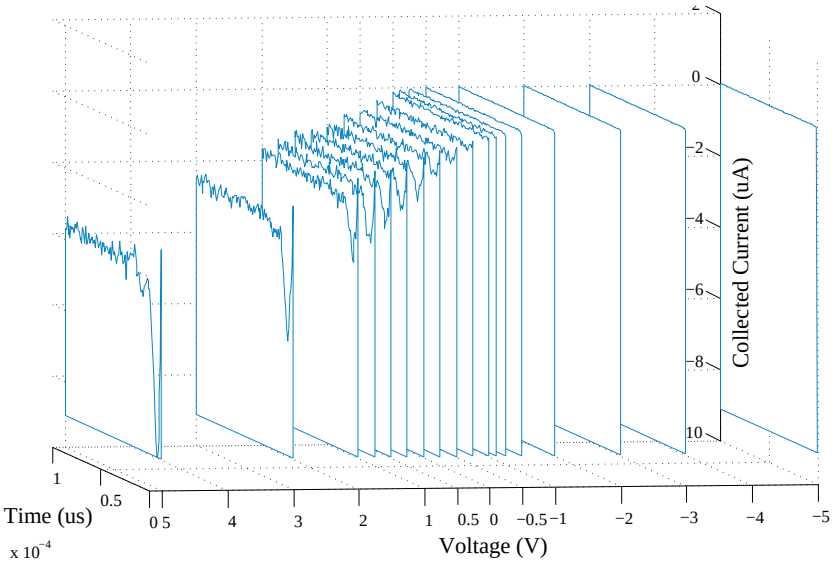

Figure 6.21: *Sampling of the current in time to reconstruct the sweep via the V values listen in Table 6.21.*

Sphere B PIC, larger simulation box

Simulation runs implementing a CAD model of Figure 5.7 whose geometrical properties are detailed in Table 5.7

Table 6.22: *Imposed parameters, Sphere.*

Parameter		Imposed Value	
Electron temperature	T_e	0.2	eV
Ion temperature	T_i	0.2	eV
Electron density	n_e	$1 \cdot 10^{12}$	m^{-3}
Ion density	n_i	$1 \cdot 10^{12}$	m^{-3}
Drift velocity	v_d	7800	m/s
Debye length	λ_D	10	mm
Potential range	Φ	*Table*	V
Sphere radious	r_P	3.8	mm
Simulation box diameter	$b_\varnothing$	138	mm
Numerical speed up		42	
Number of tetrahedrons		$3.5 \cdot 10^5$	
Number of macro-particles		$1.75 \cdot 10^6$	

Table 6.23: *Average collected current for 1V and 2V bias voltages, Sphere.*

Voltage (V)	2.0	1.0
Current (μA)	-2.30423	-1.25542

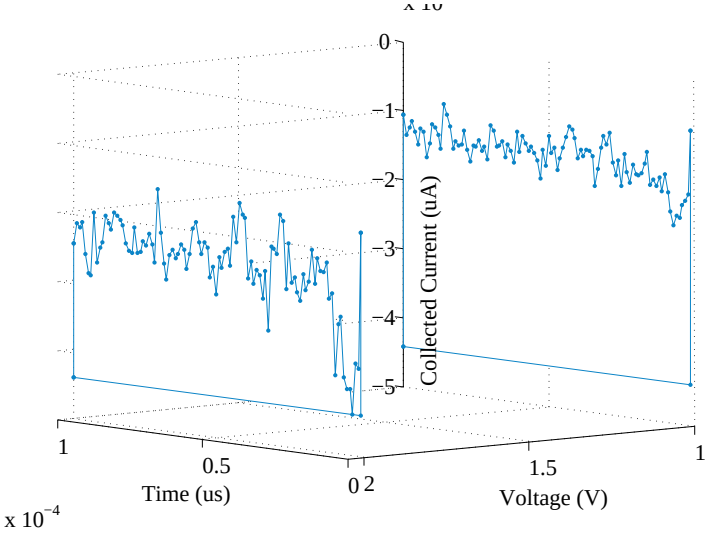

Figure 6.22: *Sampling of the current in time to reconstruct the sweep via the V values listen in Table 6.23.*

Sphere and stub drift PIC

Simulation run implementing a CAD model of Figure 5.7 whose geometrical properties are detailed in Table 5.7.

Table 6.24: *Imposed parameters, Sphere-Stub.*

Parameter		Imposed Value	
Electron temperature	T_e	0.2	eV
Ion temperature	T_i	0.2	eV
Electron density	n_e	$1 \cdot 10^{11}$	m^{-3}
Ion density	n_i	$1 \cdot 10^{11}$	m^{-3}
Drift velocity	v_d	7800	m/s
Debye length	λ_D	1.7	mm
Potential range	Φ	*Table*	V
Sphere radious	r_P	3.8	mm
Stub radius	r_S	1.5	mm
Stub length	l_S	30	mm
Simulation box diameter (max extension)	$b_\oslash$	95	mm
Numerical speed up		42	
Number of tetrahedrons		$1.25 \cdot 10^5$	
Number of macro-particles		$6.25 \cdot 10^6$	

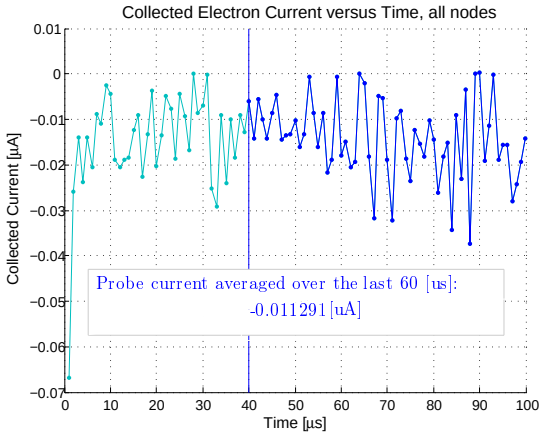

Figure 6.23: *Current to Sphere for* $-0.6\,V$ *biased sphere and stub.*

Full probe-simplified s/c model drift PIC

Simulation run implementing a CAD model of Figure 5.8 which geometrical properties are detailed in Table 5.8.

Table 6.25: *Imposed parameters, full probe and simplified s/c portion.*

Parameter		Imposed Value	
Electron temperature	T_e	0.2	eV
Ion temperature	T_i	0.2	eV
Electron density	n_e	$1 \cdot 10^{11}$	m^{-3}
Ion density	n_i	$1 \cdot 10^{11}$	m^{-3}
Drift velocity	v_d	7800	m/s
Debye length	λ_D	1.7	mm
Potential range	Φ	*Table*	V
Sphere radious	r_P	3.8	mm
Stub radius	r_S	1.5	mm
Stub length	l_S	30	mm
Simulation box diameter (max extension)	$b_\oslash$	95	mm
Numerical speed up		42	
Number of tetrahedrons		$1.25 \cdot 10^5$	
Number of macro-particles		$6.25 \cdot 10^6$	

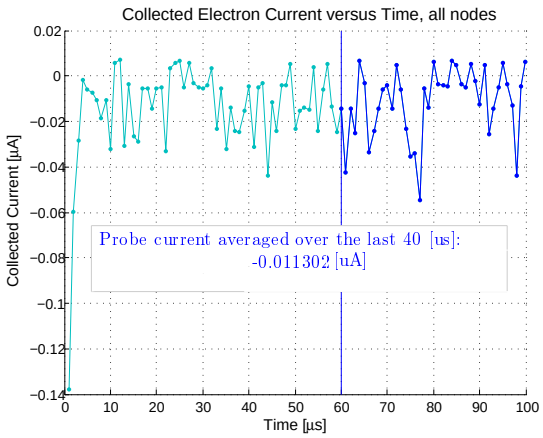

Figure 6.24: *Current to Sphere for* $-0.6\,V$ *biased sphere, stub, boom and simplified s/c portion.*

6.4.3 Stabilized values of collected species current

Table 6.26 for $\lambda_D \approx 1.7\,\text{mm}$ and Table 6.27 for $\lambda_D \approx 10\,\text{mm}$ resume all the stabilized values of collected currents. By considering these two tables, I-V-t maps are simplified to I-V maps to enable data discussion; curves are plotted in the following chapter.

Table 6.26: *Collected current for the probe's models set.*

Voltage (V)	Sphere PIC (μA)	Sphere MB electrons (μA)	Sphere-Stub PIC (μA)	Sphere-Stub R (μA)	Sphere-Stub R Drift PIC (μA)	Sphere-Stub V PIC (μA)	Sphere V PIC (μA)	Stub PIC (μA)
5.0	−47.89551		−31.07232	-30.67928		-32.07453		-33.855
3.0	−32.96122		−22.59314			-26.00494		-24.04242
2.0	−24.16883		−17.69486	-17.74597	−21.48771	-20.70815	−34.12045	-18.46331
1.5	−19.39611							
1.0	−14.27363		−11.00537	-11.01931	−13.09374	-12.88028	−18.74421	-12.01453
0.5	−8.50657		−6.75019			-7.48714	−10.2878	-7.48714
0.1	−2.89158		−2.36675	-2.39615		-2.31279		-3.51832
0.05	−2.01414		−1.68863	-1.68952		-1.59498		-2.69521
0.0	−1.06293	-1.06181	−0.91979			-0.83596	−0.95881	-1.59446
-0.01	−0.87214	-0.86737	−0.77635			-0.69708	−0.78845	-1.33824
-0.05	−0.40007	-0.38058	−0.34783	-0.38009		-0.29971		-0.61078
-0.1	−0.14019	-0.12616	−0.12932			-0.08027		-0.23888
-0.2	0.00381	0.00818	−0.00202			0.03642	−0.33366	0.00877
-0.3	0.03201	0.03355	0.02479			0.05217		0.03088
-0.5	0.06321	0.05005			0.056591	0.05681		0.04753
-1.0	0.08471	0.08406	0.06577					0.07271
-1.5		0.08508						
-2.0		0.14331	0.10313			0.06895		0.11244
-3.0	0.19063		0.13064					0.14777
-5.0		0.28889	0.17946			0.09408	0.11114	0.20597

Table 6.27: *Collected current for the probe's models set.*

Voltage (V)	Sphere PIC (μA)	Sphere B PIC (μA)	Sphere-Stub PIC (μA)	Sphere-Stub drift PIC (μA)	Full probe PIC (μA)
5.0	−5.34149		−3.86281		
3.0	−3.31681		−2.55882		
2.0	−2.31	2.30423	−1.80248		
1.75	−2.051		−1.62565		
1.5	−1.7761		−1.43859		
1.25	−1.517		−1.25821		
1.0	−1.25643	-1.25542	−1.05659		
0.75	−1.00648		−0.85444		
0.5	−0.74268		−0.62414		
0.25	0.47404		−0.41576		
0.0	−0.20925		−0.19202		
-0.1	−0.12815		−0.11539		
-0.25	−0.05768		−0.052533		
-0.5	−0.01424		−0.01407		
-0.6				-0.01130	−0.01129
-0.75	0.00187		−0.00002		
-1.0	0.00640		0.00534		
-2.0	0.01456		0.01186		
-3.0	0.02071		0.01652		
-5.0	0.03315		0.02521		

7

Results & Conclusions

Stabilized current values resumed in Chapter 6 are here plotted in terms of I-V characteristics. Collected currents for the models Sphere, Sphere-Stub and Sphere-Stub in flowing plasma are confronted for the two sets of ambient parameters. The modelled plasma measurements for all the implemented probe geometries is resumed in a single plot for each case. Figures 7.2 a and 7.3 a refers to $\lambda_D \approx 1.7\,\text{mm}$ while Figures 7.2 b and 7.3 b refers to $\lambda_D \approx 10\,\text{mm}$.

7.1 Spherical case

7.1.1 Overview of comparisons

The current collected by the spherical probes within PIC simulations is compared to the OML limit deduced in Chapter 2 and to the Laframboise current parametrized in Chapter 3. As the ratio λ_D/r_p increases, the current collected by the probe converges to the OML limit [1]. As the ratio decreases, the current collection decreases. This occurs because the bump in the effective potential shown by Equation 2.13 that prevents particles to reach the surface [6].

7.1.2 Sphere PIC simulations vs Laframboise's results

For negative bias voltages, Laframboise's current mirrors the Spis current with a confidence level controlled by the metafit of polynomial coefficients (Section

3.4.2, Chapter 3) and by the noise level resulting from the kinetic resolution of the 5 macroparticles/cell. PIC and analytical results reproduce each other along the whole bias range for the less dense case as the curves relative deviation is of about 1.7 % at 5 V and 0.4 % at 2 V, Figure 7.2 b. In the high dense scenario, the Spis I-V curve loses 3.5 % of current at 2 V and about the 10 % at 5 V, Figure 7.2 a. This last situation pushes for further considerations concerning weather extending or not the reliability of the simulations to 5 V. On one hand, Figure 6.2 of Section 6.2 in Chapter 5 shows that 2 V is the bias voltage at which the remainder of the potential pairs the electron temperature at the boundaries. It follows that the effects of box dimensions can influence the Spis solution as the sheath grows and introduces an undesired deviations from the LF curve. On the other hand, Figure 7.4 and Figure 7.5 show that this deviation starts to appear at low bias voltages where the box effects are less relevant as the box fully contains the sheath. The digression starts just after the floating potential and propagates at low bias where the potential remainder drops below the electron temperature. Because such digression develops homogeneously from the floating potential to 5 V, it is not univocally possible to attribute its cause to boundary effects. One alternative explanation is that the effect is due to numerical error introduced by insufficient mapping of the electric field caused by to too few macroparticles and/or tetrahedra because the E-field is modelled as constant within each tetrahedron. These arguments are based on the discussions of Section 5.1.3 and Section 5.2.2 in Chapter 5. This situation would introduce numerical errors in the solutions along the whole bias range and it would explain the constant deviation.

7.1.3 Sphere PIC simulation vs OML limit

The current collected by the spherical probes within PIC simulations is compared to the OML limit to quantify the decrease in current collection from the ideal case. The amount of deviation from the OML limit is 3.5 % at 5 V and 1.5 % at 1 V for the less dense plasma. This result is expected as these simulations have been designed to closely reproduce the results of the OML theory at low voltages, Section 5.1.2, Chapter 5. Also as expected, the OML curve does not emulate the simulated current behavior in the high density scenario and the collected current is half of the ideal case. From a comparison between the two types of simulations it follows that, as the plasma coditions shifts from $\lambda_D \approx 1\,\text{mm}$ to $\lambda_D \approx 10\,\text{mm}$, the sheath becomes less effective in particle shielding and the collected current

converges towards the OML limit.

7.2 Sphere-Stub

The stub surfaces is significantly larger than in the sphere as they are respectively $\sim 283\,mm^2$ and $\sim 180\,mm^2$. Their independent contributions in collected current are compared in Figure 7.1.

The probe of the Sphere-Stub model collects less current than the Sphere model, we interpret this as the stub attracts particles whose trajectory would have been captured by the probe, Figures 7.2 and 7.3.

7.3 Sphere-Stub drift

This scenario investigates the effects of non negligible ion drift velocity and it is simulated for high dense plasma only because of the relevant digression from the OML limit. The sheath, streatched by the flowing plasma, is less effective in particles shielding than stationary situations because the kinetic energy of incoming particles overcomes the potential barrier represented by the bump in potential induced by the sheath discussed in Section 2.8.2, Chapter 2. At bias values higher than the equivalent kinetic energy of an ion in the flow (4 eV for O^+), we can expect that the collected current should be about the same as in the stationary case. This is verified in Figure 7.2 a; at 5 V where the collected current in the flowing plasma and plasma at rest cases is almost the same.

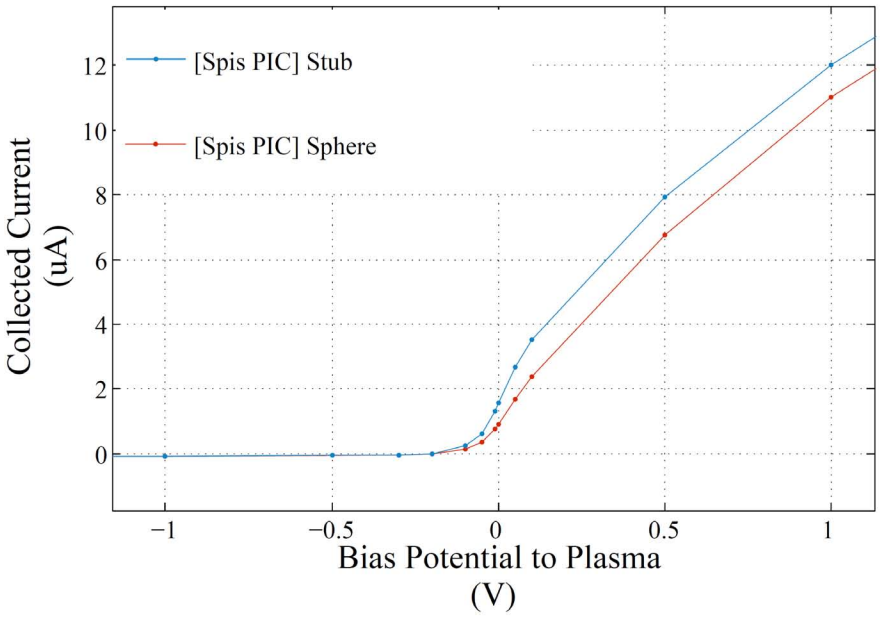

Figure 7.1: *Single element contribution in current collection in the* $\lambda_D \approx 10\,mm$ *case.*

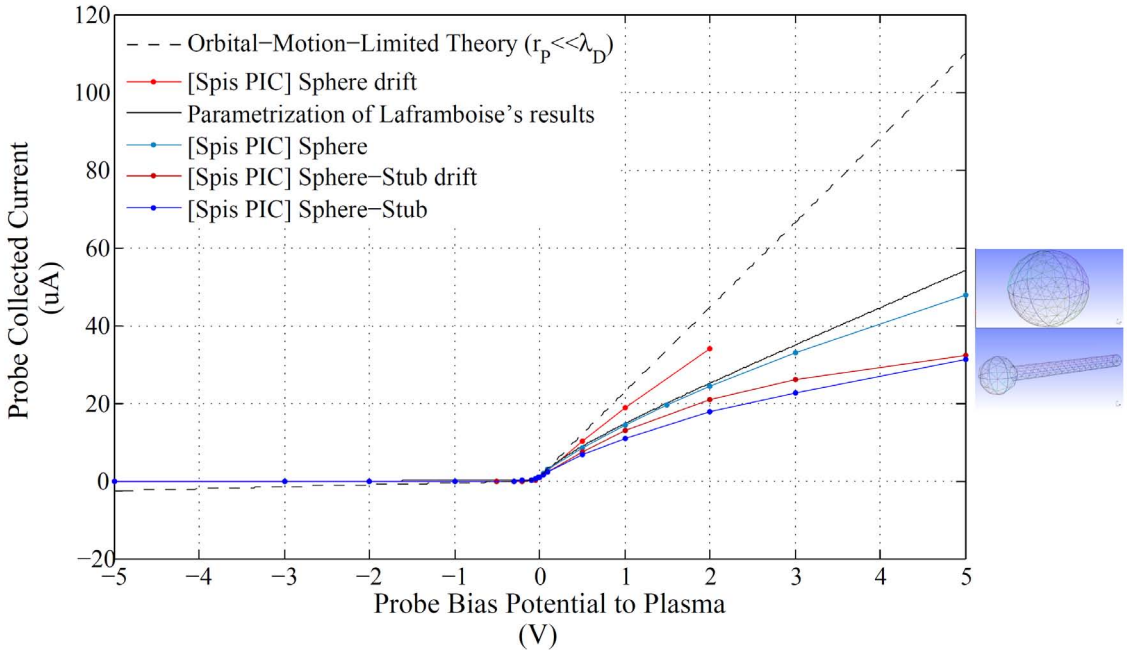

(a) $\lambda_D \approx 1.7\,\text{mm}$.

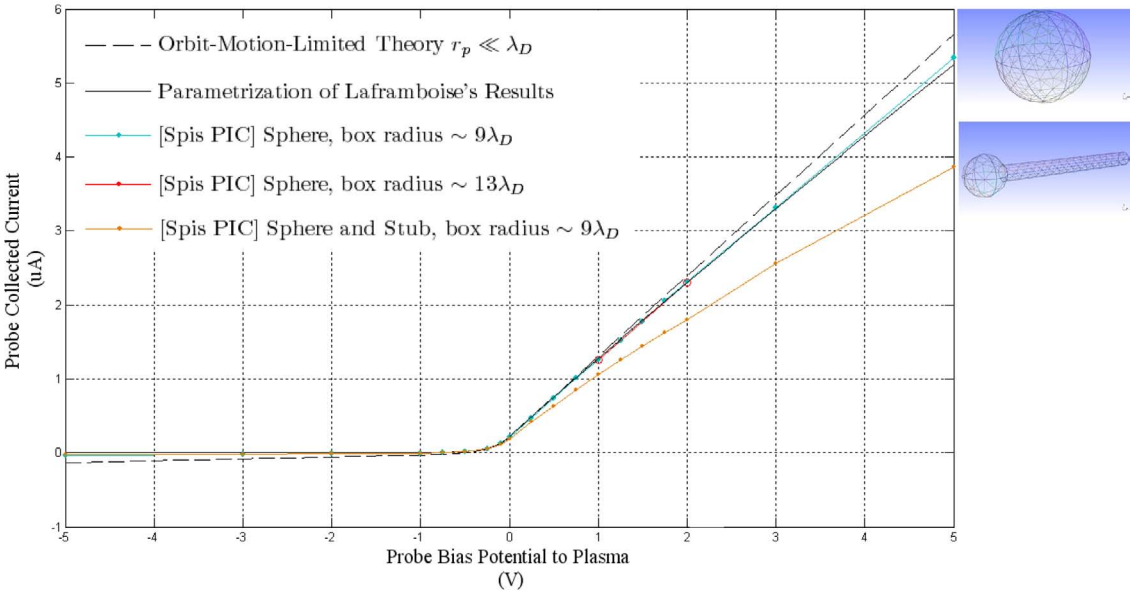

(b) $\lambda_D \approx 10\,\text{mm}$.

Figure 7.2: *Spis simulations of I-V characteristics for the Swarm LP (Sphere and Sphere-Stub) and comparisons to parametrized LF results [1] and to the OML limit.*

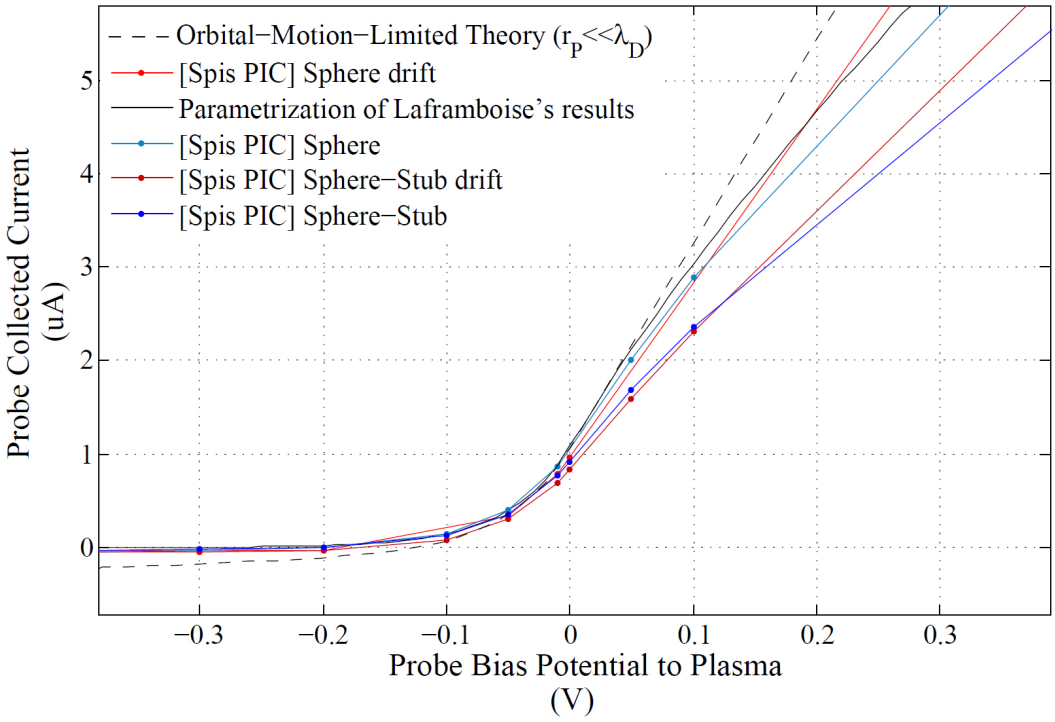

(a) $\lambda_D \approx 1.7\,\text{mm}$ case.

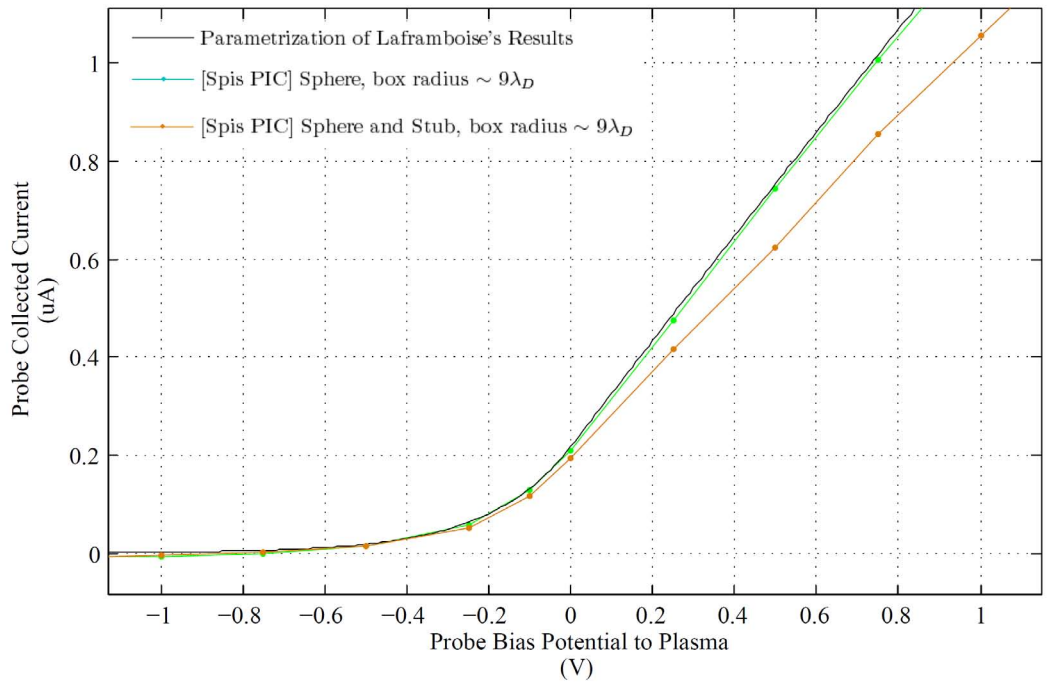

(b) $\lambda_D \approx 10\,\text{mm}$ case.

Figure 7.3: *Details of the exponential regions.*

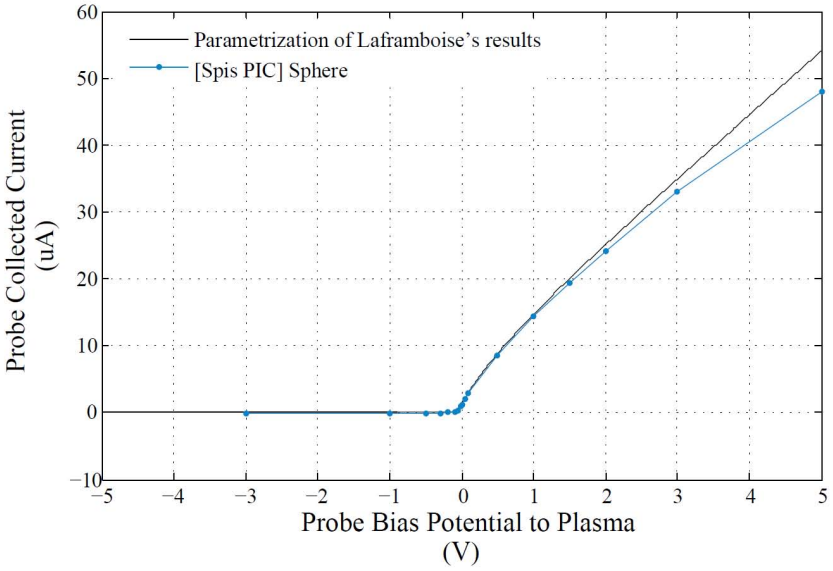

Figure 7.4: $\lambda_D \approx 1\,mm$*: Spis vs parametrized LF results [1],* $V = [-5, +5]$.

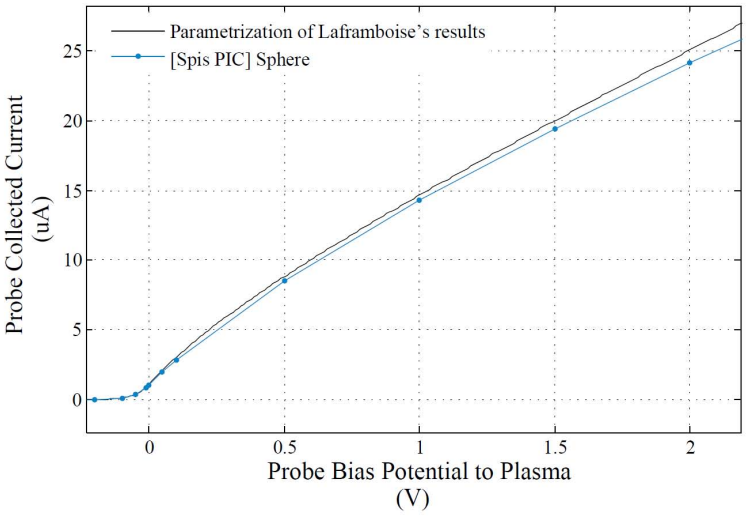

(a) Close-in V = $[-1, +2]$.

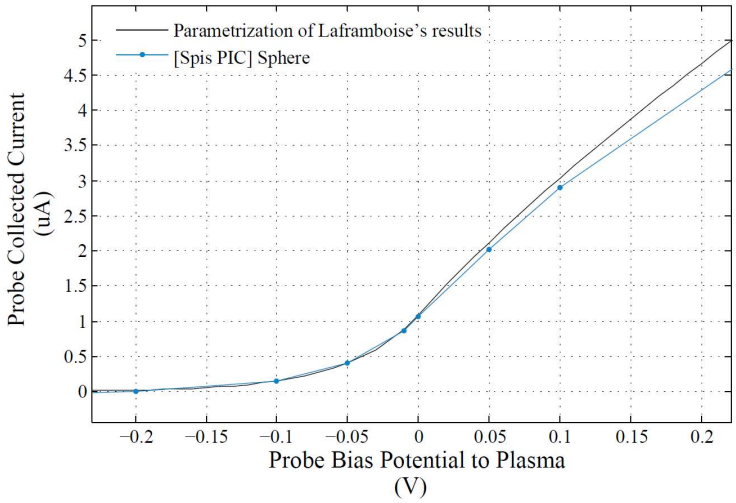

(b) Close-in V = $[-0.2, +0.2]$.

Figure 7.5: $\lambda_D \approx 1\,mm$*: Spis vs parametrized LF results [1].*

7.4 Sheath structures at different bias voltages

7.4.1 Sphere and Sphere-Stub cases

Electric potential and densities of species are shown for the flowing plasma scenario. The models are the Sphere and the Sphere-Stub in the high density case and the full probe in the low density scenario.

The first example concerns the sphere biased at 2 V, Figure 7.6 shows a clear demarcation between the sheath and the relatively[1] unperturbed plasma within the box. Electrons are absorbed in the ram side where the ions are shielded from the back side. The focusing of ions around the edge of the wake enhances locally the charge density and the wake structure contributes in shaping the structure of the potential.

The Sphere-Stub model is shown at five bias voltages: ±5 V, ±0.5 V and 0 V, Figures 7.7-7.11. An horizontal comparison among the examples shows the dependence of the hypersonic conic angle on the applied voltage hence on the sheath size. The cone aperture angle is broader as the imposed voltage grows and it is sligthly negative in the 0 V case because of the thermal motion of the electrons that induces a filling effect at the wake boundaries, Figures 7.7-7.9. At 0 V the bias effects are neglected and the colours show the unperturbed plasma throughout the box and outside the wake.

At negative bias, the focusing of ions around the edge is the predominant effect. This makes the wake much less marked and it effects less the potential.

The particles distribution around the probe does not reflect the potential distribution which is symmetrical due to the higher electron mobility with respect of the ions, Figures 7.10-7.11.

[1] See discussion about the potential remainer in Section 6.2.1

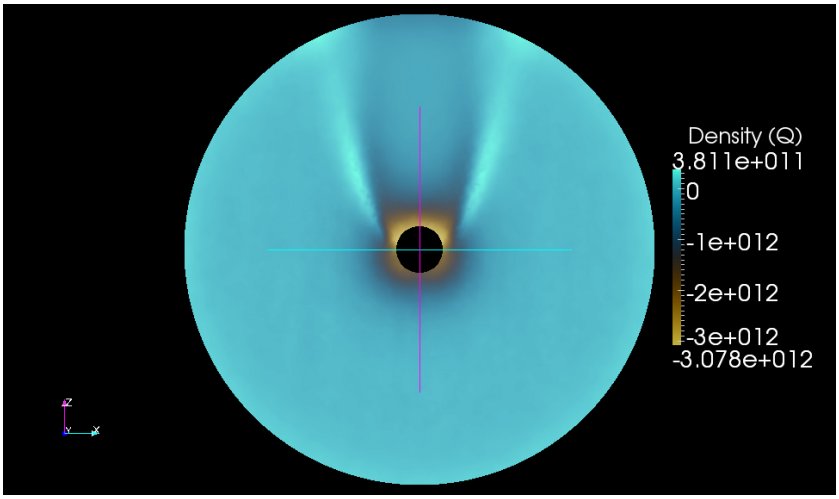

(a) Charge density.

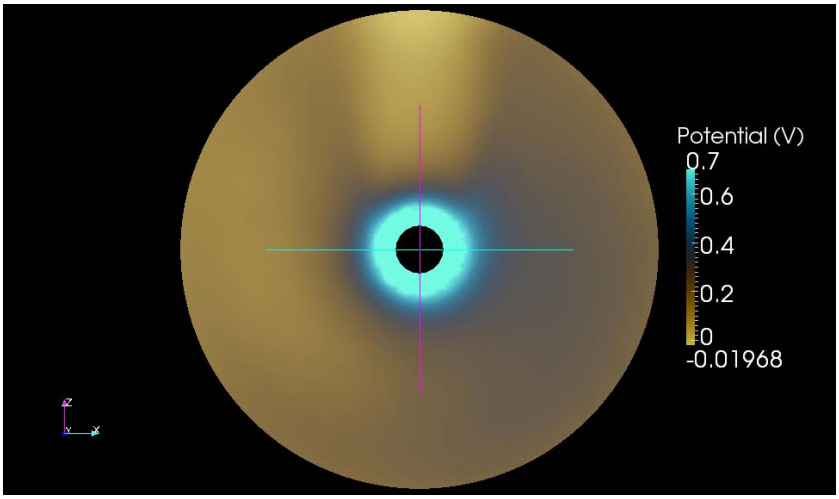

(b) Rescaled potential.

Figure 7.6: 2 *V bias potential on Sphere model and flowing plasma,* $\lambda_D \approx 1.7\,mm$.

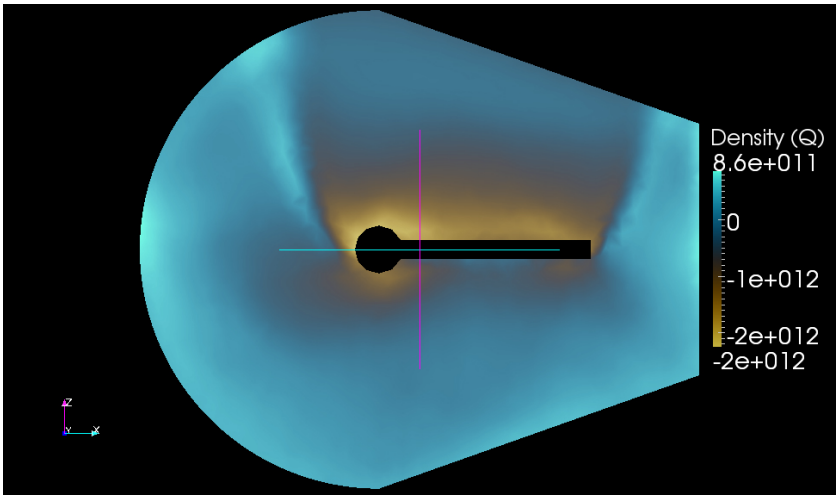

(a) Charge density.

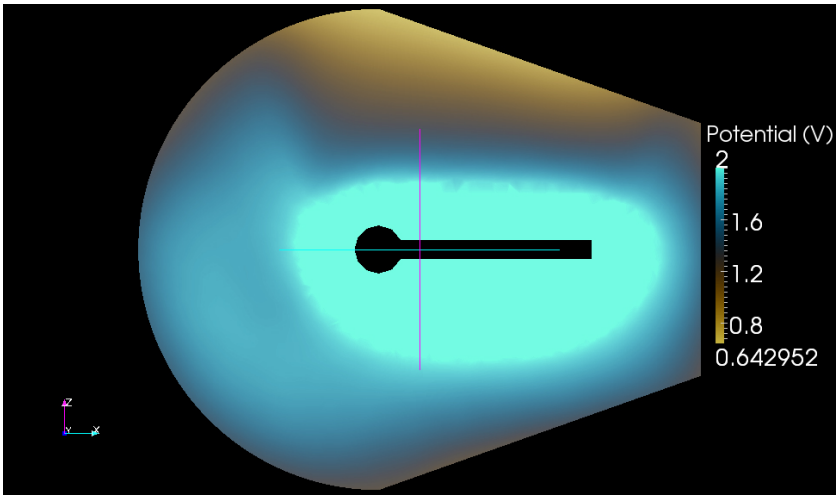

(b) Rescaled potential.

Figure 7.7: 5 *V bias potential on Sphere-Stub model and flowing plasma,* $\lambda_D \approx 1.7\,mm$.

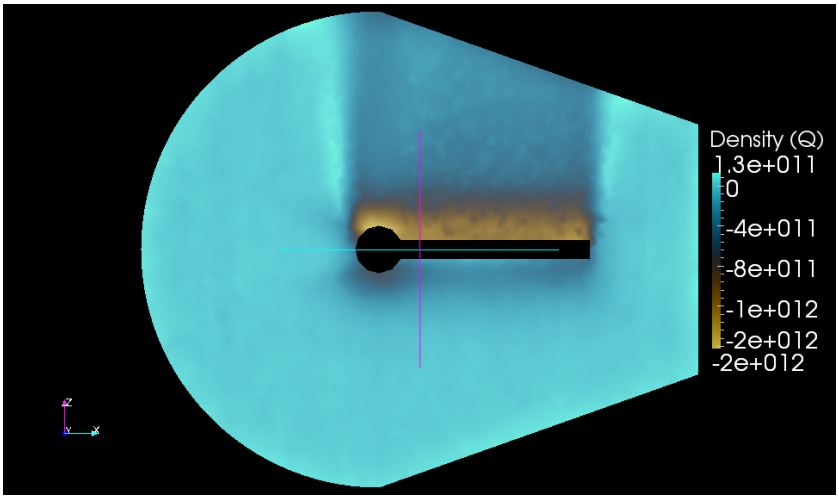

(a) Charge density.

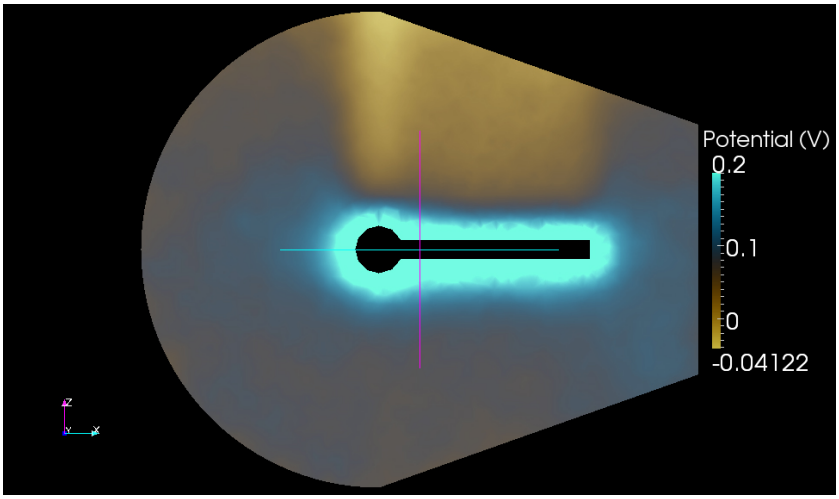

(b) Rescaled potential.

Figure 7.8: 0.5 *V bias potential on Sphere-Stub model and flowing plasma,* $\lambda_D \approx 1.7\,mm$.

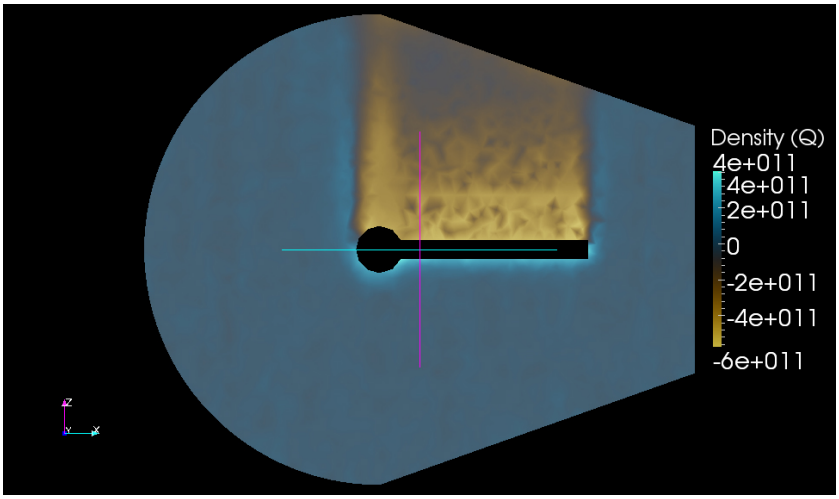

(a) Charge density.

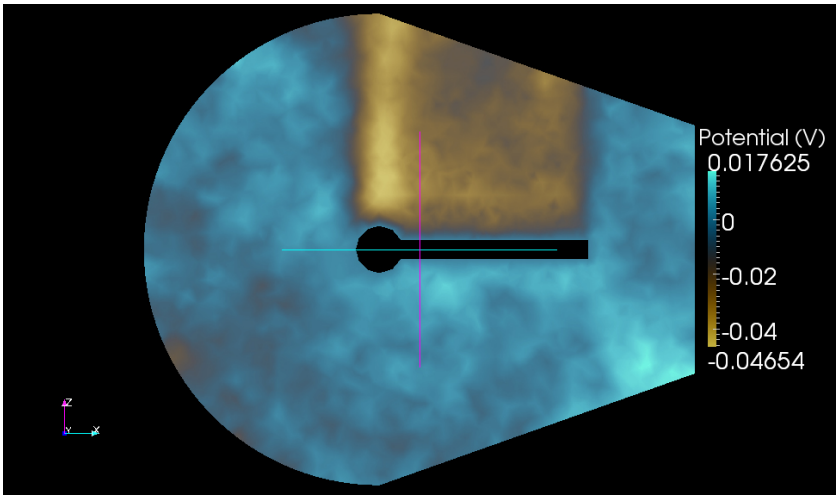

(b) Potential.

Figure 7.9: $0\,V$ *bias potential on Sphere-Stub model and flowing plasma,* $\lambda_D \approx 1.7\,mm$.

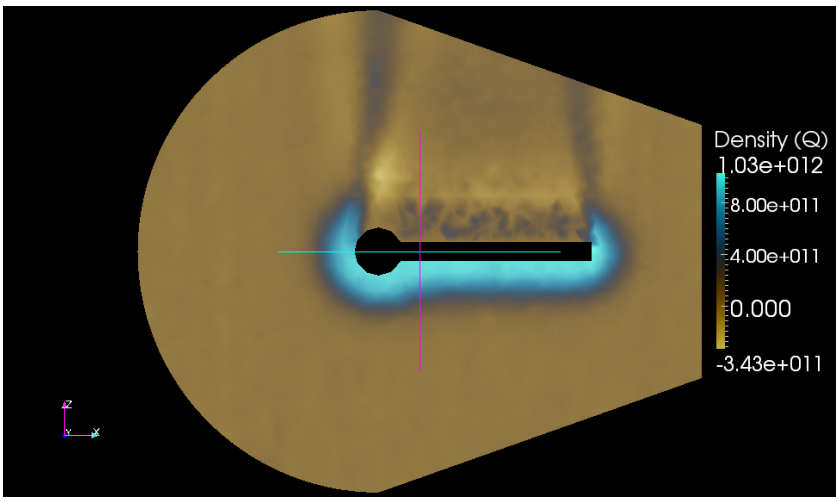

(a) Charge density.

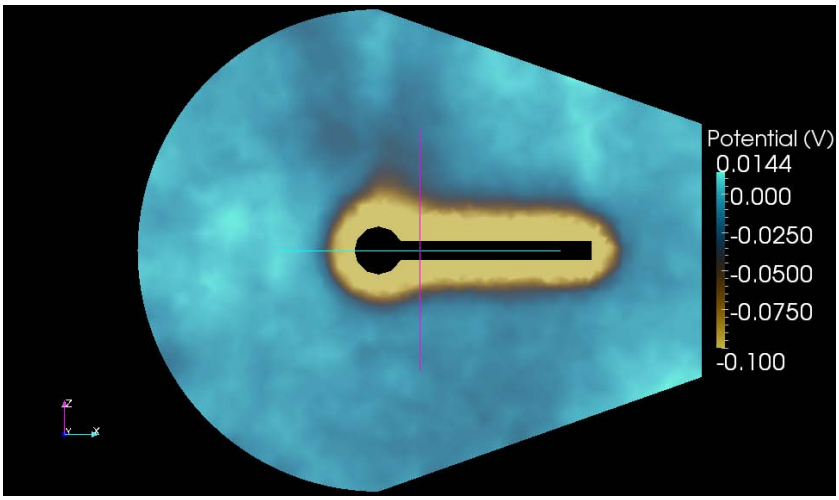

(b) Rescaled potential.

Figure 7.10: $-0.5\,V$ *bias potential on Sphere-Stub model and flowing plasma,* $\lambda_D \approx 1.7\,mm$.

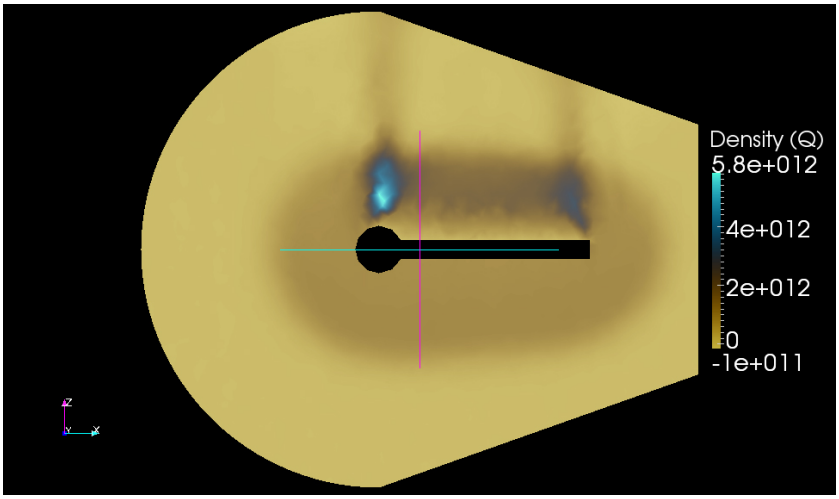

(a) Charge density.

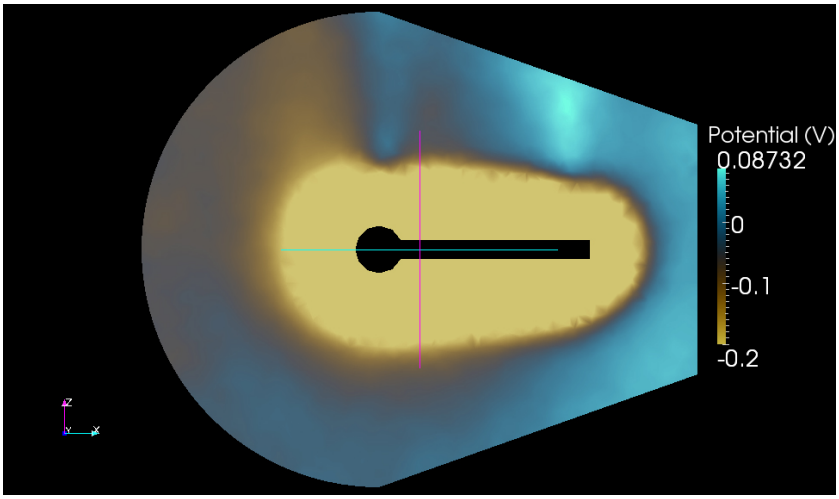

(b) Rescaled potentia.

Figure 7.11: *$-5\,V$ bias potential on Sphere-Stub model and flowing plasma, $\lambda_D \approx 1.7\,mm$.*

7.4.2 Full probe case

The near-spacecraft environment is complex due to higher applied voltages and to the presence of the wake. In order to verify the effects of a portion of spacecraft on the wake a single simulation has been carried out. Figures 7.12 and 7.13 show the sheath and the wake structures of the full probe attached to a simplified s/c portion both biased at the floating potential which is set to $-0.6\,\mathrm{V}$. The potential structures are compared to the high density case for similar voltages and the related smaller boxes are included in the pictures. The sheaths around the instruments are comparable and the s/c polarized area does not interfere with the probe area as the electron density increases due to the presence of the wall only around the boom, Figure 7.13 a. Figure 7.13 b shows that the ions charge density creates a wake behind the probe and the spacecraft support.

Because the sheath is broader in the low dense plasma, the perturbing effect of peripheral s/c walls are not expected to influence the current collection also in the high dense scenario, in particular at low voltages.

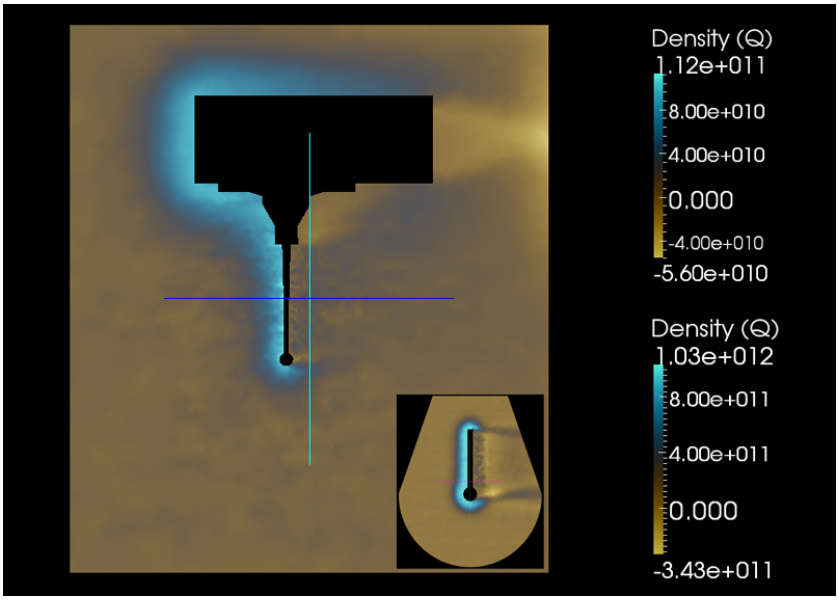

(a) Charge density.

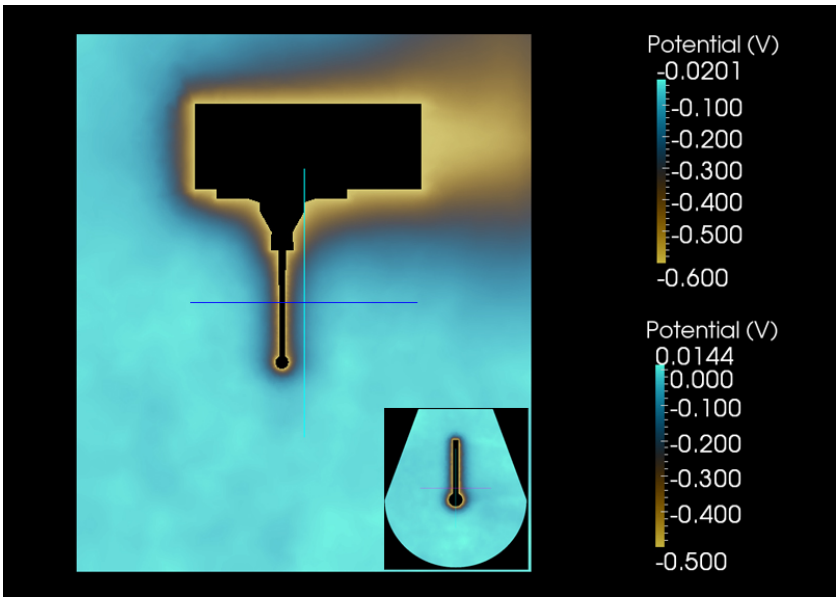

(b) Potentia.

Figure 7.12: $-0.6\,V$ *bias potential and flowing plasma. Comparison between full probe model and s/c portion* ($\lambda_D \approx 10\,mm$) *and Sphere-Stub model* ($\lambda_D \approx 1.7\,mm$).

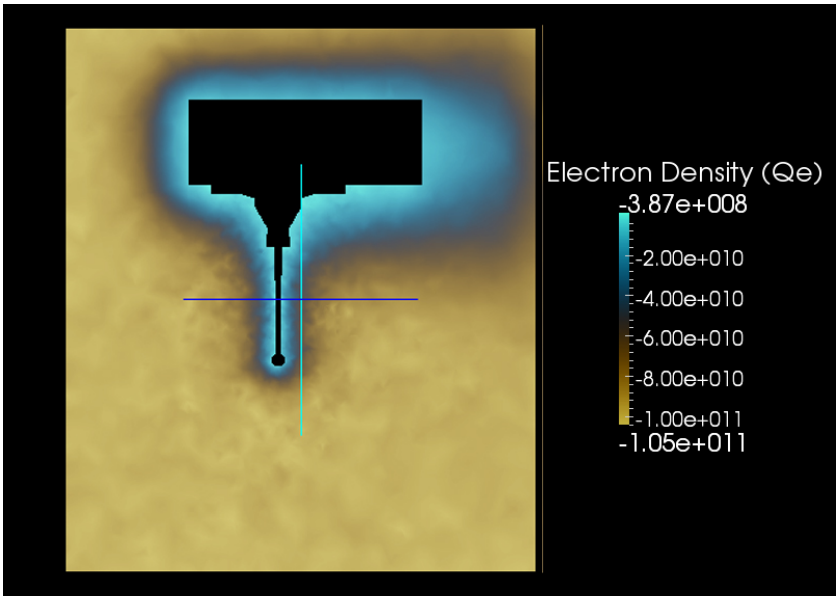

(a) Electrons charge density.

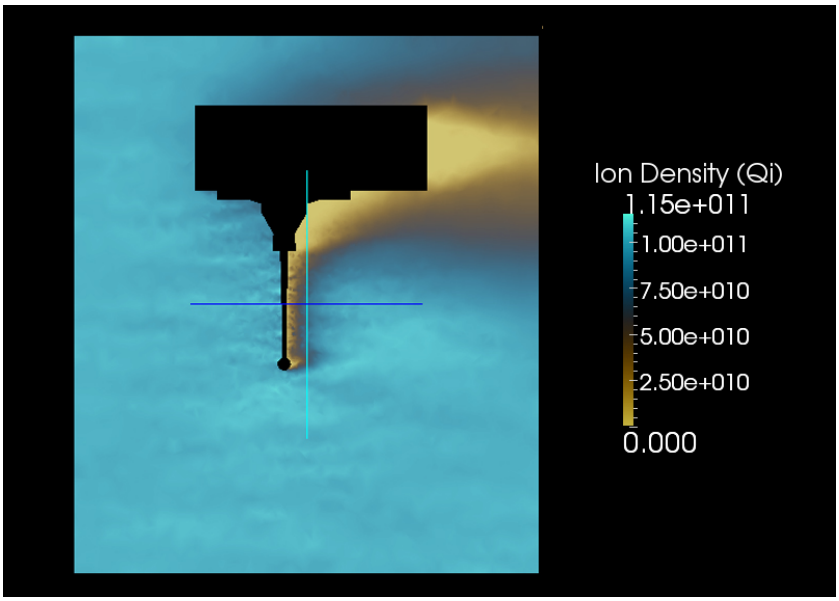

(b) Ions charge density.

Figure 7.13: $-0.6\,V$ *bias and flowing plasma, full probe model and s/c portion.*

7.5 Conclusions and future work

The I-V characteristics show a good matching between numerical solution obtained from different methods. Since the simulations do not include the magnetic field, a full study may need to be performed. A larger amount of macroparticles should be included to avoid time consuming horizontal comparisons. If the hardware does not support enough macroparticles, it occurs a lack of statistics that might result into too few particles collection, the problem can be partially solved by backtracking particles injected at the boundaries.

When the assumption that no ions are absorbed by the probe is reasonable, a light or very light ion mass can be implemented in order to speed up the simulation process. Maxwell Boltzmann simulations, when can be applied, are appropriate for the double purpose to speed up the simulations at negative bias voltages and for looking at the ”big picture” of larger portion of the spacecraft as less memory consuming.

BIBLIOGRAPHY

[1] J. G. Laframboise. *Theory of Spherical and Cylindrical Langmuir Probes in a Collisionless, Maxwellian Plasma at Rest.* PhD thesis, University of Toronto (Canada), 1966.

[2] I. Langmuir and K. T. Compton. Electrical Discharges in Gases Part II. Fundamental Phenomena in Electrical Discharges. *Reviews of Modern Physics*, 3:191–257, April 1931.

[3] H. M. Mott-Smith and I. Langmuir. The Theory of Collectors in Gaseous Discharges. *Physical Review*, 28:727–763, October 1926.

[4] D. Hastings and H. Garrett. *Spacecraft-Environment Interactions*. Cambridge University Press, August 2004.

[5] P. M. Chung, L. Talbot, and K. J. Touryan. Electric probes in stationary and flowing plasmas: Theory and application. *NASA STI/Recon Technical Report A*, 75:25150– +, 1975.

[6] A. Barjatya. *Langmuir Probe Measurements in the Ionosphere*. Phd thesis, Utah State University (USA), 2007.

[7] V. A. Davis and L. W. Gordon. Spacecraft surface charging handbook. Technical report, November 1992.

[8] S. H. Høymork, editor. *Sensors and Instruments for Space Exploration*, chapter 7. Langmuir probes, pages 121–145. Swedish Institute of Space Physics, Kiruna, 2000.

[9] E. C. Whipple. Potentials of surfaces in space. *Reports on Progress in Physics*, 44:1197–1250, November 1981.

[10] R. Haagmans, E. Friis-Christensen, H. Lühr, and G. Hulot. Swarm- The Earth's Magnetic Field and Environment Explorers. *AGU Fall Meeting Abstracts*, pages A4+, December 2004.

[11] E. Friis-Christensen, H. Lühr, D. Knudsen, and R. Haagmans. Swarm An Earth Observation Mission investigating Geospace. *Advances in Space Research*, 41:210–216, 2008.

[12] S. Maus. Improving the Resolution of the Lithospheric Magnetic Field From CHAMP and Upcoming SWARM Satellite Measurements. *AGU Fall Meeting Abstracts*, pages D4+, December 2003.

[13] J. Burchill, D. Knudsen, and A. Eriksson. Swarm Measurements of Ionospheric Electric Field and Plasma. *AGU Spring Meeting Abstracts*, pages A5+, May 2009.

[14] F. F. Chen. *Introduction to plasma physics and controlled fusion*. Springer, 2006.

[15] W. Baumjohann and R. A. Treumann. *Basic space plasma physics*. Imperial College Press, 1996.

[16] J.-F. Roussel, F. Rogier, G. Dufour, J.-C. Mateo-Velez, J. Forest, A. Hilgers, D. Rodgers, L. Girard, and D. Payan. SPIS Open-Source Code: Methods, Capabilities, Achievements, and Prospects. *IEEE Transactions on Plasma Science*, 36:2360–2368, October 2008.

[17] S. N. Ghosh. *The neutral upper atmosphere*. Kluwer Academic Publisher, Dordrecht, July 2002.

[18] T. E. Cravens. *Physics of Solar System Plasmas*. Cambridge University Press, November 2004.

[19] D. Bilitza, W. R. Hoegy, L. H. Brace, and R. F. Theis. Evaluation of the international reference ionosphere with the large AE-C and DE2 data bases. *Advances in Space Research*, 8:209–212, 1988.

[20] C.K. Birdsall. *Plasma physics via computer simulation*. Adam Hilger, 1991.

[21] I. Katz, G. A. Jongeward, V. A. Davis, M. J. Mandell, and R. A. Kuharski. Structure of the bipolar plasma sheath generated by SPEAR I. *Journal of Geophysical Research*, 94:1450–1458, February 1989.

[22] J. Rubinstein and J. G. Laframboise. Theory of a spherical probe in a collisionless magnetoplasma. *Physics of Fluids*, 25:1174–1182, July 1982.

[23] F. F. Chen, C. Etievant, and D. Mosher. Measurement of Low Plasma Densities in a Magnetic Field. *Physics of Fluids*, 11:811–821, April 1968.

[24] M. Sugawara, editor. *Plasma Etching*. Oxford Science Publications, Tucson, USA, 1998.

[25] R. F. Fernsler. Modeling Langmuir probes in multi-component plasmas. *Plasma Sources Science Technology*, 18(1):014012–+, February 2009.

A

GMSH SCRIPTS

A.1 Gmsh approach

The Gmsh is freeware program available on the website http://www.geuz.org/gmsh together with detailed documentation. Gmsh follows a bottom-up approach which defines the physical domain of the mesh starting by defining the simplest elements, the points, in order to define segments hence surfaces and volumes according to a hierarchical order. The comments to the following codes are organized according to this criteria.

A.2 Model: Sphere in high density plasma

```
///// [Model: Sphere][ne=ni= 1e12 m-3]

///// Probe geometry: Spherical probe model
///// Probe universe: 2 concentrical spherical boxes

///// Minimal probe-box distance: Debye length = 1.7mm

//////////////////////////////////////////////////////

///// Define[mesh size][m]:

///// mesh size inner box, probe surface
```

```
smsh = 0.001;

///// mesh size inner box, box surface
ismsh = 0.001;

///// mesh size outern sphere, surface
cmsh = 0.0017;


/////Define[geometry]:

///// Spherical probe:
Point(1) = {0, 0, 0, smsh};
Point(2) = {0, 0.003805, 0, smsh};
Point(3) = {0, -0.003805, 0, smsh};
Point(4) = {0.003805, 0, 0, smsh};
Point(5) = {-0.003805, 0, 0, smsh};
Point(6) = {0, 0, 0.003805, smsh};
Point(7) = {0, 0, -0.003805, smsh};

Circle(1) = {2, 1, 4};
Circle(2) = {4, 1, 3};
Circle(3) = {3, 1, 5};
Circle(4) = {5, 1, 2};
Circle(5) = {5, 1, 7};
Circle(6) = {7, 1, 4};
Circle(7) = {5, 1, 6};
Circle(8) = {6, 1, 4};
Circle(9) = {2, 1, 7};
Circle(10) = {7, 1, 3};
Circle(11) = {3, 1, 6};
Circle(12) = {6, 1, 2};


///// Inner spherical box
Point(26) = {0.008, 0, 0, ismsh};
Point(27) = {-0.008, 0, 0, ismsh};
Point(28) = {0, 0.008, 0, ismsh};
Point(29) = {0, -0.008, 0, ismsh};
Point(30) = {0, 0, 0.008, ismsh};
Point(31) = {0, 0, -0.008, ismsh};

Circle(21) = {28, 1, 30};
Circle(22) = {30, 1, 29};
Circle(23) = {29, 1, 31};
```

```
Circle(24) = {31, 1, 28};
Circle(25) = {28, 1, 26};
Circle(26) = {28, 1, 27};
Circle(27) = {27, 1, 29};
Circle(28) = {29, 1, 26};
Circle(29) = {26, 1, 31};
Circle(30) = {31, 1, 27};
Circle(31) = {27, 1, 30};
Circle(32) = {30, 1, 26};


///// Outer  sphere:
Point(8) = {0.03805, 0, 0, cmsh};
Point(9) = {-0.03805, 0, 0, cmsh};
Point(10) = {0, 0.03805, 0, cmsh};
Point(11) = {0, -0.03805, 0, cmsh};
Point(12) = {0, 0, 0.03805, cmsh};
Point (13) = {0, 0, -0.03805, cmsh};

Circle(33) = {13, 1, 8};
Circle(34) = {8, 1, 12};
Circle(35) = {12, 1, 9};
Circle(36) = {9, 1, 13};
Circle(37) = {13, 1, 11};
Circle(38) = {11, 1, 12};
Circle(39) = {12, 1, 10};
Circle(40) = {10, 1, 13};
Circle(41) = {9, 1, 10};
Circle(42) = {9, 1, 11};
Circle(43) = {11, 1, 8};
Circle(44) = {8, 1, 10};


///// Define others: elementary entities & physicals groups

///// Define[Surfaces]

///// Ruled surfaces of Outhern sphere
Line Loop(45) = {40, -36, 41};
Ruled Surface(46) = {45};
Line Loop(47) = {41, -39, 35};
Ruled Surface(48) = {47};
Line Loop(49) = {39, -44, 34};
Ruled Surface(50) = {49};
Line Loop(51) = {40, 33, 44};
```

```
Ruled Surface(52) = {51};
Line Loop(53) = {33, -43, -37};
Ruled Surface(54) = {53};
Line Loop(55) = {43, 34, -38};
Ruled Surface(56) = {55};
Line Loop(57) = {37, -42, 36};
Ruled Surface(58) = {57};
Line Loop(59) = {38, 35, 42};
Ruled Surface(60) = {59};


///// Ruled surfaces of Inner spherical box
Line Loop(61) = {23, 30, 27};
Ruled Surface(62) = {61};
Line Loop(63) = {24, 26, -30};
Ruled Surface(64) = {63};
Line Loop(65) = {26, 31, -21};
Ruled Surface(66) = {65};
Line Loop(67) = {24, 25, 29};
Ruled Surface(68) = {67};
Line Loop(69) = {25, -32, -21};
Ruled Surface(70) = {69};
Line Loop(71) = {29, -23, 28};
Ruled Surface(72) = {71};
Line Loop(73) = {32, -28, -22};
Ruled Surface(74) = {73};
Line Loop(75) = {22, -27, 31};
Ruled Surface(76) = {75};


///// Ruled surface of Inner spherical probe
Line Loop(77) = {8, -1, -12};
Ruled Surface(78) = {77};
Line Loop(79) = {10, 3, 5};
Ruled Surface(80) = {79};
Line Loop(81) = {11, -7, -3};
Ruled Surface(82) = {81};
Line Loop(84) = {11, 8, 2};
Ruled Surface(85) = {84};
Line Loop(86) = {2, -10, 6};
Ruled Surface(87) = {86};
Line Loop(88) = {6, -1, 9};
Ruled Surface(89) = {88};
Line Loop(90) = {5, -9, -4};
Ruled Surface(91) = {90};
```

```
Line Loop(92) = {4, -12, -7};
Ruled Surface(93) = {92};

///// Define[spatial volumes]

///// Volume [from] outher spherical box [to] inner spherical box
Surface Loop(94) = {60, 56, 54, 52, 46, 58, 48, 50};
Surface Loop(95) = {76, 74, 70, 68, 64, 66, 62, 72};
Volume(96) = {94, 95};

///// Volume [from] inner spherical box [to] spherical probe
Surface Loop(97) = {93, 91, 80, 87, 85, 82, 78, 89};
Volume(98) = {95, 97};

///// Define[Physical surfaces]

///// order:  outher sphere(99), spherical probe(100)
Physical Surface(99) = {56, 60, 50, 48, 46, 52, 54, 58};
Physical Surface(100) = {80, 82, 91, 93, 89, 85, 87, 78};

///// Define[physical volume = plasma volume]

///// volume in which the plasma moves
Physical Volume(101) = {96, 98};
```

A.3 Model: Sphere-Stub in high density plasma

```
///// [Model: Sphere-Stub][ne=ni= 1e12 m-3]

///// Probe geometry: Spherical probe model and attached stub
///// Probe universe: 2 spherical boxes

///// Minimal probe-box distance: Debye length = 1.7mm

///// 2 models are implemented: unresolved & resolved

////////////////////////////////////////////////////////////

///// Define[mesh size][m]:

///// mesh size inner box, probe surface
smsh = 0.0017;

///// mesh size inner box, box surface  //////////////////////
///// mesh size outern sphere, surface  /////unresolved///////
cmsh = 0.002;                          //////////////////////

///// mesh size inner box, box surface  //////////////////////
///// mesh size outern sphere, surface  ///////resolved////////
cmsh = 0.0017;                         //////////////////////


/////Define[geometry]:

///// Spherical probe:
Point(1) = {0, 0, 0, smsh};
Point(2) = {0, 0.003805, 0, smsh};
Point(3) = {0, -0.003805, 0, smsh};
Point(4) = {-0.003805, 0, 0, smsh};
Point(5) = {0, 0, 0.003805, smsh};
Point(6) = {0, 0, -0.003805, smsh};

///// Spherical probe-stub connection:
Point(7) = {0.00349685930515, 0.0015, 0, smsh};
Point(8) = {0.00349685930515, -0.0015, 0, smsh};
Point(9) = {0.00349685930515, 0, -0.0015, smsh};
Point(10) = {0.00349685930515, 0, 0.0015, smsh};
Point(11) = {0.00349685930515, 0, 0, smsh};
```

```
///// Stub base
Point(12) = {0.03370809924355, 0, 0, smsh};
Point(13) = {0.03370809924355, 0.0015, 0, smsh};
Point(14) = {0.03370809924355, -0.0015, 0, smsh};
Point(15) = {0.03370809924355, 0, 0.0015, smsh};
Point(16) = {0.03370809924355, 0, -0.0015, smsh};

///// Outer box: cone base
Point(17) = {0.051, 0, 0, cmsh};
Point(18) = {0.051, 0.02, 0, cmsh};
Point(20) = {0.051, 0, 0.02, cmsh};
Point(21) = {0.051, -0.02, 0, cmsh};
Point(22) = {0.051, 0, -0.02, cmsh};

///// Outer box: cone-hemisphere connection
Point(23) = {-0.03805, 0, 0, cmsh};
Point(24) = {0, 0.03805, 0, cmsh};
Point(25) = {0, 0, 0.03805, cmsh};
Point(26) = {0, -0.03805, 0, cmsh};
Point(27) = {0, 0, -0.03805, cmsh};

///// Inner box: cylinder base
Point(117) = {0.03871, 0, 0, cmsh};
Point(118) = {0.03871, 0.008805, 0, cmsh};
Point(120) = {0.03871, 0, 0.008805, cmsh};
Point(121) = {0.03871, -0.008805, 0, cmsh};
Point(122) = {0.03871, 0, -0.008805, cmsh};

///// Inner box: cylinder-hemisphere connection
Point(123) = {-0.008805, 0, 0, cmsh};
Point(124) = {0, 0.008805, 0, cmsh};
Point(125) = {0, 0, 0.008805, cmsh};
Point(126) = {0, -0.008805, 0, cmsh};
Point(127) = {0, 0, -0.008805, cmsh};

///// Circles and Lines related to the probe and the boxes
Circle(1) = {4, 1, 3};
Circle(2) = {4, 1, 2};
Circle(3) = {3, 1, 8};
Circle(4) = {2, 1, 7};
Circle(5) = {2, 1, 6};
Circle(6) = {6, 1, 3};
Circle(7) = {3, 1, 5};
Circle(8) = {5, 1, 2};
```

```
Circle(9) = {4, 1, 6};
Circle(10) = {4, 1, 5};
Circle(11) = {6, 1, 9};
Circle(12) = {5, 1, 10};
Circle(13) = {16, 12, 14};
Circle(14) = {16, 12, 13};
Circle(15) = {13, 12, 15};
Circle(16) = {15, 12, 14};
Line(17) = {9, 16};
Line(18) = {13, 7};
Line(19) = {10, 15};
Line(20) = {14, 8};
Circle(21) = {9, 11, 8};
Circle(22) = {8, 11, 10};
Circle(23) = {10, 11, 7};
Circle(24) = {7, 11, 9};
Circle(25) = {126, 1, 125};
Circle(26) = {126, 1, 127};
Circle(27) = {127, 1, 124};
Circle(28) = {124, 1, 125};
Circle(29) = {121, 117, 120};
Circle(30) = {121, 117, 122};
Circle(31) = {122, 117, 118};
Circle(32) = {118, 117, 120};
Circle(33) = {126, 1, 123};
Circle(34) = {123, 1, 127};
Circle(35) = {124, 1, 123};
Circle(36) = {125, 1, 123};
Line(37) = {125, 120};
Line(38) = {118, 124};
Line(39) = {122, 127};
Line(40) = {126, 121};
Line(41) = {25, 20};
Line(42) = {21, 26};
Line(43) = {22, 27};
Line(44) = {18, 24};
Circle(45) = {18, 17, 22};
Circle(46) = {22, 17, 21};
Circle(47) = {21, 17, 20};
Circle(48) = {20, 17, 18};
Circle(49) = {27, 1, 26};
Circle(50) = {26, 1, 25};
Circle(51) = {25, 1, 24};
Circle(52) = {24, 1, 27};
Circle(53) = {26, 1, 23};
```

```
Circle(54) = {23, 1, 25};
Circle(55) = {23, 1, 24};
Circle(56) = {23, 1, 27};


///// Define[Surfaces]

///// Ruled surfaces
Line Loop(58) = {2, -8, -10};
Ruled Surface(58) = {58};
Line Loop(60) = {10, -7, -1};
Ruled Surface(60) = {60};
Line Loop(62) = {2, 5, -9};
Ruled Surface(62) = {62};
Line Loop(64) = {9, 6, -1};
Ruled Surface(64) = {64};
Line Loop(66) = {5, 11, -24, -4};
Ruled Surface(66) = {66};
Line Loop(68) = {4, -23, -12, 8};
Ruled Surface(68) = {68};
Line Loop(70) = {6, 3, -21, -11};
Ruled Surface(70) = {70};
Line Loop(72) = {12, -22, -3, 7};
Ruled Surface(72) = {72};
Line Loop(74) = {19, 16, 20, 22};
Ruled Surface(74) = {74};
Line Loop(76) = {19, -15, 18, -23};
Ruled Surface(76) = {76};
Line Loop(78) = {20, -21, 17, 13};
Ruled Surface(78) = {78};
Line Loop(80) = {14, 18, 24, 17};
Ruled Surface(80) = {80};
Line Loop(82) = {15, 16, -13, 14};
Plane Surface(82) = {82};
Line Loop(84) = {28, 36, -35};
Ruled Surface(84) = {84};
Line Loop(86) = {36, -33, 25};
Ruled Surface(86) = {86};
Line Loop(88) = {34, -26, 33};
Ruled Surface(88) = {88};
Line Loop(90) = {34, 27, 35};
Ruled Surface(90) = {90};
Line Loop(92) = {27, -38, -31, 39};
Ruled Surface(92) = {92};
Line Loop(94) = {26, -39, -30, -40};
```

```
Ruled Surface(94) = {94};
Line Loop(96) = {40, 29, -37, -25};
Ruled Surface(96) = {96};
Line Loop(98) = {37, -32, 38, 28};
Ruled Surface(98) = {98};
Line Loop(100) = {30, 31, 32, -29};
Plane Surface(100) = {100};
Line Loop(102) = {56, 49, 53};
Ruled Surface(102) = {102};
Line Loop(104) = {56, -52, -55};
Ruled Surface(104) = {104};
Line Loop(106) = {55, -51, -54};
Ruled Surface(106) = {106};
Line Loop(108) = {54, -50, 53};
Ruled Surface(108) = {108};
Line Loop(110) = {43, -52, -44, 45};
Ruled Surface(110) = {110};
Line Loop(112) = {48, 44, -51, 41};
Ruled Surface(112) = {112};
Line Loop(114) = {47, -41, -50, -42};
Ruled Surface(114) = {114};
Line Loop(116) = {46, 42, -49, -43};
Ruled Surface(116) = {116};
Line Loop(118) = {48, 45, 46, 47};
Plane Surface(118) = {118};


///// Define[spatial volumes]

///// Volume [from] outher box [to] inner box
Surface Loop(121) = {112, 118, 110, 116, 114, 108, 106, 104,
102, 98, 96,94, 88, 90, 92, 100, 84, 86};
Volume(121) = {121};

///// Volume [from] inner box [to] spherical probe
Surface Loop(123) = {98, 96, 94, 88, 90, 92, 100, 84, 86,
72, 68, 66, 62, 58, 60, 64, 70, 78, 74, 76, 82, 80};
Volume(123) = {123};


///// Define[Physical surfaces]

///// order: spherical probe, stub, stub base, outher box
Physical Surface(124) = {58, 60, 62, 64, 66, 68, 70, 72};
Physical Surface(125) = {74, 76, 78, 80};
```

```
Physical Surface(126) = {82};
Physical Surface(127) = {102, 104, 106, 108, 110, 112, 114,
116, 118};


///// Define[physical volume = plasma volume]

///// Volume in which the plasma moves
Physical Volume(128) = {123, 121};
```

A.4 Model: Sphere in low density plasma

```
///// [Model: Sphere][ne=ni= 1e12 m-3]

///// Probe geometry: Spherical probe model
///// Probe universe: 2 concentrical spherical boxes

///// Minimal probe-box distance: Debye length = 1.7mm

////////////////////////////////////////////////////

///// Define[mesh size][m]:

///// mesh size inner box, probe surface
smsh = 0.001;

///// mesh size inner box, box surface
ismsh = 0.001;

///// mesh size outern sphere, surface
cmsh = 0.0017;


/////Define[geometry]:

///// Spherical probe:
Point(1) = {0, 0, 0, smsh};
Point(2) = {0, 0.003805, 0, smsh};
Point(3) = {0, -0.003805, 0, smsh};
Point(4) = {0.003805, 0, 0, smsh};
Point(5) = {-0.003805, 0, 0, smsh};
Point(6) = {0, 0, 0.003805, smsh};
Point(7) = {0, 0, -0.003805, smsh};

Circle(1) = {2, 1, 4};
Circle(2) = {4, 1, 3};
Circle(3) = {3, 1, 5};
Circle(4) = {5, 1, 2};
Circle(5) = {5, 1, 7};
Circle(6) = {7, 1, 4};
Circle(7) = {5, 1, 6};
Circle(8) = {6, 1, 4};
Circle(9) = {2, 1, 7};
```

```
Circle(10) = {7, 1, 3};
Circle(11) = {3, 1, 6};
Circle(12) = {6, 1, 2};


///// Inner spherical box
Point(26) = {0.008, 0, 0, ismsh};
Point(27) = {-0.008, 0, 0, ismsh};
Point(28) = {0, 0.008, 0, ismsh};
Point(29) = {0, -0.008, 0, ismsh};
Point(30) = {0, 0, 0.008, ismsh};
Point(31) = {0, 0, -0.008, ismsh};

Circle(21) = {28, 1, 30};
Circle(22) = {30, 1, 29};
Circle(23) = {29, 1, 31};
Circle(24) = {31, 1, 28};
Circle(25) = {28, 1, 26};
Circle(26) = {28, 1, 27};
Circle(27) = {27, 1, 29};
Circle(28) = {29, 1, 26};
Circle(29) = {26, 1, 31};
Circle(30) = {31, 1, 27};
Circle(31) = {27, 1, 30};
Circle(32) = {30, 1, 26};


///// Outer  sphere:
Point(8) = {0.03805, 0, 0, cmsh};
Point(9) = {-0.03805, 0, 0, cmsh};
Point(10) = {0, 0.03805, 0, cmsh};
Point(11) = {0, -0.03805, 0, cmsh};
Point(12) = {0, 0, 0.03805, cmsh};
Point (13) = {0, 0, -0.03805, cmsh};

Circle(33) = {13, 1, 8};
Circle(34) = {8, 1, 12};
Circle(35) = {12, 1, 9};
Circle(36) = {9, 1, 13};
Circle(37) = {13, 1, 11};
Circle(38) = {11, 1, 12};
Circle(39) = {12, 1, 10};
Circle(40) = {10, 1, 13};
Circle(41) = {9, 1, 10};
Circle(42) = {9, 1, 11};
```

```
Circle(43) = {11, 1, 8};
Circle(44) = {8, 1, 10};


///// Define others: elementary entities & physicals groups

///// Define[Surfaces]

///// Ruled surfaces of Outhern sphere
Line Loop(45) = {40, -36, 41};
Ruled Surface(46) = {45};
Line Loop(47) = {41, -39, 35};
Ruled Surface(48) = {47};
Line Loop(49) = {39, -44, 34};
Ruled Surface(50) = {49};
Line Loop(51) = {40, 33, 44};
Ruled Surface(52) = {51};
Line Loop(53) = {33, -43, -37};
Ruled Surface(54) = {53};
Line Loop(55) = {43, 34, -38};
Ruled Surface(56) = {55};
Line Loop(57) = {37, -42, 36};
Ruled Surface(58) = {57};
Line Loop(59) = {38, 35, 42};
Ruled Surface(60) = {59};


///// Ruled surfaces of Inner spherical box
Line Loop(61) = {23, 30, 27};
Ruled Surface(62) = {61};
Line Loop(63) = {24, 26, -30};
Ruled Surface(64) = {63};
Line Loop(65) = {26, 31, -21};
Ruled Surface(66) = {65};
Line Loop(67) = {24, 25, 29};
Ruled Surface(68) = {67};
Line Loop(69) = {25, -32, -21};
Ruled Surface(70) = {69};
Line Loop(71) = {29, -23, 28};
Ruled Surface(72) = {71};
Line Loop(73) = {32, -28, -22};
Ruled Surface(74) = {73};
Line Loop(75) = {22, -27, 31};
Ruled Surface(76) = {75};
```

```
///// Ruled surface of Inner spherical probe
Line Loop(77) = {8, -1, -12};
Ruled Surface(78) = {77};
Line Loop(79) = {10, 3, 5};
Ruled Surface(80) = {79};
Line Loop(81) = {11, -7, -3};
Ruled Surface(82) = {81};
Line Loop(84) = {11, 8, 2};
Ruled Surface(85) = {84};
Line Loop(86) = {2, -10, 6};
Ruled Surface(87) = {86};
Line Loop(88) = {6, -1, 9};
Ruled Surface(89) = {88};
Line Loop(90) = {5, -9, -4};
Ruled Surface(91) = {90};
Line Loop(92) = {4, -12, -7};
Ruled Surface(93) = {92};

///// Define[spatial volumes]

///// Volume [from] outher spherical box [to] inner spherical box
Surface Loop(94) = {60, 56, 54, 52, 46, 58, 48, 50};
Surface Loop(95) = {76, 74, 70, 68, 64, 66, 62, 72};
Volume(96) = {94, 95};

///// Volume [from] inner spherical box [to] spherical probe
Surface Loop(97) = {93, 91, 80, 87, 85, 82, 78, 89};
Volume(98) = {95, 97};

///// Define[Physical surfaces]

///// order:  outher sphere(99), spherical probe(100)
Physical Surface(99) = {56, 60, 50, 48, 46, 52, 54, 58};
Physical Surface(100) = {80, 82, 91, 93, 89, 85, 87, 78};

///// Define[physical volume = plasma volume]

///// volume in which the plasma moves
Physical Volume(101) = {96, 98};
```

A.5 Model: Sphere-Stub in low density plasma

```
///// [Model: Sphere-Stub][ne=ni= 1e11 m-3]

///// Probe geometry: Spherical probe model and attached stub
///// Probe universe: 2 spherical boxes

///// Minimal probe-box distance: Debye length = 10mm

///// 2 models are implemented: unresolved & resolved

////////////////////////////////////////////////////////////

///// Define[mesh size][m]:

///// mesh size inner box, probe surface
smsh = 0.0017;

///// mesh size inner box, box surface
///// mesh size outern sphere, surface
cmsh = 0.006;


/////Define[geometry]:

///// Spherical probe:
Point(1) = {0, 0, 0, smsh};
Point(2) = {0, 0.003805, 0, smsh};
Point(3) = {0, -0.003805, 0, smsh};
Point(4) = {-0.003805, 0, 0, smsh};
Point(5) = {0, 0, 0.003805, smsh};
Point(6) = {0, 0, -0.003805, smsh};

///// Spherical probe-stub connection:
Point(7) = {0.00349685930515, 0.0015, 0, smsh};
Point(8) = {0.00349685930515, -0.0015, 0, smsh};
Point(9) = {0.00349685930515, 0, -0.0015, smsh};
Point(10) = {0.00349685930515, 0, 0.0015, smsh};
Point(11) = {0.00349685930515, 0, 0, smsh};

///// Stub base
Point(12) = {0.03370809924355, 0, 0, smsh};
Point(13) = {0.03370809924355, 0.0015, 0, smsh};
```

```
Point(14) = {0.03370809924355, -0.0015, 0, smsh};
Point(15) = {0.03370809924355, 0, 0.0015, smsh};
Point(16) = {0.03370809924355, 0, -0.0015, smsh};

///// Outer box
Point(23) = {-0.095125, 0, 0, cmsh};
Point(24) = {0, 0.095125, 0, cmsh};
Point(25) = {0, 0, 0.095125, cmsh};
Point(26) = {0, -0.095125, 0, cmsh};
Point(27) = {0, 0, -0.095125, cmsh};
Point(28) = {0.095125, 0, 0, cmsh};

///// Inner box: cylinder base
Point(117) = {0.0437081, 0, 0, cmsh};
Point(118) = {0.0437081, 0.013805, 0, cmsh};
Point(120) = {0.0437081, 0, 0.013805, cmsh};
Point(121) = {0.0437081, -0.013805, 0, cmsh};
Point(122) = {0.0437081, 0, -0.013805, cmsh};

///// Inner box: cylinder-hemisphere connection
Point(123) = {-0.013805, 0, 0, cmsh};
Point(124) = {0, 0.013805, 0, cmsh};
Point(125) = {0, 0, 0.013805, cmsh};
Point(126) = {0, -0.013805, 0, cmsh};
Point(127) = {0, 0, -0.013805, cmsh};

///// Circles and Lines related to the probe and the boxes
Circle(1) = {4, 1, 5};
Circle(2) = {4, 1, 6};
Circle(3) = {4, 1, 2};
Circle(4) = {4, 1, 3};
Circle(5) = {5, 1, 3};
Circle(6) = {5, 1, 2};
Circle(7) = {2, 1, 6};
Circle(8) = {6, 1, 3};
Circle(9) = {2, 1, 7};
Circle(10) = {6, 1, 9};
Circle(11) = {3, 1, 8};
Circle(12) = {5, 1, 10};
Circle(13) = {10, 11, 8};
Circle(14) = {8, 11, 9};
Circle(15) = {9, 11, 7};
Circle(16) = {7, 11, 10};
Circle(17) = {15, 12, 14};
Circle(18) = {14, 12, 16};
```

```
Circle(19) = {16, 12, 13};
Circle(20) = {13, 12, 15};
Line(21) = {8, 14};
Line(22) = {10, 15};
Line(23) = {13, 7};
Line(24) = {9, 16};
Circle(25) = {126, 1, 125};
Circle(26) = {125, 1, 124};
Circle(27) = {124, 1, 127};
Circle(28) = {127, 1, 126};
Circle(29) = {126, 1, 123};
Circle(30) = {123, 1, 124};
Circle(31) = {123, 1, 127};
Circle(32) = {123, 1, 125};
Circle(33) = {120, 117, 118};
Circle(34) = {120, 117, 121};
Circle(35) = {121, 117, 122};
Circle(36) = {122, 117, 118};
Line(37) = {125, 120};
Line(38) = {126, 121};
Line(39) = {127, 122};
Line(40) = {124, 118};
Circle(41) = {23, 1, 24};
Circle(42) = {24, 1, 28};
Circle(43) = {28, 1, 26};
Circle(44) = {26, 1, 23};
Circle(45) = {27, 1, 28};
Circle(46) = {28, 1, 25};
Circle(47) = {25, 1, 23};
Circle(48) = {23, 1, 27};
Circle(49) = {24, 1, 27};
Circle(50) = {27, 1, 26};
Circle(51) = {26, 1, 25};
Circle(52) = {25, 1, 24};


///// Define[Surfaces]

///// Ruled surfaces
Line Loop(55) = {3, -6, -1};
Ruled Surface(55) = {55};
Line Loop(57) = {1, 5, -4};
Ruled Surface(57) = {57};
Line Loop(58) = {3, 7, -2};
Ruled Surface(58) = {58};
```

```
Line Loop(60) = {2, 8, -4};
Ruled Surface(60) = {60};
Line Loop(62) = {7, 10, 15, -9};
Ruled Surface(62) = {62};
Line Loop(64) = {9, 16, -12, 6};
Ruled Surface(64) = {64};
Line Loop(66) = {10, -14, -11, -8};
Ruled Surface(66) = {66};
Line Loop(68) = {11, -13, -12, 5};
Ruled Surface(68) = {68};
Line Loop(70) = {13, 21, -17, -22};
Ruled Surface(70) = {70};
Line Loop(72) = {21, 18, -24, -14};
Ruled Surface(72) = {72};
Line Loop(74) = {19, 23, -15, 24};
Ruled Surface(74) = {74};
Line Loop(76) = {20, -22, -16, -23};
Ruled Surface(76) = {76};
Line Loop(78) = {17, 18, 19, 20};
Plane Surface(78) = {78};
Line Loop(80) = {31, 28, 29};
Ruled Surface(80) = {80};
Line Loop(82) = {29, 32, -25};
Ruled Surface(82) = {82};
Line Loop(84) = {32, 26, -30};
Ruled Surface(84) = {84};
Line Loop(86) = {30, 27, -31};
Ruled Surface(86) = {86};
Line Loop(88) = {25, 37, 34, -38};
Ruled Surface(88) = {88};
Line Loop(90) = {38, 35, -39, 28};
Ruled Surface(90) = {90};
Line Loop(92) = {40, -33, -37, 26};
Ruled Surface(92) = {92};
Line Loop(94) = {40, -36, -39, -27};
Ruled Surface(94) = {94};
Line Loop(96) = {36, -33, 34, 35};
Plane Surface(96) = {96};
Line Loop(98) = {41, 49, -48};
Ruled Surface(98) = {98};
Line Loop(100) = {41, -52, 47};
Ruled Surface(100) = {100};
Line Loop(102) = {42, 46, 52};
Ruled Surface(102) = {102};
Line Loop(104) = {46, -51, -43};
```

```
Ruled Surface(104) = {104};
Line Loop(106) = {47, -44, 51};
Ruled Surface(106) = {106};
Line Loop(108) = {44, 48, 50};
Ruled Surface(108) = {108};
Line Loop(110) = {43, -50, 45};
Ruled Surface(110) = {110};
Line Loop(112) = {45, -42, 49};
Ruled Surface(112) = {112};


///// Define[spatial volumes]

///// Volume [from] outher box [to] inner box
Surface Loop(115) = {98, 100, 102, 112, 110, 104, 106, 108,
94, 92, 96, 88, 82, 80, 86, 84, 90};
Volume(115) = {115};

///// Volume [from] inner box [to] spherical probe
Surface Loop(117) = {94, 92, 96, 88, 82, 80, 86, 84, 90, 76,
78, 70, 68, 66, 62, 58, 55, 64, 57, 60, 74, 72};
Volume(117) = {117};


///// Define[Physical surfaces]

///// order: spherical probe, stub, stub base, outher box
Physical Surface(118) = {55, 57, 58, 60, 62, 64, 66, 68};
Physical Surface(119) = {70, 72, 74, 76};
Physical Surface(120) = {78};
Physical Surface(121) = {98, 100, 102, 104, 106, 108, 110, 112};


///// Define[physical volume = plasma volume]

///// Volume in which the plasma moves
Physical Volume(122) = {115, 117};
```

A.6 Model: Sphere in big box in low density plasma

```
///// [Model: Sphere 19][ne=ni= 1e11 m-3]

///// Probe geometry: Spherical probe model
///// Probe universe: 2 concentrical spherical boxes

///// Minimal probe-box distance: Debye length = 10mm

////////////////////////////////////////////////////

///// Define[mesh size][m]:

///// mesh size inner box, probe surface
smsh = 0.001;

///// mesh size inner box, box surface
ismsh= 0.005

///// mesh size outern sphere, surface
cmsh = 0.01;


/////Define[geometry]:

///// Spherical probe:
Point(1) = {0, 0, 0, 0.001};
Point(2) = {0, 0.003805, 0, 0.001};
Point(3) = {0, -0.003805, 0, 0.001};
Point(4) = {0.003805, 0, 0, 0.001};
Point(5) = {-0.003805, 0, 0, 0.001};
Point(6) = {0, 0, 0.003805, 0.001};
Point(7) = {0, 0, -0.003805, 0.001};

///// Outer spherical box
Point(8) = {0.19025, 0, 0, 0.01};
Point(9) = {-0.19025, 0, 0, 0.01};
Point(10) = {0, 0.19025, 0, 0.01};
Point(11) = {0, -0.19025, 0, 0.01};
Point(12) = {0, 0, 0.19025, 0.01};
Point(13) = {0, 0, -0.19025, 0.01};

///// Inner spherical box
```

```
Point(26) = {0.013805, 0, 0, 0.005};
Point(27) = {-0.013805, 0, 0, 0.005};
Point(28) = {0, 0.013805, 0, 0.005};
Point(29) = {0, -0.013805, 0, 0.005};
Point(30) = {0, 0, 0.013805, 0.005};
Point(31) = {0, 0, -0.013805, 0.005};

///// Circles related to the probe and the boxes
Circle(1) = {2, 1, 4};
Circle(2) = {4, 1, 3};
Circle(3) = {3, 1, 5};
Circle(4) = {5, 1, 2};
Circle(5) = {5, 1, 7};
Circle(6) = {7, 1, 4};
Circle(7) = {5, 1, 6};
Circle(8) = {6, 1, 4};
Circle(9) = {2, 1, 7};
Circle(10) = {7, 1, 3};
Circle(11) = {3, 1, 6};
Circle(12) = {6, 1, 2};
Circle(21) = {28, 1, 30};
Circle(22) = {30, 1, 29};
Circle(23) = {29, 1, 31};
Circle(24) = {31, 1, 28};
Circle(25) = {28, 1, 26};
Circle(26) = {28, 1, 27};
Circle(27) = {27, 1, 29};
Circle(28) = {29, 1, 26};
Circle(29) = {26, 1, 31};
Circle(30) = {31, 1, 27};
Circle(31) = {27, 1, 30};
Circle(32) = {30, 1, 26};
Circle(33) = {13, 1, 8};
Circle(34) = {8, 1, 12};
Circle(35) = {12, 1, 9};
Circle(36) = {9, 1, 13};
Circle(37) = {13, 1, 11};
Circle(38) = {11, 1, 12};
Circle(39) = {12, 1, 10};
Circle(40) = {10, 1, 13};
Circle(41) = {9, 1, 10};
Circle(42) = {9, 1, 11};
Circle(43) = {11, 1, 8};
Circle(44) = {8, 1, 10};
```

```
///// Define[Surfaces]

///// Ruled surface
Line Loop(46) = {40, -36, 41};
Ruled Surface(46) = {46};
Line Loop(48) = {41, -39, 35};
Ruled Surface(48) = {48};
Line Loop(50) = {39, -44, 34};
Ruled Surface(50) = {50};
Line Loop(52) = {40, 33, 44};
Ruled Surface(52) = {52};
Line Loop(54) = {33, -43, -37};
Ruled Surface(54) = {54};
Line Loop(56) = {43, 34, -38};
Ruled Surface(56) = {56};
Line Loop(58) = {37, -42, 36};
Ruled Surface(58) = {58};
Line Loop(60) = {38, 35, 42};
Ruled Surface(60) = {60};
Line Loop(62) = {23, 30, 27};
Ruled Surface(62) = {62};
Line Loop(64) = {24, 26, -30};
Ruled Surface(64) = {64};
Line Loop(66) = {26, 31, -21};
Ruled Surface(66) = {66};
Line Loop(68) = {24, 25, 29};
Ruled Surface(68) = {68};
Line Loop(70) = {25, -32, -21};
Ruled Surface(70) = {70};
Line Loop(72) = {29, -23, 28};
Ruled Surface(72) = {72};
Line Loop(74) = {32, -28, -22};
Ruled Surface(74) = {74};
Line Loop(76) = {22, -27, 31};
Ruled Surface(76) = {76};
Line Loop(78) = {8, -1, -12};
Ruled Surface(78) = {78};
Line Loop(80) = {10, 3, 5};
Ruled Surface(80) = {80};
Line Loop(82) = {11, -7, -3};
Ruled Surface(82) = {82};
Line Loop(85) = {11, 8, 2};
Ruled Surface(85) = {85};
Line Loop(87) = {2, -10, 6};
```

```
Ruled Surface(87) = {87};
Line Loop(89) = {6, -1, 9};
Ruled Surface(89) = {89};
Line Loop(91) = {5, -9, -4};
Ruled Surface(91) = {91};
Line Loop(93) = {4, -12, -7};
Ruled Surface(93) = {93};


///// Define[spatial volumes]

///// Volume [from] outher box [to] inner box
Surface Loop(96) = {60, 56, 54, 52, 46, 58, 48, 50, 76,
74, 70, 68, 64, 66, 62, 72};
Volume(96) = {96};

///// Volume [from] inner box [to] spherical probe
Surface Loop(98) = {76, 74, 70, 68, 64, 66, 62, 72, 93,
91, 80, 87, 85, 82, 78, 89};
Volume(98) = {98};


///// Define[Physical surfaces]

///// order: spherical probe, outher box
Physical Surface(99) = {46, 48, 50, 52, 54, 56, 58, 60};
Physical Surface(100) = {78, 80, 82, 85, 87, 89, 91, 93};


///// Define[physical volume = plasma volume]

///// Volume in which the plasma moves
Physical Volume(101) = {96, 98};
```

A.7 Model: LP-simplified s/c model in low density plasma

```
///// [Model: Complete LP-symplified s/c][ne=ni= 1e11 m-3]

///// Probe geometry: fully reproduced LP geometry;
///// Resolution: detailes smaller that Dedye length have
/////             beed omitted, see figure;
///// Probe universe: box, parallelepiped.

////////////////////////////////////////////////////////////


///// Define[mesh size][m]:

///// mesh size inner box, probe surface
smsh = 0.001;

///// mesh size inner box, box surface
ismsh = 0.001;

///// mesh size outern sphere, surface
cmsh = 0.0017;


/////Define[geometry]:

///// Spherical probe:
Point(1) = {0, 0, 0, 0.0017};
Point(2) = {0, 0.003805, 0, 0.0017};
Point(3) = {0, -0.003805, 0, 0.0017};
Point(4) = {-0.003805, 0, 0, 0.0017};
Point(5) = {0, 0, 0.003805, 0.0017};
Point(6) = {0, 0, -0.003805, 0.0017};

///// Stub:
Point(7) = {0.00349685930515, 0.0015, 0, 0.002};
Point(8) = {0.00349685930515, -0.0015, 0, 0.002};
Point(9) = {0.00349685930515, 0, -0.0015, 0.002};
Point(10) = {0.00349685930515, 0, 0.0015, 0.002};
Point(11) = {0.00349685930515, 0, 0, 0.002};

///// Boom:
Point(12) = {0.0341, 0, 0, 0.002};
```

```
Point(13) = {0.0341, 0.0015, 0, 0.002};
Point(14) = {0.0341, -0.0015, 0, 0.002};
Point(15) = {0.0341, 0, 0.0015, 0.002};
Point(16) = {0.0341, 0, -0.0015, 0.002};

///// Boom-First conical support
Point(17) = {0.0644, 0, 0, 0.003};
Point(18) = {0.0644, 0.00231, 0, 0.003};
Point(19) = {0.0644, -0.00231, 0, 0.003};
Point(20) = {0.0644, 0, 0.00231, 0.003};
Point(21) = {0.0644, 0, -0.00231, 0.003};

///// First conical support base
Point(22) = {0.0644, 0, 0, 0.003};
Point(23) = {0.0644, 0.00654, 0, 0.003};
Point(24) = {0.0644, -0.00654, 0, 0.003};
Point(25) = {0.0644, 0, 0.00654, 0.003};
Point(26) = {0.0644, 0, -0.00654, 0.003};

///// First conical support-Second conical support
Point(27) = {0.0746, 0, 0, 0.003};
Point(28) = {0.0746, 0.006015, 0, 0.003};
Point(29) = {0.0746, -0.006015, 0, 0.003};
Point(30) = {0.0746, 0, 0.006015, 0.003};
Point(31) = {0.0746, 0, -0.006015, 0.003};

///// Second conical support base-Cilinder
Point(32) = {0.08690000000000001, 0, 0, 0.003};
Point(33) = {0.08690000000000001, 0.01301, 0, 0.003};
Point(34) = {0.08690000000000001, -0.01301, 0, 0.003};
Point(35) = {0.08690000000000001, 0, 0.01301, 0.003};
Point(36) = {0.08690000000000001, 0, -0.01301, 0.003};


///// Cilinder-Third conical support connection
Point(37) = {0.09161999999999999, 0, 0, 0.003};
Point(38) = {0.09161999999999999, 0.01301, 0, 0.003};
Point(39) = {0.09161999999999999, -0.01301, 0, 0.003};
Point(40) = {0.09161999999999999, 0, 0.01301, 0.003};
Point(41) = {0.09161999999999999, 0, -0.01301, 0.003};

///// Third conical support base
Point(42) = {0.09401, 0, 0, 0.003};
Point(43) = {0.09401, 0.02015, 0, 0.003};
Point(44) = {0.09401, -0.02015, 0, 0.003};
```

```
Point(45) = {0.09401, 0, 0.02015, 0.003};
Point(46) = {0.09401, 0, -0.02015, 0.003};

///// LP cindrical base
Point(47) = {0.09401, 0, 0, 0.003};
Point(48) = {0.09401, 0.0375, 0, 0.003};
Point(49) = {0.09401, -0.0375, 0, 0.003};
Point(50) = {0.09401, 0, 0.0375, 0.003};
Point(51) = {0.09401, 0, -0.0375, 0.003};

///// LP cindrical base-S/c wall
Point(52) = {0.09901, 0, 0, 0.003};
Point(53) = {0.09901, 0.0375, 0, 0.003};
Point(54) = {0.09901, -0.0375, 0, 0.003};
Point(55) = {0.09901, 0, 0.0375, 0.003};
Point(56) = {0.09901, 0, -0.0375, 0.003};

///// S/c wall facing the LP probe
Point(57) = {0.09901, 0.05, 0.09, 0.008};
Point(58) = {0.09901, 0.05, -0.09, 0.008};
Point(59) = {0.09901, -0.08, 0.09, 0.008};
Point(60) = {0.09901, -0.08, -0.09, 0.008};

///// S/c wall far side
Point(61) = {0.148, 0.05, 0.09, 0.01};
Point(62) = {0.148, 0.05, -0.09, 0.01};
Point(63) = {0.148, -0.08, 0.09, 0.01};
Point(64) = {0.148, -0.08, -0.09, 0.01};

///// Parallelepiped, box
Point(65) = {0.188, 0.118, 0.168, 0.01};
Point(66) = {0.188, -0.143, 0.168, 0.01};
Point(67) = {0.188, 0.118, -0.168, 0.01};
Point(68) = {0.188, -0.143, -0.168, 0.01};
Point(69) = {-0.12, 0.118, 0.168, 0.01};
Point(70) = {-0.12, -0.143, 0.168, 0.01};
Point(71) = {-0.12, 0.118, -0.168, 0.01};
Point(72) = {-0.12, -0.143, -0.168, 0.01};

///// Circles and Lines related to the LP and to the box
Circle(1) = {6, 1, 3};
Circle(2) = {3, 1, 5};
Circle(3) = {5, 1, 2};
Circle(4) = {2, 1, 6};
Circle(5) = {6, 1, 4};
```

```
Circle(6) = {4, 1, 5};
Circle(7) = {3, 1, 4};
Circle(8) = {4, 1, 2};
Circle(9) = {3, 1, 8};
Circle(10) = {6, 1, 9};
Circle(11) = {2, 1, 7};
Circle(12) = {5, 1, 10};
Circle(13) = {10, 11, 8};
Circle(14) = {8, 11, 9};
Circle(15) = {9, 11, 7};
Circle(16) = {7, 11, 10};
Circle(17) = {14, 12, 16};
Circle(18) = {16, 12, 13};
Circle(19) = {13, 12, 15};
Circle(20) = {15, 12, 14};
Line(21) = {8, 14};
Line(22) = {16, 9};
Line(23) = {7, 13};
Line(24) = {15, 10};
Line(25) = {14, 19};
Line(26) = {16, 21};
Line(27) = {13, 18};
Line(28) = {15, 20};
Circle(29) = {19, 17, 21};
Circle(30) = {21, 17, 18};
Circle(31) = {18, 17, 20};
Circle(32) = {20, 17, 19};
Circle(33) = {24, 17, 26};
Circle(34) = {26, 17, 23};
Circle(35) = {23, 17, 25};
Circle(36) = {25, 17, 24};
Circle(37) = {29, 27, 30};
Circle(38) = {29, 27, 31};
Circle(39) = {31, 27, 28};
Circle(40) = {28, 27, 30};
Line(41) = {24, 29};
Line(42) = {30, 25};
Line(43) = {26, 31};
Line(44) = {28, 23};
Line(45) = {28, 33};
Line(46) = {31, 36};
Line(47) = {29, 34};
Line(48) = {30, 35};
Circle(49) = {36, 32, 33};
Circle(50) = {33, 32, 35};
```

```
Circle(51) = {35, 32, 34};
Circle(52) = {34, 32, 36};
Line(53) = {36, 41};
Line(54) = {34, 39};
Line(55) = {33, 38};
Line(56) = {35, 40};
Circle(57) = {41, 37, 39};
Circle(58) = {39, 37, 40};
Circle(59) = {40, 37, 38};
Circle(60) = {38, 37, 41};
Circle(61) = {44, 42, 46};
Circle(62) = {46, 42, 43};
Circle(63) = {43, 42, 45};
Circle(64) = {45, 42, 44};
Line(65) = {45, 40};
Line(66) = {44, 39};
Line(67) = {46, 41};
Line(68) = {38, 43};
Line(69) = {44, 49};
Line(70) = {51, 46};
Line(71) = {48, 43};
Line(72) = {45, 50};
Line(73) = {49, 54};
Line(74) = {50, 55};
Line(75) = {51, 56};
Line(76) = {48, 53};
Circle(77) = {55, 52, 53};
Circle(78) = {53, 52, 56};
Circle(79) = {56, 52, 54};
Circle(80) = {54, 52, 55};
Circle(81) = {50, 42, 48};
Circle(82) = {48, 42, 51};
Circle(83) = {51, 42, 49};
Circle(84) = {50, 42, 49};
Line(85) = {19, 24};
Line(86) = {26, 21};
Line(87) = {23, 18};
Line(88) = {20, 25};
Line(177) = {57, 58};
Line(178) = {57, 59};
Line(179) = {58, 60};
Line(180) = {60, 59};
Line(181) = {57, 61};
Line(182) = {58, 62};
Line(183) = {62, 61};
```

```
Line(184) = {61, 63};
Line(185) = {62, 64};
Line(186) = {64, 63};
Line(187) = {63, 59};
Line(188) = {64, 60};
Line(189) = {65, 66};
Line(190) = {66, 68};
Line(191) = {68, 67};
Line(192) = {67, 65};
Line(193) = {65, 69};
Line(194) = {67, 71};
Line(195) = {66, 70};
Line(196) = {68, 72};
Line(197) = {69, 70};
Line(198) = {71, 72};
Line(199) = {69, 71};
Line(200) = {70, 72};


///// Define[Surfaces]

///// Ruled surface
Line Loop(202) = {3, -8, 6};
Ruled Surface(202) = {202};
Line Loop(204) = {6, -2, 7};
Ruled Surface(204) = {204};
Line Loop(206) = {8, 4, 5};
Ruled Surface(206) = {206};
Line Loop(208) = {5, -7, -1};
Ruled Surface(208) = {208};
Line Loop(210) = {10, 15, -11, 4};
Ruled Surface(210) = {210};
Line Loop(212) = {11, 16, -12, 3};
Ruled Surface(212) = {212};
Line Loop(214) = {13, -9, 2, 12};
Ruled Surface(214) = {214};
Line Loop(216) = {10, -14, -9, -1};
Ruled Surface(216) = {216};
Line Loop(218) = {22, 15, 23, -18};
Ruled Surface(218) = {218};
Line Loop(220) = {23, 19, 24, -16};
Ruled Surface(220) = {220};
Line Loop(222) = {14, -22, -17, -21};
Ruled Surface(222) = {222};
Line Loop(224) = {24, 13, 21, -20};
```

```
Ruled Surface(224) = {224};
Line Loop(226) = {28, 32, -25, -20};
Ruled Surface(226) = {226};
Line Loop(228) = {25, 29, -26, -17};
Ruled Surface(228) = {228};
Line Loop(230) = {26, 30, -27, -18};
Ruled Surface(230) = {230};
Line Loop(232) = {27, 31, -28, -19};
Ruled Surface(232) = {232};
Line Loop(234) = {86, 30, -87, -34};
Plane Surface(234) = {234};
Line Loop(236) = {35, -88, -31, -87};
Plane Surface(236) = {236};
Line Loop(238) = {86, -29, 85, 33};
Plane Surface(238) = {238};
Line Loop(240) = {85, -36, -88, 32};
Plane Surface(240) = {240};
Line Loop(242) = {43, 39, 44, -34};
Ruled Surface(242) = {242};
Line Loop(244) = {44, 35, -42, -40};
Ruled Surface(244) = {244};
Line Loop(246) = {42, 36, 41, 37};
Ruled Surface(246) = {246};
Line Loop(248) = {41, 38, -43, -33};
Ruled Surface(248) = {248};
Line Loop(250) = {48, 51, -47, 37};
Ruled Surface(250) = {250};
Line Loop(252) = {45, 50, -48, -40};
Ruled Surface(252) = {252};
Line Loop(254) = {46, -52, -47, 38};
Ruled Surface(254) = {254};
Line Loop(256) = {39, 45, -49, -46};
Ruled Surface(256) = {256};
Line Loop(258) = {51, 54, 58, -56};
Ruled Surface(258) = {258};
Line Loop(260) = {54, -57, -53, -52};
Ruled Surface(260) = {260};
Line Loop(262) = {53, -60, -55, -49};
Ruled Surface(262) = {262};
Line Loop(264) = {59, -55, 50, 56};
Ruled Surface(264) = {264};
Line Loop(266) = {65, 59, 68, 63};
Ruled Surface(266) = {266};
Line Loop(268) = {64, 66, 58, -65};
Ruled Surface(268) = {268};
```

```
Line Loop(270) = {66, -57, -67, -61};
Ruled Surface(270) = {270};
Line Loop(272) = {60, -67, 62, -68};
Ruled Surface(272) = {272};
Line Loop(274) = {84, -69, -64, 72};
Plane Surface(274) = {274};
Line Loop(276) = {72, 81, 71, 63};
Plane Surface(276) = {276};
Line Loop(278) = {62, -71, 82, 70};
Plane Surface(278) = {278};
Line Loop(280) = {69, -83, 70, -61};
Plane Surface(280) = {280};
Line Loop(282) = {73, -79, -75, 83};
Ruled Surface(282) = {282};
Line Loop(284) = {82, 75, -78, -76};
Ruled Surface(284) = {284};
Line Loop(286) = {77, -76, -81, 74};
Ruled Surface(286) = {286};
Line Loop(288) = {84, 73, 80, -74};
Ruled Surface(288) = {288};
Line Loop(291) = {180, -178, 177, 179, -78, -77, -80, -79};
Plane Surface(291) = {291};
Line Loop(293) = {188, -179, 182, 185};
Plane Surface(293) = {293};
Line Loop(295) = {188, 180, -187, -186};
Plane Surface(295) = {295};
Line Loop(297) = {187, -178, 181, 184};
Plane Surface(297) = {297};
Line Loop(299) = {183, -181, 177, 182};
Plane Surface(299) = {299};
Line Loop(301) = {186, -184, -183, 185};
Plane Surface(301) = {301};
Line Loop(303) = {196, -198, -194, -191};
Plane Surface(303) = {303};
Line Loop(305) = {189, 190, 191, 192};
Plane Surface(305) = {305};
Line Loop(307) = {190, 196, -200, -195};
Plane Surface(307) = {307};
Line Loop(309) = {197, 200, -198, -199};
Plane Surface(309) = {309};
Line Loop(311) = {194, -199, -193, -192};
Plane Surface(311) = {311};
Line Loop(313) = {193, 197, -195, -189};
Plane Surface(313) = {313};
```

```
///// Define[spatial volumes]

///// Volume [from] outher box [to] inner box
Surface Loop(316) = {303, 307, 305, 313, 311, 309, 212, 210, 216, 222,
218, 220, 232, 230,228, 226, 240, 238, 234, 236, 244, 242, 248, 246,
250, 252, 256, 262, 260, 258, 268, 274, 288,282, 291, 295, 293, 299,
301, 297, 284, 278, 272, 270, 280, 266, 264, 276, 286, 254, 224, 214,
204, 202, 206, 208};
Volume(316) = {316};


///// Define[Physical surfaces]

///// order: spherical probe, stub, resting LP mechanical components
and s/c, outher box
Physical Surface(317) = {202, 204, 206, 208, 210, 212, 214, 216};
Physical Surface(318) = {218, 220, 222, 224};
Physical Surface(319) = {226, 228, 230, 232, 234, 236, 238, 240, 242,
244, 246, 248, 250, 252,254, 256, 258, 260, 262, 264, 266, 268, 270,
272, 274, 276, 278, 280, 282, 284, 286, 288, 291,293, 295, 297, 299,
301};
Physical Surface(320) = {303, 305, 307, 309, 311, 313};


///// Define[physical volume = plasma volume]

///// Volume in which the plasma moves
Physical Volume(321) = {316};
```

B

MATLAB SCRIPTS

Presented here are the Matlab routines used to derive the results described in Chapter 3. These results are also based on other programs not included because not conceptually relevant.

```
% PARAMERIZATION OF LAFRAMBOISE'S RESULTS

% Marco Chiaretta & Anders.Eriksson@irfu.se 2010-03-17

% Searching the coefficients of the plolynomials that fits the
% Laframboise's table; data in input are firstly plotted hence fitted


% Part1-Search for Coefficients

%%%%%%%%%%%%%%%%%%%%%%%%%%%%%%%%%%%%%%%%%%%%%%%%%%%%%%%%%%%%%%%%%%%%%%%%%%%%%%%
%  Inputs description
%
%  Inputs are from Laframboise Report No. 100.
%  Title: "Theory of Spherical and Cylindrical probes in a collisionless
%  plasma at rest"; pag.86, table 5c, tile:
%  "Computed Values of Attracted Maxwellian Species Current i+ and i-,
%  at equilibrium T+/T-=1".
%%%%%%%%%%%%%%%%%%%%%%%%%%%%%%%%%%%%%%%%%%%%%%%%%%%%%%%%%%%%%%%%%%%%%%%%%%%%%%%

% Inputs source, table 5c = tabNR.txt
tab = load('lafr_curr.txt');    % Ip/Ip0
vp = load('lafr_pot.txt');      % eVp/KTe
rp = load('lafr_rp.txt');       % r_p/lambda_D
```

```
% Locate coefficients into zmat matrix
zmat = zeros(14,4);

for(i=1:14)
    i
  y = tab(:,i);  % Current
  x = vp;        % Voltage

  % Table 5c is not complete hence empity slots are ignored
  ind =find(isnan(y));
  x(ind) =[];
  y(ind) =[];

    % Lenght of the vector has to be at least 6 for good interpolation
    if(length(x)>5)

        % Assign values to axis
        current = y;
        normalpot = 1+x;

        % Arbitrarily weight the Vp = 0 point by 1e4
        current = [current' current(1)*ones(1,1e4)]';
        normalpot = [normalpot' normalpot(1)*ones(1,1e4)]';

        % Fit and plot
        z = polyfit(log(normalpot), log(current), 3);
        zmat(i,:) = z;

        % Generate a basis on x axis instead of using the potential vector
        % as a basis. This is done by adding more points for a better
        % resolution
        %
        % +1 is given to avoid the singularity in the log function

        v =1 +(0:0.1:25);

        subplot(1,2,1)
          plot(normalpot, current, '.', v, exp(polyval(z,log(v))));
          hold on;

          %ColorSet = varycolor1(50);
          %set(gca, 'ColorOrder', ColorSet);
          hold all;
```

```
        ylabel('Normalized Current'); xlabel('Normal Potential');

        subplot(1,2,2);
          loglog(normalpot, current, '.', v, exp(polyval(z,log(v))));
          hold on

          % ColorSet = varycolor2(50);
         % set(gca, 'ColorOrder', ColorSet);
          hold all;

          ylabel('Normalized Current'); xlabel('Normalized Potential');

          h =legend('R/l=0, OML theory','polyn 0','R/l=0.5',...
              'polyn 0.5','R/l=1','polyn 1','R/l=2','polyn 2','R/l=3',...
              'polyn 3','R/l=5','polyn 5','R/l=10','ploy 10','R/l=20',...
              'polyn 20','R/l=50','ploy 50','R/l=100','polyn 100');
          set(h,'Interpreter','latex');

    end
end

% [ax4,h3] =suplabel('Computed Values of Attracted Species Currents' ,'t');
% set(h3,'FontSize',12);

save lafr_coeff.txt zmat -ascii


% Meta-parametrization of Laframboise's results

% Marco Chiaretta & Anders.Eriksson@irfu.se 2010-03-17

% Part2-Plot of Coefficients Versus R/lbda

%%%%%%%%%%%%%%%%%%%%%%%%%%%%%%%%%%%%%%%%%%%%%%%%%%%%%%%%%%%%%%%%%%%%%%%%%%%%%%%
% From part 1 we obtain zmat
% Goal: find a function that fits the variations of these coefficients
% Interpolation of coefficients -> generation of a new set of coefficients
%%%%%%%%%%%%%%%%%%%%%%%%%%%%%%%%%%%%%%%%%%%%%%%%%%%%%%%%%%%%%%%%%%%%%%%%%%%%%%%

% Inputs source, table 5c = tabNR.txt


tab = load('lafr_curr.txt');    % Ip/Ip0
vp = load('lafr_pot.txt');      % eVp/KTe
rp = load('lafr_rp.txt');       % r_p/lambda_D
```

```
zmat = load('lafr_coeff.txt');

% rp values for which Laframboise's results are OK
rpok =[0 0.5 1 2 3 5 10 20 50 100]';
ind = [];
for i=1:length(rp)
    if(find(rpok == rp(i)))
        ind = [ind i];
    end
end

zmat2 = zmat(ind,:);
rp2 = rp(ind);

%xlabel('Normalized radius of the probe [R/lbda]');
%ylabel('Polynomial Coefficients');
%legend('3rd order','2nd order','1st order','0','Location','SouthEast')

% Locate coefficients into cmat matrix
order = 4;
cmat = zeros(4,order + 1);

dat = zeros(4,1000);
 rp1 = linspace(min(rp),max(rp),1000);

for j=1:4;
  % OBS: log(n+rp)->
  % log generates a better fit
  % n+rp avoids a singularity

  % conditioning the fit by weighting coefficients for the OML coloumn
  % in order to get a better percentage error when confronted to numerical
  % Laframboise's results (table 5c)
  polv = zmat2(:,j);

  % The following is to heavily weight the the rp/lambda_D = 0 case, so as
  % to ensure consistency in the low density limit.
  weight = 10;
  polv = [polv' polv(1)*ones(1,weight)]';
  rpmod = [rp2 zeros(1,weight)]';

  %cmat(j,:)=polyfit(log(3+rp),zmat(:,j),order);
  cmat(j,:) = polyfit(log(3+rpmod),polv,order);
```

```
  dat(j,:) = polyval(cmat(j,:),log(3+rp1));
end

save meta_pol.txt cmat -ascii

figure(2);


plot(rp1,dat,rp2,zmat2,'o')
grid on
xlabel('Normalized radius of the probe [R/lbda]');
ylabel('Polynomial Coefficients');
legend('3rd order','2nd order','1st order','0','Location','SouthEast')


% Part 3-Complete and extend Laframboise's table

%%%%%%%%%%%%%%%%%%%%%%%%%%%%%%%%%%%%%%%%%%%%%%%%%%%%%%%%%%%%%%%%%%%%%%%%%%%%%%%
% Now have been created 4 plynoms, 1 for each coefficient interpolation
% Every row is describing an order
%%%%%%%%%%%%%%%%%%%%%%%%%%%%%%%%%%%%%%%%%%%%%%%%%%%%%%%%%%%%%%%%%%%%%%%%%%%%%%%

polycoff =zeros(1,4);
len = length(rp);
lafr = zeros(14,len);

for(k=1:len)
  % ProbeRadius =input('Set the Probe Radius: ')
  ProbeRadius = rp(k);

  % Coefficient of the first polnomia coefficient
  polycoff(1,1) =polyval(cmat(1,:), log(3+ProbeRadius));

  % Coefficient of the second polnomial coefficient
  polycoff(1,2) =polyval(cmat(2,:), log(3+ProbeRadius));

  % Coefficient of the third polnomial coefficient
  polycoff(1,3) =polyval(cmat(3,:), log(3+ProbeRadius));

  % Coefficient of the fourth polnomial coefficient
  polycoff(1,4) =polyval(cmat(4,:), log(3+ProbeRadius));


  % Interpolate the current
  % potential= 0.1:0.1:50;
```

```
  potential = tab(:,1);
  interpolCurrent= exp(polyval(polycoff, log(1+potential)));

  lafr(:,k) = interpolCurrent;
end

% figure(3);
% plot(potential, interpolCurrent)
% hold on
% plot(tab(:,1), tab(:,13),'cyan:o')
%
% lafr(:,2:3) = [];
% tab2=tab(:,[2 5 6 7 9 11 12 13]);
```

C

AVERAGED VALUES OF COLLECTED SPECIES CURRENTS

C.1 Reference table

Resume of collected currents from the simulations in Table C.1. Averaged values are listed for each simulation and the amount of points over which the average is taken is indicated.

Table C.1: *Simulations.*

$T_e = 0.05V$, $n_{O^+} = n_{e^-} = 10^{12}m^{-3} \Rightarrow \lambda_D \approx 1.7\,\text{mm}$		
$\lambda_D \approx 1.7\,\text{mm}$	Sphere PIC	
	Sphere MB	Maxwell Boltzmann electrons
	Sphere-Stub PIC	
	Sphere-Stub R PIC	λ_D resolved in the external box
	Sphere-Stub drift R PIC	
	Sphere-Stub drift V PIC	speed up= 13
	Sphere PIC drift	speed up= 13
	Stub PIC	
$T_e = 0.2V$, $n_{O^+} = n_{e^-} = 10^{12}m^{-3} \Rightarrow \lambda_D \approx 10\,\text{mm}$		
$\lambda_D \approx 10\,\text{mm}$	Sphere PIC	
	Sphere B PIC	
	Sphere-Stub PIC	
	Sphere-Stub drift PIC	
	Full probe-simplified s/c model drift PIC	

C.2 High density plasma

$n_{O^+} = n_{e^-} = 10^{12}$ particles·m^{-3} $\lambda_D \approx 1.7$ mm

C.2.1 Sphere PIC, $\lambda_D = 1mm$

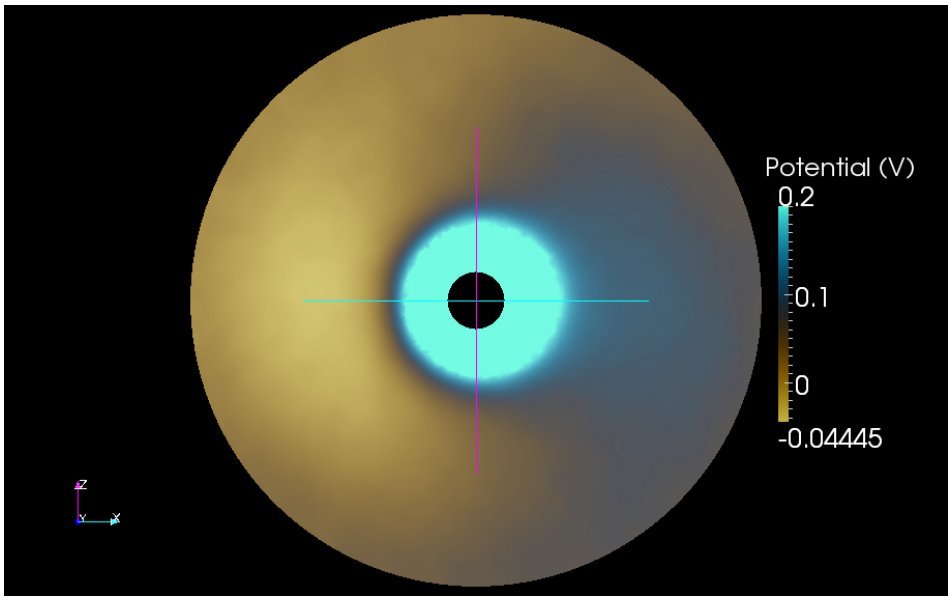

Figure C.1: *Potential map: bias = 2V, rescaled to 0.2V*

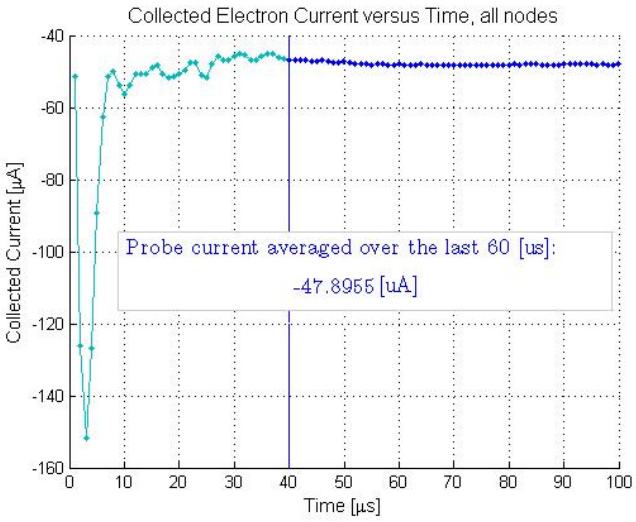

Figure C.2: *5V*

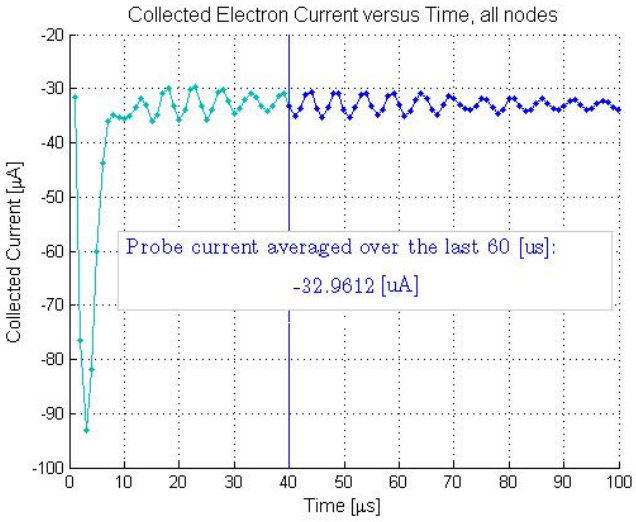

Figure C.3: *3V*

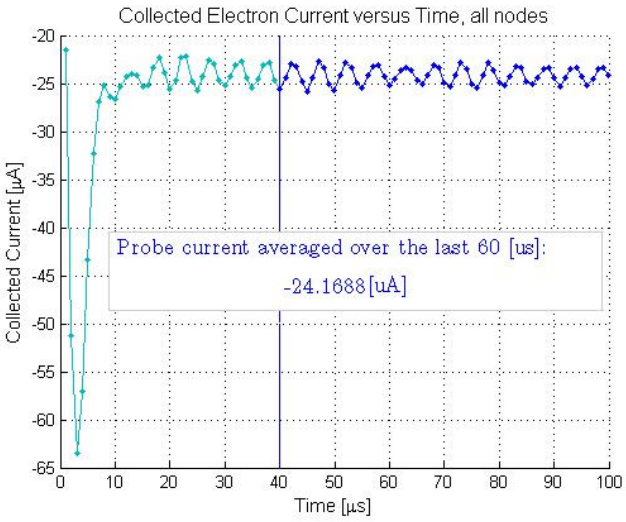

Figure C.4: *2V*

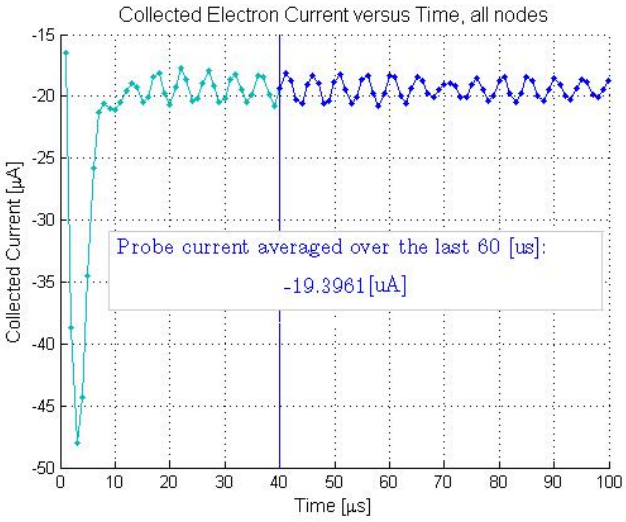

Figure C.5: *1.5V*

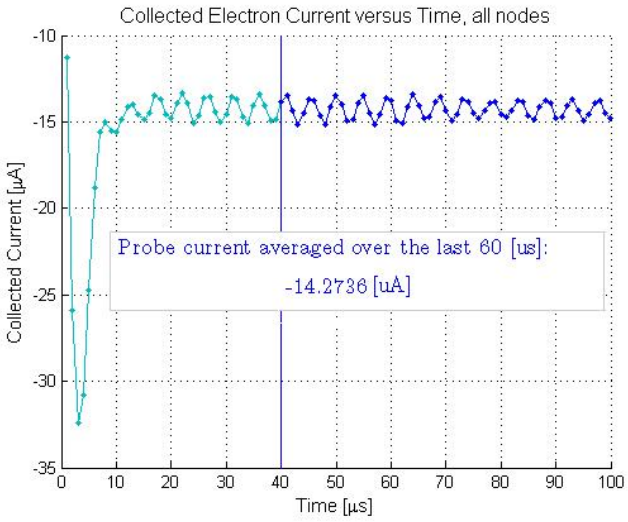

Figure C.6: *1V*

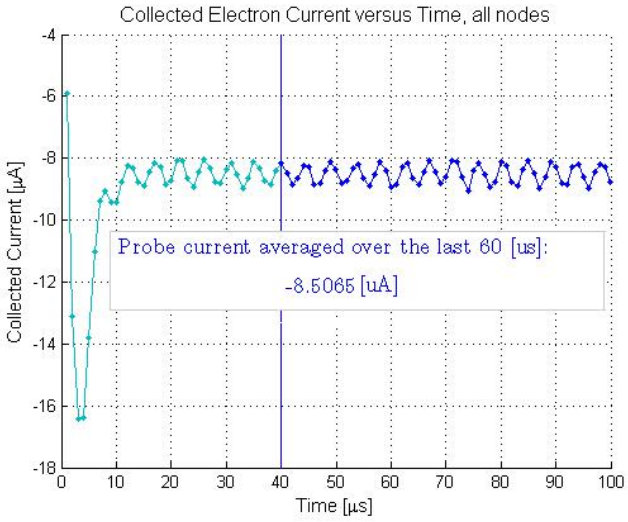

Figure C.7: *0.5V*

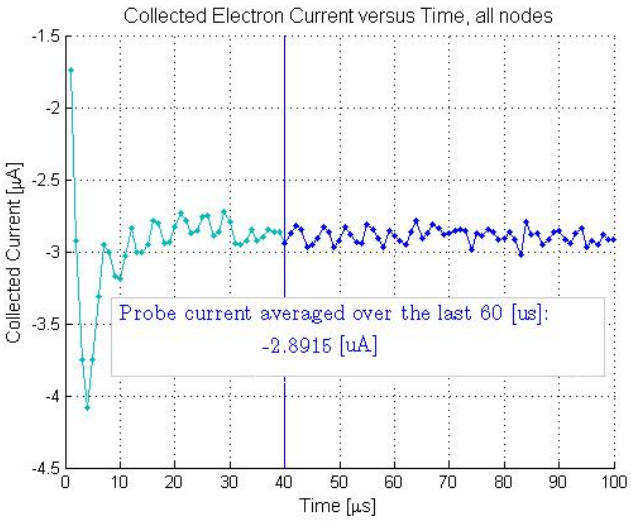

Figure C.8: *0.1V*

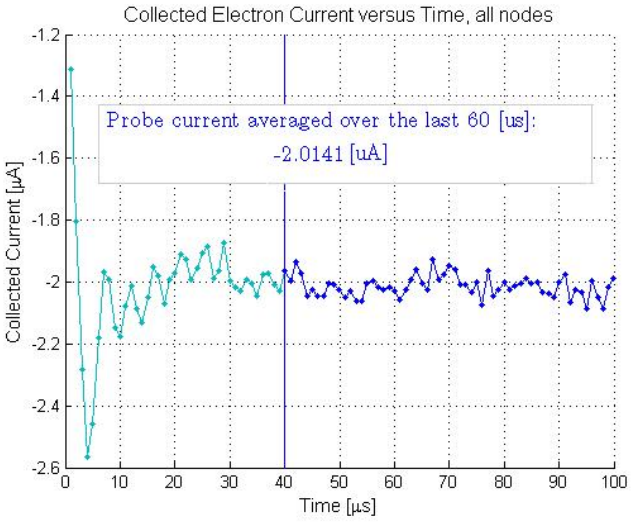

Figure C.9: *0.05V*

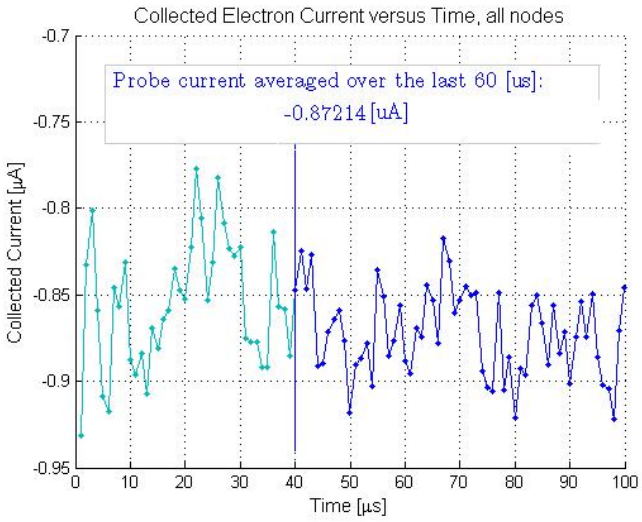

Figure C.10: *-0.01V*

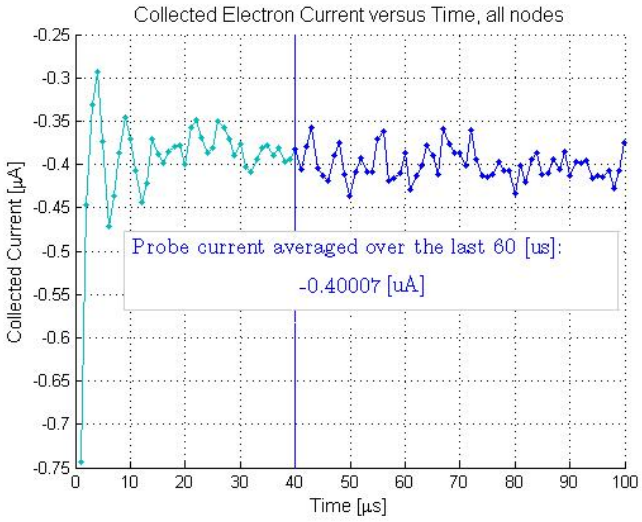

Figure C.11: *-0.05V*

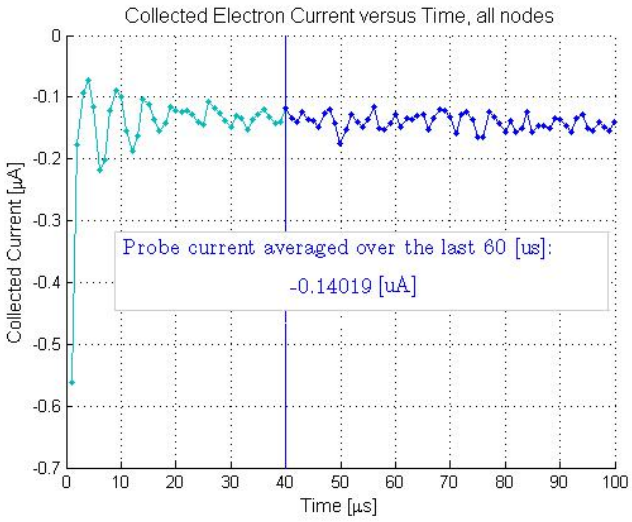

Figure C.12: *-0.1V*

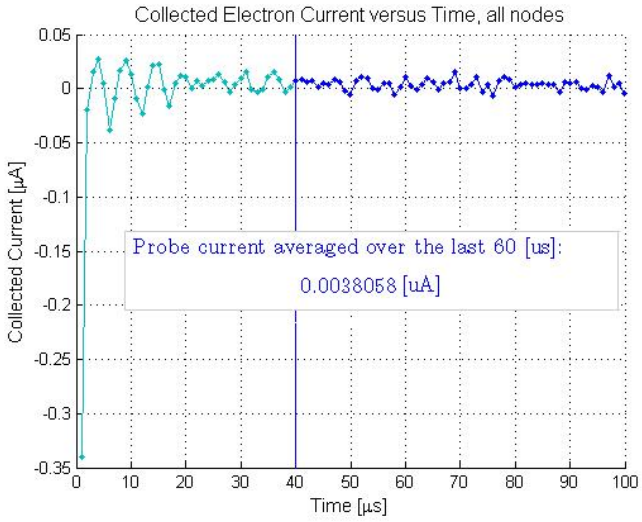

Figure C.13: *-0.2V*

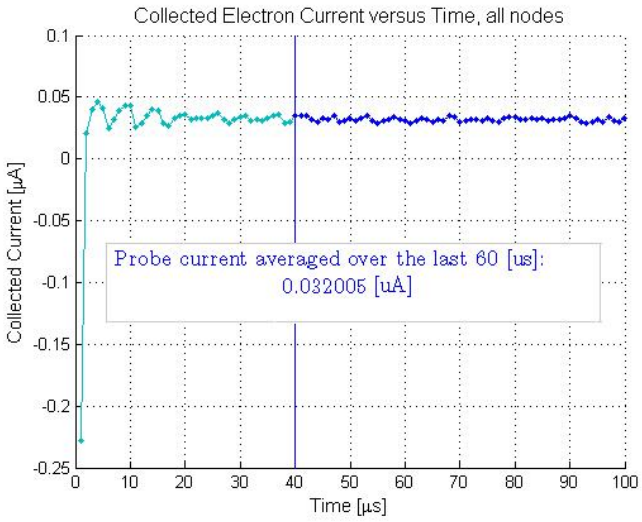

Figure C.14: *-0.3V*

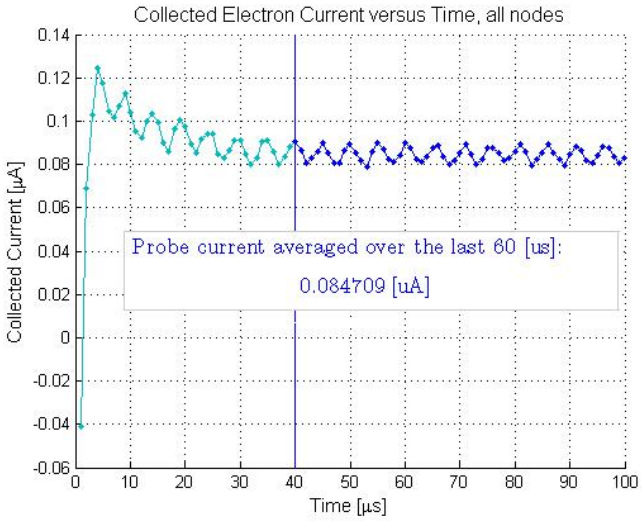

Figure C.15: *-2V*

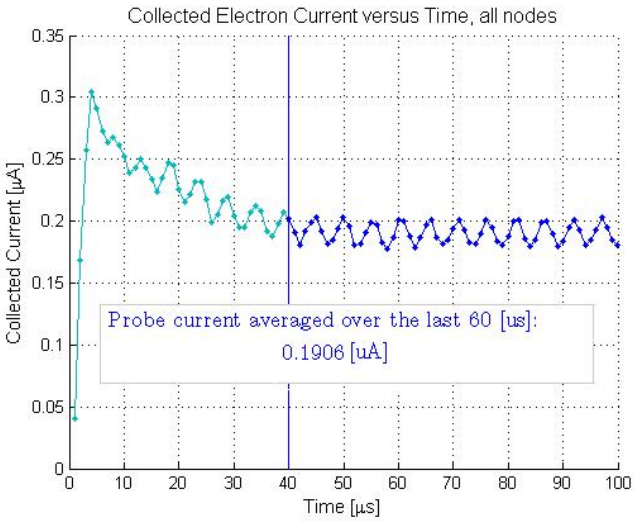

Figure C.16: *-3V*

C.2.2 Sphere MB, $\lambda_D \approx 1.7$mm and Boltzmann electrons

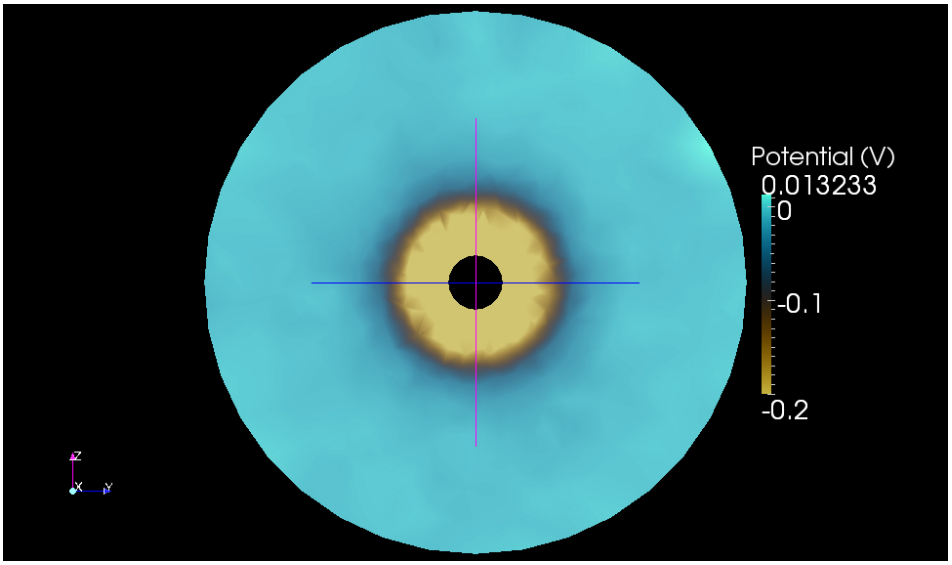

Figure C.17: *Potential map: bias = 2V, rescaled to 0.2V*

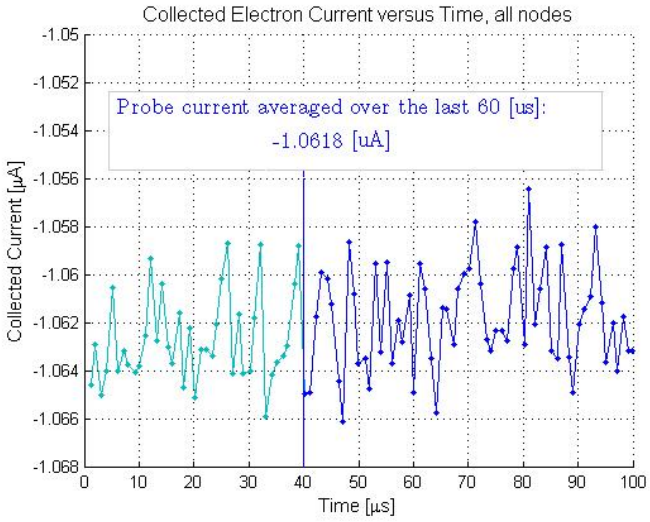

Figure C.18: *0V*

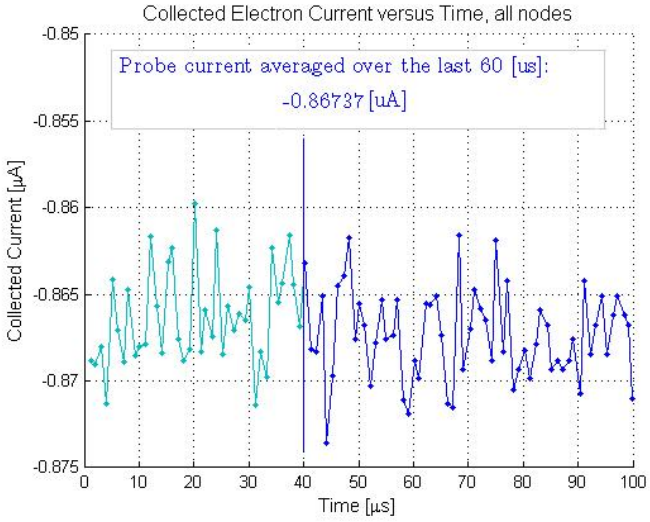

Figure C.19: *-0.01V*

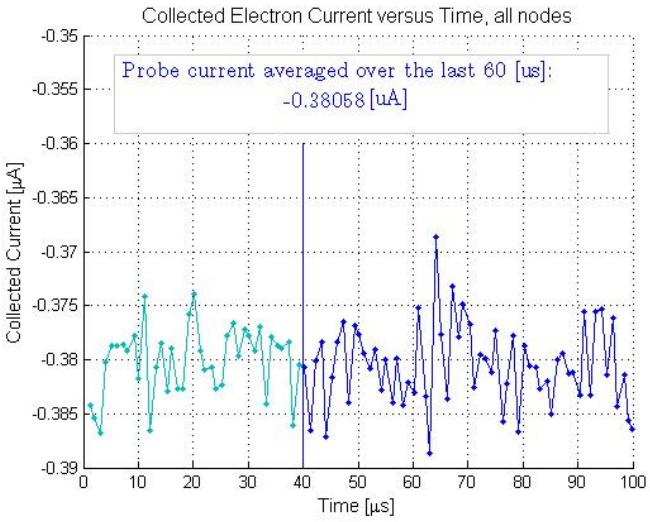

Figure C.20: *-0.05V*

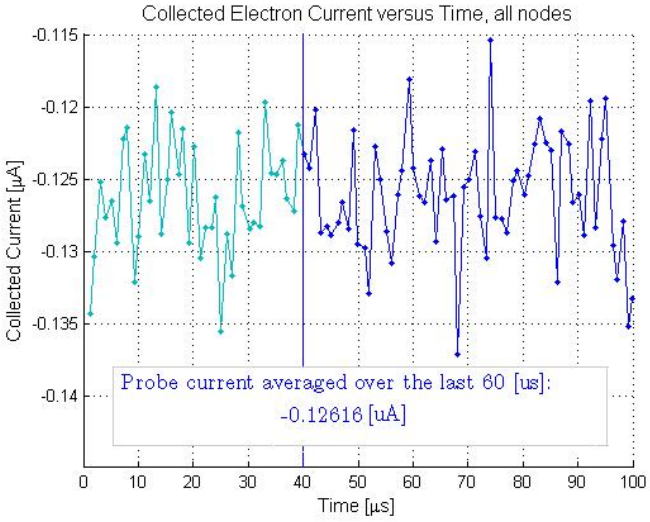

Figure C.21: *-0.1V*

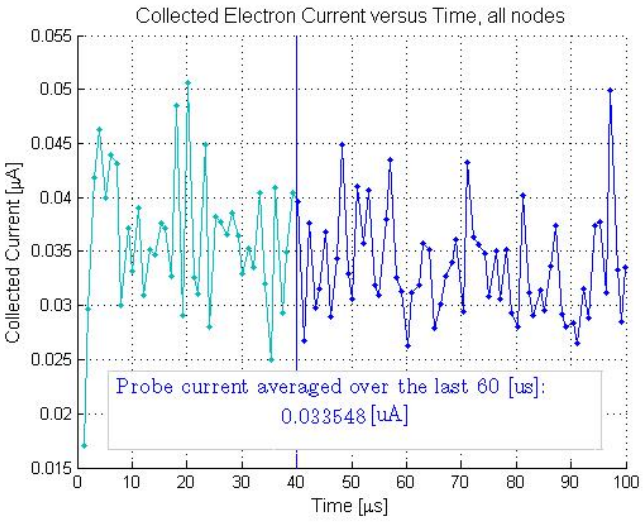

Figure C.22: *-2V*

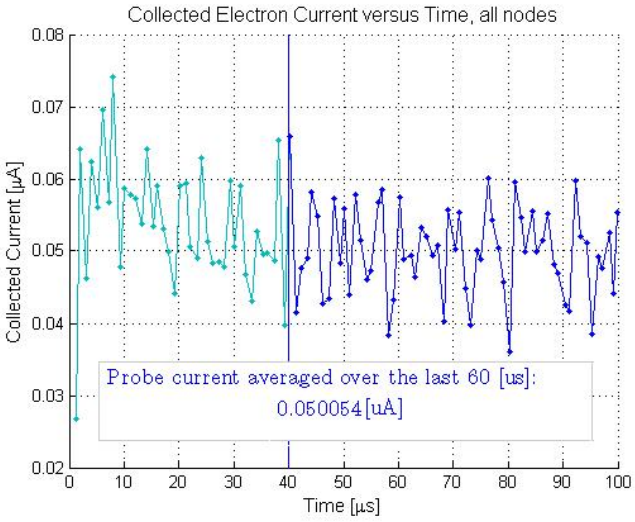

Figure C.23: *-0.5V*

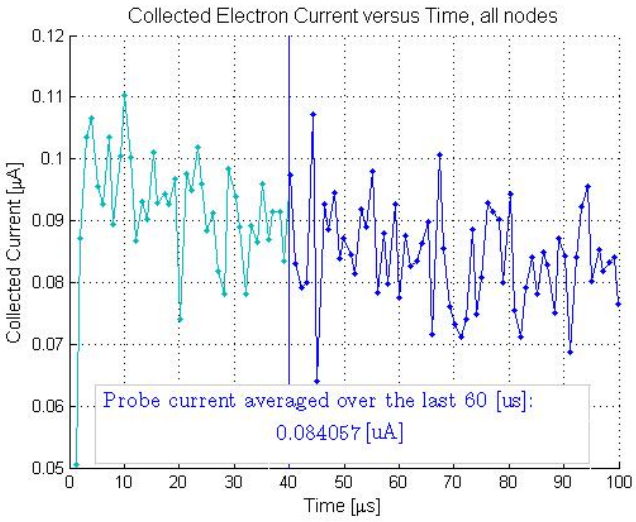

Figure C.24: *-1V*

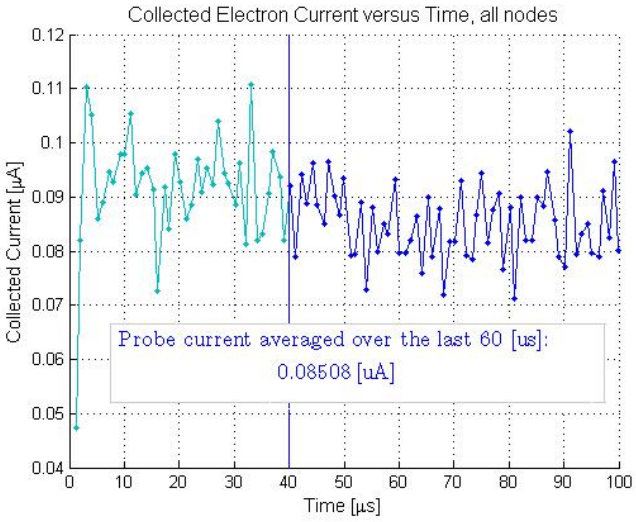

Figure C.25: *-1.5V*

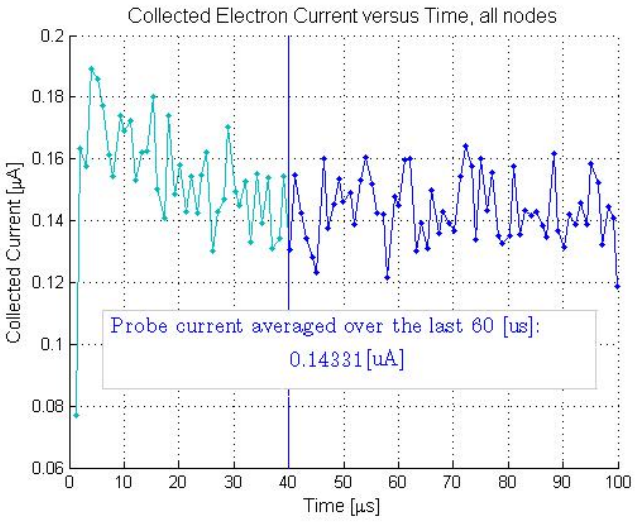

Figure C.26: *-2V*

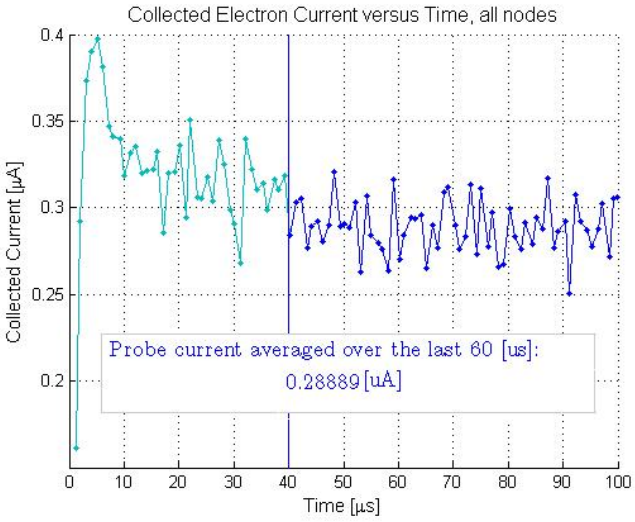

Figure C.27: *-5V*

C.2.3 Sphere-Stub PIC, $\lambda_D \approx 1.7$mm

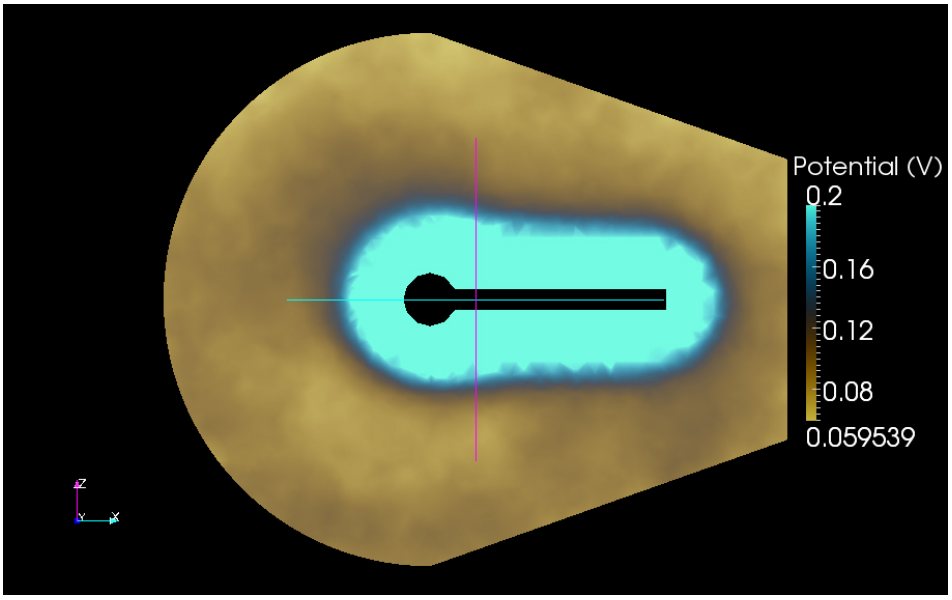

Figure C.28: *Potential map: bias = 2V, rescaled to 0.2V*

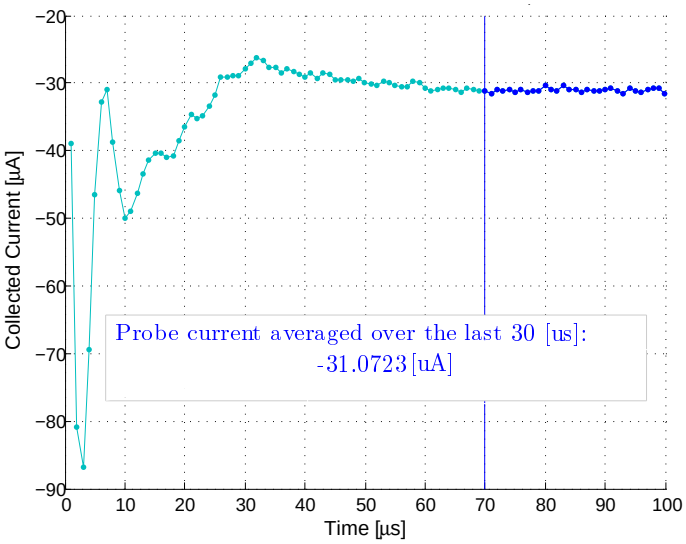

Figure C.29: *5V*

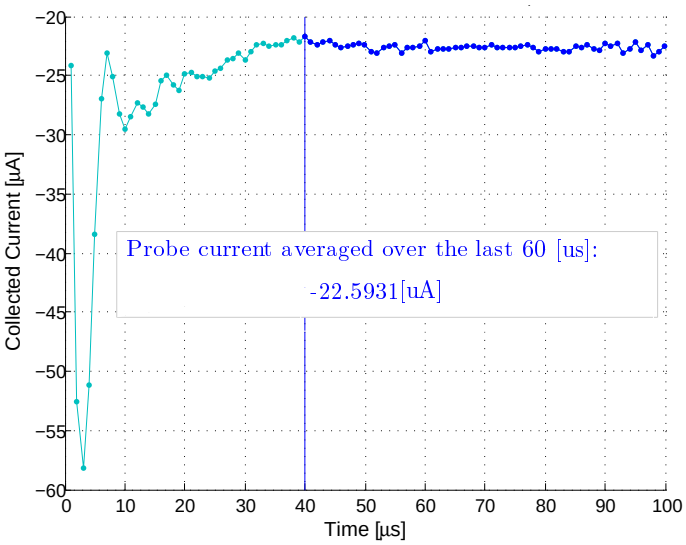

Figure C.30: *3V*

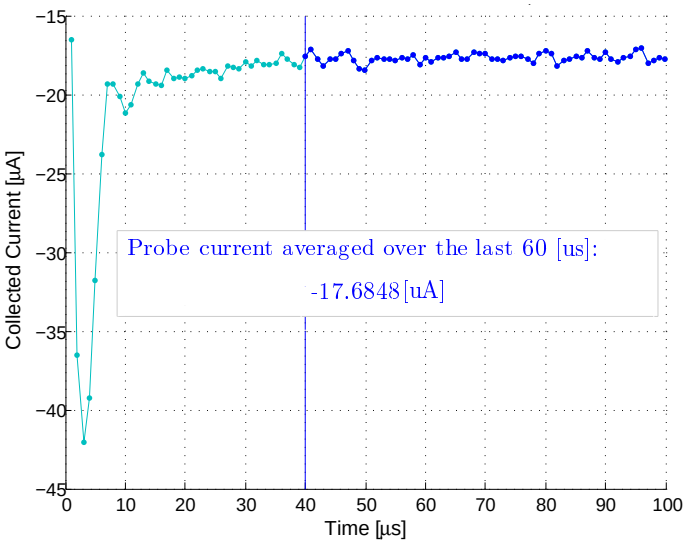

Figure C.31: *2V*

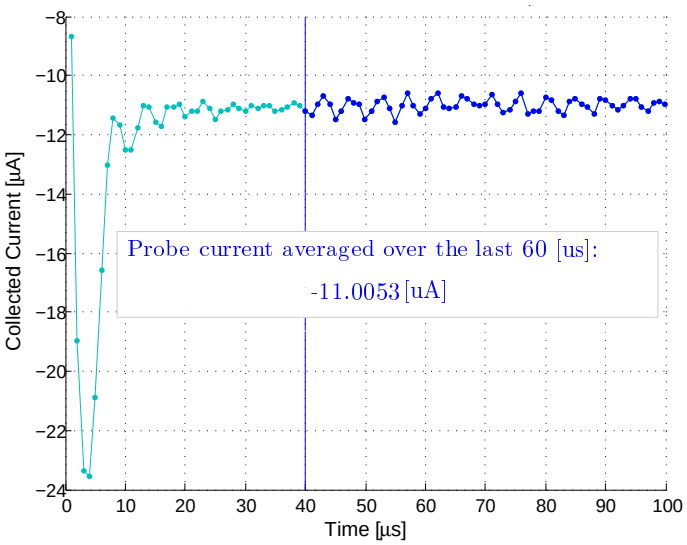

Figure C.32: *1V*

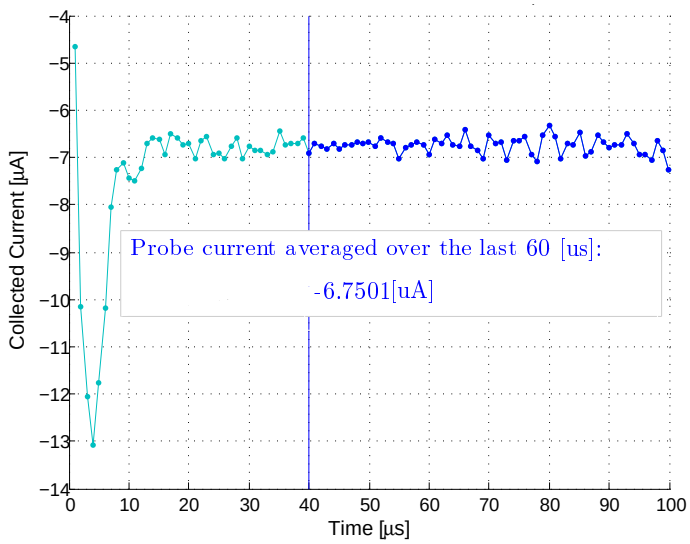

Figure C.33: *0.5V*

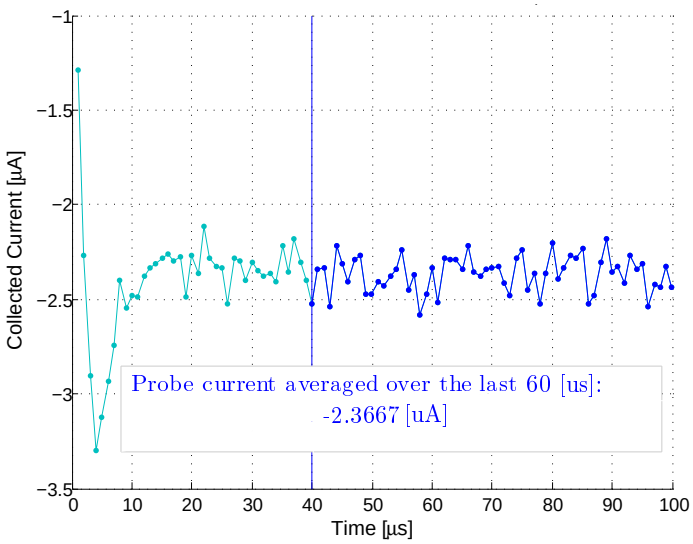

Figure C.34: *0.1V*

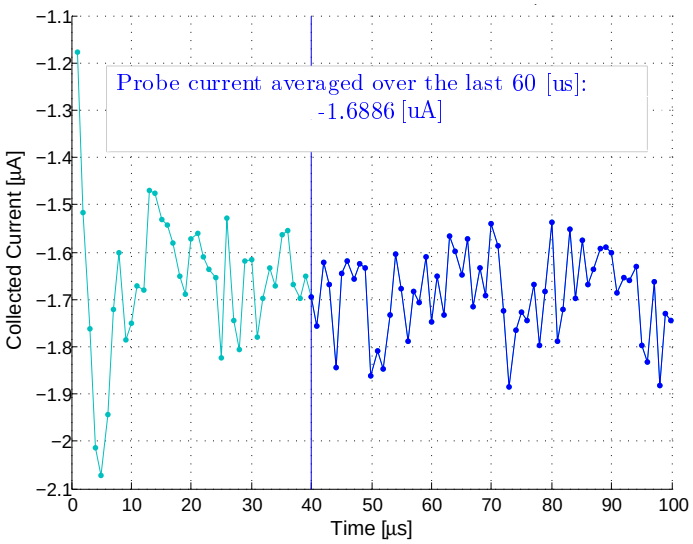

Figure C.35: *0.05V*

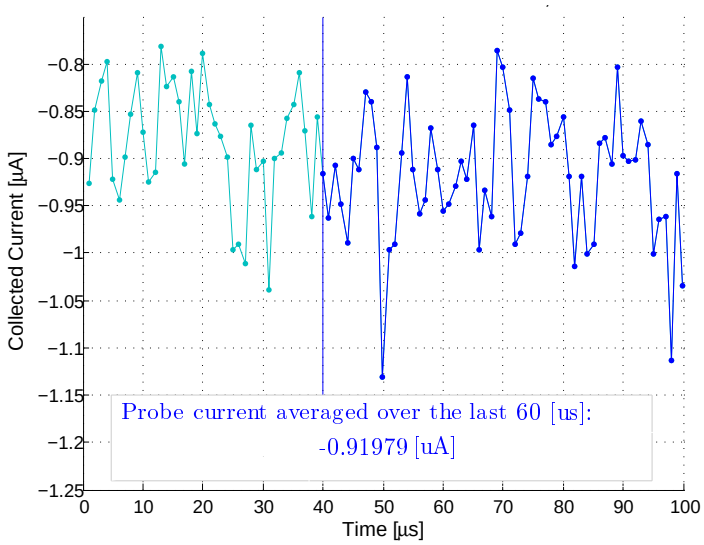

Figure C.36: *0V*

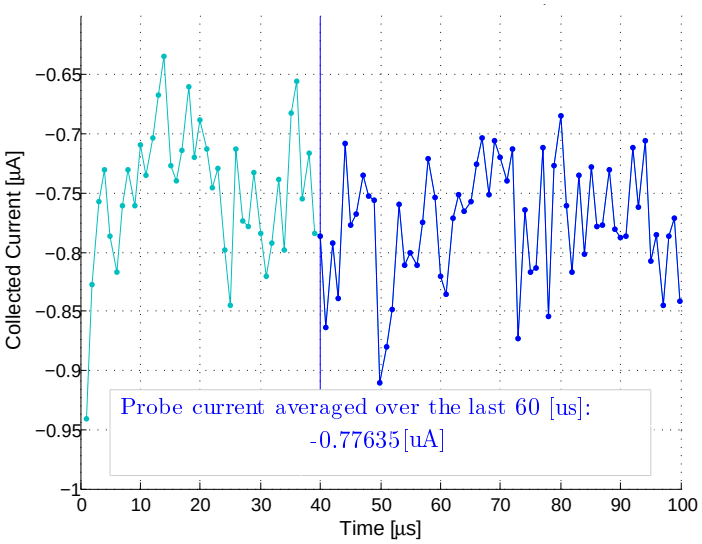

Figure C.37: *-0.01V*

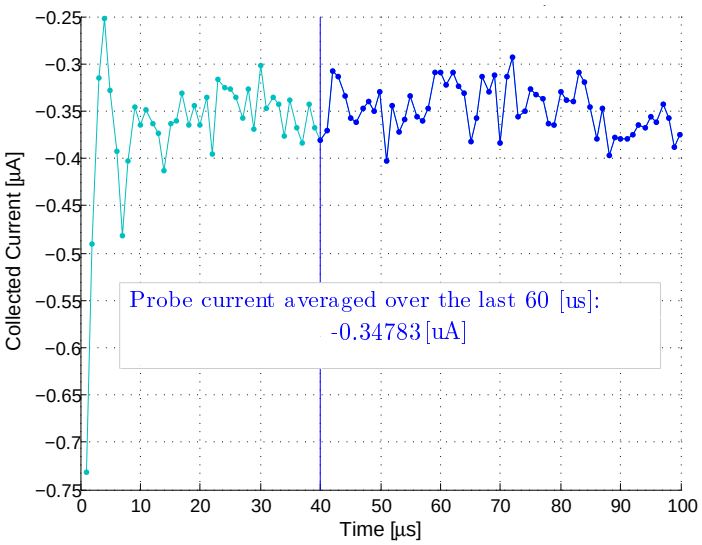

Figure C.38: *-0.05V*

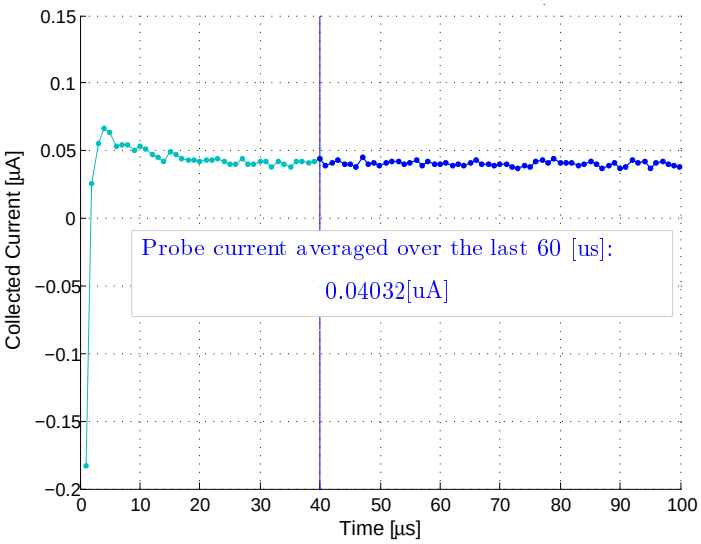

Figure C.39: *-0.5V*

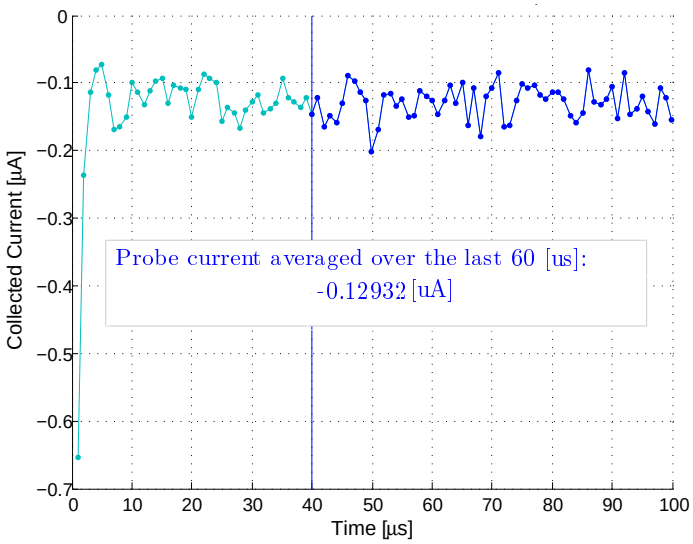

Figure C.40: *-0.1V*

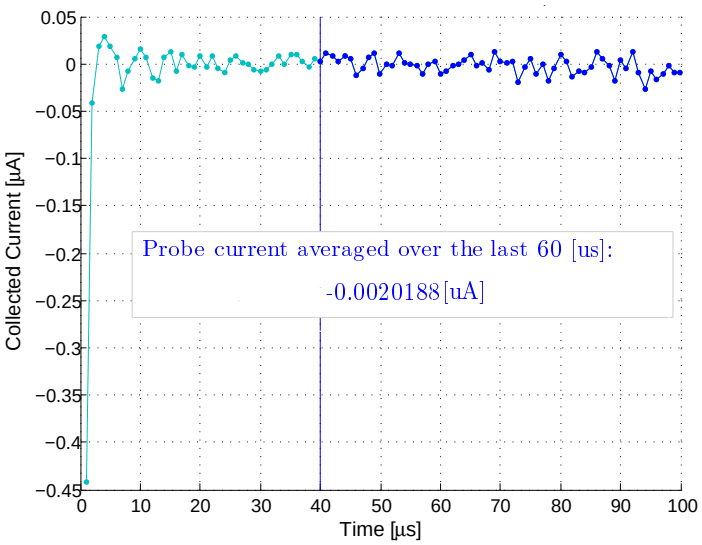

Figure C.41: *-0.2V*

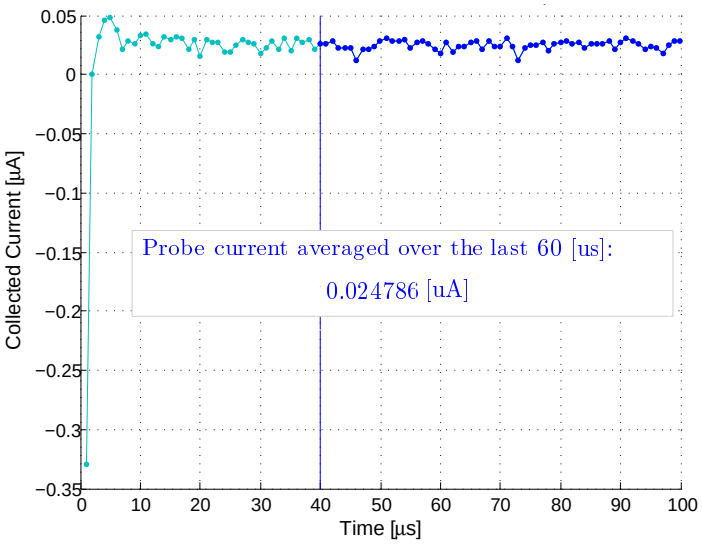

Figure C.42: *-0.3V*

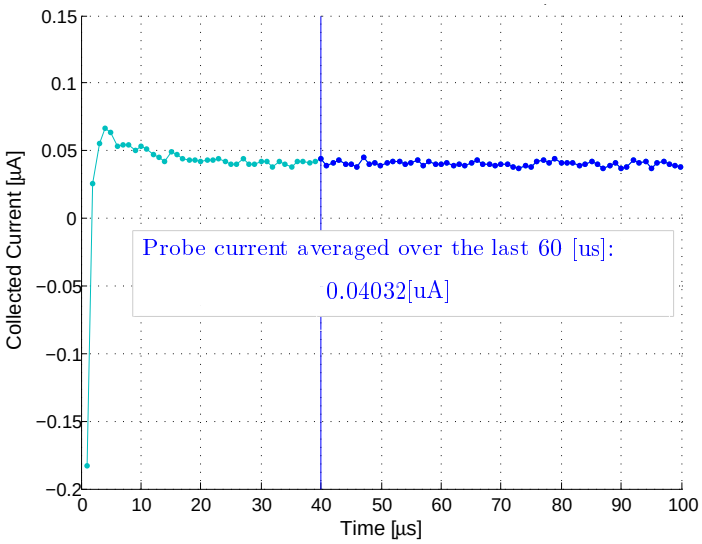

Figure C.43: *-0.5V*

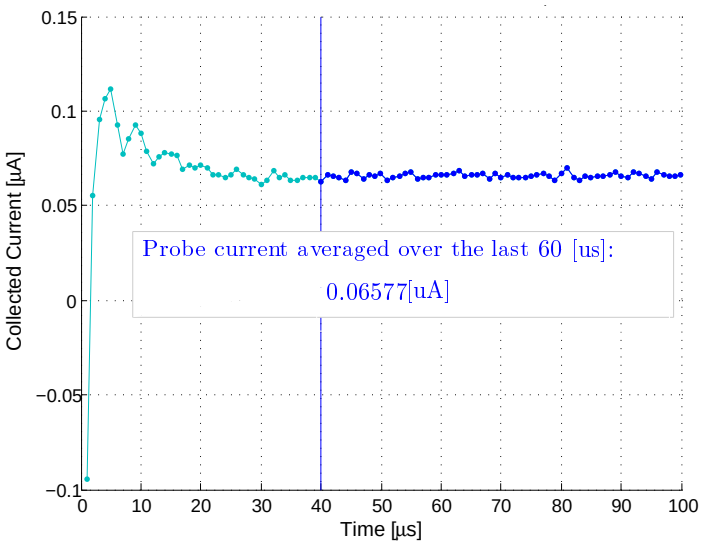

Figure C.44: *-1V*

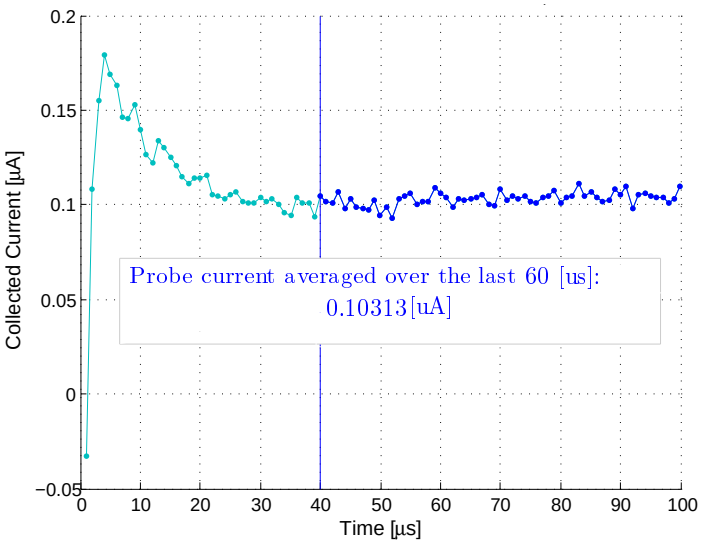

Figure C.45: *-2V*

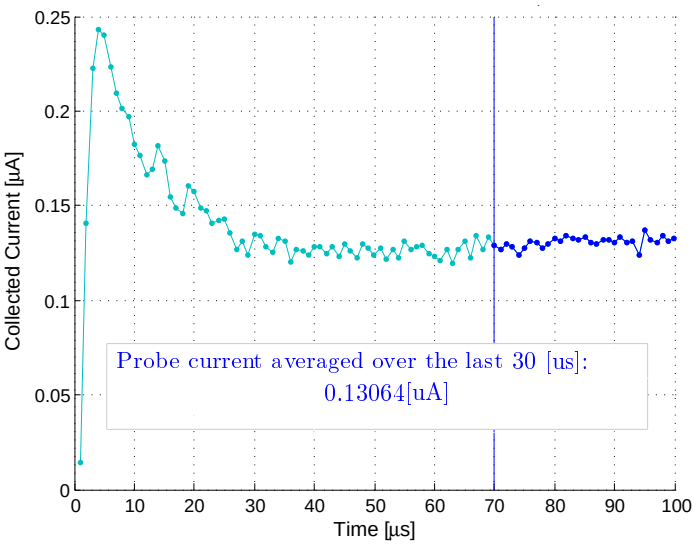

Figure C.46: *-3V*

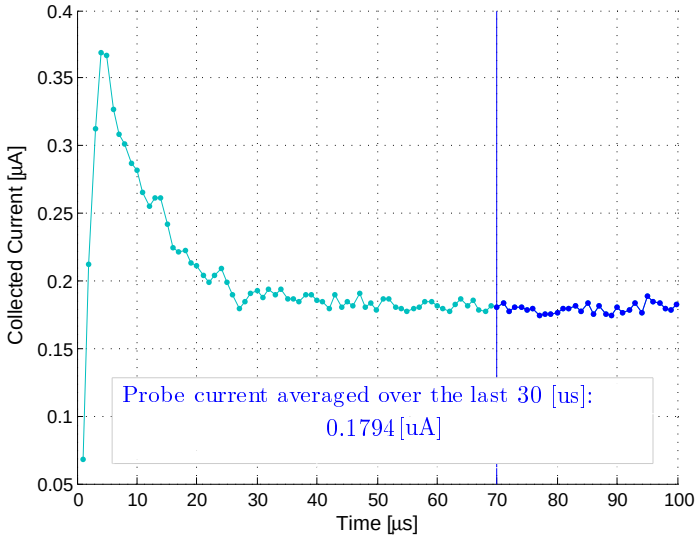

Figure C.47: *-5V*

C.2.4 Sphere-Stub R PIC, $\lambda_D \approx 1.7$mm

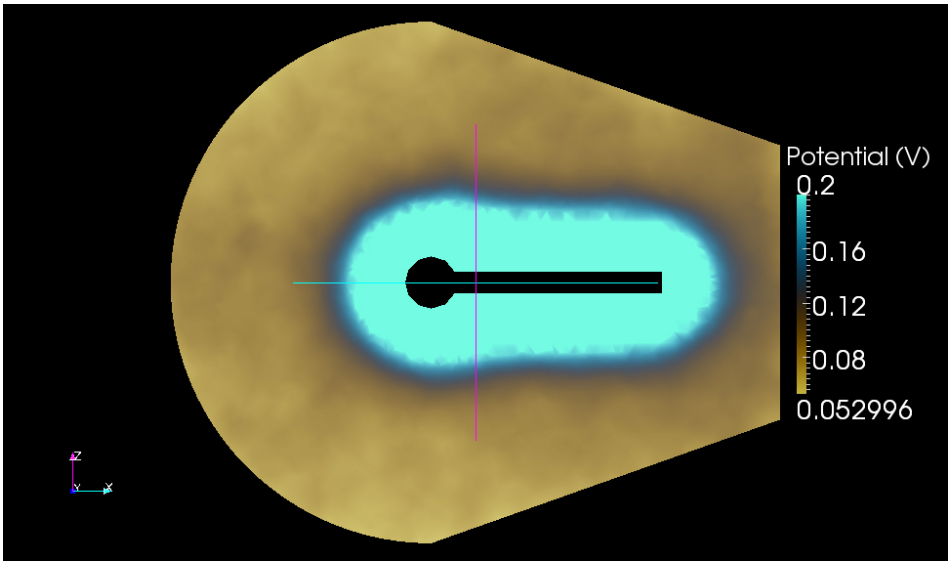

Figure C.48: *Potential map: bias = 2V, rescaled to 0.2V*

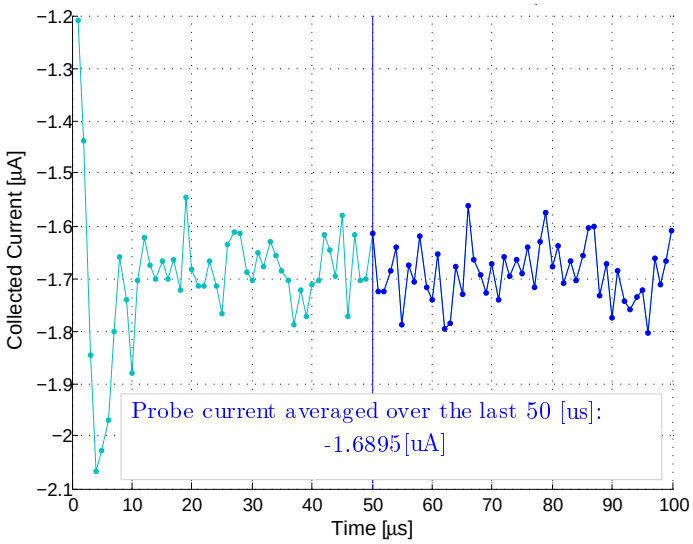

Figure C.49: *0.05V*

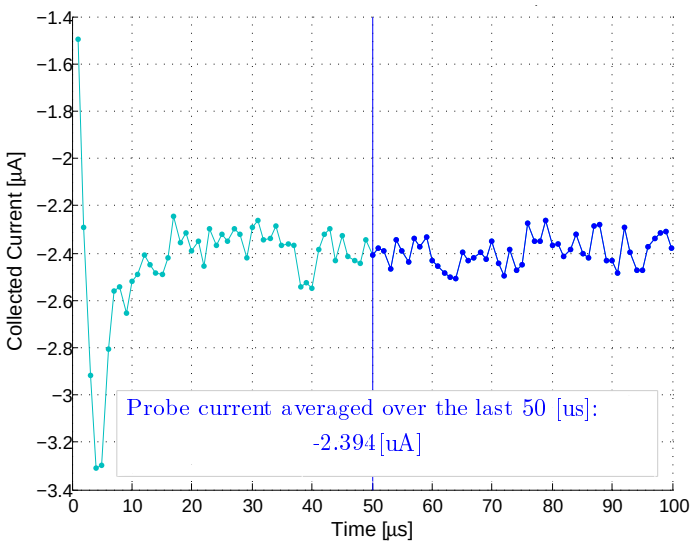

Figure C.50: *0.1V*

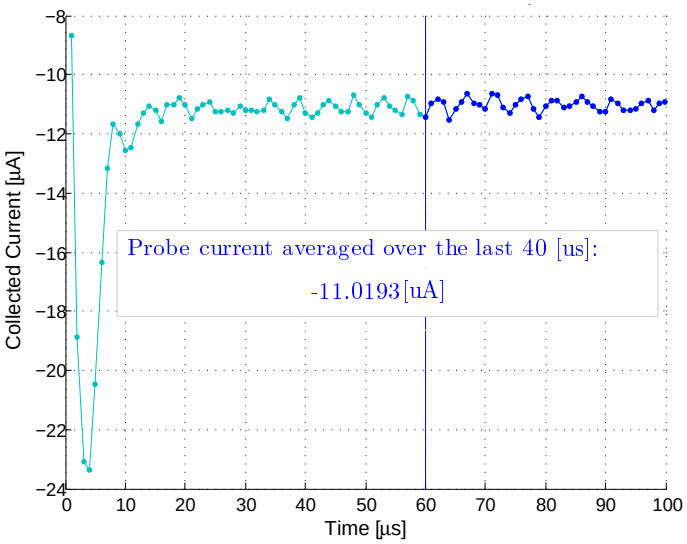

Figure C.51: *1V*

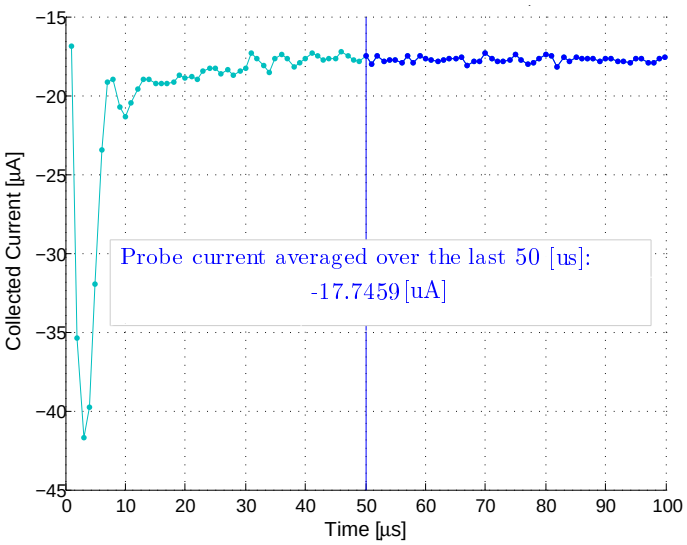

Figure C.52: *2V*

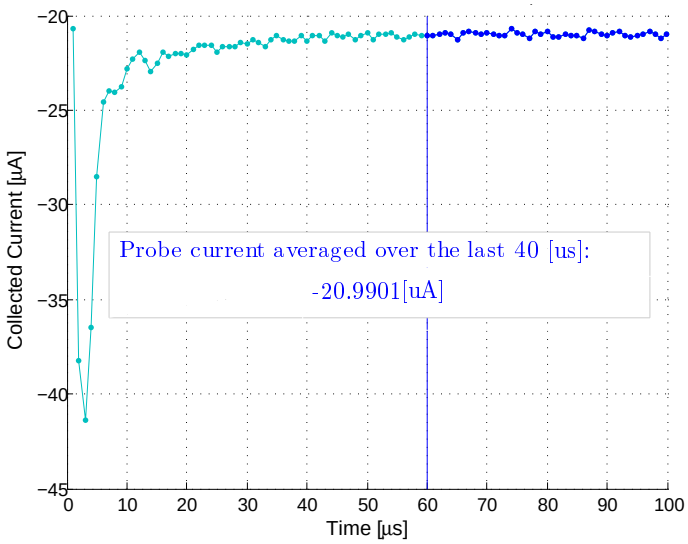

Figure C.53: *3V*

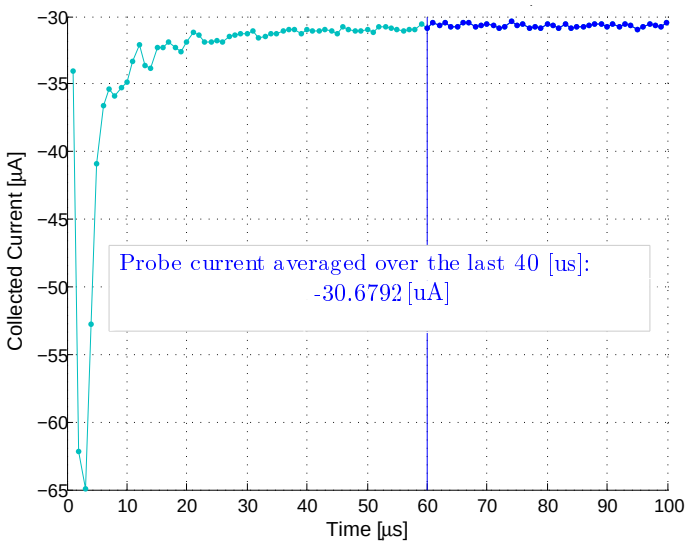

Figure C.54: *5V*

C.2.5 Sphere-Stub R drift PIC, $\lambda_D \approx 1.7$mm

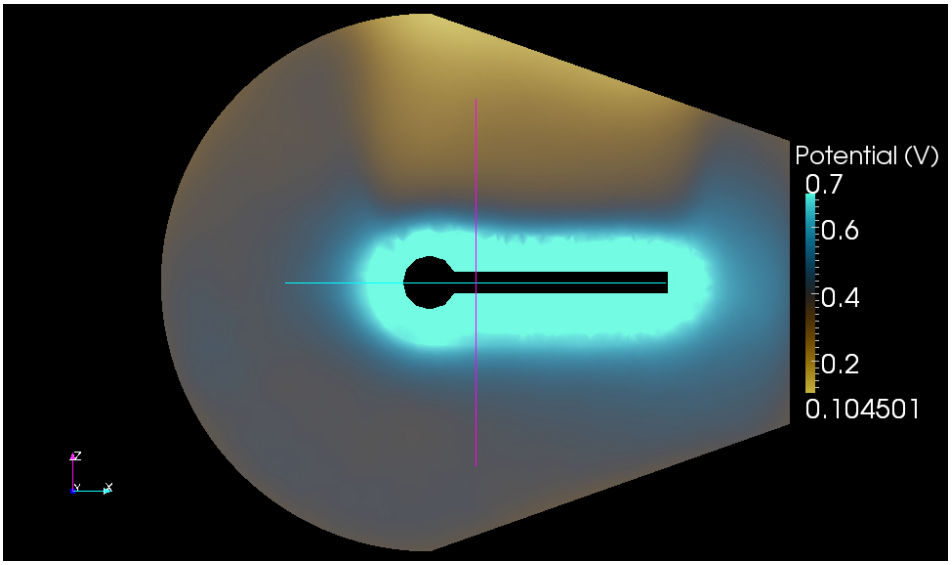

Figure C.55: *Potential map: bias = 2V, rescaled to 0.7V*

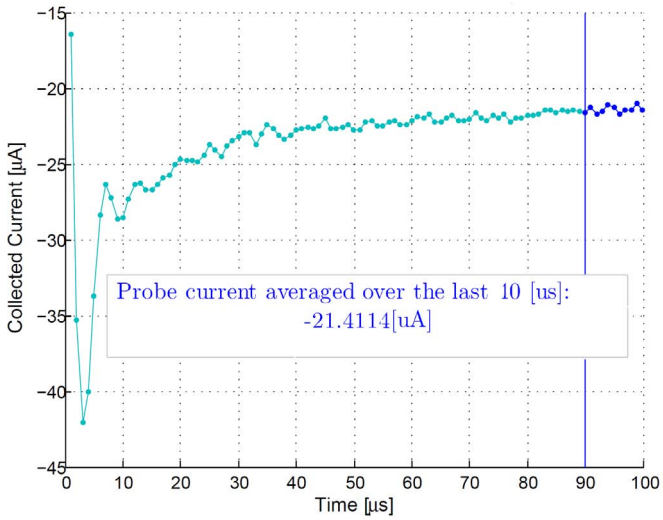

Figure C.56: *2V*

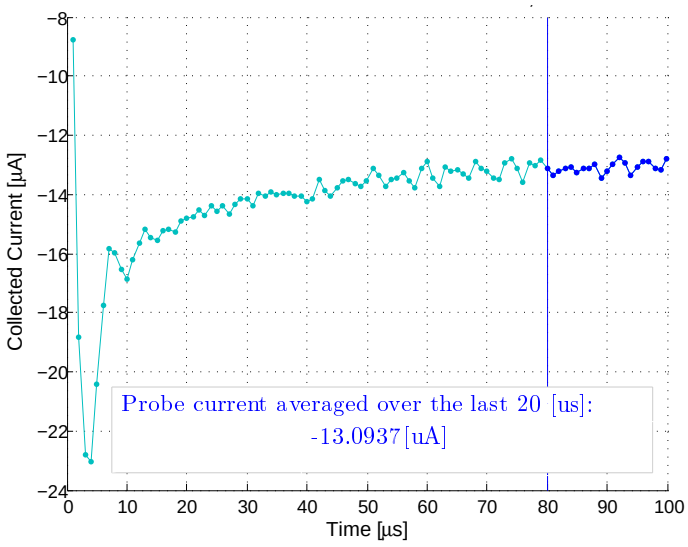

Figure C.57: *1V*

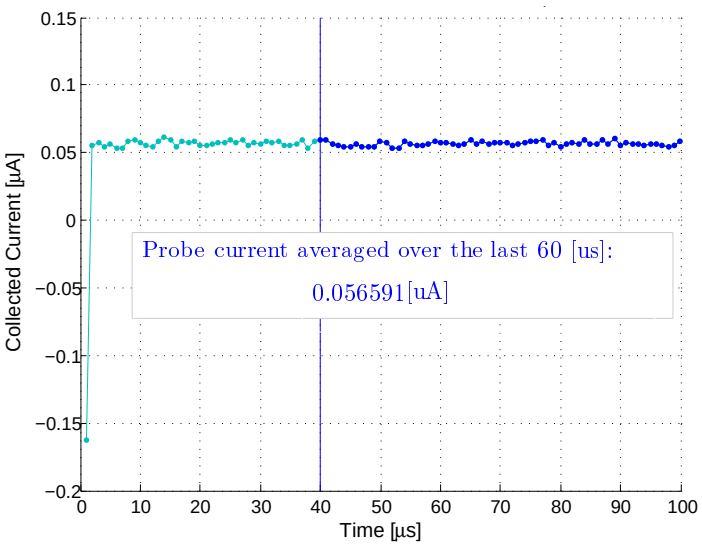

Figure C.58: *-0.5V*

C.2.6 Sphere-Stub V drift PIC, speed up= 13

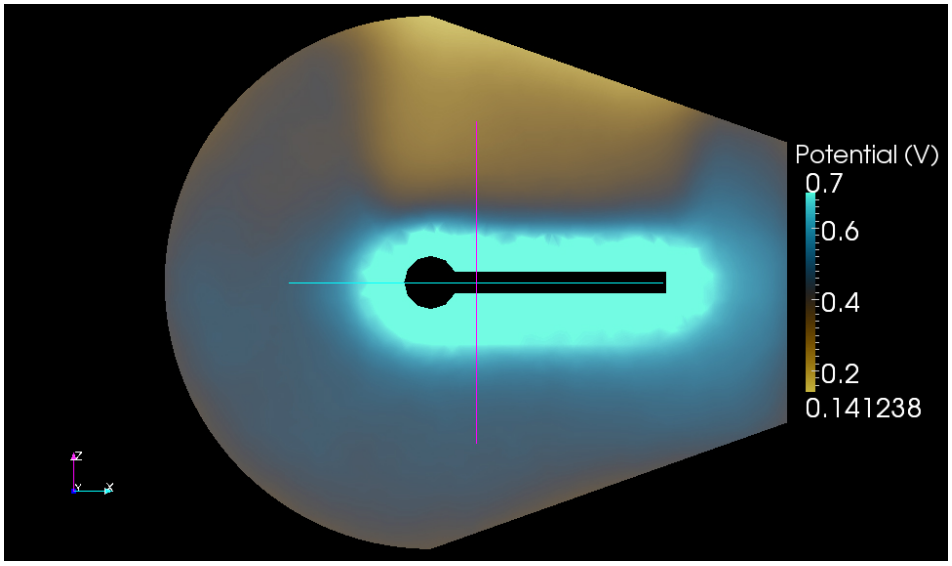

Figure C.59: *Potential map: bias = 2V, rescaled to 0.7V*

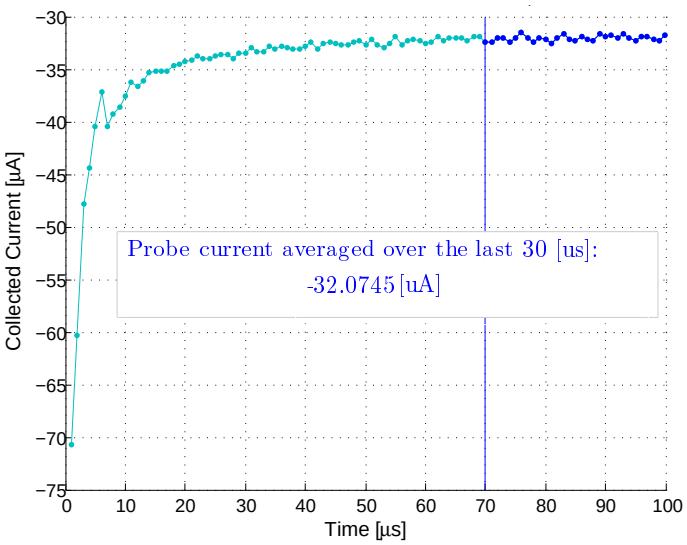

Figure C.60: *5V*

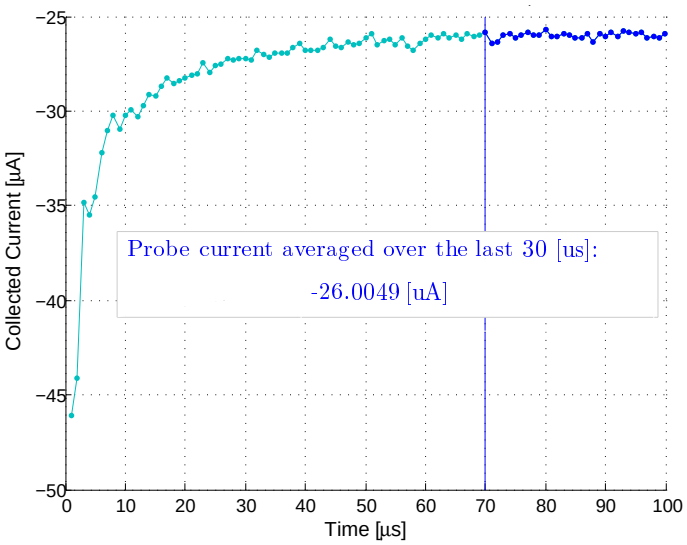

Figure C.61: *3V*

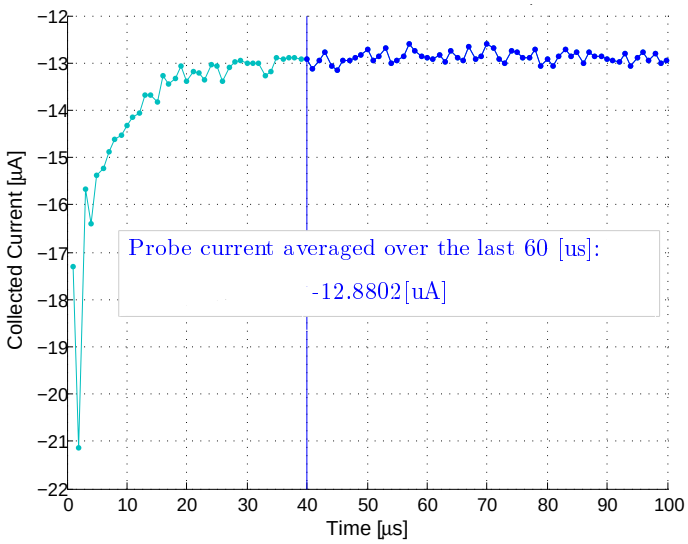

Figure C.62: *1V*

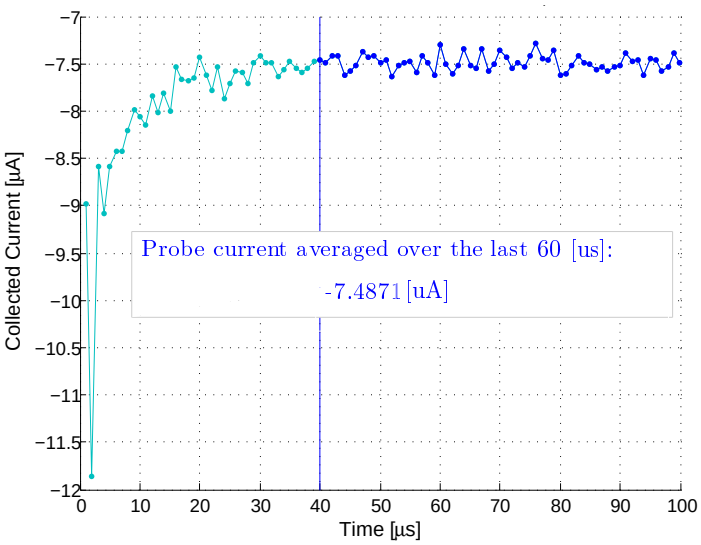

Figure C.63: *0.5V*

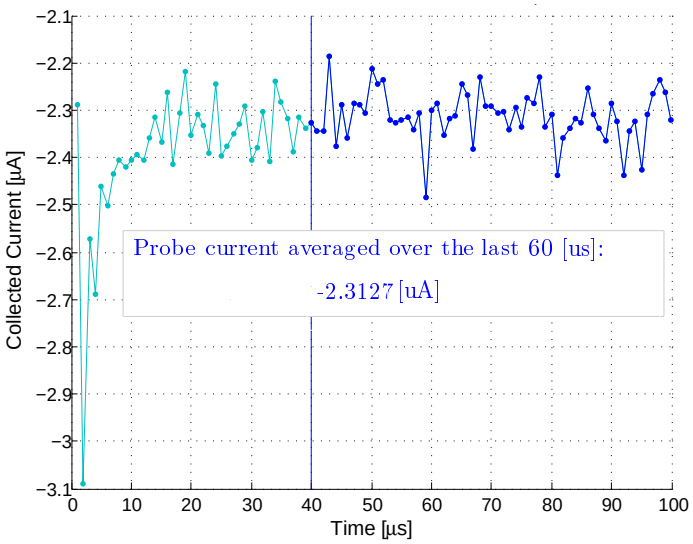

Figure C.64: *0.1V*

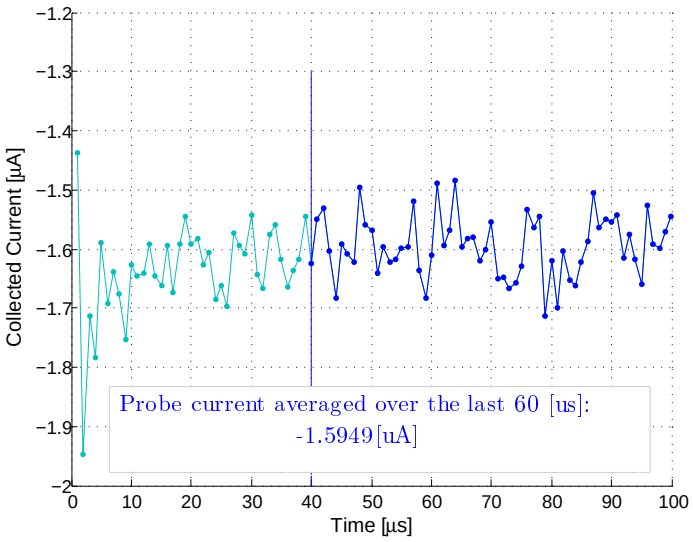

Figure C.65: *0.05V*

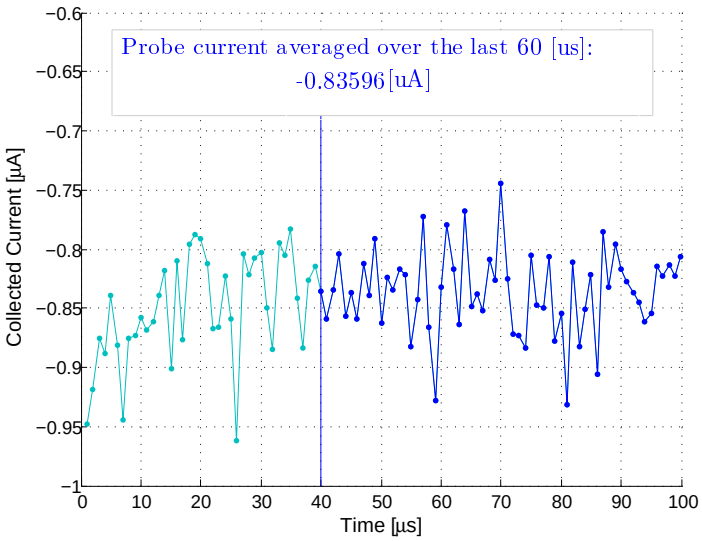

Figure C.66: *0V*

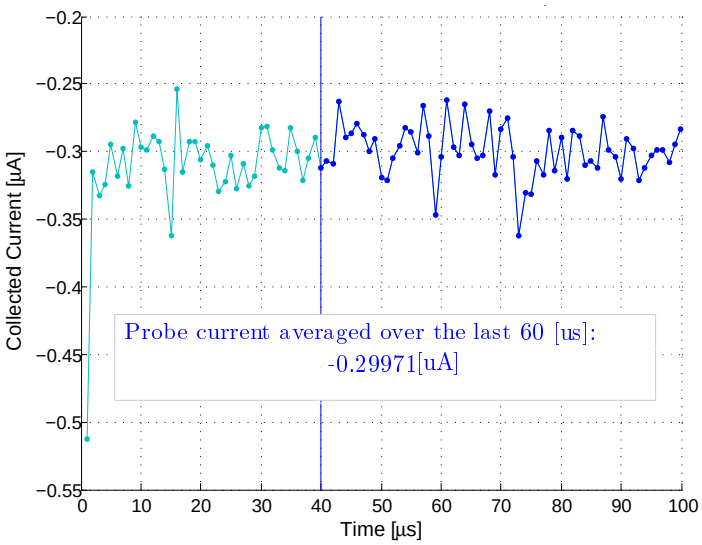

Figure C.67: *-0.05V*

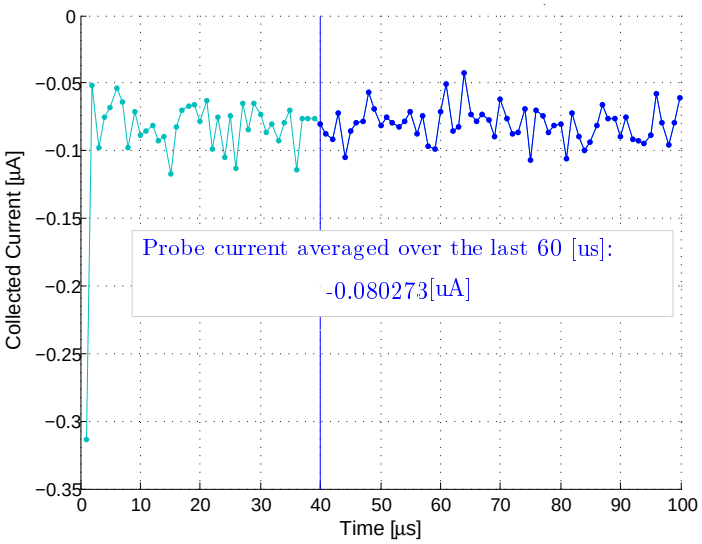

Figure C.68: *-0.1V*

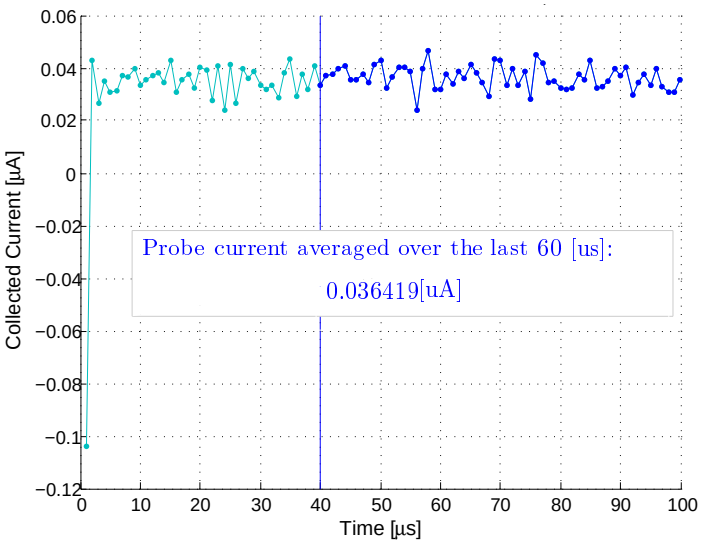

Figure C.69: *-0.2V*

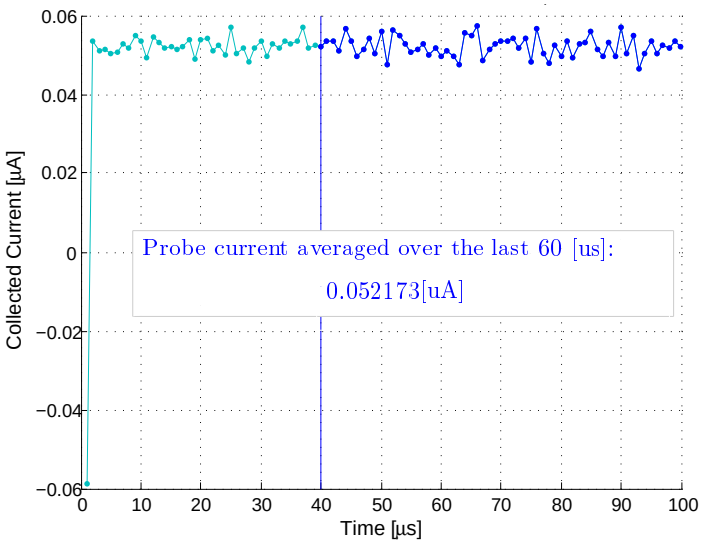

Figure C.70: *-0.3V*

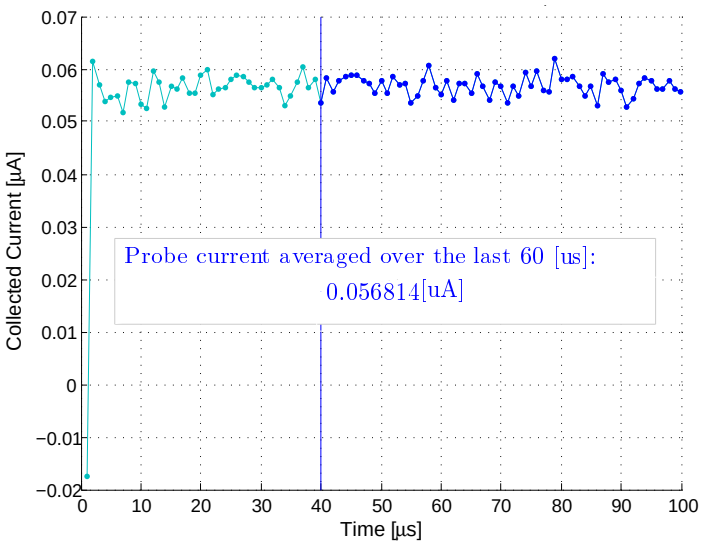

Figure C.71: *-0.5V*

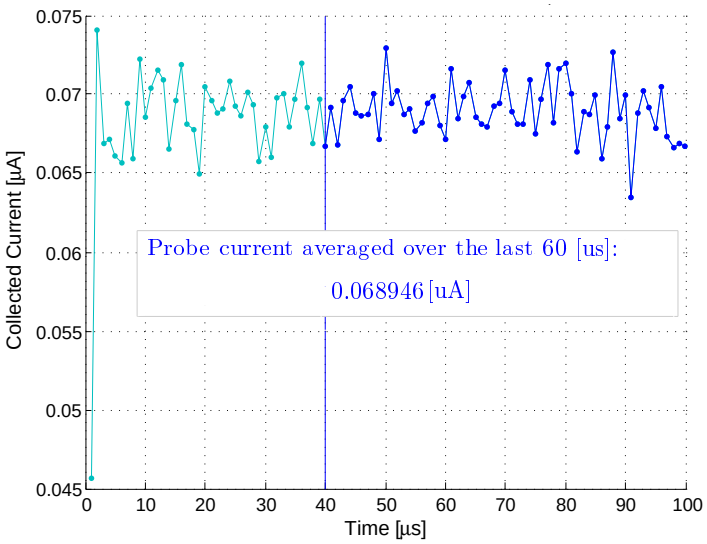

Figure C.72: *-2V*

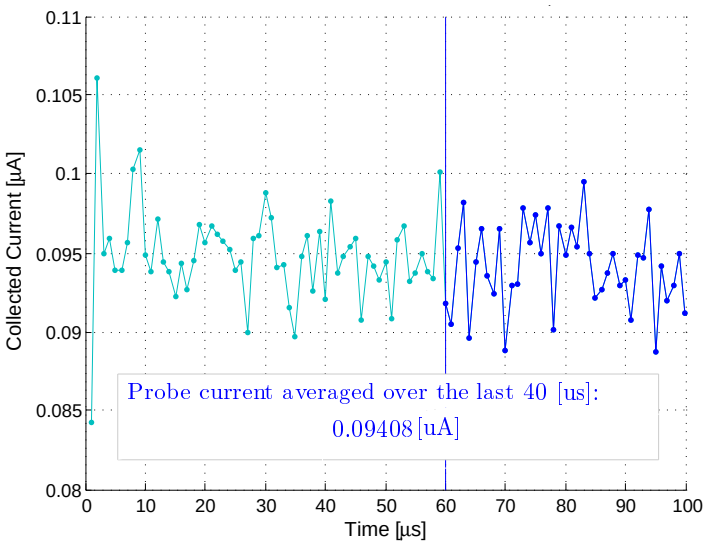

Figure C.73: *-5V*

C.2.7 Stub PIC, $\lambda_D \approx 1.7$mm

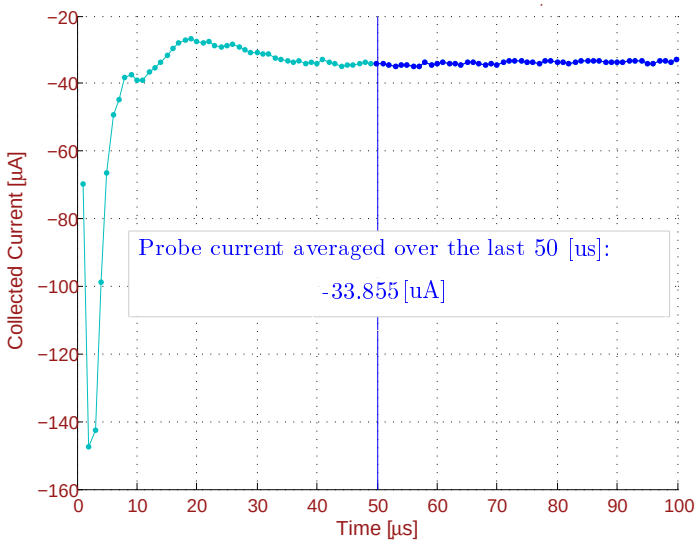

Figure C.74: *5V*

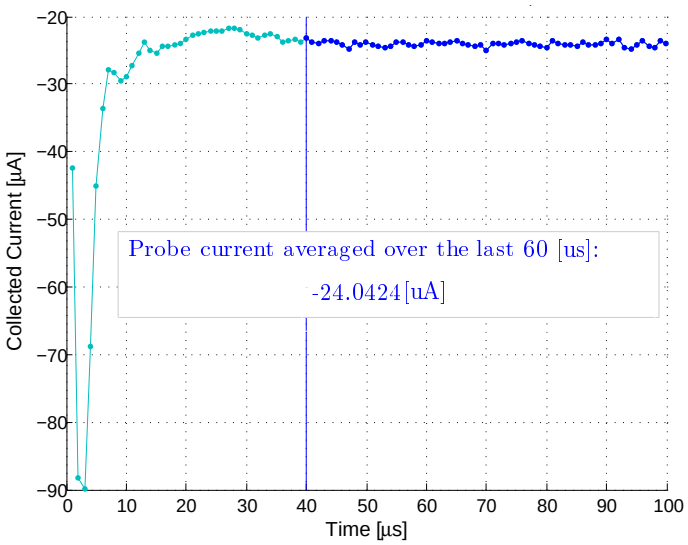

Figure C.75: *3V*

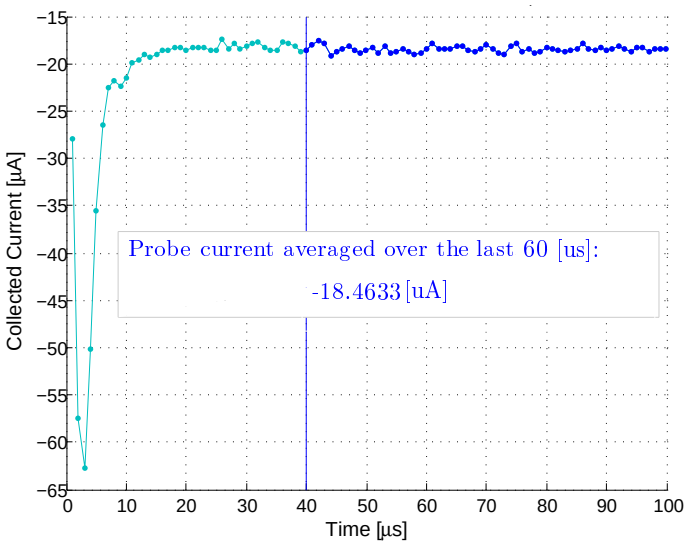

Figure C.76: *2V*

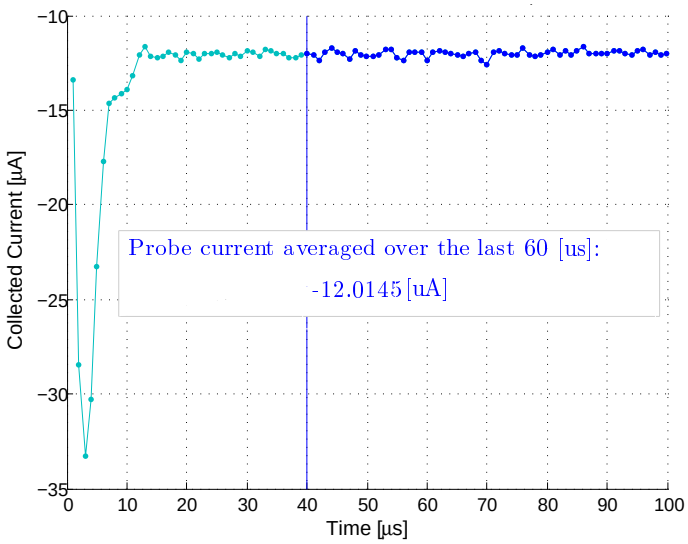

Figure C.77: *1V*

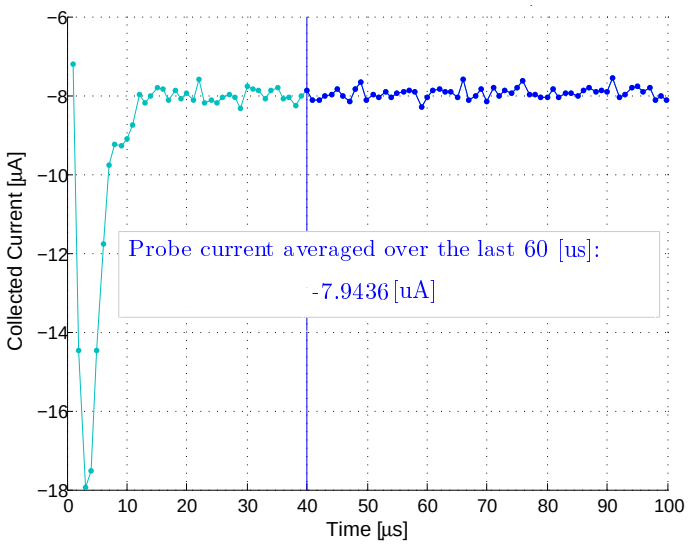

Figure C.78: *0.5V*

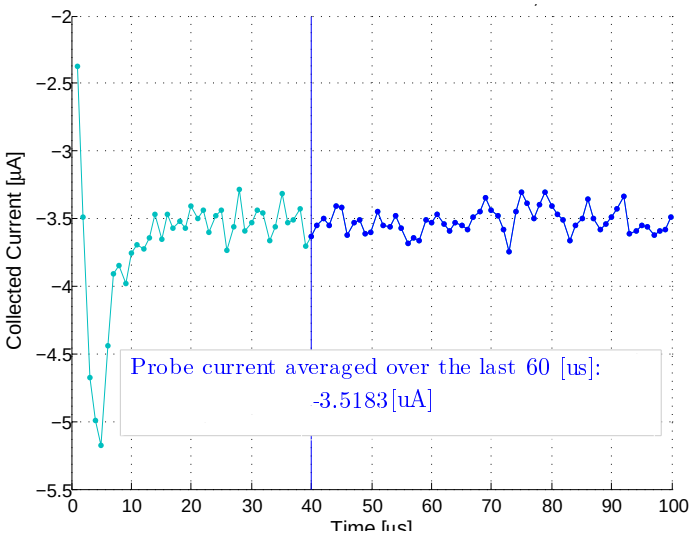

Figure C.79: *0.1V*

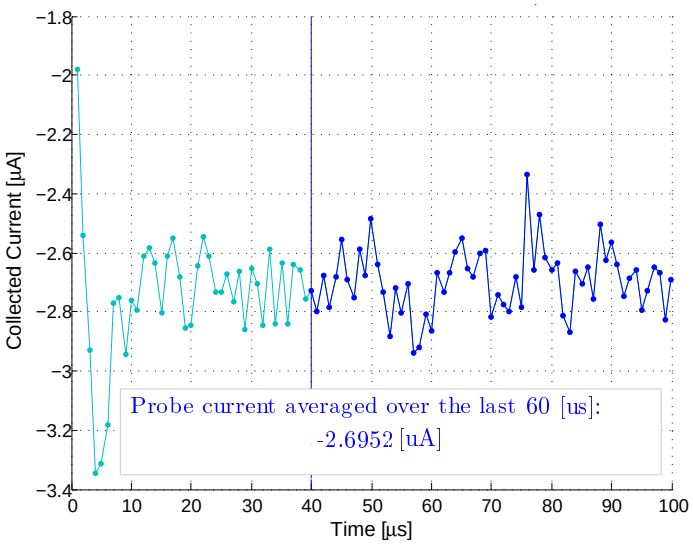

Figure C.80: *0.05V*

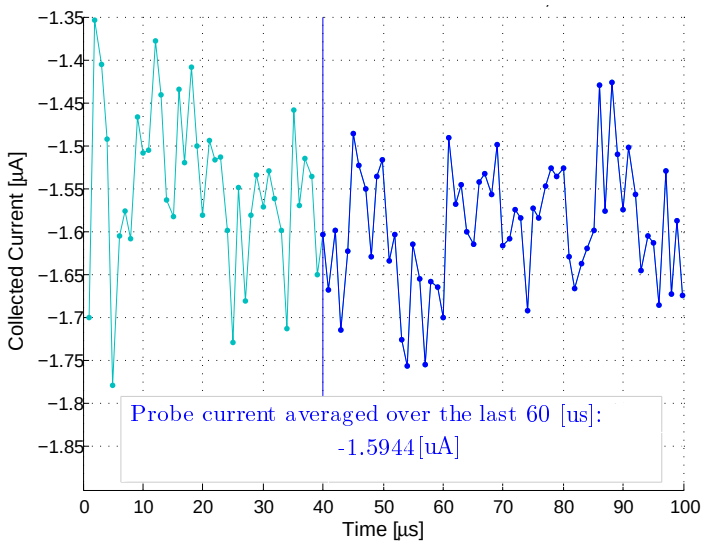

Figure C.81: *0V*

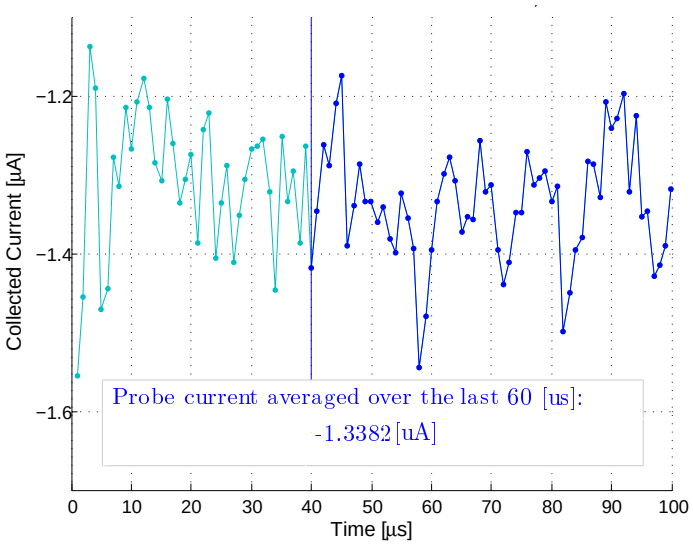

Figure C.82: *-0.01V*

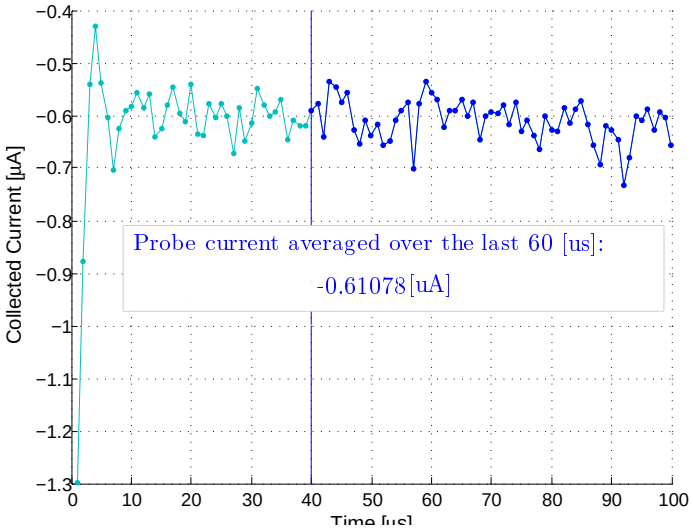

Figure C.83: *-0.05V*

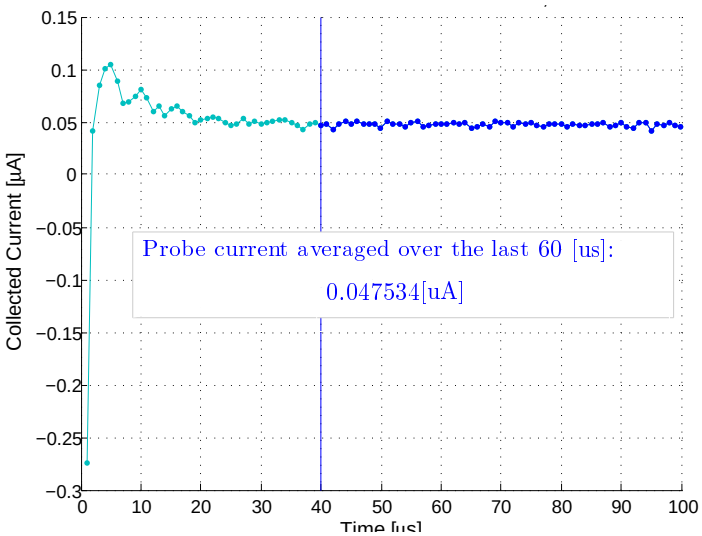

Figure C.84: *-0.5V*

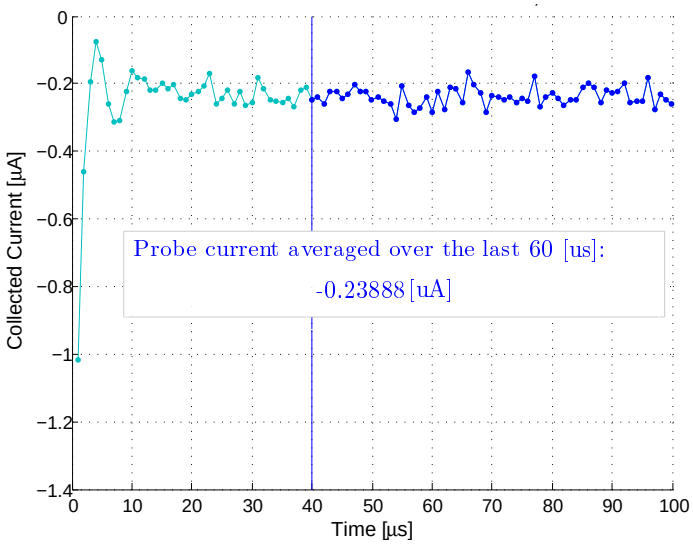

Figure C.85: *-0.1V*

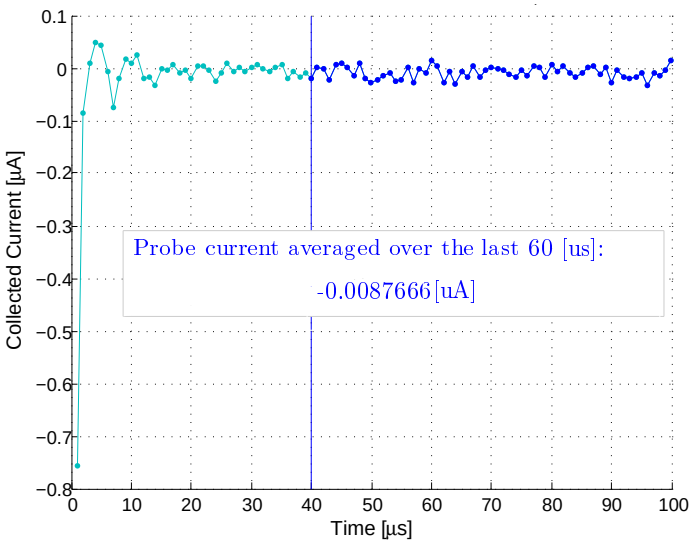

Figure C.86: *-0.2V*

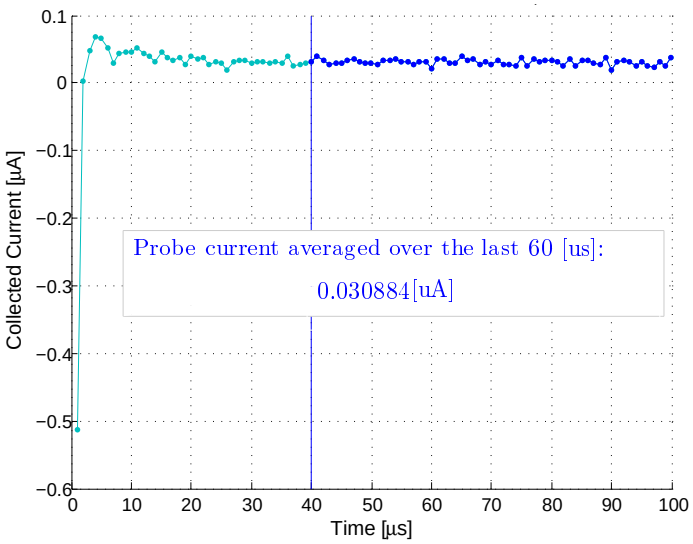

Figure C.87: *-0.3V*

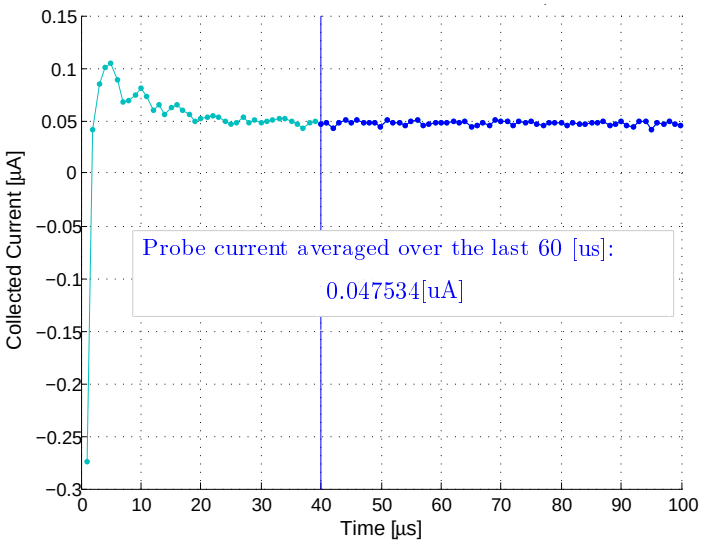

Figure C.88: *-0.5V*

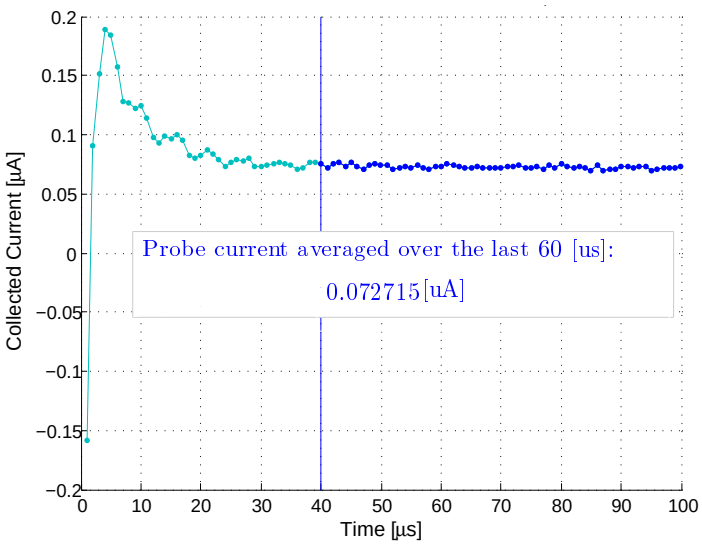

Figure C.89: *-1V*

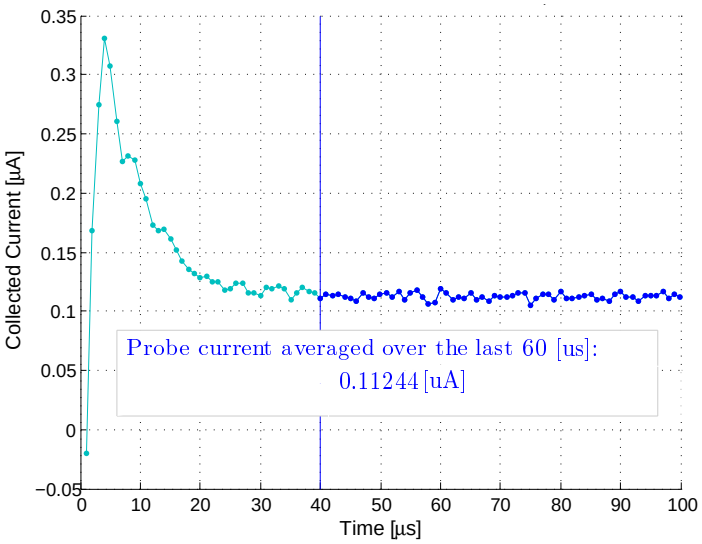

Figure C.90: *-2V*

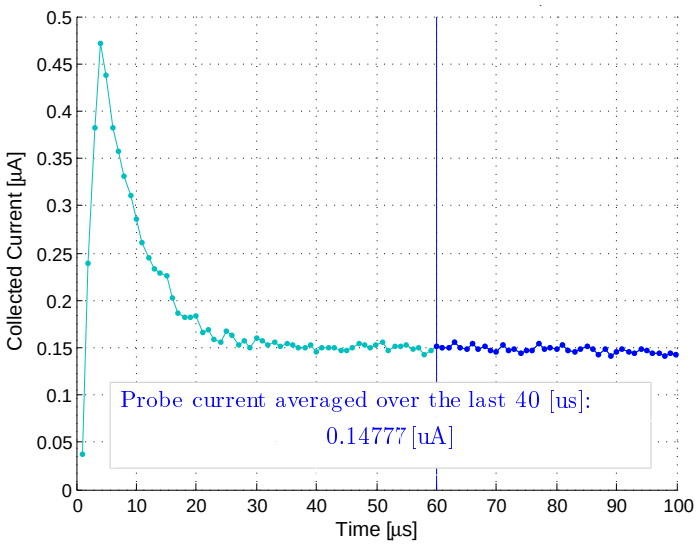

Figure C.91: *-3V*

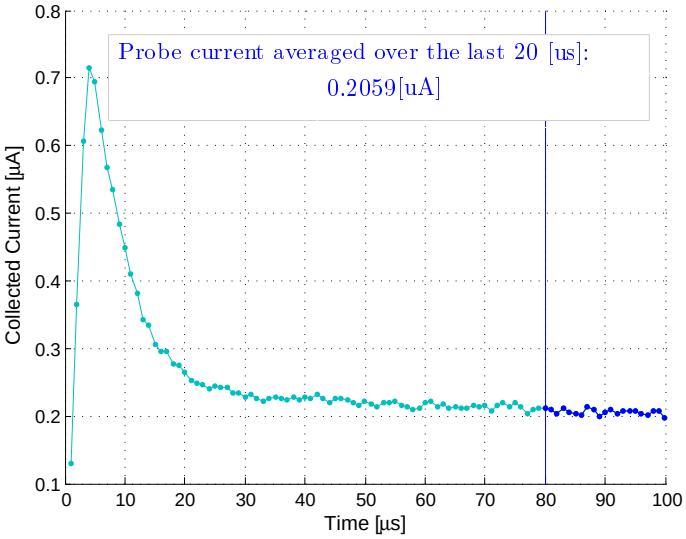

Figure C.92: *-5V*

C.2.8 Sphere drift PIC, speed up=13 and $\lambda_D \approx 1.7$mm

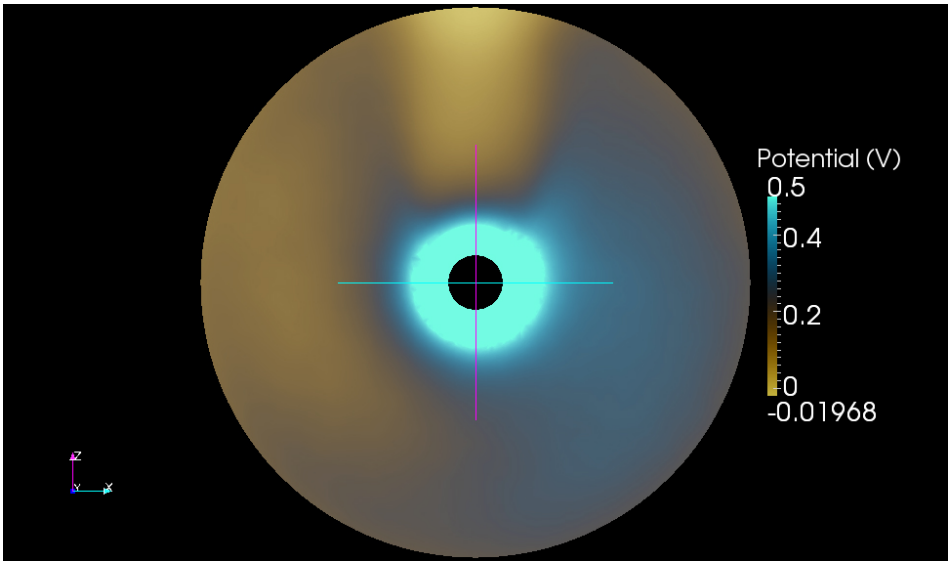

Figure C.93: *Potential map: bias = 2V, rescaled to 0.7V*

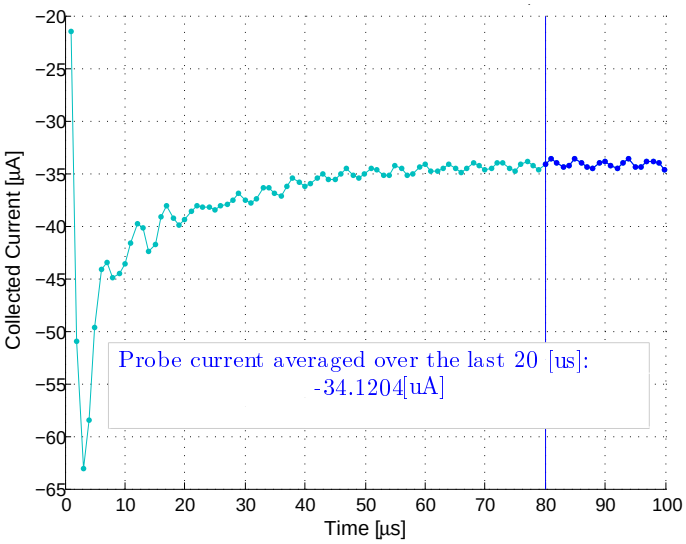

Figure C.94: *2V*

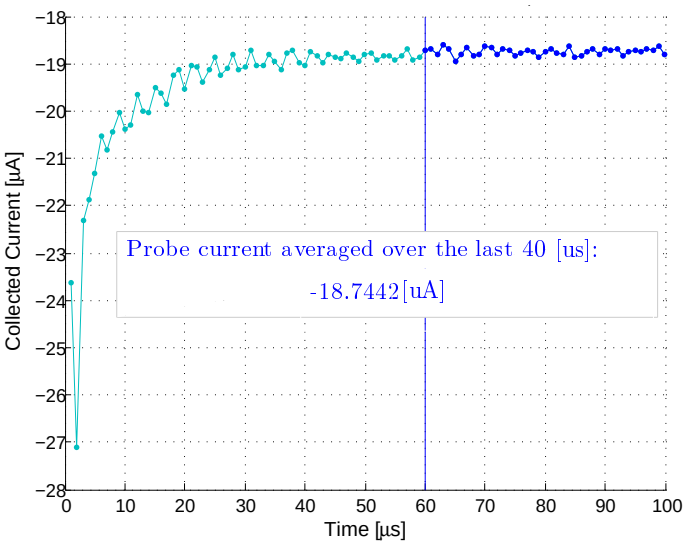

Figure C.95: *1V*

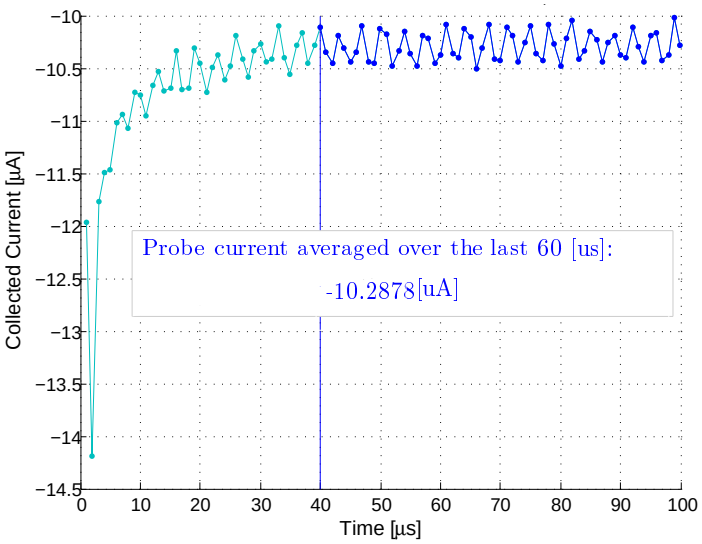

Figure C.96: *05V*

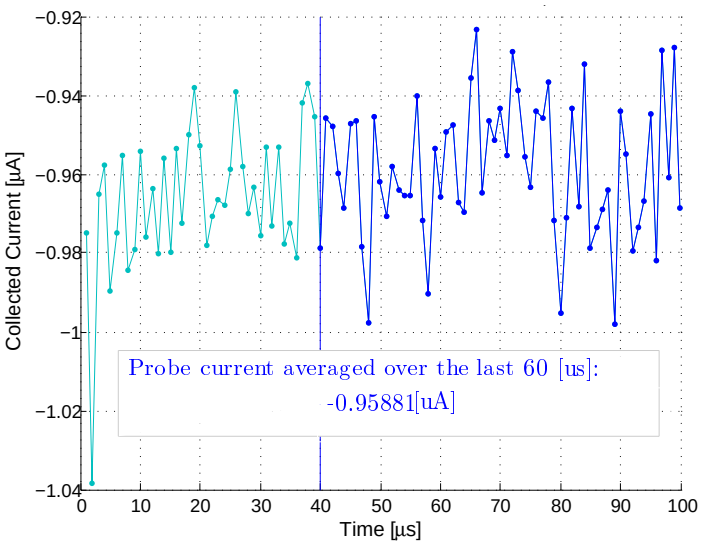

Figure C.97: *2V*

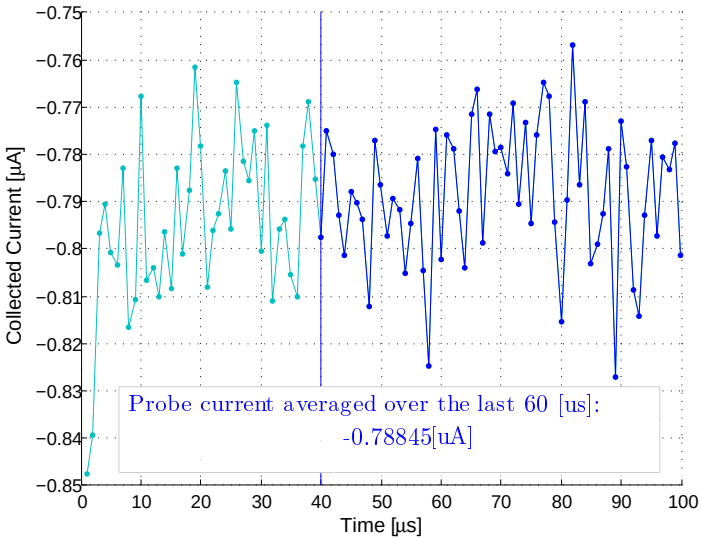

Figure C.98: *-0.01V*

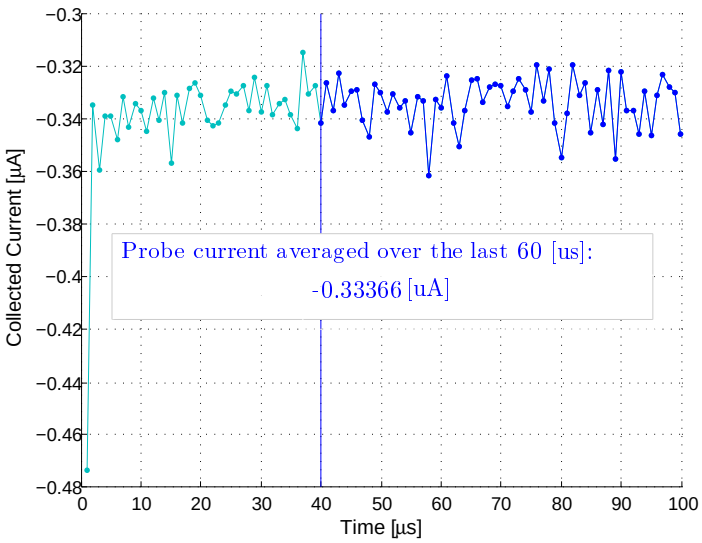

Figure C.99: *-0.05V*

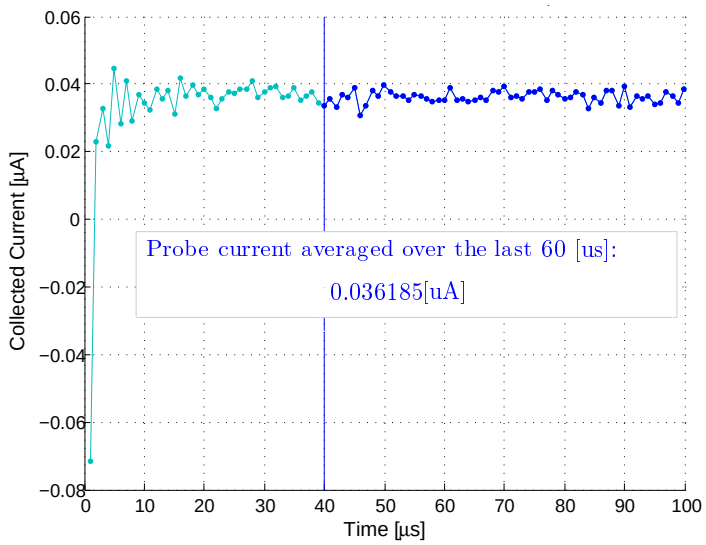

Figure C.100: *-0.2V*

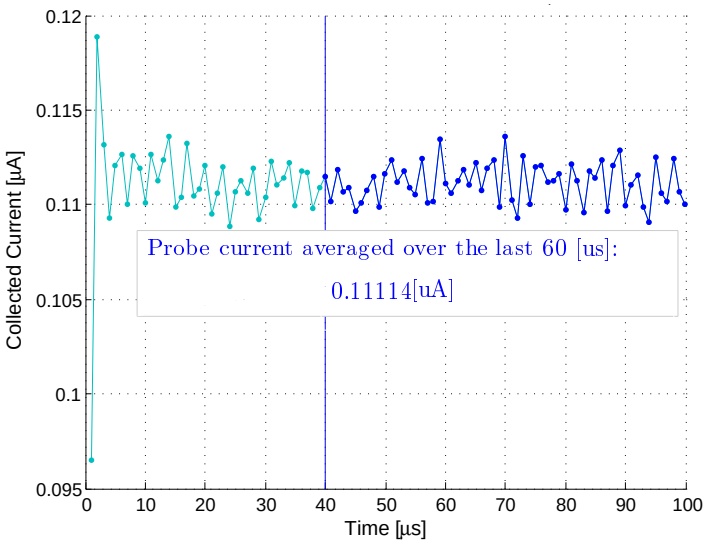

Figure C.101: *-5V*

C.3 Average density plasma

$n_{O^+} = n_{e^-} = 10^{11}\mathrm{m}^{-3}$ $\lambda_D \approx 10\,\mathrm{mm}$

C.3.1 Sphere PIC, $\lambda_D \approx 10$mm

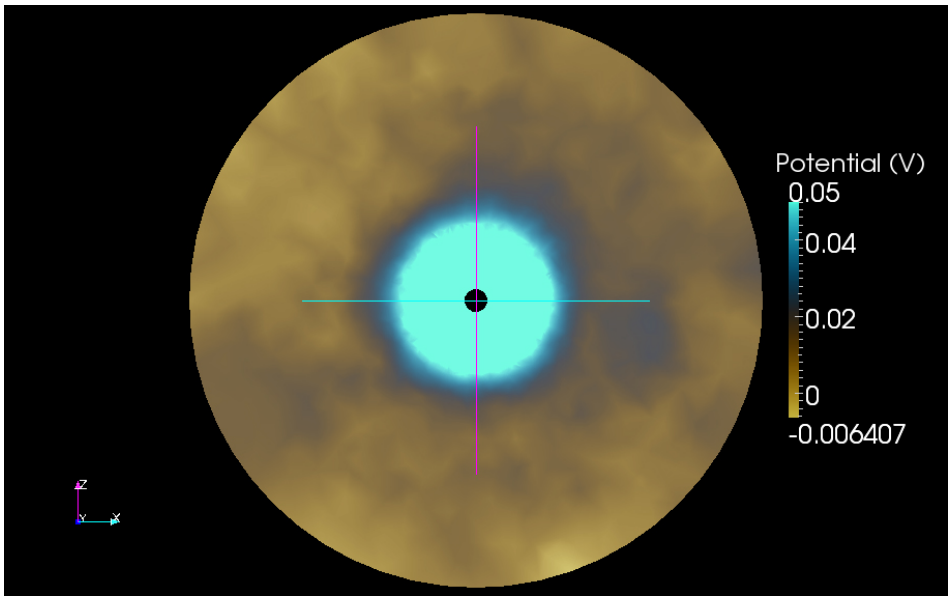

Figure C.102: *Potential map: bias = 2V, rescaled to 0.05V*

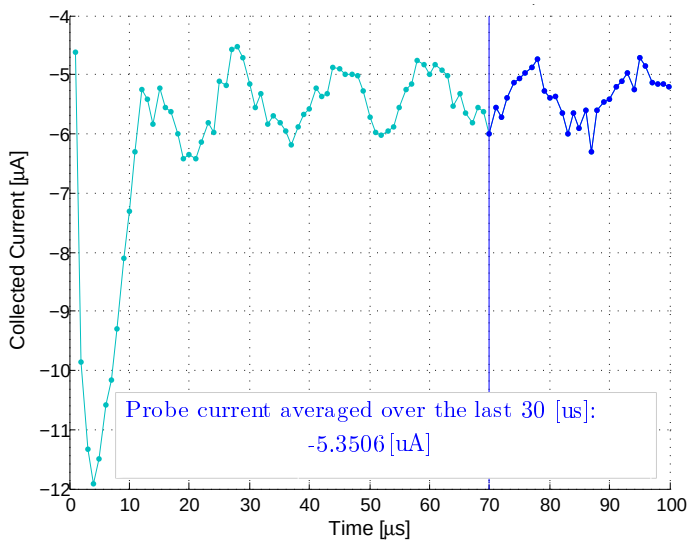

Figure C.103: *5V*

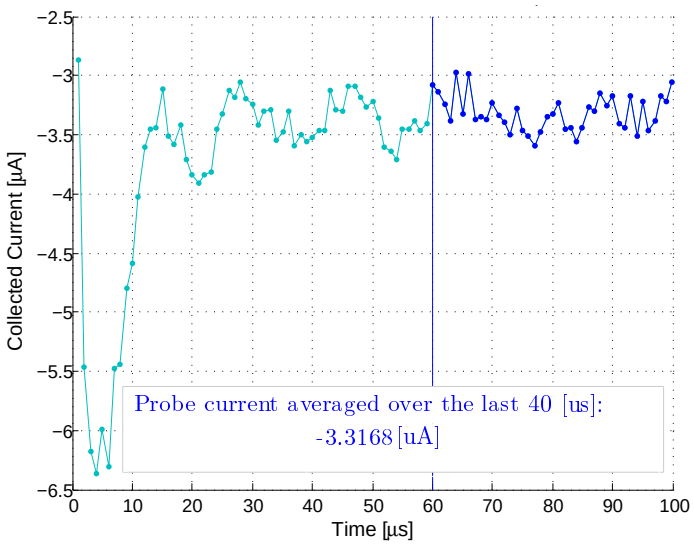

Figure C.104: *3V*

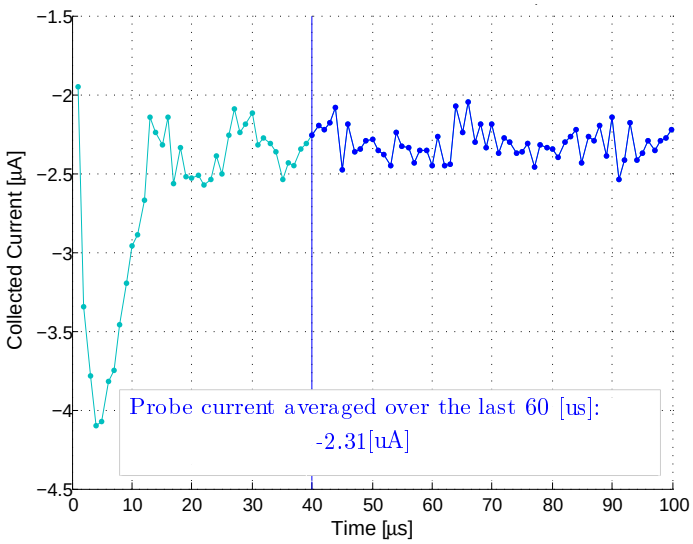

Figure C.105: *2V*

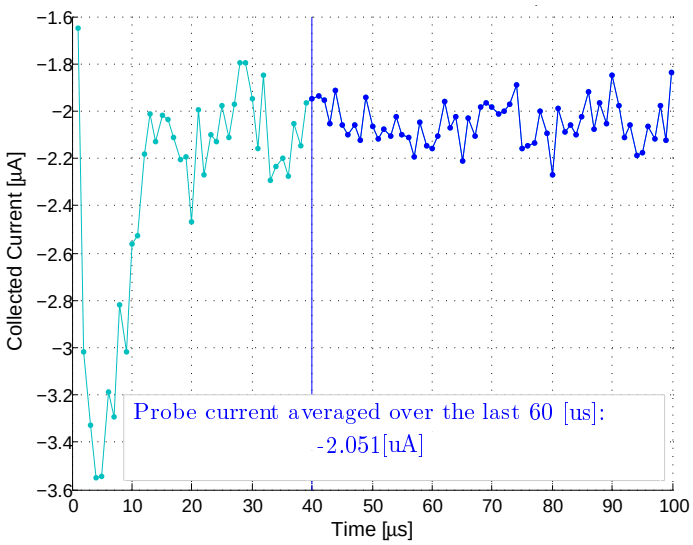

Figure C.106: *1.75V*

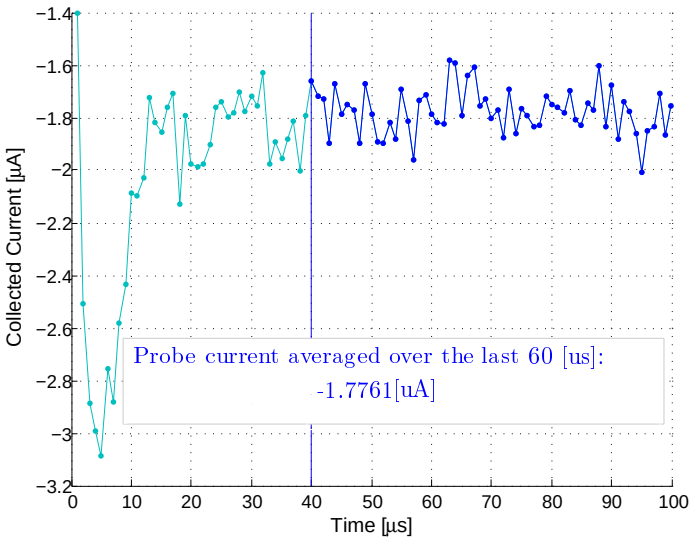

Figure C.107: *1.5V*

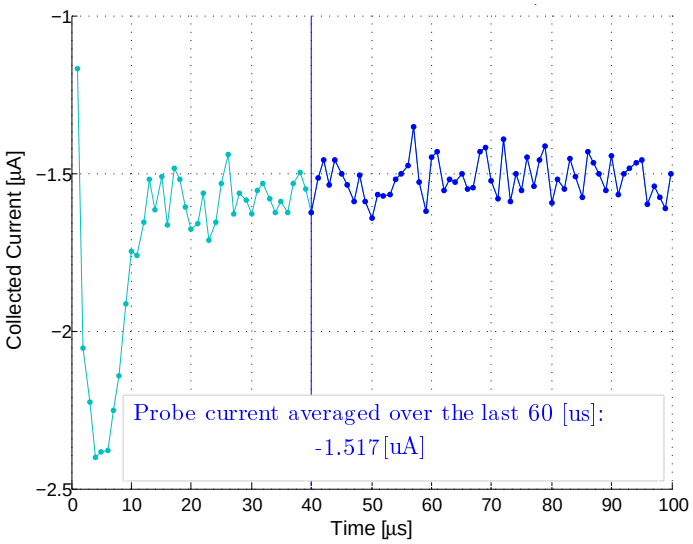

Figure C.108: *1.25V*

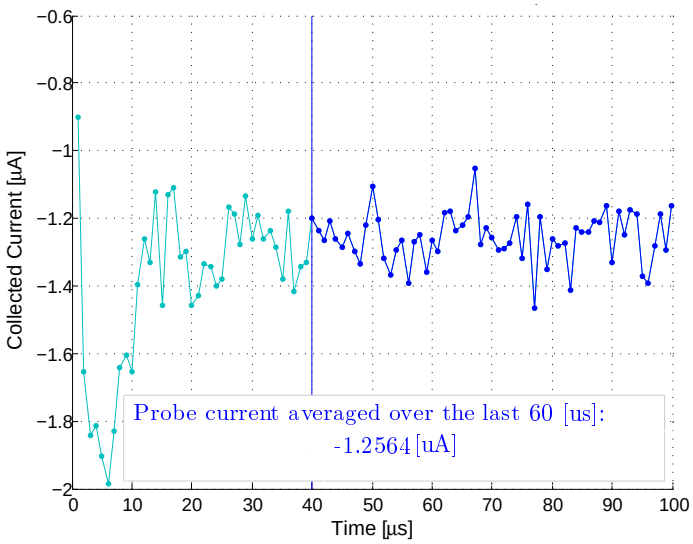

Figure C.109: *1V*

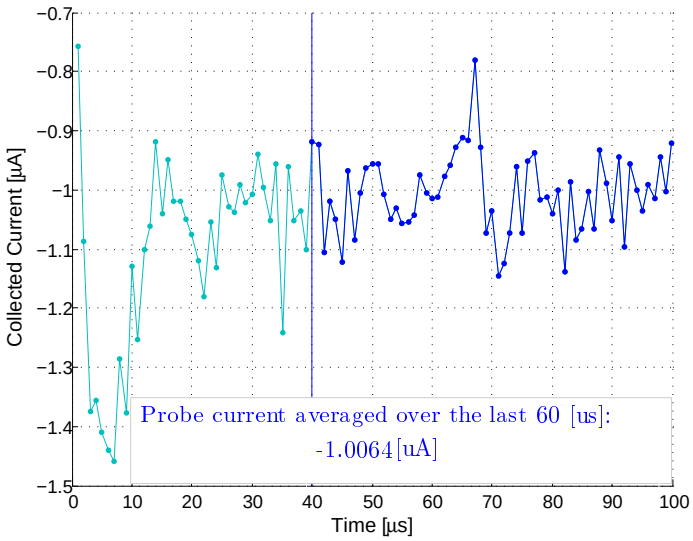

Figure C.110: *0.75V*

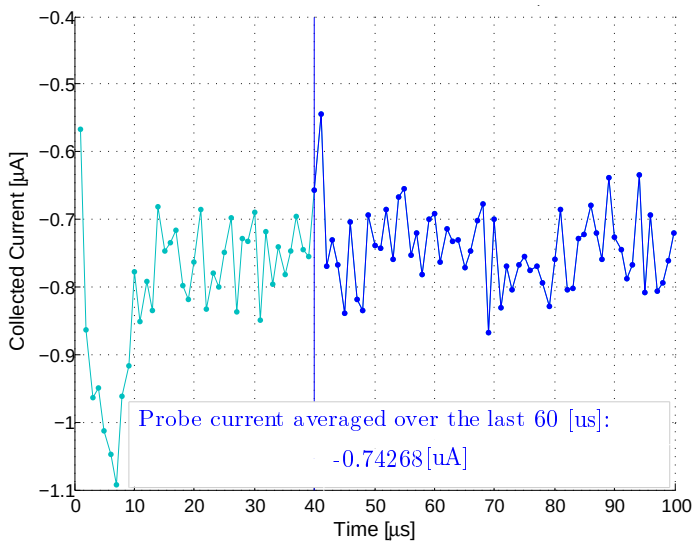

Figure C.111: *0.5V*

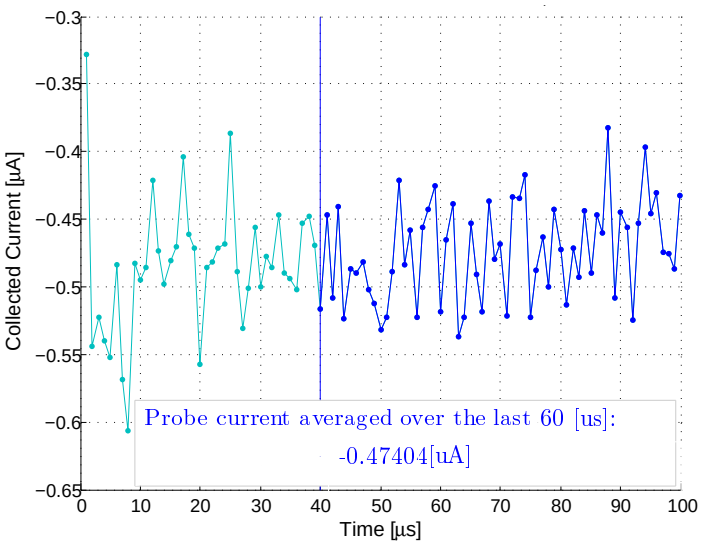

Figure C.112: *0.25V*

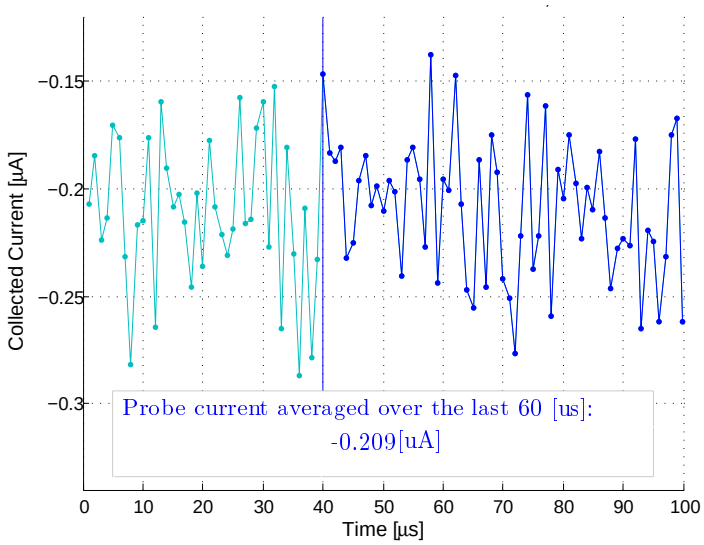

Figure C.113: *0V*

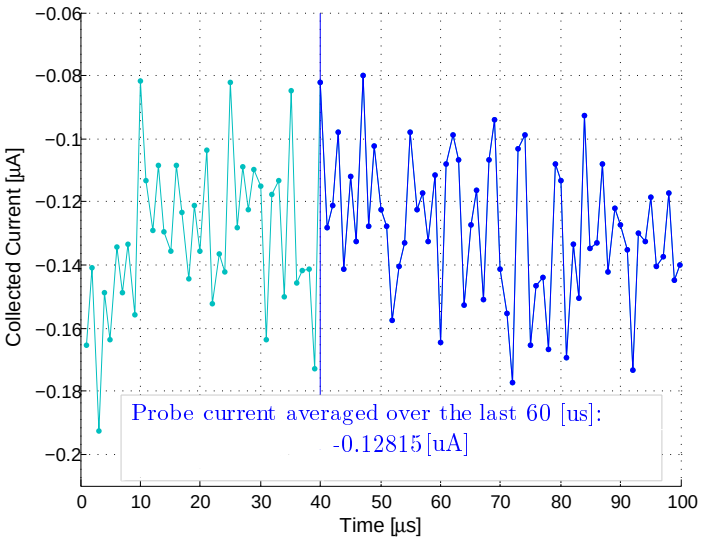

Figure C.114: *-0.1V*

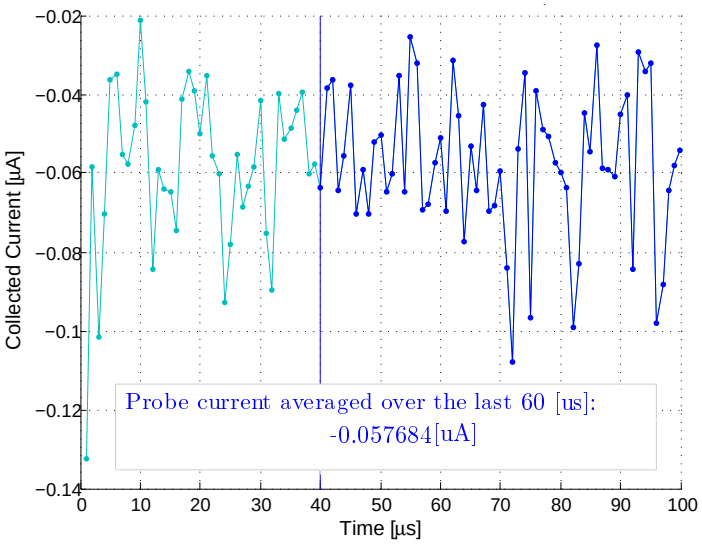

Figure C.115: *-0.25V*

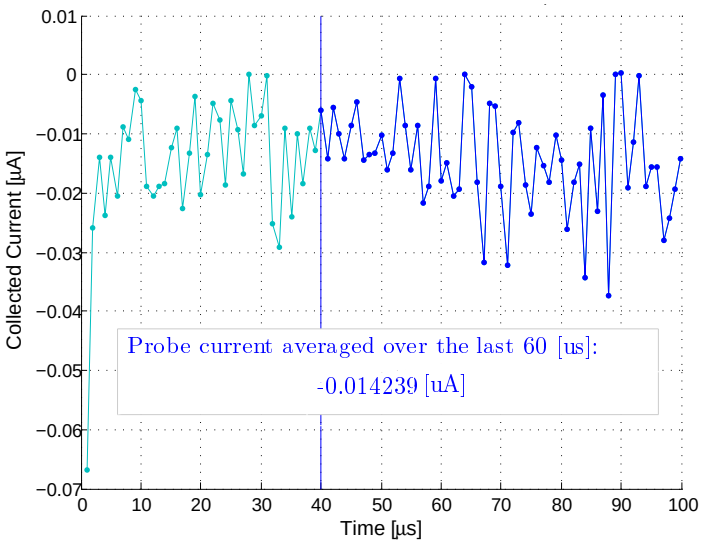

Figure C.116: *-0.5V*

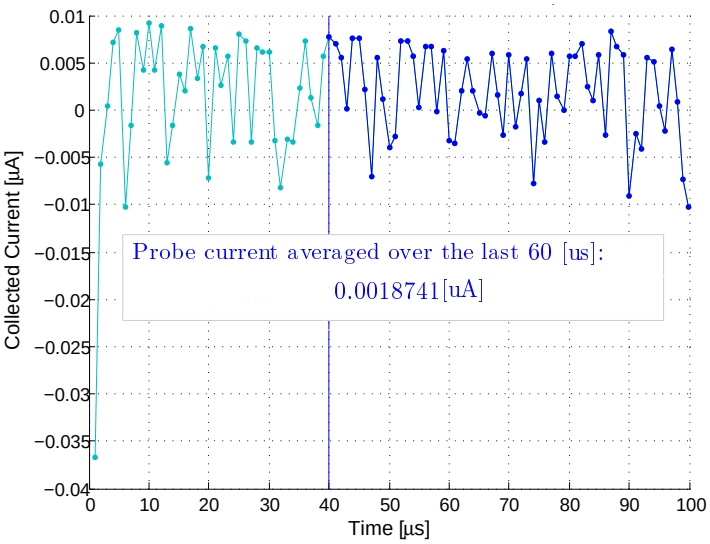

Figure C.117: *-0.75V*

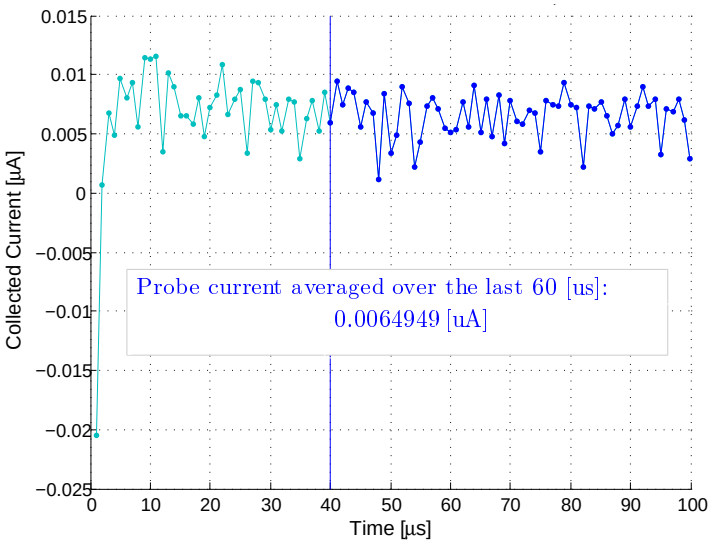

Figure C.118: *-1V*

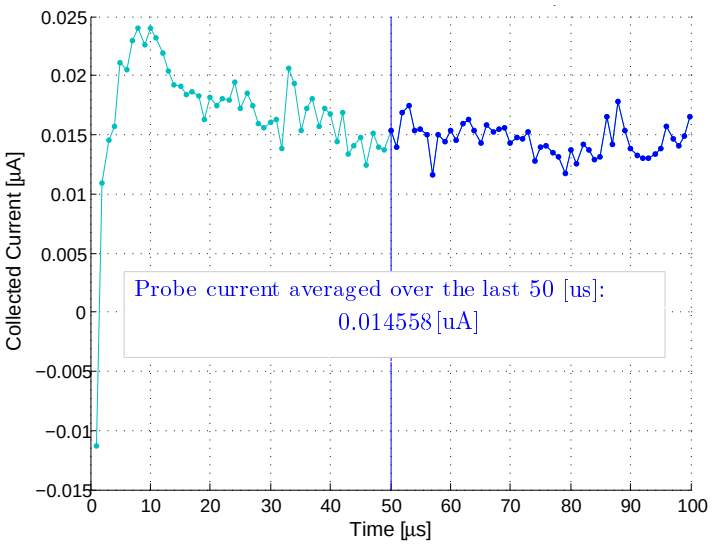

Figure C.119: *-2V*

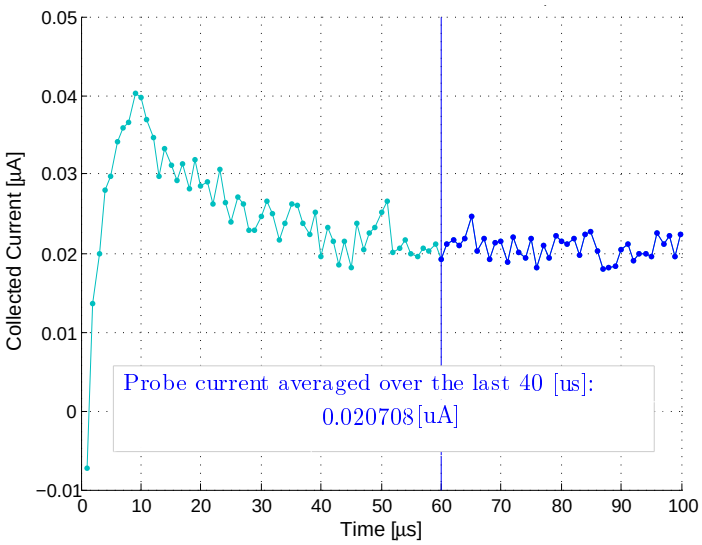

Figure C.120: *-3V*

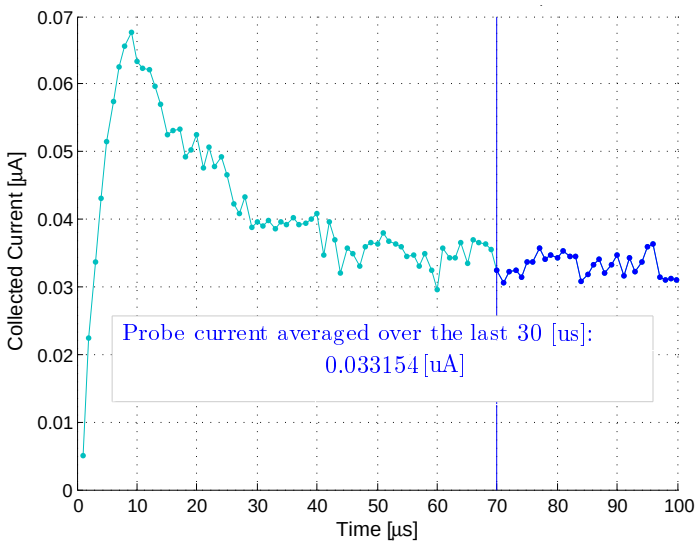

Figure C.121: *-5V*

C.3.2 Sphere B PIC, $\lambda_D \approx 10$mm

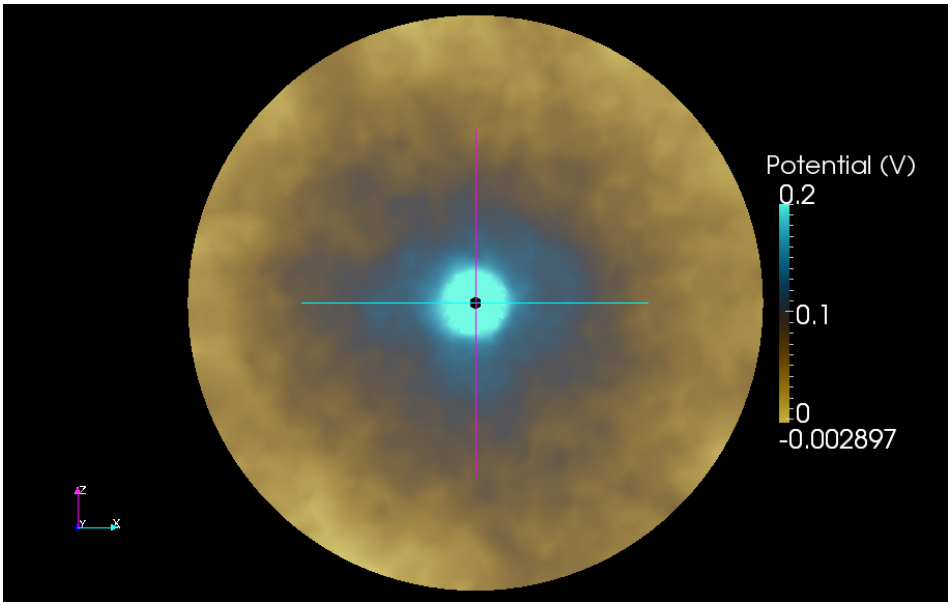

Figure C.122: *Potential map: bias = 2V, rescaled to 0.05V*

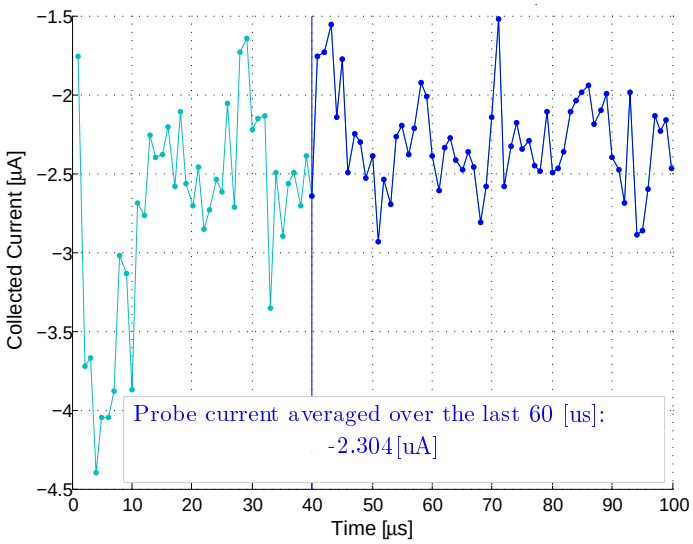

Figure C.123: *2V*

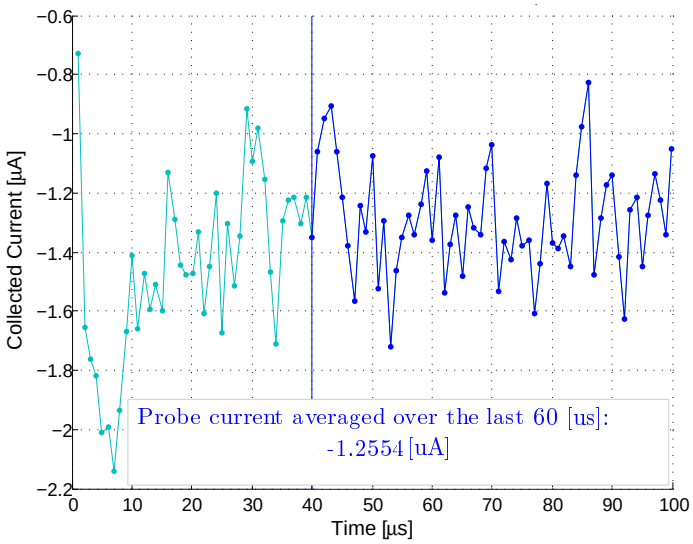

Figure C.124: *1V*

C.3.3 Sphere-Stub PIC, $\lambda_D \approx 10\,\text{mm}$

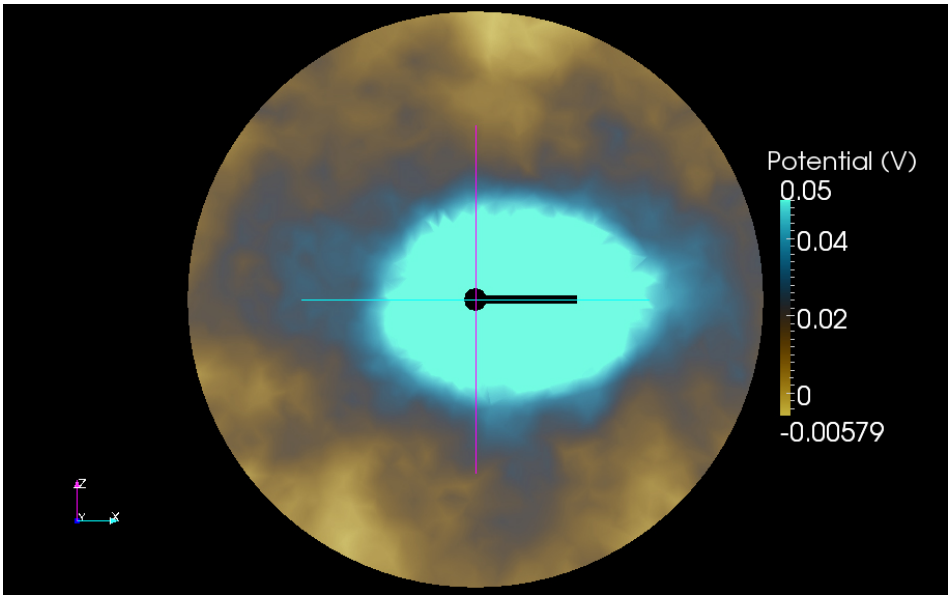

Figure C.125: *Potential map: bias = 2V, rescaled to 0.05V*

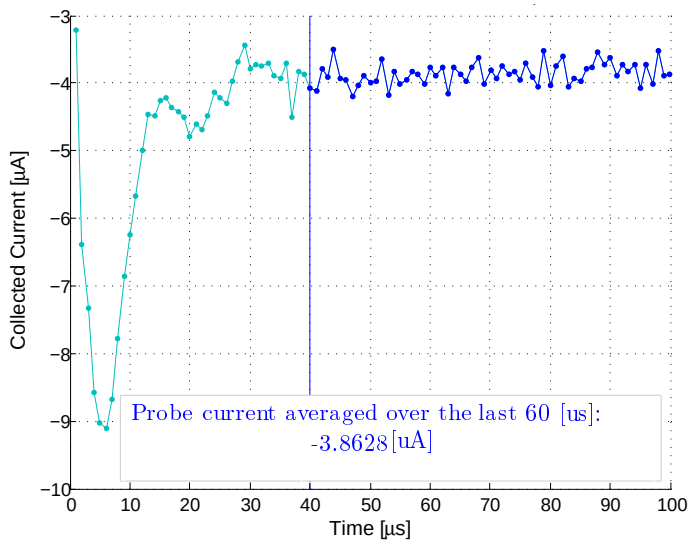

Figure C.126: *5V*

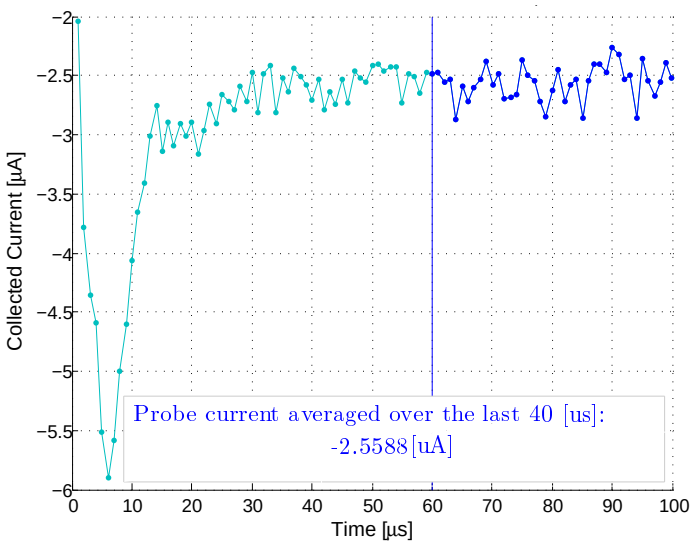

Figure C.127: *3V*

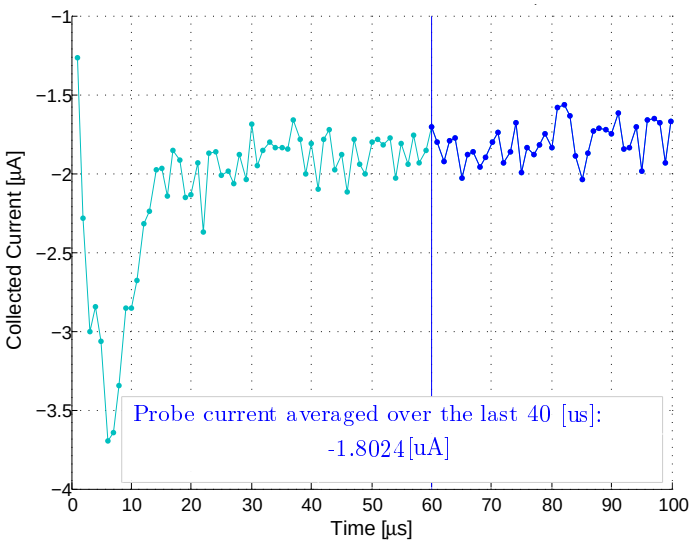

Figure C.128: *2V*

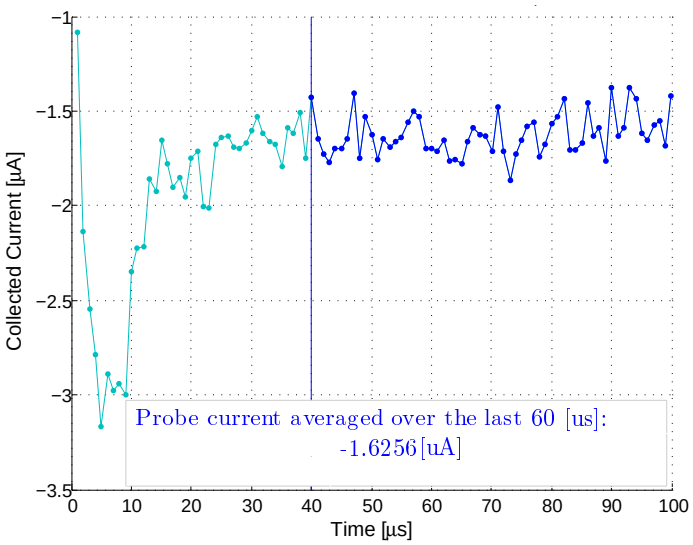

Figure C.129: *1.75V*

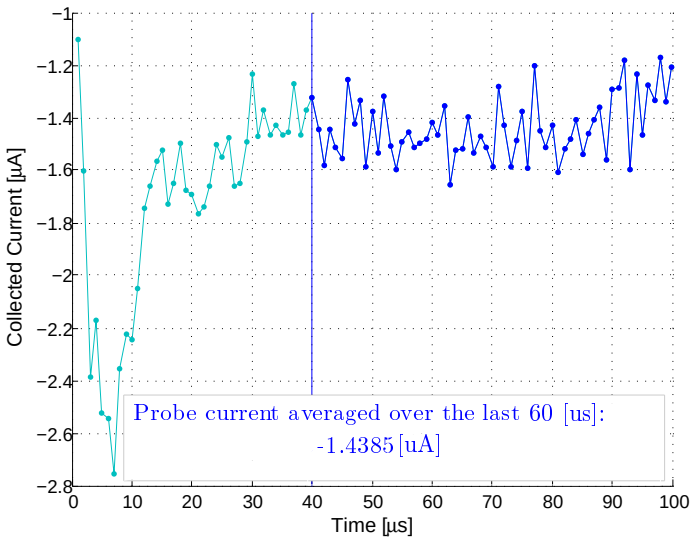

Figure C.130: *1.5V*

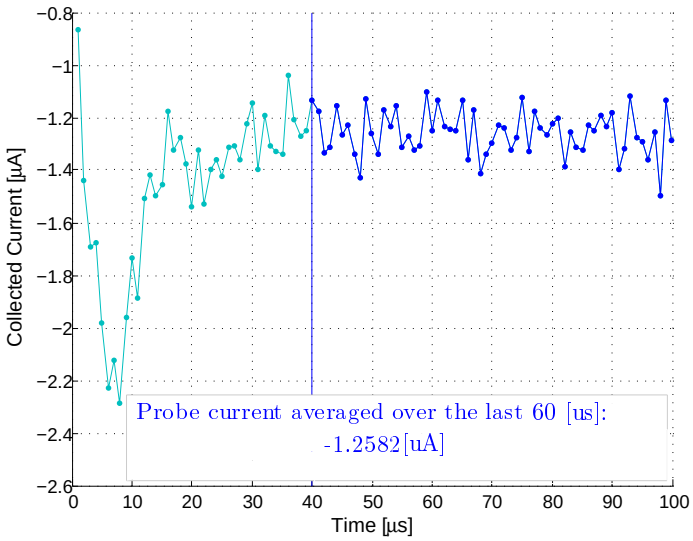

Figure C.131: *1.25V*

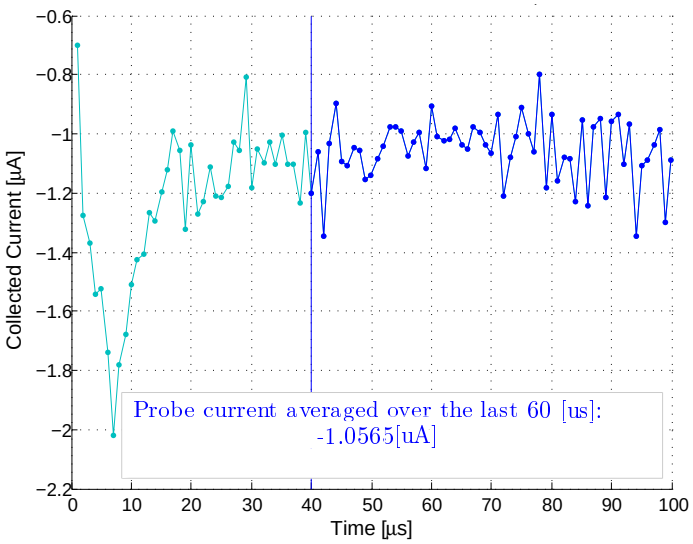

Figure C.132: *1V*

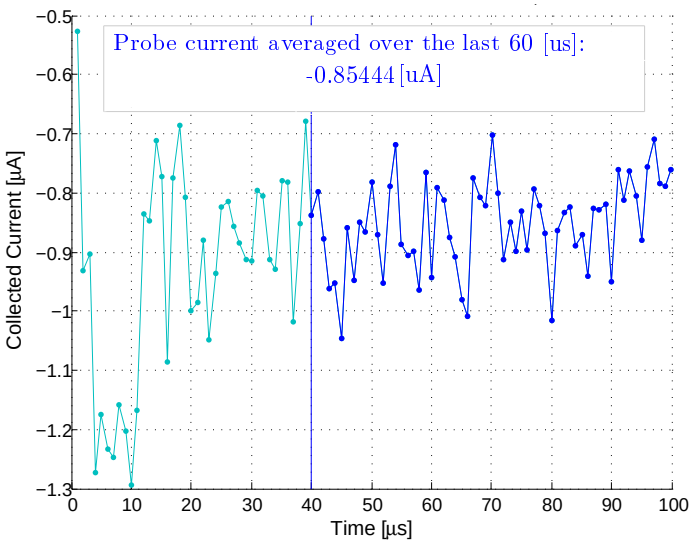

Figure C.133: *0.75V*

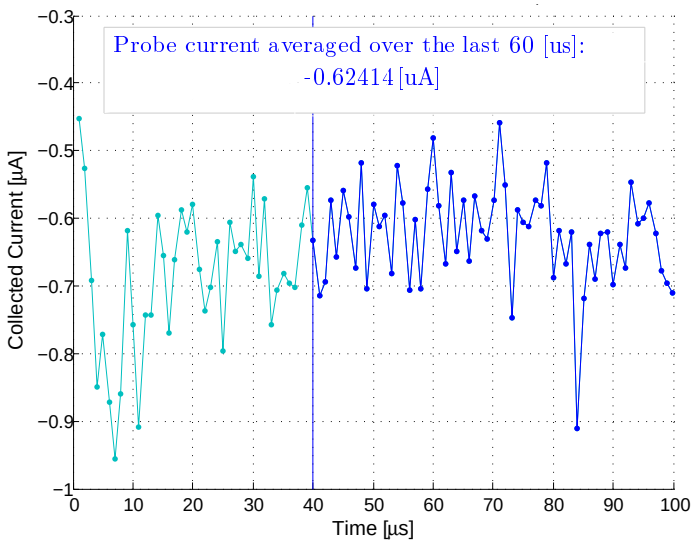

Figure C.134: *0.5V*

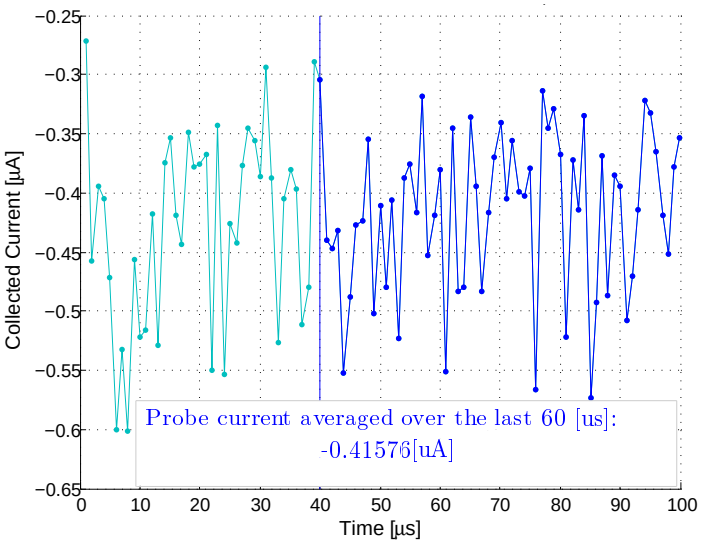

Figure C.135: *0.25V*

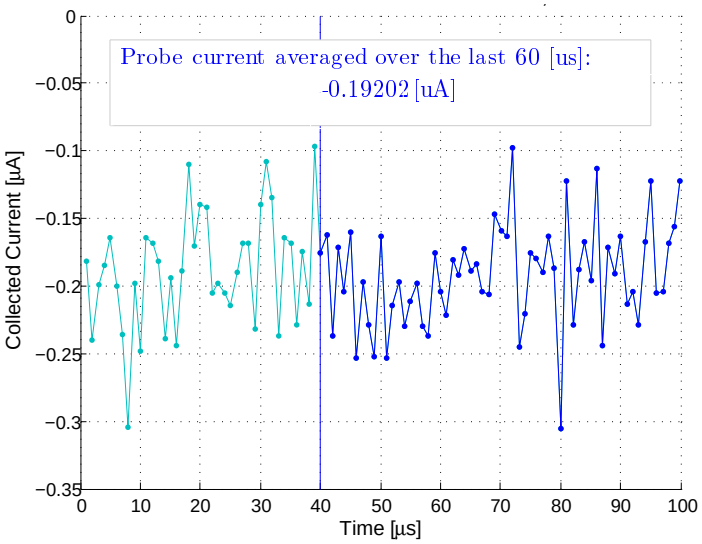

Figure C.136: *0V*

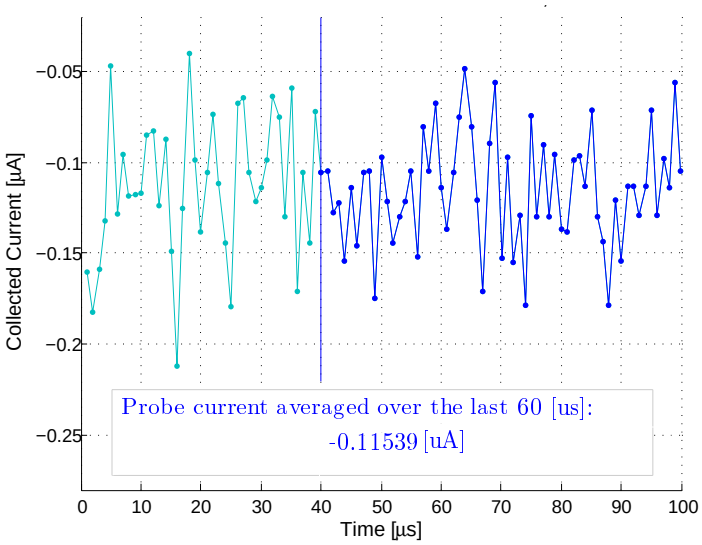

Figure C.137: *-0.1V*

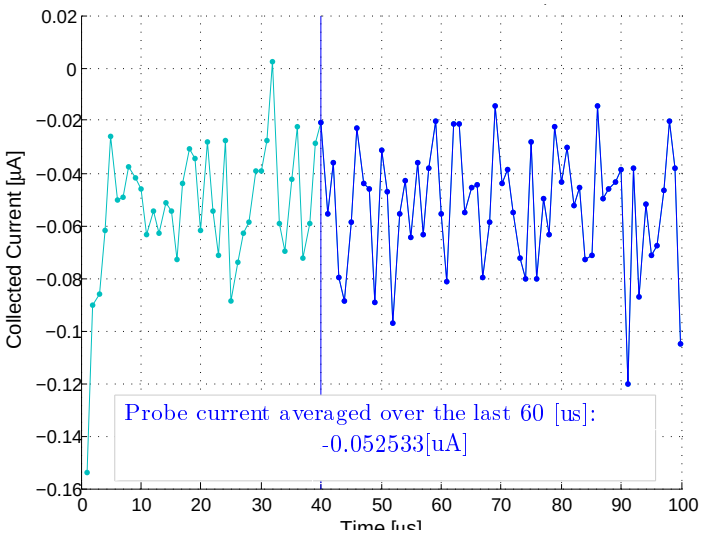

Figure C.138: *-0.25V*

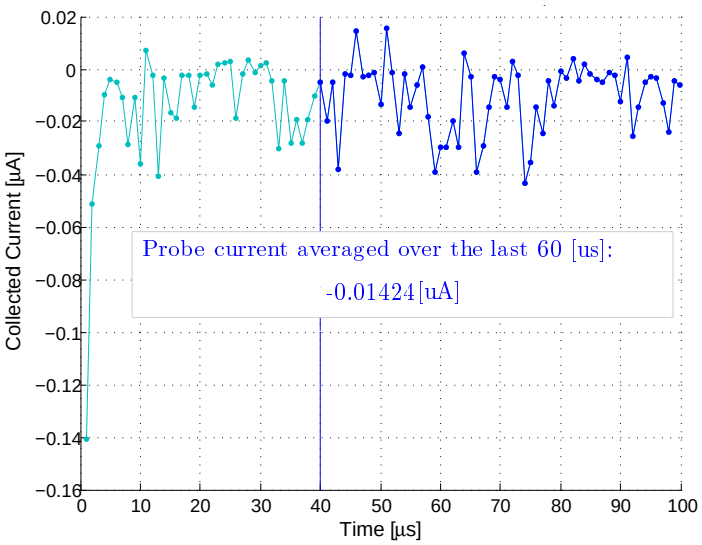

Figure C.139: *-0.5V*

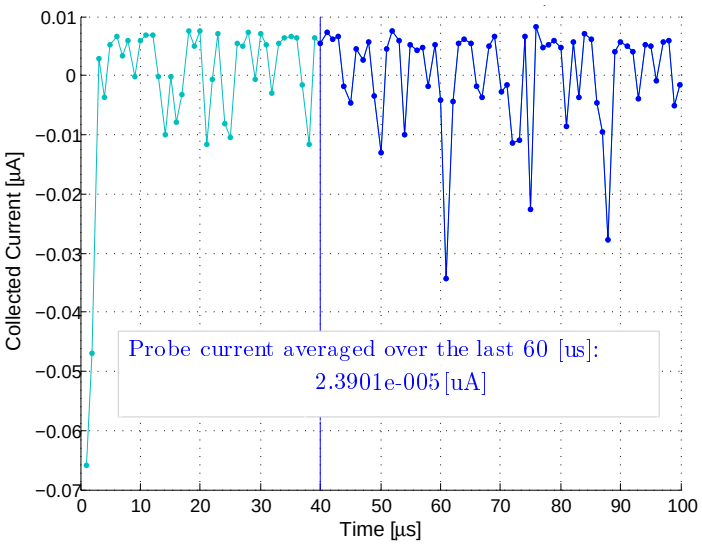

Figure C.140: *-0.75V*

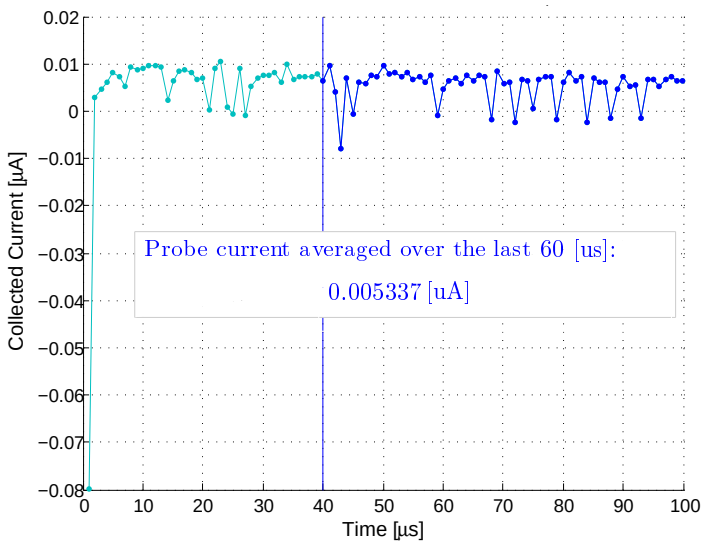

Figure C.141: *-1V*

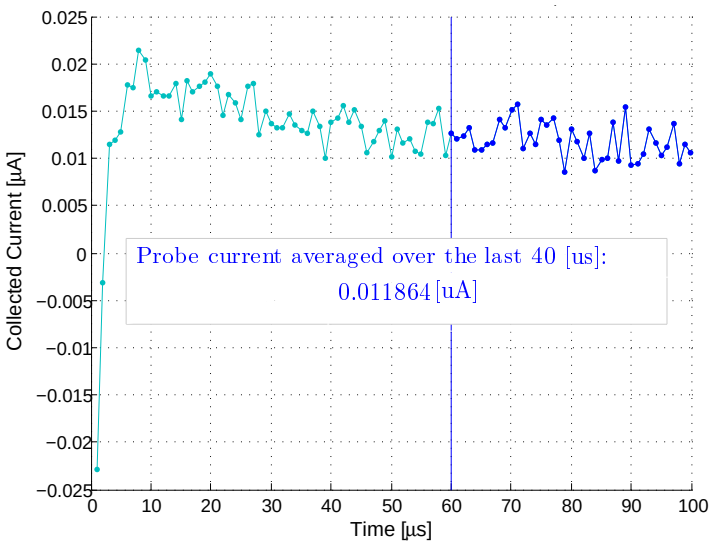

Figure C.142: *-2V*

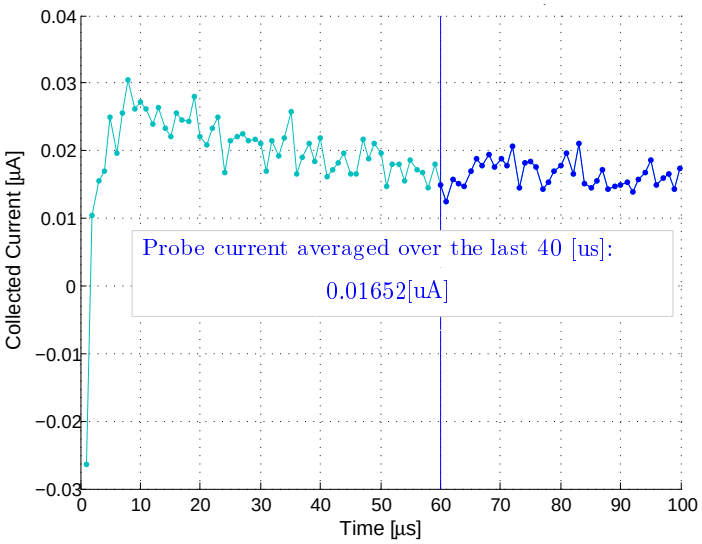

Figure C.143: *-3V*

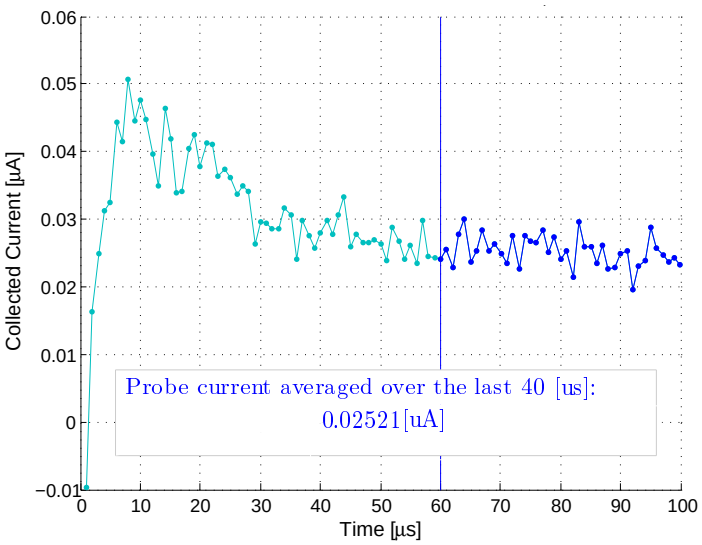

Figure C.144: *-5V*

C.3.4 Sphere-Stub drift PIC, $\lambda_D \approx 10\,\text{mm}$

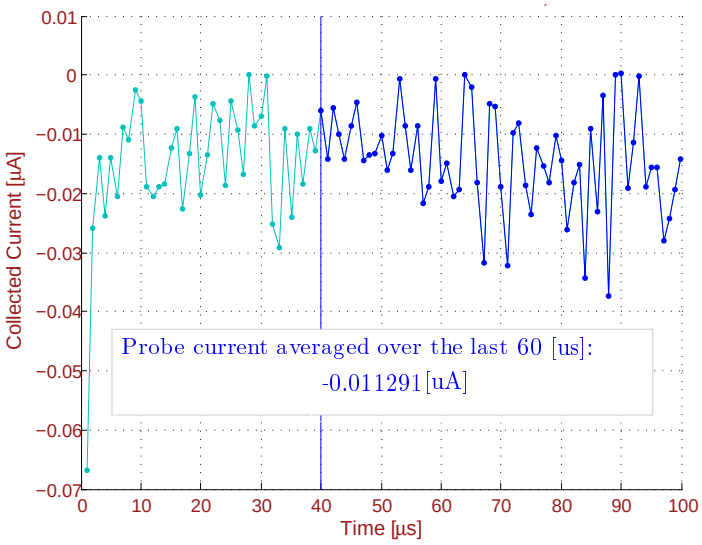

Figure C.145: *-0.6V*

C.3.5 Full probe-simplified s/c model PIC, $\lambda_D \approx 10\,\text{mm}$

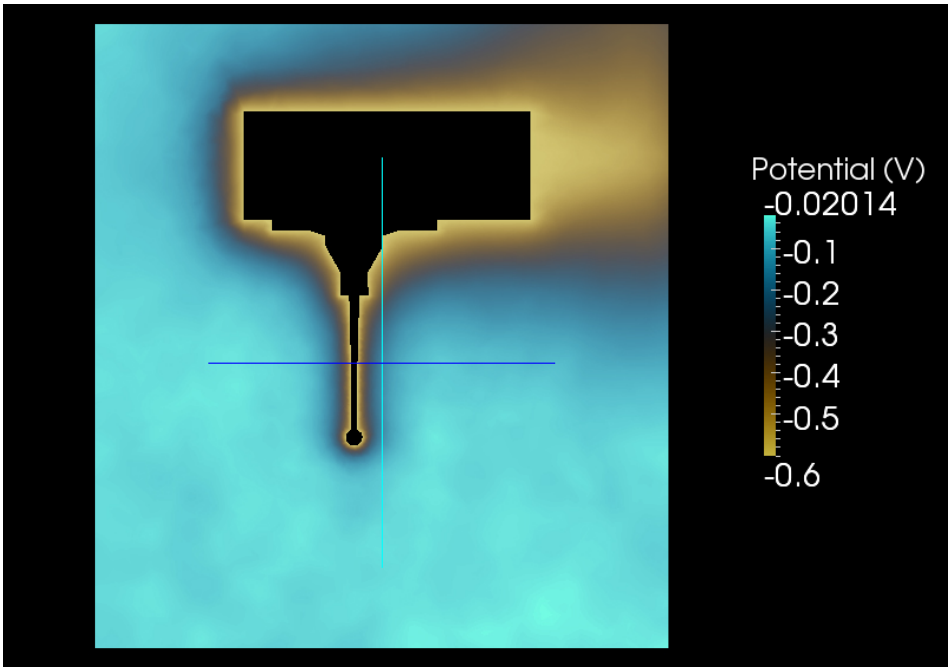

Figure C.146: *Potential map: bias = 2V, rescaled to 0.05V*

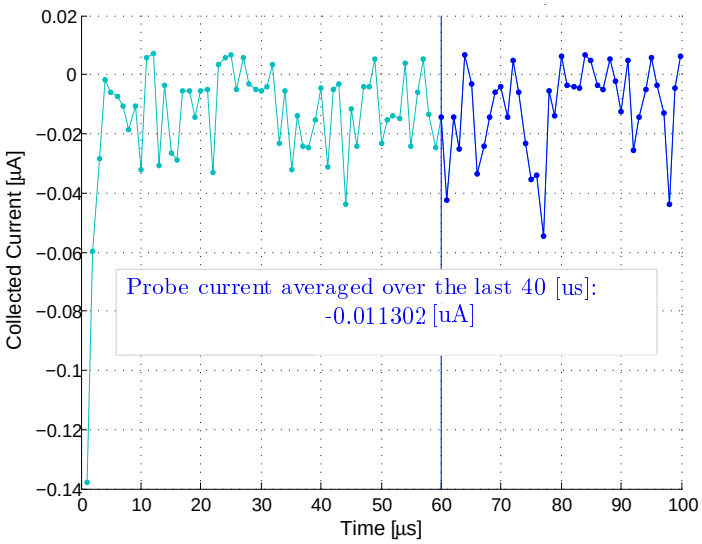

Figure C.147: *-0.6V*